Reactivity of Cu(100)-Fe surfaces

De reactiviteit van Cu(100)-Fe oppervlakken.
(met een samenvatting in het Nederlands)

PROEFSCHRIFT

TER VERKRIJGING VAN DE GRAAD VAN DOCTOR AAN DE RIJKSUNIVERSITEIT TE UTRECHT OP GEZAG VAN DE RECTOR MAGNIFICUS, PROF. DR. J.A. VAN GINKEL INGEVOLGE HET BESLUIT VAN HET COLLEGE VAN DECANEN IN HET OPENBAAR TE VERDEDIGEN OP MAANDAG 28 FEBRUARI 1994 DES NAMIDDAGS TE 2.30 UUR.

door

Hans-Peter den Daas

GEBOREN OP 8 DECEMBER 1965 TE MEPPEL

promotor : Prof. Ir. J.W. Geus
co-promotor : Dr. O.L.J. Gijzeman
(Beiden verbonden aan de Faculteit der Scheikunde van de Rijksuniversiteit te Utrecht)

CIP-GEGEVENS KONINKLIJKE BIBLIOTHEEK, DEN HAAG

Daas, Hans-Peter den

Reactivity of Cu(100)-Fe surfaces / Hans-Peter den Daas. -
Utrecht : Universiteit Utrecht, Faculteit Scheikunde
Proefschrift Universiteit Utrecht. - Met lit. opg. - Met
samenvatting in het Nederlands.
ISBN 90-393-0110-7
Trefw.: ijzer ; reactiviteit / fysische chemie

Voorwoord

Het in dit proefschrift beschreven werk is grotendeels uitgevoerd in de werkgroep oppervlaktechemie (thans onderdeel van de vakgroep Anorganische chemie, toen ik in dienst kwam onderdeel van de vakgroep Fysische en Colloïdchemie en gedurende mijn hele onderzoeksperiode deel van het Debye Instituut) en voor een gedeelte bij het Dipartimento di Fysica, Università dell'Aquila (It.).

Iedereen die, op zijn eigen manier, heeft bijgedragen aan het tot stand komen van dit proefschrift wil ik hier graag bedanken:

Mijn promotores John Geus en Onno Gijzeman, de technici Ad Mens en Kees Rietveld met hun onmisbare steun op het lab, de studenten Joep van Giezen, Manon Jeurissen, Chloé Laszlo en Erwin Voogt (de laatste ook nog 3 maanden als collega), mijn collegae in de groep Ruud Balkenende, Robert-Jan Vreeburg, Wijnand van Kooten en Rob van Wijk en de audio-visuele dienst onder leiding van Jan den Boesterd. Ook voor de steun van Jan Verhoeven (AMOLF), met name aan het begin van mijn onderzoek en in de voorbereidingsfase, ben ik zeer erkentelijk.

Furthermore I am very grateful to Luca Lozzi, Maurizio Passacantando, Pietro Picozzi and Sandro Santucci who are responsible for my enjoyable and productive 6 months visit to their laboratory in l'Aquila and the grant of the EC Human Capital and Mobility Programme offered to me by the INFM. Last (but no least) I would like to thank Maurizio De Crescenzi (Dipartimento di Fysica, Università di Roma II and Dipartimento di Fysica, Università di Camerino) for introducing me to the l'Aquila group during my one month visit to his lab in Rome, October 1990.

Contents

This thesis is based on the following papers:

Chapter 3 Oxidation of ultra thin iron layers on Cu(100). Composition of the oxide films.
H. den Daas, O.L.J. Gijzeman and J.W. Geus, Surf. Sci. **285** (1993) 15.

Chapter 4 Oxidation of one monolayer of iron on Cu(100) studied with AES peak shape analysis.
H. den Daas, O.L.J. Gijzeman and J.W. Geus, Surf. Sci. **290** (1993) 26.

Chapter 5 The interaction of Cu(100)-Fe surfaces with oxygen studied with photoelectron spectroscopy I.
H. den Daas, M. Passacantando, L. Lozzi, S. Santucci and P. Picozzi, submitted to Surf. Sci.

Chapter 6 The interaction of Cu(100)-Fe surfaces with oxygen studied with photoelectron spectroscopy II.
H. den Daas, M. Passacantando, L. Lozzi, S. Santucci and P. Picozzi, submitted to Surf. Sci.

Chapter 7 The interaction of CO and H_2 with oxidised Cu(100)-Fe surfaces.
H. den Daas, O.L.J. Gijzeman and J.W: Geus, Appl. Surf. Sci. **68** (1993) 557.

Chapter 8 The interaction of CO with Cu(100)-Fe surfaces. H. den Daas, E.H. Voogt, O.L.J. Gijzeman and J.W. Geus, accepted for publication in Surf. Sci.

Chapter 9 Low Energy Auger Electron Spectroscopy of clean and oxidised Cu(100) and Cu(100)-Fe surfaces.
H. den Daas, O.L.J. Gijzeman and J.W. Geus, Surf. and Interface Anal. **18** (1992) 397.

Related papers:

'Structural and electronic studies of clean and oxidised thin Fe films on polycrystalline copper.', S. Di Nardo, M. Passacantando, P. Picozzi, S. Santucci, L. Lozzi, M. De Crescenzi and H. den Daas, Surf. Interface Anal. **18** (1992) 98.

'Extended energy loss fine structure and X-ray photoelectron spectroscopy studies of clean and oxidised Fe thin films on polycrystalline copper.', S. Di Nardo, M. Passacantando, P. Picozzi, S. Santucci, L. Lozzi, M. De Crescenzi and H. den Daas, Surf. Interface Anal. **19** (1992) 478.

1

Introduction

1.1 Bimetallic surfaces and their reactivity.

In recent literature quite a lot of work dedicated to Cu-Fe surfaces can be found. The reasons that authors give for their investigations depend on their field of interest but can basically be reduced to the fact that the properties of the Cu-Fe system cannot be described by a simple addition of the bulk properties of both metals. Of course this observation is not restricted to the Cu-Fe system.

So the first reason to study bimetallic systems is the fundamental question which (new) properties are induced when two metals are put together. Answers to this question result in a better understanding of matter in general. Sometimes the new properties can be made profitable to mankind and that is where applied research comes in. So the second reason to study bimetallic systems is that the understanding of these systems can improve existing applications or lead to new applications.

As for the pure metals, in bimetallic systems differences exist between bulk and surface properties. These differences are not only interesting from a physical point of view (for example crystalline and electronic structure, magnetic properties, or surface composition compared to bulk composition) but also from a chemical point of view. One may be curious to know what the reactivity of a bimetallic surface is compared to that of the single constituents.

On the more practical side the interaction of surfaces with gases may be disastrous when one thinks of corrosion, but also very worthwhile because, for example, in heterogeneous

catalysis metals (or metal compounds) are often used to produce desirable products. In principle catalysts are used to enhance chemical reactions in order to permit (industrial) processes to be carried out under better (= cheaper) conditions. Since present day requirements in industry ask for a more careful use of reactants, catalysts with a better performance must be developed. This means higher selectivity for the desired product without loosing activity or reducing the lifetime of the catalyst. This requires a good understanding of the mechanisms of the reactions taking place on the surface of the catalyst. Though the differences between catalysts and model surfaces like single crystals are huge, the study of model systems is a convenient way to get a better insight in processes occurring on the surface. Campbell states it even stronger in his review paper on bimetallic surface chemistry [1]: "The well-defined bimetallic surfaces offered for first time an ability to correlate surface chemical reactivity with atomic level surface structure."

When studying the reactivity of well-defined surfaces it is sensible to use relatively simple molecules like oxygen, carbon monoxide and hydrogen. However, even these simple molecules can result in complicated processes. Furthermore, because oxygen is an element involved in many surface processes both the reactivity of surfaces towards molecular oxygen and the reactivity of oxygen adsorbed (or incorporated in the surface in some way) towards gases other than oxygen is an important subject. Information about the interaction of CO and H_2 can be used to get more information about structure and composition of oxidised surfaces. And, on the other hand, it can give an indication of what kind of sites are involved in the interaction. The same can be said for the interaction of CO with unoxidised surfaces.

1.2 Cu-Fe surfaces.

For this thesis the most important differences between copper and iron are the crystal structure at room temperature, the surface free energy and the reactivity towards oxygen and carbon monoxide. These and other properties of both metals are listed in Table 1.

Many studies have been done on the Cu-Fe system [7-28]. Several of them concern the magnetic properties of these surfaces [22-28], or in close relation to that, the structure of iron grown on copper single crystal surfaces [7-13]. Also the chemical reactivity of the Cu-Fe surfaces has been subject of quite a number of studies [29-37].

The growth of iron on Cu(100) has been studied with a large number of techniques. Though some discussion still exists about details in the growth mechanism, all authors agree about the formation of an fcc iron layer when iron is evaporated at or below 300 K. Since the discussion concerns mostly the exact number of monolayers at which the growth mode changes and the exact temperature at which those changes happen, just an outline of the growth without mentioning many numbers or temperatures will be given.

Evaporating iron at room temperature initially gives epitaxial iron islands on the copper surface followed by a layer-by-layer growth (4 - 11 ML) [7-13]. According to Wuttig et al. [13] the presence of CO during evaporation induces a longer region of layer-by-layer growth. This effect is already found for CO pressures of $7 \cdot 10^{-8}$ Pa. The copper/iron surfaces are not stable, even at room temperature slow changes occur [7-11]. The Cu(100)-Fe system has been studied with STM by Brodde et al. [9] and by Chambliss et al. [10]. They report an iron induced diffusion of copper atoms starting at room temperature. This is confirmed by an ion-scattering spectroscopy study [12]. Brodde et al. [9] also found that annealing the surfaces

Table 1. Some properties of copper and iron.

	copper	**iron**
Bulk		
molecular weight (g/mol)	63.546	55.847
density (g/cm^3 298 K)	8.92	7.86 (bcc)
melting point (K)	1356	1808
$T_{transition}$ (K) bcc⁄fcc [2]	--	T < 1180 bcc T > 1223 fcc
nearest neighbour (Å)	2.55	2.48 (bcc)
refractive index [3]	0.25 + 3.6i	2.87 + 3.36i
ΔG_f oxides (kJ/mol, 298 K) [4]	Cu_2O -198.3 CuO -168.8	FeO -283.7 Fe_3O_4 -1159.1 Fe_2O_3 -849.5
surface		
γ (ergs/cm^2) [5]	1670 (1320 K)	2150 (1673 K)
ΔH_{ads} for CO (kJ/mol) (at θ_{CO}=0, 300 K)	69.4 [5] Cu(100)	100 ± 5 [6] Fe(100)*)
s_0 oxygen (300 K)	0.01	1

*) on most Fe single crystal surfaces CO dissociates at 300 K

causes an extensive migration of copper atoms. The copper atoms even seem to cover the iron islands.

Van Pruissen et al. [29-34] studied the reactivity of Cu(111)-Fe and Cu(110)-Fe surfaces quite extensively. However, the use of iron pentacarbonyl to deposit iron on the copper surfaces results in less well-defined surfaces as one might desire. The possibility to deposit iron on the surface by means of evaporation and the relative good knowledge of the growth of iron on the Cu(100) plane led to the choice to study the reactivity of the Cu(100)-Fe surfaces. Direct comparison with the work of Van Pruissen is thus impossible, but a simple heat treatment of the surface should take away most of the differences caused by the two preparation methods and leave differences caused by the different copper planes.

1.3 Scope of this thesis.

The central theme of this thesis is how oxygen reacts with the well-defined Cu(100)-Fe surfaces and what the composition of the surface is after the reaction. The influence of the iron coverage on the interaction and the composition is taken into account. Since the oxidation of iron can result in different kinds of iron oxide, much attention is paid to the oxide formed and to the intermediates that exist during the reaction. Chapter 3 describes the results of the oxidation of Cu(100)-Fe surfaces studied with Auger electron spectroscopy (AES), ellipsometry and low energy electron diffraction (LEED). In chapter 4 a more detailed analysis of the Fe $M_{2,3}VV$ Auger transition during oxidation is given. Chapter 5 and 6 are dedicated to photo-emission results (XPS and UPS respectively).

The reactivity of the oxidised surfaces to hydrogen and carbon monoxide is also a matter of interest since it tells more about the structure of the oxide (surface). In chapter 7 the study of this reactivity is described.

The formation of fcc iron on the Cu(100) surfaces opens the possibility to study this type of iron at temperatures where bulk fcc iron is unstable. The interaction of carbon monoxide with iron is probably influenced by the structure of the iron on an atomic level. Chapter 8 deals with the interesting features of the interaction CO with Cu(100)-Fe surfaces.

The results described in chapter 4 could only be obtained after an improvement in data acquisition and analysis of the AES spectra. Chapter 2 gives, besides a general description of the techniques used in this thesis, also a description and discussion of a better method for data acquisition of AES spectra. The necessary changes in the data analysis are described in chapter 9.

2

Experimental

2.1 Introduction. Ultra high vacuum.

The interest in solid-gas (or solid-vacuum) interfaces has been increasing rapidly during the last three decades. On one hand this is due to the practical importance of these interfaces in daily life (read: 'industrial purposes') as found in heterogeneous catalysis, micro-electronics and corrosion, and on the other hand it is due to the possibility of studying these interesting interfaces under appropriate conditions: ultra high vacuum (UHV). The reason UHV is appropriate for these studies is twofold: First, many surface sensitive analytical techniques require pressures below 10^{-6} Pa because they use low energy charged or neutral particles as probes (for electrons typically energies up to 10^{3} eV are used). The mean free path of these particles in vacuum depends on the energy and the pressure. Second, since the interest often concerns clean surfaces or surfaces containing known amounts of hetero atoms/compounds, the partial pressure of contaminating compounds must be below a certain level to be able to maintain the surfaces in the desired condition during a reasonable time interval. In practice this means that in UHV systems base pressures in the 10^{-8} Pa range are maintained. Development and improvement of adequate pump systems and welding technology during the last decades make these pressures now readily obtainable.

Besides vacuum technology many techniques were developed to study surface composition and structure (both electronic and geometric) of different kinds of samples. Apart from giving different types of information some techniques are destructive, some non-

destructive and others enhance or influence chemical processes on the surfaces. Thus special care is required in choosing the proper techniques and in interpreting the data correctly. As all techniques have their own special qualities several of them are required to get proper insight in the surface (-processes).

In order to get information about the reactivity, composition and structure of Cu(100)-Fe (oxide) surfaces AES, ellipsometry, LEED, XPS and UPS are used in combination. Since all these techniques are well described in the literature [38-42], only features of the techniques that are of special interest for the studies described in this thesis will be explained in greater detail in the next sections. More attention is paid towards data acquisition and analysis for AES because the procedures as used in this thesis differ from the common procedures.

Finally a description of the UHV-systems used in this thesis and the methods for sample preparation will be given.

2.2 Auger electron spectroscopy.

Auger electron spectroscopy (AES) uses the electrons resulting from the Auger decay process [40]. The energy of an Auger electron depends on the energy of the orbitals involved and thus is characteristic for an element. Due to the small inelastic mean free path (imfp) of the Auger electrons (ca. 3 - 15Å for energies between 40 and 1000 eV) the information depth is reduced to about 2 - 10 atomic layers [43]. Thus AES gives (quantitative) information about the atomic composition of the top layers of the surface.

Since in AES the (core) holes required for the Auger process are usually created by high energy (ca. 2 - 5 keV) electrons the number of so called secondary electrons is much higher than in the case of X-ray induced holes. These secondary electrons are the result of a number of inelastic scattering processes in the surface region. In the spectra the electrons of interest are thus superimposed on a background which is at least one order of magnitude higher in number. In the past the most convenient way to make the data accessible was to detect the derivative (or second derivative depending on the analyser) using a phase sensitive amplifier (lock-in-amplifier) and a x-y recorder. In this way small signals can be 'separated' from a large background with relatively high signal-to-noise levels. An other 'advantage' of this procedure is that a slowly changing background can be (must be) neglected. Correction methods have been developed for steep backgrounds [44].

Nowadays, the availability of cheap personal computers (a 80286 can do the job) and 14 bit or more analogue-to-digital converters eliminates all reasons not to use more sophisticated methods. However, the peak-to-peak heights of the differentiated Auger spectra are still used by many scientists to determine the surface composition. It is relatively easy to compare the spectra with those of Auger handbooks and to use relative sensitivity factors to calculate the chemical composition of the surface. This presupposes the same peak shape for both the sample and the elemental standard used. Identical conditions are required in both cases: modulation amplitudes and all other instrument specific functions have to be the same. Although, even then, it can be dangerous to use the differentiated spectra for quantitative analysis. Both the overlap of peaks of different elements and a change in peak shape can cause errors in quantification. To illustrate this argument the results obtained from differentiated spectra are compared with results obtained using the original N(E) vs. E spectra and a background subtraction as described in chapter 9.

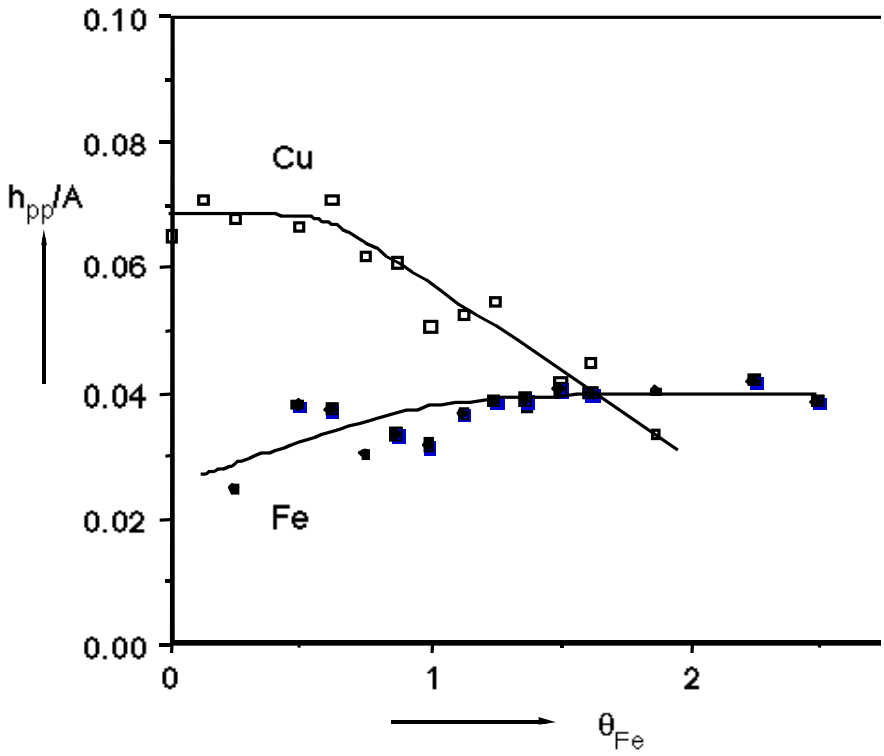

Figure 1 *The ratio of the peak-to-peak height and the peak area of the Cu and Fe $M_{2,3}VV$ peaks during evaporation of iron on Cu(100). Lines are drawn to guide the eye.*

Fig. 1 shows the ratio of the peak-to-peak height (h_{pp}) and the peak area (A) of the Fe and the Cu $M_{2,3}VV$ peaks obtained during the evaporation of Fe on Cu(100) as function of θ_{Fe} (the same spectra were used to obtain Fig. 8 in chapter 9). The differentiated spectra were obtained by means of numerical differentiation of the original spectra. It is clear that h_{pp}/A is not constant with changing peak intensities. A constant h_{pp}/A is expected when the peak shape does not change. For the metallic Cu(100)-Fe system no shape change of the $M_{2,3}VV$ peaks is observed within experimental error for both the Fe and the Cu $M_{2,3}VV$ peak [45]. So the changing h_{pp}/A must be due to effects of the overlap of both peaks. In that case one should expect the deviations to be largest for θ_{Fe} values for which one of both peaks is small in respect to the other. In fact this is the case. A similar effect is visible in Fig. 2. In this figure h_{pp}/A of the Cu and Fe $M_{2,3}VV$ peaks is given as function of the amount of oxygen on a Cu(100) surface containing one monolayer (ML) of iron. (The same spectra were used in Fig. 5 in chapter 4.) Here the decrease of h_{pp}/A for the Cu $M_{2,3}VV$ peak is caused by the increasing overlap with the Fe $M_{2,3}VV$ peak. The h_{pp}/A for the Fe $M_{2,3}VV$ peak decreases fast during the adsorption of the first ML of oxygen because most of the shape change in the Fe $M_{2,3}VV$ peak occurs during this part of the oxidation [46]. Quantitatively the derivative spectra are deluding in the described cases. In the last case it is also difficult to extract useful information about the oxidation.

To show that in some cases there is no difference in both methods, results of the analysis of the O KLL and Fe the LMM peaks obtained during the oxidation of Fe(100) are presented in Fig. 3. The ratio of the O and Fe peak areas is given as function of the ratio of the h_{pp} of the O $KL_{2,3}L_{2,3}$ (515 eV) and the Fe $L_3M_{4,5}M_{4,5}$ (705 eV) peaks. The straight line is the

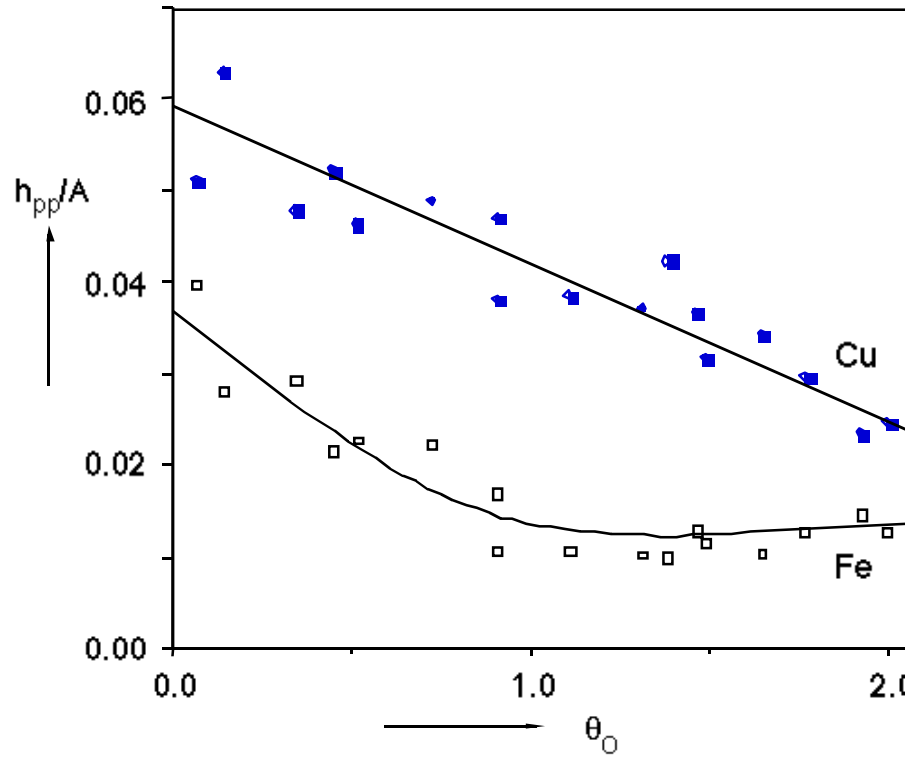

Figure 2 *The ratio of the peak-to-peak height and the peak area of the Cu and Fe $M_{2,3}VV$ peaks during oxidation of one monolayer of iron on Cu(100). The lines are drawn to guide the eye.*

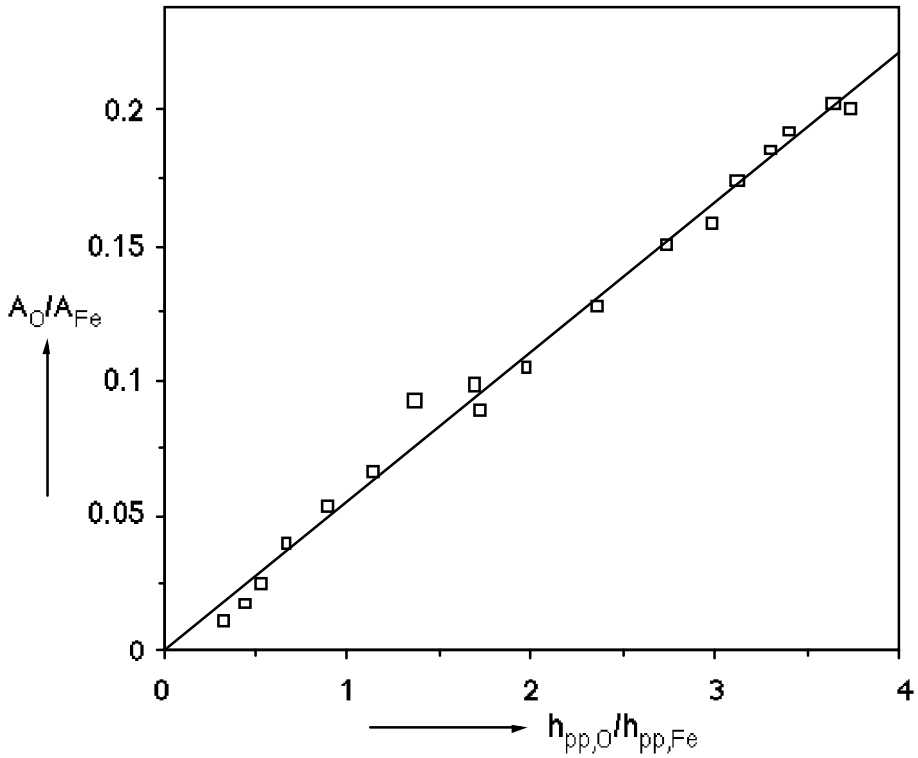

Figure 3 *The ratio of the O KLL and the Fe LMM peak area plotted against the ratio of the peak-to-peak height of the largest peaks during oxidation of Fe(100).*

linear fit through the points. The line indicates that both methods give the same results in quantification. One remark must be made: a possible shape change of the Fe $L_3M_{4,5}M_{4,5}$ peak might be invisible in the spectra used since they were obtained using a modulation amplitude of 8 V_{pp} (section 2.2.1 of this chapter gives more details about data acquisition).

It may be clear now that for reasons of accuracy it is better to collect (and use) the N(E) vs. E spectra. The use of this kind of spectra, however, introduces an other problem: background subtraction. In chapter 9 a method is described that appeared to give satisfactory backgrounds. Unless stated otherwise the AES spectra in this thesis were collected and handled as described in the next sections.

2.2.1 Instrumentation and data acquisition.

The AES spectra were produced by exciting the top-layer atoms using an electron beam perpendicular to the surface with an energy of 2500 eV and a beam current of 1-3 μA. For the subtraction of a good background on the high energy part of the AES spectra a higher primary beam energy (5 keV) would have favourable but the electron gun did not admit that. The lower limit of the intensity of the beam current was determined by the sensitivity of the detection system.

A 4 grid retarding field analyser (RFA, also used as LEED optics) with an on-axis electron gun was used to analyse the energy of the emitted electrons. The angle of acceptance of the RFA was 120°, the resolution 0.3%. The often used bias voltage of 200 V on the collector was not necessary because of a soot coating on the collector. The production of extra secondary electrons on the grids was prevented by a carbon coating which was evaporated on the grids. The retarding field was controlled by a computer. The voltage could be changed in steps of 60 mV from 0 to 2000 V. The step width used was 120 mV for the MVV region (20 - 80 eV) and 240 mV for the other parts of the spectrum.

A lock-in-amplifier (LIA) was used to obtain the first derivative of the I versus E spectra. A modulation frequency of 2.4 kHz was used. The spectra in the MVV region were collected with a peak-to-peak modulation amplitude of 0.7 V_{pp}, the sulphur LMM and the carbon KLL with 4.0 V_{pp} and the other spectra with a modulation amplitude of 8.0 V_{pp}. The output of the LIA was sampled either by integrating for 500 ms or by adding 10 samples from an analogue-to-digital converter at each energy step. The settings given above were chosen to compromise between the signal to noise ratio, the resolution and the time needed to collect a spectrum. Usually two scans were collected and added in order to check for drift and to increase the signal to noise ratio.

2.2.2 Data analysis.

The Fe $M_{2,3}VV$, Cu $M_{2,3}VV$ and O KLL peaks were extracted from the spectra by means of a background subtraction method proposed by Peacock [45,47]. Areas of the Fe $L_{2,3}M_{2,3}V$ and Cu $L_{2,3}VV$ peaks were calculated after subtraction of a linear background because the use of a primary beam energy of 2500 eV in combination with the long region in the spectrum containing Auger features for these surfaces (470 - 950 eV) makes it very difficult to use a more sophisticated method. The validity of this method for quantitative use was checked by using the peak-to-peak heights from numerically differentiated spectra.

Because of day to day changes in the electron gun emission it was necessary to correct the peak areas for changes in the beam current. For the $M_{2,3}VV$ spectra this could done by using the height of the background at 79 eV as internal standard [45, 48, 49] but for the high energy peaks a more complicated method had to be used. Since the surfaces only contained copper, iron and oxygen the sum of the Cu $L_{2,3}VV$, Fe $L_{2,3}M_{2,3}V$ and O $KL_{2,3}L_{2,3}$ peak areas multiplied by their relative sensitivity factors (RSF's) was taken to represent the beam current. The RSF's have to be used because the three components have different cross sections and inelastic mean free paths (imfp). The RSF's ($f_{Fe,Cu}$ and $f_{O,Cu}$) were determined relative to the Cu $L_{2,3}VV$ peak. The RSF of Fe was determined from the Fe $L_{2,3}M_{2,3}V$ intensity of 16 ML of Fe on the Cu(100) surface. The Fe $L_{2,3}M_{2,3}V$ intensity of this surface is the same as Cu $L_{2,3}VV$ intensity from the clean Cu surface. The RSF of Fe $L_{2,3}M_{2,3}V$ relative to Cu $L_{2,3}VV$ ($f_{Fe,Cu}$) could now be taken to be unity. To check the reliability of this number the imfp of the I_{Fe} vs. θ_{Fe} plot (ASt-plot) is calculated assuming a perfect first monolayer (the influence of a slightly imperfect first monolayer on the calculation is expected to be negligible). The resulting imfp is 1.2 ± 0.2 nm, which is in good agreement with calculations of Tanuma et al. [50]. As the preparation of a pure oxygen surface is impossible, the signal of the known saturation value of oxygen on Cu(100) (0.52±0.05 ML [51]) and an imfp of 1.0 nm for the O $KL_{2,3}L_{2,3}$ electrons were used to calculate the RSF. This appeared to be $f_{O,Cu} = 1.4 \pm 0.2$. When also the O $KL_1L_{2,3}$ and the O KL_1L_1 peak areas are included $f_{O,Cu}$ becomes unity. Here should be noted that the magnitude of the RSF depends sensitively on the background procedure. Thus the values mentioned here are useful only for the data handling as performed in this thesis. An other important point here is that the corrected intensities (f_xI_x/Sf_iI_i) do not necessarily represent mole fractions because that interpretation requires a homogeneous distribution of the atoms in the surface layers. Though in some special cases the error in the so determined mole fraction is small [52], mole fractions are not useful in the work presented here.

2.3 Photoelectron spectroscopy.

Photoelectron spectroscopy uses the electrons emitted from an atom by means of photon-excitation. In this thesis only Mg K_α (1253.6 eV) X-rays (XPS) and He I and II (respectively 21.2 and 40.8 eV) ultra violet radiation (UPS) are used. With the use of X-ray excitation is easy to determine the different elements present in the surface. The depth sensitivity of both UPS and XPS as used in this thesis is similar to that of AES. The usefulness comes from the possibility to determine the chemical surrounding of the element because the core levels are sensitive to this. Due to the low energy of the UV radiation for He I and He II UPS is especially (if not only) suitable for the study of the valence band. Since the valence band of multiple element systems often consists of overlapping contributions of those elements more information can in some cases be obtained using different excitation energies. This is due to different excitation cross-sections that change differently with changing excitation energy. The energy of the structures in the valence band can sometimes be used to discriminate between oxidation states of the component.

2.3.1 Instrumentation and data acquisition.

The X-ray photoelectrons were excited by Mg K_α radiation produced by a fresh Mg/Al anode operated at 20 mA and 14 kV. Using a new anode and the relatively low current ensured the absence of the Al K_α induced Cu 2p ghosts which disturb -when present- the Fe 2p spectra. A hemispherical analyser was operated at a pass energy of 35.75 eV and steps of 0.1 eV were used to obtain the Fe 2p (736-699 eV), the Cu $2p_{3/2}$ (940-925 eV) and the O 1s (535-525 eV) spectra. A sample time of 500 ms/step was used and respectively 10, 2 and 10 scans were added to improve the signal to noise ratio. Shirley backgrounds (using 5 iterations) were used to obtain the Fe 2p and Cu $2p_{3/2}$ peaks; for the O 1s peak a second order polynomial was subtracted because the presence of Fe and Cu Auger peaks on both sides of the O 1s made the use of a Shirley background impossible.

The UPS spectra were collected using a He discharge lamp the same analyser as used for the XPS spectra. The analyser was operated at a pass energy of 4.25 V and steps of 0.025 and 0.10 V were used for respectively He I (21.2 eV) and He II (40.8 eV) photoemission spectra. Scans were sampled until a reasonable signal to noise ratio was obtained.

2.4 Ellipsometry.

Ellipsometry is a technique that uses photons to determine (the change in) optical properties of the surface. This means that changes in the electron distribution of the surface layer can be determined. These changes can be caused by chemical processes or by changes in the surface structure. Great advantages of ellipsometry over other techniques are first that the photons used (He-Ne laser, 632.8 nm, ca. 2 eV) do not influence reactions and can be used at all pressures, second that the sample depth is about two orders of magnitude larger than for AES meaning that also atoms migrated into the bulk can be detected to some extent and third that the complete instrument is situated outside the UHV.

The useful information is obtained from the change in the state of polarisation of the reflected beam. Analysis of this change results in two parameters Δ and Ψ. Values of Δ and Ψ can also be calculated for a surface when the composition and the refractive indices (or other physical properties that can be used to calculate the refractive indices) of the constituents are known [38,53]. For many bulk materials these data are readily available [54]. However, the optical properties of very thin films (up to a few ML) are different from bulk values and for the films studied in this thesis even bulk properties are unknown. This may seem rather distressing but fortunately an empirical calibration is possible.

For oxygen adsorption and the oxidation of several metal single crystal surfaces an absolute calibration has recently been done by means of nuclear reaction analysis (NRA) [51,55]. It appeared that on all metals that were examined the change in Δ was linear with the change in the amount of sorbed oxygen with an exception for 'chemisorbed' oxygen on Ni, Co and Fe. Thus reactions concerning oxygen can easily be followed using ellipsometry. Also adsorption of CO causes a change in Δ but in this case calibration (especially for linearity) is difficult. However, good results based on the assumption of linearity are reported in literature [6,29,58].

In oxidation experiments under mild conditions of metals such as Ni, Fe, Co and Cu, the change in Ψ is usually small with respect to that of Δ and not necessarily linear with the oxygen uptake. Therefore much more attention is paid to changes in Δ than to changes in Ψ.

Due to the set-up of the UHV system sample movement is required for performing the different techniques. This means that absolute Δ and Ψ values can be reproduced with an accuracy of only several tenths of degrees. However, when performing ellipsometry with a fixed sample position changes in Δ and Ψ can be determined with two orders of magnitude better accuracy. For this reason $\delta\Delta$ and $\delta\Psi$ are used. $\delta\Delta$ and $\delta\Psi$ represent Δ^0-Δ and Ψ^0-Ψ respectively where Δ^0 and Ψ^0 as used in this thesis are the Δ and Ψ values of the surface after evaporation of iron. *This means that the initial values of Δ and Ψ (Δ^0 and Ψ^0) are different for surfaces containing different amounts of iron.*

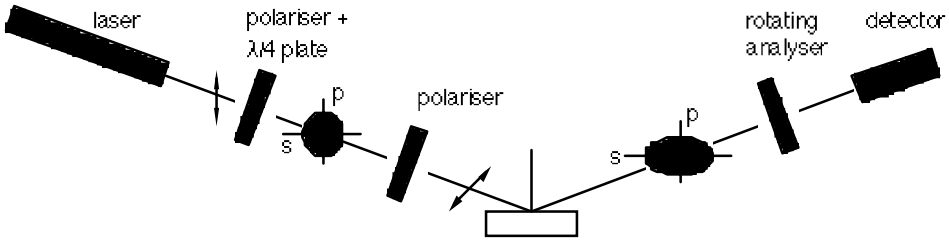

Figure 4 Experimental set-up of the ellipsometer.

2.4.1 Instrumentation and data acquisition.

Ellipsometry was performed in a configuration using a rotating analyser [38]. The set-up which is shown in Fig. 4 consists of a 10 mW He-Ne laser (λ=632.8 nm), a polariser and a quarter wave plate connected to each other (the axes making an angle of 45° in order to produce circular polarised light), a polariser to choose the desired angle of polarisation, the sample, a rotating analyser and finally a detector. Before and after the windows of the UHV system pin-holes were placed to stop unwanted reflections. The angle of incidence of the beam is 69.5°. The polariser/quarter wave plate assembly is used to enable a stepless change of the intensity. This is more convenient in respect to grey tone filters or pin-holes to reduce the intensity. The angle of the analyser is determined by means of an encoder plate connected to the polarisation filter which gives 1024 pulses per revolution on one channel and one 'master-pulse' per revolution on a second channel. An ADC converts the intensity as determined by the detector directly when a pulse is detected, starting each revolution at the master-pulse. The analyser rotates with about 5 Hz and usually the results of 8 revolutions are added before calculating Δ and Ψ. This procedure to determine a couple of Δ and Ψ values takes about 2.5 s. Since the time required to stabilise a desired reactant pressure is about 30 s the time needed to determine Δ and Ψ is not limiting for the experiments. In practice Δ and Ψ are determined every 5 s (and for slow changes even 10 or 30 s in order to reduce to amount of data).

Values that represent the intensity of the beam and the angle of the master-pulse with respect to the direction of the polarisation filter are required to determine Δ and Ψ. These values were determined before each experiment using light with an angle of polarisation of 90° with respect to the plane of incidence.

2.5 Experimental set-up.

2.5.1 The systems.

The UHV system used in Utrecht (chapters 3,4,7-9) was pumped by a turbomolecular pump (50 l/s), an ion-pump (200 l/s) and two titanium sublimation pumps. The base pressure was usually in the low 10^{-8} Pa range. To reach this pressure the system was baked by internal heating with lamps for two days. The system was equipped with an AES/LEED system, windows to perform ellipsometry, an electron beam evaporation source, an ion-gun, a Bayard-Alpert and a hot cathode pressure gauge and a rest-gas analyser. The pressure gauges could be read into the computer via the 4 ADC inputs of the LIA. To admit gases two gas inlet systems each containing the possibility to attach 4 lecture bottles were connected to the system by means of two leak-valves. Both systems could be pumped with the turbo pump separately from the main chamber. The crystal was mounted into a manipulator which could be moved in 3 orthogonal directions, rotated around the vertical axis (360°.) and tilted around a horizontal axis for 110°. The manipulator contained a heater with which the sample could be heated from 300 K to about 900 K. The temperature was determined by means of a chromel/alumel thermocouple pressed by force to the rear of the crystal. The crystal had to be moved to place it in the right positions to perform the different techniques. AES and LEED were performed with the crystal in the focus position of the LEED optics. For ellipsometry the position of the crystal was determined by the space required to let the beam pass through the windows and along the LEED optics without scattering.

The UHV system used in l'Aquila (chapters 5 and 6) was equipped with AES, LEED, XPS, UPS and an evaporation source which is in an other small chamber connected with the main system by means of a transport system. The complete system was pumped by an ion-pump (400 l/s).

2.5.2 The crystal.

The Cu(100) crystal was spark cut from a 5N copper rod within 0.5 deg of the [100] direction, mechanically polished and mounted in the manipulator. The cleaning procedure consisted of repeated Ar ion bombardment (600 V, 1-3μA/cm2) and annealing until no contamination could be detected with AES. In the end the crystal was annealed for 15 min. at 725 K. A sharp (1x1) LEED pattern could be observed after this procedure and cooled down to 300 K.

2.5.3 Gas handling.

The argon, oxygen, hydrogen and carbon monoxide used had purities of better than 5.0, 4.5, 4.5 and 4.5 respectively. During the experiments involving gas exposures the gas was admitted in the system while still pumping with the turbo pump (though with reduced pump speed) in order to establish a continuous refreshing of the gas inside the chamber.

2.5.4 Evaporation of iron.

The electron beam evaporation source was loaded with 4N iron and thoroughly degassed before use. A metal shield with three apertures was placed over the source to prevent the iron to cover the complete system. One is used for a mirror permitting to monitor the iron when evaporating, the second for a micro balance thickness monitor and the third was equipped with a shutter. The source was situated about 35 cm below the sample. The micro balance thickness monitor was calibrated for its position by means of a second monitor temporarily placed in the position of the sample. The calibration was performed for fluxes between 0.3 and 5 ML/min (at the position of the sample). The ratio between the fluxes determined by both monitors appeared to be independent of the flux for this range. When using the evaporation source all pumps were used. However, this could not prevent the pressure to rise to ca. 10^{-6} Pa. The oxygen contamination at the surface was usually lower than 5% of a ML and only few times could carbon be detected. Here must be mentioned that working with gases as CO and oxygen in the same chamber as where the evaporation source is used increases the amount of contamination in the iron (and the pressure during evaporation).

The amount of iron (and also of other components on the surface) is given in monolayers (ML), where one ML is equivalent to the number of atoms per unit area of the Cu(100) surface, i.e. $1.53 \cdot 10^{19}$ m^{-2}.

In l'Aquila the iron (purity better than 0.9999%) was evaporated from a electrically heated crucible. The flux was determined by means of a quartz micro balance thickness monitor placed at the same height as the sample. The iron was deposited at fluxes varying between 3 and 6 ML/min.

3

Oxidation of ultra thin iron layers on Cu(100) studied with AES and ellipsometry.

Abstract

The oxidation of Cu(100)-Fe surfaces containing 0-2.7 ML of Fe was studied at room temperature using Auger electron spectroscopy, ellipsometry and low energy electron diffraction. The initial oxidation rate was independent of θ_{Fe} which means that oxygen adsorption proceeds via a precursor mechanism. On all surfaces saturation of the oxidation occurred. For $\theta_{Fe}<2$ all iron was oxidised to $FeO_{1.43\pm0.07}$ (Fe_2O_3) and a surplus of $\theta_O=0.5$ was present, probably at the Cu-Fe_2O_3 interface. For iron coverages exceeding 2 ML the oxidation stopped after the uptake of 3.3±0.3 ML of oxygen. LEED experiments on a surface containing 0.8 ML of oxidised iron gave evidence for the formation of ordered domains of oxide in two (perpendicular) orientations. The distances of the spots indicate that a strong contraction of the oxide lattice takes place in order to match the Cu(100) lattice.

1 Introduction.

This chapter focuses on the reactivity of Cu(100) surfaces containing up to 2.7 ML Fe towards oxygen at room temperature and the composition and the structure of the surface after oxidation. The techniques used in this study are AES, ellipsometry and LEED.

The oxidation of Cu(111)-Fe and Cu(110)-Fe alloys was studied extensively by Van Pruissen et al. [30-34]. They prepared their alloys by decomposition of $Fe(CO)_5$ on clean Cu surfaces at elevated temperatures. The disadvantage of this procedure is the mixing of the Cu and Fe in the surface layers and a carbon and oxygen contamination at the surface. The exact amount of Fe deposited is unknown. On Cu(111) iron segregates upon oxidation and at high Fe contents γ-Fe_2O_3 is formed as determined from H_2 reduction experiments using ellipsometry. Also on Cu(110) iron oxide is formed at the surface. The stoichiometry on this surface was determined with LEED and AES and appeared to be $Fe_{0.95}O$ (wüstite).

The oxidation at room temperature of the Cu(100)-Fe system has been studied by Kishi and Nishioka [35] using XPS. The shifts of the Fe $2p_{3/2}$ peak after exposure of 750 L (0.1 Pa·s) O_2 to surfaces containing 0.3, 0.6 and 2.0 ML Fe were ascribed to FeO like species for the two lowest coverages and Fe_3O_4 like species for 2 ML of iron. So the type of oxide formed seems to depend on the amount of Fe present at the surface.

For Fe deposited on polycrystalline copper Di Nardo et al. [36,37] observed different Fe $2p_{3/2}$ peak positions for different Fe coverages after an oxygen exposure of 50 L (6.6 mPa·s). These exposures are too small to oxidise the Fe completely at room temperature, so it is hard to say from these experiments which kind of oxide is stable at room temperature.

3.2 Results.

3.2.1 Ellipsometry.

Cu(100) surfaces containing 0-2.7 ML Fe were exposed to oxygen. The O_2 pressure varied between $1 \cdot 10^{-6}$ and $1 \cdot 10^{-2}$ Pa and the crystal was kept at room temperature. In Fig. 1 $\delta\Delta$ and $\delta\Psi$ are plotted as function of the oxygen exposure for different Fe coverages (0-3 ML of Fe). For reasons of clearness not all oxidation curves are given, but the curves in Fig. 1 are representative for those of surfaces containing other amounts of iron. For all Fe coverages the reaction probability was first order in the oxygen pressure. The $\delta\Delta$ curves in Fig. 1a have an identical shape and the same initial slope. Though not visible on this scale, the $\delta\Delta$ curve of clean Cu(100) has a smaller initial slope. For all surfaces $\delta\Delta$ reaches its saturation value after 3-5 Pa·s (these values are also shown in Fig. 1a), whereas $\delta\Psi$ reaches its saturation value already after 0.2 Pa·s. The surface was taken to be saturated when the change in Δ could not be distinguished from drift, i.e. $|d\Delta/dt| < 0.05 \bullet\ hr^{-1}$. It is obvious that the value of $\delta\Delta$ at saturation increases with θ_{Fe}. The saturation value of $\delta\Psi$, however, decreases with θ_{Fe}. Therefore the saturation values $\delta\Delta_{sat}$ and $\delta\Psi_{sat}$ are plotted as function of θ_{Fe} in Fig. 2. The saturation values of 16 ML Fe on Cu(100) are also shown in Fig. 2. There is obviously no linear or other simple relationship between $\delta\Delta_{sat}$ and θ_{Fe}. The lines plotted in Fig. 2 represent the $\delta\Delta_{sat}$ and $\delta\Psi_{sat}$ values calculated according to a model that will be discussed together with the three indicated regions in section 3.4.2.2.

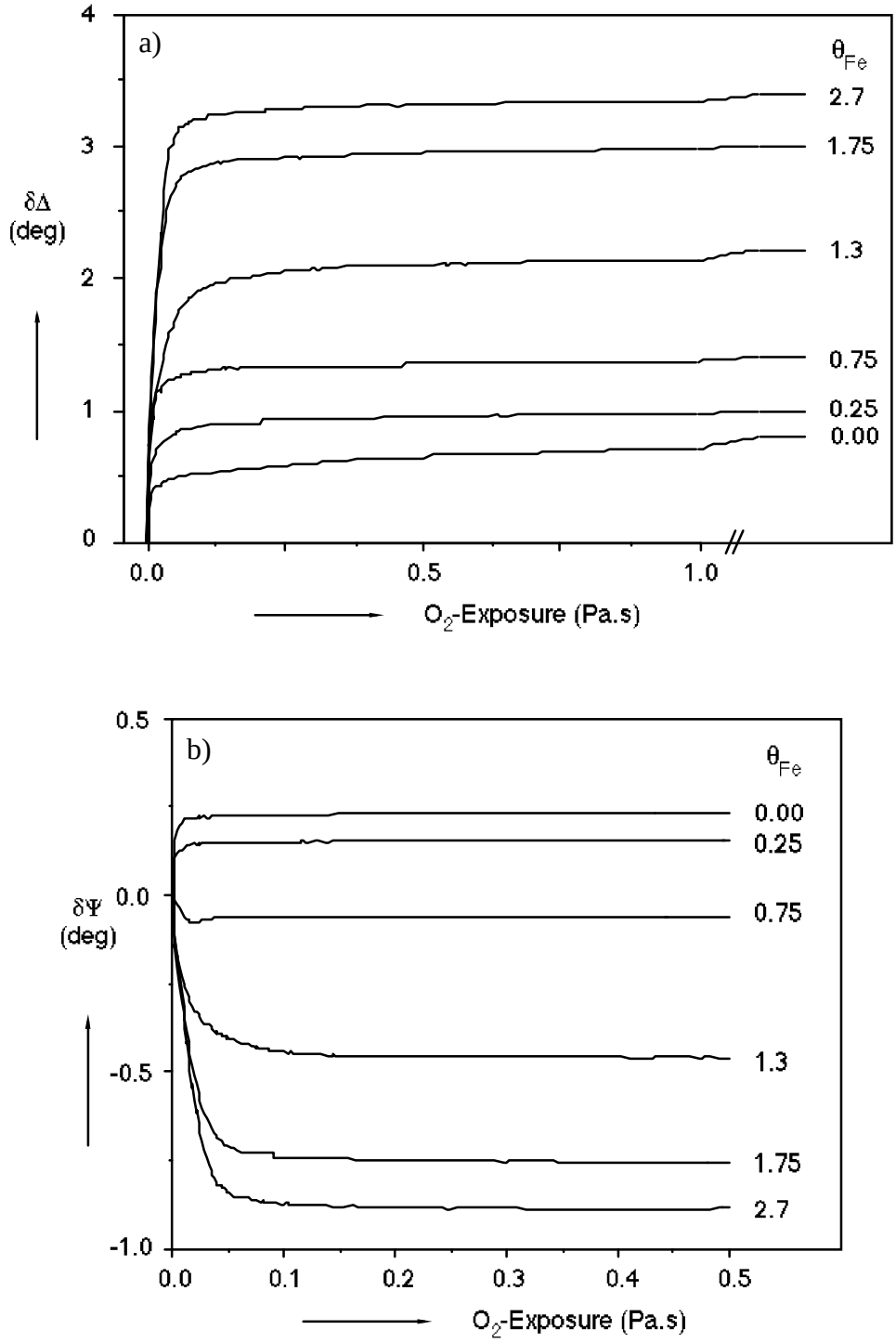

Figure 1 *The change in Δ (a) and Ψ (b) as function of the oxygen exposure for different coverages of iron on Cu(100) at 300K. The saturation values of δΔ of these surfaces are also given.*

3.2.2 AES.

The intensity of the O $KL_{2,3}L_{2,3}$ Auger peak at saturation ($f_{O,Cu} \cdot I_{O,sat}$) is plotted in Fig. 3 as function of the iron coverage. The saturation value of a surface containing 16 ML of Fe is given too. The drawn line is the best fit for $\theta_{Fe}<0.5$. The oxygen intensity does not vary linearly with θ_{Fe} at higher coverages. At $\theta_{Fe}>2$ ML the amount of oxygen is almost saturated.

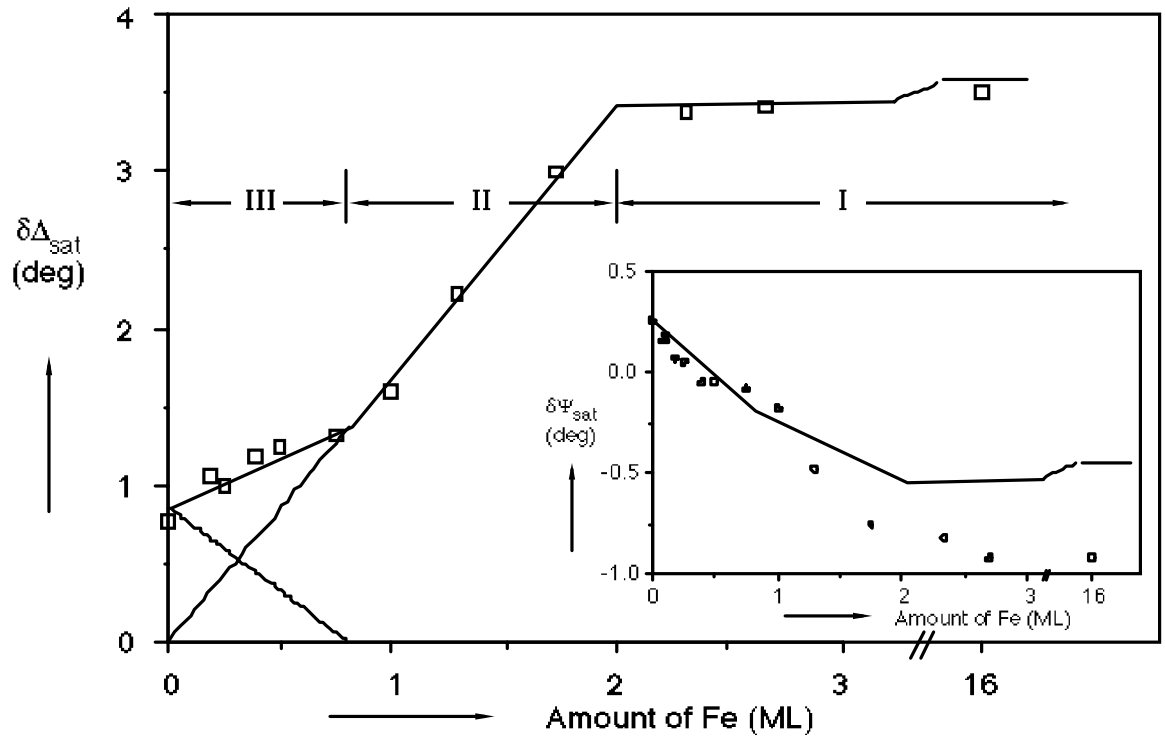

Figure 2 *The saturation value of $\delta\Delta$ as function of θ_{Fe} for oxidation of Cu(100)-Fe surfaces at room temperature. The meaning of the lines and regions is explained in the discussion. In the inset the saturation value of $\delta\Psi$ as function of θ_{Fe} is shown.*

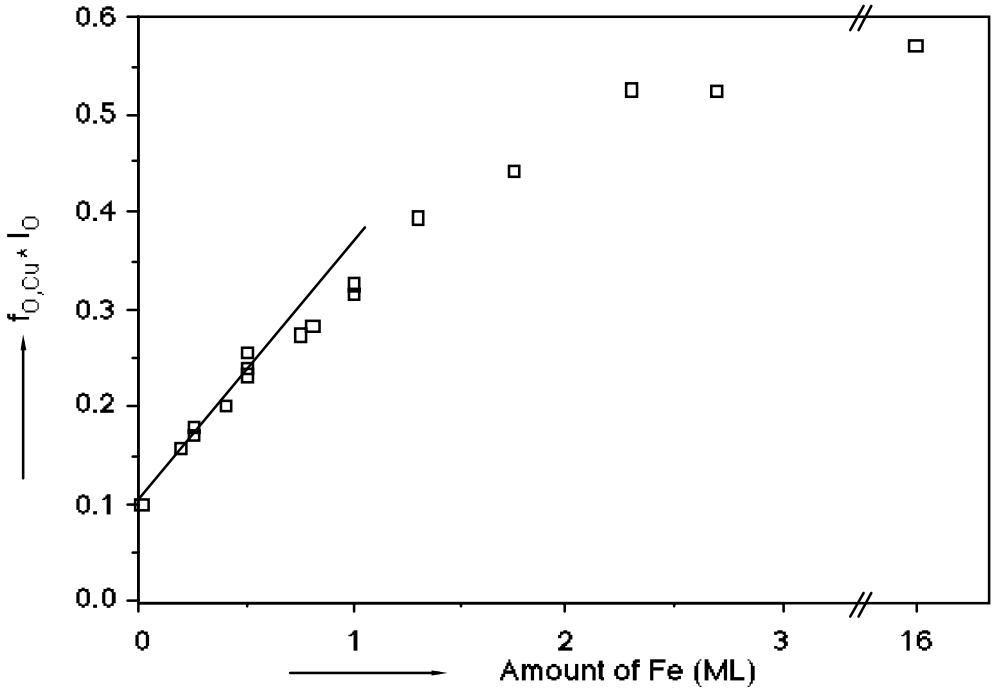

Figure 3 *The intensity of the O $KL_{2,3}L_{2,3}$ peak corrected for the relative sensitivity factor at saturation as function of θ_{Fe}. The line represents a linear fit through the data up to 0.5 ML.*

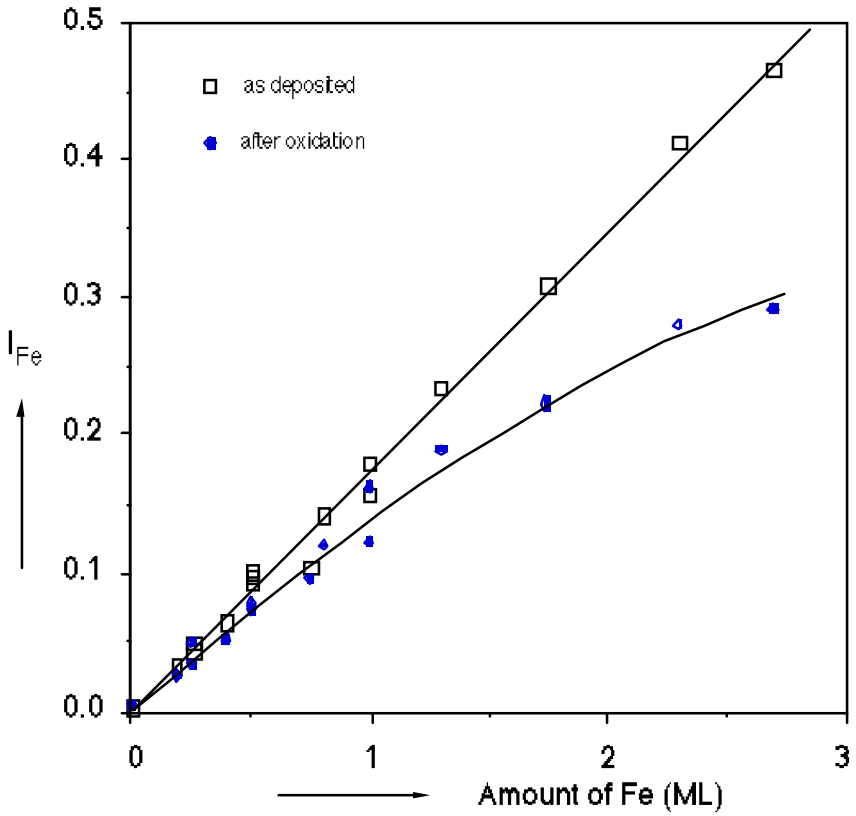

Figure 4 *The intensity of the Fe $L_{2,3}M_{2,3}V$ peak before and after oxidation as function of θ_{Fe}. The line through the points before oxidation is a linear fit, the line through the points after oxidation is to guide the eye.*

The deviation from linearity is also found for the Fe Auger intensity after oxidation. Fig. 4 shows I_{Fe} versus θ_{Fe} before and after oxidation. The line through the points taken before oxidation is a linear fit, the line through the points after oxidation is just to guide the eye. The decrease in signal after oxidation can be ascribed to screening of the Auger electrons due to the spreading of Fe atoms over more layers.

The Fe $M_{2,3}VV$ peaks from oxygen saturated surfaces containing different amounts of Fe were collected and compared in Fig. 5. Both the background and the Cu $M_{2,3}VV$ peak are removed from these spectra. To be able to compare the peak shape with the more frequently used derivative spectra the numerically differentiated spectrum of 2.3 ML Fe (oxidised until saturation) is shown in the inset.

3.2.3 LEED.

Fig. 6 shows the LEED pattern of a surface containing 0.8 ML Fe after oxidation at room temperature. Surfaces containing less Fe exhibited the same pattern but more diffuse. Also annealing at 600 K made the patterns more diffuse. The LEED-spots are arranged in two hexagons. The spots of one hexagon appear to be slightly elliptical with the axes parallel. The hexagons are rotated by 90° with respect to each other.

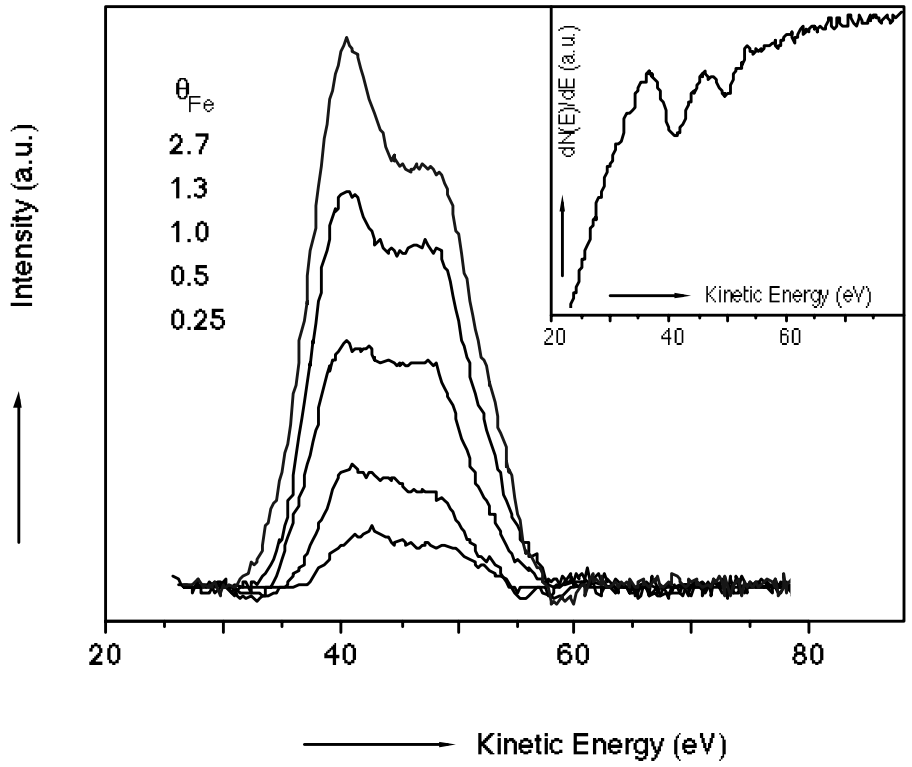

Figure 5 *The Fe $M_{2,3}VV$ peak of completely oxidised surfaces containing different amounts of iron. The inset shows the derivative of a Fe $M_{2,3}VV$ peak of a oxidised surface containing 2.3 ML of iron.*

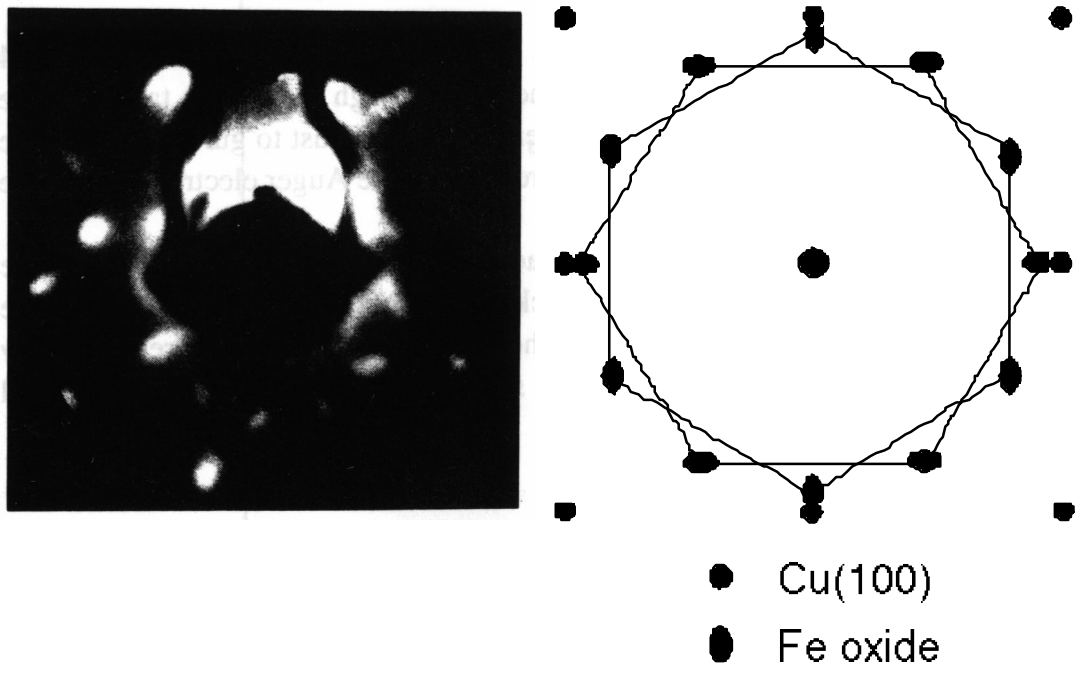

Figure 6 *The LEED pattern of a Cu(100) surface containing 0.8 ML of iron after oxidation until saturation. The beam energy was 119 eV.*

3.3 Discussion.

3.3.1 Oxidation mechanism.

In the curves of $\delta\Delta$ vs. the O_2-exposure of Fig. 1a no sharp changes in slope are visible. Also enlargement of the first 1 mPa·s of oxygen exposure does not reveal any changes. Such breakpoints were found by Van Pruissen et al. [30] for the oxidation of Cu(111)-Fe. They ascribed these breakpoints to a change from the oxidation of Fe to the oxygen adsorption on Cu. The value of $\delta\Delta$ at the breakpoint showed a linear relationship with the iron content of the surface. Breakpoints may be expected when free Cu surface sites are available after oxidation of all iron. Assuming an equal growth in three directions of the oxide coverages of more than 0.6 ML Fe can cover the surface completely. The calculation of this number is based on bulk atomic densities of fcc Fe and Fe_2O_3. The lack of these breakpoints in the oxidation curves with $\theta_{Fe}<0.6$ (though not shown in Fig. 1a, several curves for surfaces containing 0.19, 0.25, 0.40 and 0.50 ML of Fe were collected) may have two reasons. First of all Cu(111) has a smaller reactivity towards O_2 than Cu(100), implying a larger change in reaction rate going from oxidation of iron to adsorption of O_2 on Cu(111). The difference in sticking coefficient between clean Cu(100) and clean Cu(111) is about a factor 10 at $\theta_O=0$ [57,58]. So, if the sticking coefficients are about equal for oxygen on copper and iron sites, no changes would be visible. Second, the breakpoints may not be visible because $\delta\Delta$ has a different (i.e. smaller) sensitivity for oxygen adsorbed on Fe than on for oxygen on Cu.

So from Fig. 1a it is impossible to say much about the oxidation kinetics, apart from the slope at $\delta\Delta=0°$, which is independent of θ_{Fe} (for $\theta_{Fe}>0$). The initial slope of the oxidation curve of Cu(100) is much smaller. For this surface an initial sticking probability of 0.01 can be calculated. This agrees well with the results of Habraken et al. [57]. The slope of the other curves is about twice the value measured on Fe(100) [59]. As the sensitivity of $\delta\Delta$ for oxygen on Fe(100) is smaller for small amounts of oxygen than for larger amounts (a discussion on this will follow in the next section), it is hard to determine the absolute sticking probability of O_2 for the Cu(100)-Fe surfaces. Though, as the initial sticking probability is independent of θ_{Fe}, the oxygen adsorption should follow a precursor mechanism, as it does on Cu(100) [58].

3.3.2 Structure and stoichiometry.

3.3.2.1. AES.

From Fig. 3 it seems that the amount of oxygen adsorbed is not linearly dependent of the iron coverage. The deviation from linearity at $\theta_{Fe}>0.5$ may have two explanations: First there could be a change in the (mean) stoichiometry of the oxide. Second, the oxide may screen part of the O $KL_{2,3}L_{2,3}$ electrons due to the small inelastic mean free path (imfp) of the O $KL_{2,3}L_{2,3}$ Auger electrons relative to the thickness of the oxide layer.

A change in the stoichiometry is difficult to determine from the experiments as performed here. Although Seo et al. [60] claim that different iron oxides have different $M_{2,3}VV$ peak shapes this might not be the case as will be shown in chapter 4. Nevertheless Fig. 5 shows clearly that all peaks have the same features (two overlapping peaks) and the only difference is the relative contribution of both. No contribution of the metallic $M_{2,3}VV$ which lies in the

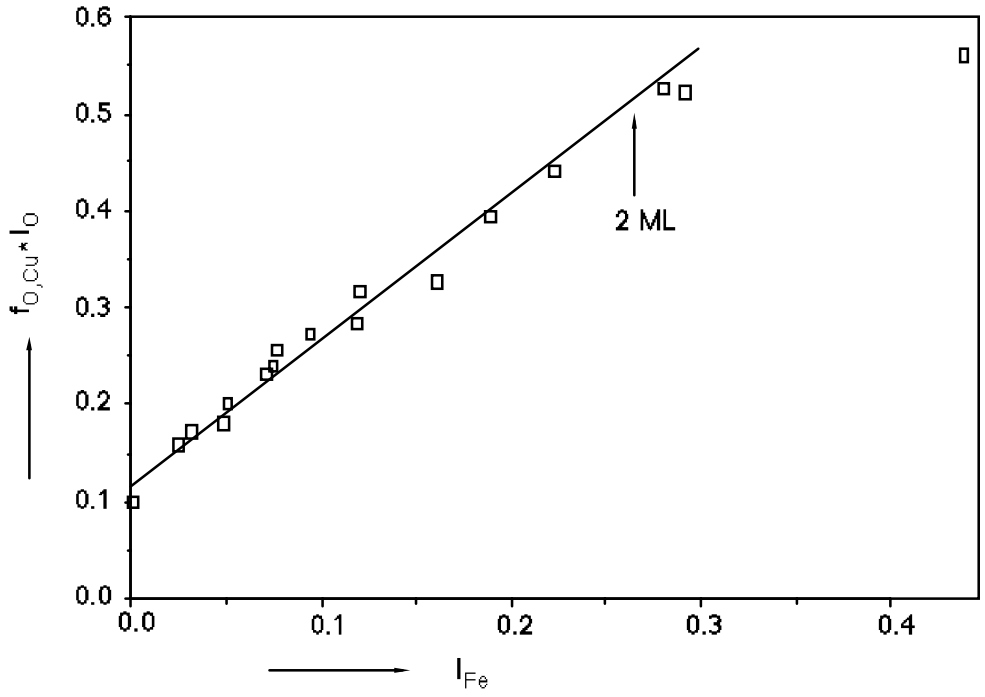

Figure 7 *The O $KL_{2,3}L_{2,3}$ intensity as function of the Fe $L_{2,3}M_{2,3}V$ intensity for surfaces oxidised to saturation. The line represents a linear fit through the points up to 1.75 ML of Fe. The arrow indicates the iron intensity calculated for 2.0 ML Fe.*

middle of the two oxidic peaks could be found. So metallic iron is certainly not present in the top layers.

The screening of part of the O $KL_{2,3}L_{2,3}$ electrons by the oxide layer was mentioned as a second reason for a deviation in linearity in Fig. 3. Fig. 4 shows clearly that the screening effect can not be neglected for Fe $L_{2,3}M_{2,3}V$ electrons in the oxide, at least not for iron coverages exceeding one half of a monolayer. Because the Fe $L_{2,3}M_{2,3}V$ electrons have a slightly larger imfp than the O $KL_{2,3}L_{2,3}$ electrons, I_O should be effected more by the screening. So it seems better to investigate the oxygen intensity as function of the iron intensity using for both signals the intensities corrected for the relative sensitivity factors. Therefore $f_{O,Cu} \cdot I_O$ is plotted against I_{Fe} (determined after oxidation; $f_{Fe,Cu} = 1$) in Fig. 7. The slope of the calculated line, which is also shown, is 1.43±0.07 (the error is based on the linear regression calculation) and the intercept is 0.12±0.02 which corresponds to a value of θ_O=0.5. The same oxygen/iron ratio can be calculated from the line drawn in Fig. 3. So the stoichiometry calculated from the oxygen intensities indicates the formation of Fe_2O_3. This is not consistent with the results of Kishi and Nishioka [35]. They determined FeO or Fe_3O_4 to be present depending on the amount of Fe at the surface. Their conclusions are based on the shape of the Fe $2p_{3/2}$ peak as measured with XPS. However, their surfaces were far from saturated with oxygen. In chapter 5 it will be shown that surfaces saturated with oxygen exhibit only the shape and position of a Fe 2p peak corresponding to Fe_2O_3. As the conclusions here are based on the amount of oxygen present at the surface at saturation relative to the amount of iron, the interpretation that only Fe_2O_3 is formed is preferred.

A deviation from linearity is also visible in Fig. 7. For $\theta_{Fe} \geq 2.3$ the oxygen intensity is almost constant, whereas the Fe intensity still increases.The constant oxygen intensity can be

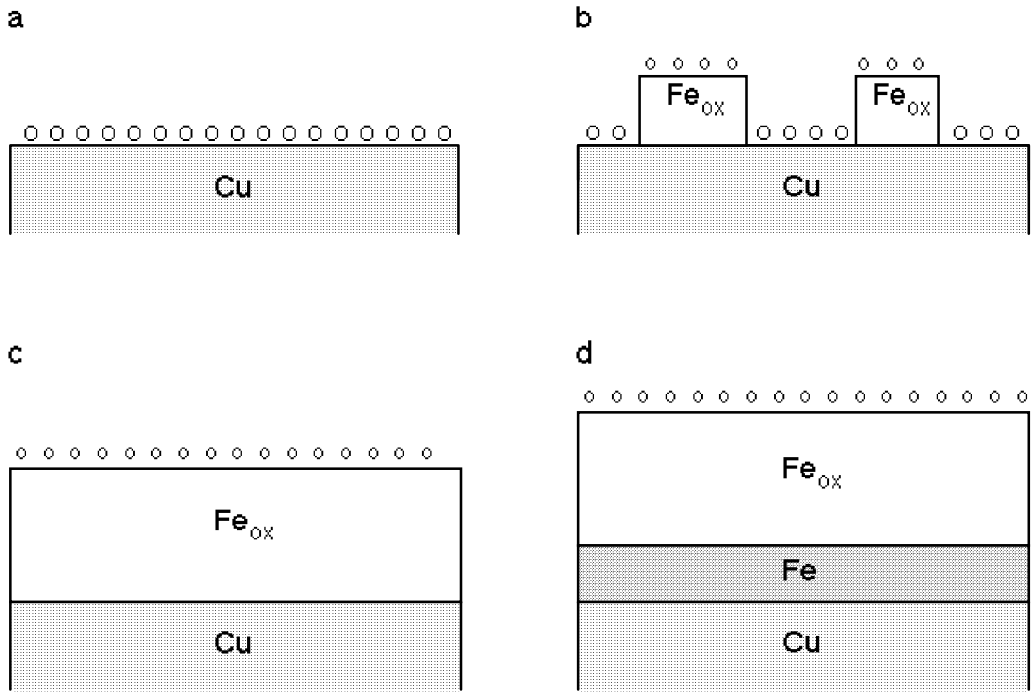

Figure 8 *A schematic model for the oxidised surfaces containing different amounts of Fe. a) $\theta_{Fe} = 0$, b) $0 \geq \theta_{Fe} \geq 0.8$, c) $0.8 \geq \theta_{Fe} \geq 2$ and d) $\theta_{Fe} > 2$.*

explained by a saturation of the oxygen adsorption comparable to that of room temperature oxidation of Fe(100) [55,59]. Based on the amount of oxygen 2 monolayers of iron can be oxidised at this saturation value. To highlight the value of θ_{Fe}=2 the place of I_{Fe} related to θ_{Fe}=2 in Fig. 7 is indicated by an arrow. The oxygen intensity calculated for θ_{Fe}=2 using the fit is not significantly different from the experimental values of surfaces containing 2.3, 2.7 and 16 ML of iron (the experimental points on the right side of the arrow in Fig. 7). So the oxidation of iron seems to stop when 2 ML of iron are oxidised.

An other important conclusion that can be drawn from Fig. 7 is that (at least up to 2 ML of Fe) there is a 'surplus' of oxygen of half a monolayer, the intercept of Fig. 7. For $\theta_{Fe} \geq 2$ this surplus is probably present at the Cu(100)-Fe_2O_3 interface as it is for θ_{Fe}=0, where it can be stabilised by the Cu atoms. In principle it could also be at the Fe_2O_3-vacuum interface or divided over both interfaces. But it is impossible to discriminate between these possibilities using AES. At higher iron coverages the surplus can also be interpreted as a change in stoichiometry (to the lower oxidation states) below the surface. However, this must be a small region very near to the Fe_2O_3-Fe interface because when the same amount of oxygen is spread over more (deeper) layers I_O should decrease.

So based on the AES results I come to a schematic model of the structure of the surface as given in Fig. 8. At zero coverage the saturated surface contains half a monolayer of oxygen on copper, Fig. 8a. For θ_{Fe}<2 all Fe is oxidised to Fe_2O_3 and a surplus of 0.5 ML of oxygen is present. This 'excess' oxygen is partly present at the iron free Cu(100) surface and partly connected to the iron oxide (for iron coverages too small to cover all of the Cu surface), Fig. 8b, or totally in contact with the iron oxide when the oxide layer covers the copper completely, Fig. 8c. At even higher Fe coverages (θ_{Fe}>2) a layer of metallic Fe is present between the Fe_2O_3 and the Cu surface, Fig. 8d. In this situation the thickness of the metallic Fe layer depends on θ_{Fe}, whereas the thickness of the oxide layer is independent of θ_{Fe}.

3.3.2.2. Ellipsometry.

In this section the ellipsometry results and their consistency with the model as proposed above will be discussed. In the behaviour of $\delta\Delta_{sat}$ as function of θ_{Fe} (Fig.2) three regions can be distinguished. These regions are numbered I, II and III from high to low θ_{Fe} (Fig. 2). For θ_{Fe}>2 ML (region I) $\delta\Delta_{sat}$ is about 3.5° which is the same value as that for fully oxidised Fe(100). From θ_{Fe}•0.8 to θ_{Fe}=2 (region II) $\delta\Delta_{sat}$ is proportional to θ_{Fe} and for $\theta_{Fe}\leq$0.8 (region III) $\delta\Delta_{sat}$ changes linearly with θ_{Fe} with an intercept at the saturation value of an iron free Cu(100) surface.

The saturation of the surface at $\delta\Delta$=3.5° for θ_{Fe}>2 ML (region I) can easily be explained realising that also for oxidation at room temperature of Fe(100) the surface saturates at this value [55,59]. At this oxygen coverage and for this temperature the oxidation stops because migration processes in the oxide layer become very slow [61]. The absolute amount of oxygen present on Fe(100) at $\delta\Delta$=3.5° is $5.1\pm0.4\cdot10^{19}$ m^{-2} [55] which equals θ_O=3.3±0.3 relative to the atomic density of Cu(100). This agrees well with the results of the AES experiments: oxidising 2 ML of Fe to Fe_2O_3 requires 3 ML of oxygen and adding the half monolayer excess oxygen 3.5 ML is required for saturation. So in this region the surface can be described by a layer of metallic Fe on the Cu(100) crystal surface with an iron oxide layer on top (Fig. 8d).

The proportional decrease of $\delta\Delta_{sat}$ with θ_{Fe} going from θ_{Fe}=2 to $\theta_{Fe}\approx$0.8 (region II) can be explained by a decrease of the amount of oxygen with θ_{Fe}. The least-squares fit through the four points is given by eq. (1).

$$\delta\Delta = -0.04\pm0.08 + (1.72\pm0.10)\cdot\theta_{Fe} \qquad (1)$$

When the sensitivity of $\delta\Delta$ for oxygen on Fe(100) as determined by means of nuclear reaction analysis (NRA) by Leibbrandt et al. [55] of 1.1 deg/ML (taken from Fig. 3 of the reference and recalculated to the atomic density of Cu(100)) is used, a stoichiometry can be calculated of $FeO_{1.56\pm0.09}$, which means Fe_2O_3. This constitutes an independent determination of the stoichiometry which agrees well with the AES results. Although this conclusion seems reasonable (and is in fact what I believe) a literal interpretation of an extrapolation to θ_{Fe}=0 following Eq. (1) is tantamount to a decrease of the thickness of the iron oxide in Fig. 8c to zero. This means that when all of a certain amount of Fe_2O_3 is removed $\delta\Delta$ becomes zero whereas at that point half a monolayer of oxygen is still present (the 'excess' oxygen found with AES). Apparently this half monolayer is not 'visible' to $\delta\Delta$. This means, however, that for oxygen on iron the change in Δ is not proportional to the actual coverage ($\delta\Delta = k\theta_O$). In fact, although Δ starts to change immediately upon oxygen exposure to Cu(100)-Fe or Fe(100), the resulting calibration curve is non-linear [59]. Initially the sensitivity for oxygen on Cu(100)-Fe is found to be 0.55±0.06 deg/ML, which is half the value for oxygen on Fe(100). Only at higher exposures (above about $\delta\Delta$=0.5°) a calibration curve of the type $\delta\Delta = a + k\theta_O$ is found [59]. This implies that for oxygen coverages above 1.0 ML ellipsometry does not 'see' all the oxygen present, but 'misses' exactly 0.5 ML. Since the oxygen in excess of 0.5 ML will be part of the iron oxide it seems reasonable to suppose that 'oxidic' oxygen is visible for the ellipsometer. Below this coverage some oxygen will be present on the surface and some will be present as 'oxidic' oxygen. The former will be invisible for the ellipsometer, the latter gives the its usual contribution. A

similar situation occurs for the chemisorption of oxygen on nickel as studied by ellipsometry [62]. So in the extrapolation procedure in region II of Fig. 2 an intercept is expected that corresponds to 0.5 ML of invisible oxygen, i.e. zero. This oxygen is most probably situated at the Fe_2O_3-vacuum interface. In Fig. 8b-d this oxygen is represented by small symbols.

Thus in region II the thickness of the oxide layer varies with θ_{Fe}, and an excess of oxygen is present situated on top of the oxide (Fig. 8c).

In the discussion above one major assumption has been made implicitly: the possible effect of the (changing) iron layer on $\delta\Delta$ and $\delta\Psi$ is ignored. Of course this is not realistic and the negative $\delta\Psi$ values in Figs. 1 and 2 seem to be in conflict with the oxidation of the pure metals. Both on copper and on iron $\delta\Psi$ is positive upon oxidation at 300 K (though very small in the case of iron). It should be realised, however, that in this case oxidation of a Cu-Fe surface influences the state of the surface (as seen with ellipsometry) in several ways. Starting with a given amount of iron both Δ and Ψ will change upon oxidation from their initial values due to the formation of iron oxide and due to the decreased amount of iron present between the copper and iron oxide layers. The $\delta\Delta$ and $\delta\Psi$ values would thus represent for instance the difference between a copper surface with 6 monolayers of iron and a copper surface with 4 monolayers of iron and two monolayers of iron oxidised to Fe_2O_3. The only way to account for this effect is to calculate Δ and Ψ for all surfaces and extract the observed values of $\delta\Delta$ and $\delta\Psi$ by a proper subtraction.

The calculations were based on the following assumptions: 1) the presence of the components in perfect flat layers, 2) bulk refractive indices of copper and iron can be used ($\tilde{n}_{Cu}$=0.13+ 3.55i and $\tilde{n}_{Fe}$=3.5+3.7i), 3) one monolayer of iron has the same thickness as the interlayer spacing of the Cu(100) planes (1.8 Å), 4) 1 ML of Fe results in a layer of iron oxide of 3.8 Å (bulk Fe_2O_3 density) and 5) the refractive index of the iron oxide is $\tilde{n}$=5.0+0i. The index of the oxide was adjusted as to match the calculated $\delta\Delta_{sat}$ values to the experimental values. First Δ^0 and Ψ^0 were calculated for surfaces containing different amounts of iron and next the Δ and Ψ values of the final oxidised situation as described by the model. Subtraction of the proper begin and end values results in the solid lines drawn in Fig.2. It is obvious that the calculated $\delta\Delta_{sat}$ values agree well with the experimental data whereas $(\delta\Psi_{sat})_{calc}$ shows a disagreement with the experiment. The latter is not so strange when is realised that the layers are not perfectly flat and that the refractive index of bulk (bcc) iron is used whereas thin (fcc) layers are present of which the index may be different from the bulk values. Both arguments have stronger effects on Ψ than on Δ (the negative sign of $\delta\Psi_{sat}$ is completely due to the decrease of the iron layer in favour of the oxide layer during oxidation).

When the thickness of the oxide layer becomes small, formation of clusters with free Cu surface in between can be expected. This probably happens for θ_{Fe}<0.8 (region III in Fig. 2). For the line drawn through the points of region III in Fig. 2 some extra assumptions have been used in the calculation: 1) the Cu surface covered by Fe_2O_3 is proportional to θ_{Fe} until complete coverage of the copper is reached, 2) oxygen adsorbed on iron oxide free parts of Cu(100) has its normal effect on $\delta\Delta$ and $\delta\Psi$ as does the oxygen in the iron oxide (the amount of invisible oxygen is then proportional to the Fe_2O_3 coverage with a maximum of θ_O=0.5 at total coverage) and 3) the expected changes in $\delta\Delta$ for both parts of the surface may be added. The change in the equations used to calculate Δ and Ψ for this particular problem is shown in

the appendix. In Fig. 2 the iron oxide part of $\delta\Delta_{sat}$ is represented by a dashed line and the Cu(100)-O part by a dotted line. Both lines add up to the calculated solid line through the experimental points. So this model can describe $\delta\Delta_{sat}$ for $\theta_{Fe}<0.8$ satisfactorily.

3.3.3 LEED.

The LEED pattern of 0.8 ML Fe oxidised to saturation resembles strongly the pattern observed by Simmons and Dwyer [63] for small amounts of oxygen on Fe(100). They explained the two hexagons by regions of oxide with two orientations. They proposed a stoichiometry of FeO but also Fe_3O_4 and γ-Fe_2O_3 have hexagonal symmetry in the close packed oxygen planes which can lead to the LEED pattern. The O-O distances of in the close packed planes of these oxides are 0.306, 0.297 and 0.295 nm respectively. The lattice parameter calculated from Fig. 6 is 0.27±0.02 nm, which results in a contraction of (10±8)% compared to the γ-Fe_2O_3 bulk lattice parameter. This means that the oxide lattice adjusts itself to the Cu(100) lattice distances though not completely. On Fe(100) the same happens. In that case a contraction of the lattice parameter of 4.5% is required and observed [63]. Furthermore from the diffuse spots it can be concluded that the surface is not highly ordered or the clusters are relatively small (but >50 Å). Both may be due to strains caused by the lattice mismatch.

Although the Cu(100) surface was expected to be covered completely by the iron oxide for this amount of Fe it is possible to see the Cu(100) spots in the LEED pattern in Fig. 6. Thus the coverage is not yet complete.

3.4 Conclusions.

1. The initial reaction rate for O_2 adsorption is independent of θ_{Fe} ($\theta_{Fe}\geq0.19$), which means that the reaction proceeds via a precursor mechanism.
2. For $\theta_{Fe}\leq2$ complete oxidation to Fe_2O_3 occurs and an extra amount of θ_O is probably present at the Fe_2O_3-Cu(100) interface.
3. For $\theta_{Fe}>2$ the oxidation stops when the equivalent of 2 ML of Fe is oxidised to Fe_2O_3, while the extra θ_O remains present.
4. The maximum amount of oxygen on these surfaces ($\theta_{Fe}>2$) is the same as on Fe(100) for room temperature oxidation.
5. For $\theta_{Fe}\leq0.8$ ML the oxide lattice is contracted in order to fit better to the Cu(100) lattice and clusters in two orientations rotated by 90• in respect to each other are present.

Appendix.

In this appendix it is shown that it is allowed to add the ellipsometric response (at least the parameter $\delta\Delta$) of a substrate with two adjacent overlayers A and B with complex refractive indices $\tilde{n}_A$ and $\tilde{n}_B$ depicted in Fig. 9. A simple geometric model is used because the (more sophisticated) effective medium approach is not suitable for oxides and the overlayer is assumed to consist of islands of different compounds. For each overlayer the usual ellipsometric equations hold for the amplitude reflection coefficient

$$R = \frac{r_{01} + r_{12}e^{-ix}}{1 + r_{01}r_{12}e^{-ix}} \qquad (A.1)$$

where

$$x = \frac{4\pi}{\lambda_0 \tilde{n}_0} d \left(\tilde{n}_1^2 - \tilde{n}_0^2 \sin^2\varphi_0\right)^{1/2} \qquad (A.2)$$

and r_{01} and r_{12} represent the amplitude reflection coefficients for the interface 0-1 and 1-2 respectively. The values of Δ and Ψ are then found from the relation

$$\tan\Psi e^{i\Delta} = \frac{R_p}{R_s} \qquad (A.3)$$

where the subscripts on R denote the amplitude reflection coefficients for light parallel (p) or perpendicular (s) to the plane of incidence. For the system shown in Fig. 9 each reflection coefficient R_s or R_p may be expressed as

$$R = f_A R_A + (1 - f_A) R_B \exp\left\{-i\frac{4\pi}{\lambda_0}(d_A - d_B)\cos\varphi_0\right\} \qquad (A.4)$$

where R_A is the reflection coefficient appropriate for a uniform layer of thickness d_A with complex refractive index $\tilde{n}_A$ and R_B has an analogous meaning. The fraction of the surface covered by layer is f_A and the exponential term accounts for the phase difference of the incoming light beam when it reaches the surface of A and B. Eq. (A.4) is essentially the statement that, in order to obtain the amplitude reflection coefficient of a surface, one must add the amplitudes of all reflected rays, taking proper account of their phase difference. This expression neglects those regions of the surface near to the contact between A and B where, strictly speaking, one should consider light rays entering layer A but leaving the surface through layer B. If the sizes of the different patches of A and B are large this contribution is expected to be negligible. The distance y between two emerging rays in Fig. 9 is $2d_A\tan\varphi_A$, which for $\varphi_0 = 70°$, $\mathrm{Re}(\tilde{n}_A)=1$ and d = 5 Å corresponds to 27 Å. Thus, if only two reflected rays contribute to the reflection coefficient the patch size of both A and B should be larger than 27 Å in order for this approximation to be valid. Using $\mathrm{Re}(\tilde{n}_A)=3.5$ which can be calculated for iron oxide on iron, the minimum island size decreases to 5.6 Å. As a LEED pattern is visible for $\theta_{Fe}<0.8$ this condition is probably met.

Now an exact calculation is possible using Eqs. (A.4), (A.1) and (A.3). The parameters used (d_A = 3Å, $\tilde{n}_A$ = 3.5 + 1.7i, d_B = 3.8Å, $\tilde{n}_B$ = 5.0 + 0i and $\varphi_0 = 70°$) were chosen so as to

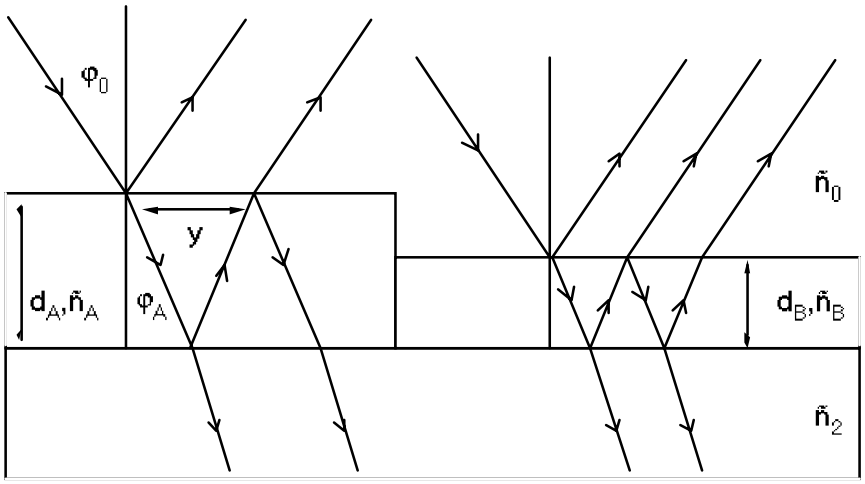

Figure 9 A schematic representation of the surface and the light rays during an ellipsometric experiment.

reflect the experimental $\delta\Delta_{sat}$ values in Fig. 2, but have no further significance. As can be seen in region III of Fig. 2 the calculation yields a linear relationship for both $\delta\Delta_{sat}$ and $\delta\Psi_{sat}$.

As the growth of iron oxide does probably not result in such well organised surfaces it is shown here that this is not very important for Δ and Ψ of thin layers on a substrate. In that case R can be expanded in Eq. (A.1) upto first order terms in x. This yields

$$R = r_{02}(1-i\beta x) \qquad (A.5)$$

where β is a function of r_{01}, r_{02} and r_{12}. Assuming just one kind of oxide present on the surface in clusters R can be given by

$$R = r_{02}\left\{1 - (1- f_A)\frac{4\pi i}{\lambda_0}d_A\cos\varphi_0 - f_A i\beta x_A\right\} \qquad (A.6)$$

The ratio R_p/R_s is then to first order in d_A

$$\tan\Psi e^{i\Delta} = \frac{r_{02\,p}}{r_{02\,s}}(1-f_A i\beta_p x_A + f_A i\beta_s x_A) \qquad (A.7)$$

and only dependent on $f_A d_A$ which means proportional to the volume of A present on the surface. So Δ and Ψ are not expected to be different for, say, two monolayers of iron on copper covering half of the crystal and one monolayer covering the total surface area. Calculations using the 'exact' Eq. (A.4) confirm this statement.

4

Oxidation of one monolayer of iron on Cu(100) studied with AES peak shape analysis.

Abstract

The peak shape of the iron $M_{2,3}VV$ Auger peak during the oxidation of one monolayer of iron on Cu(100) was studied. Peak shape analysis indicated that all iron is oxidised to Fe_2O_3 before oxygen adsorbs on the Cu(100) surface. Based on the results presented in this chapter the oxidation of iron probably proceeds at once from Fe^0 to Fe^{3+} though initially adsorbing oxygen causes a different ratio between the cross-transition and the auto-ionisation peak than later adsorbing oxygen.

4.1 Introduction.

Peak shape changes of Auger transitions due to changes in the chemical composition can be found for several elements. In most cases valence band electrons are involved in the transitions e.g. the KLL transition of carbon in graphite or carbides and the $M_{2,3}VV$ transition of the metals in titanium and vanadium nitrides and iron oxides. As the peak shape of these transitions is characteristic for a certain chemical state of the elements the shape can be used to identify the state and possibly the composition. For the examples given above this appears to be possible. Graphitic and carbidic carbon exhibit different C KLL peak shapes [40]. Dawson and Tzatzov showed the existence of a relationship between the shape of the Ti and V $M_{2,3}VV$ peaks and the amount of nitrogen present in the octahedral holes [64,65]. And for iron oxides the Fe $M_{2,3}VV$ peak shape is often used to determine which iron oxide is present at the surface [30-33,60,63,66-73].

Most peak shape analyses reported in literature are based on derivative (dN/dE or E·dN/dE) or even second derivative ($d^2N/(dE)^2$ or $E \cdot d^2N/(dE)^2$) spectra. Just a few authors use the integral (N vs. E) spectra [64,65]. Quantitative use of derivative spectra is dangerous a change of shape of the original peak also changes the peak-to-peak height in the derivative mode and the background in the low energy region (<100 eV) often changes strongly upon chemical or structural changes of the surface which thus influences the shape of the complete spectrum. So it seems better to collect N vs. E spectra and to remove the background [45,47,74-76] before performing a detailed analysis of the peak shape.

In section 2 of this chapter an overview of literature concerning the origin of the shape change of the Fe $M_{2,3}VV$ peak as caused by oxidation is given. In chapter 3 it was concluded from the high energy Auger peaks and from ellipsometric results that, for oxygen saturated surfaces containing less than 2 ML of iron, all the iron is oxidised to Fe_2O_3 and half a monolayer of oxygen is present at the Cu(100)-iron oxide interface. Since the composition at saturation is known, it is interesting to investigate the development of the Fe $M_{2,3}VV$ peak during oxidation. This is described in section 3 of this chapter.

4.2 Origin of the Fe $M_{2,3}VV$ peak shape change.

In literature there is a good agreement about the main features of the iron (oxide) $M_{2,3}VV$ peak. Because Auger spectra are usually recorded in the dN/dE (or E·dN/dE) mode the position of the negative going peak will be used here to identify the peak position. The main features of the Fe $M_{2,3}VV$ peak are found at 44, 47 and 51 eV. The energies mentioned in literature vary about 2 eV, but that is probably due to instrumental differences. The peak at 47 eV can be ascribed to the Fe $M_{2,3}M_{4,5}M_{4,5}$ super-Coster-Kronig transition and is found in spectra of surfaces (still) containing metallic iron and according to Seo et al. [60] in spectra of FeO and Fe_3O_4.

The high energy feature at 51 eV is generally ascribed to an auto-ionisation transition [67,68,77]. For this transition the 3p core hole is formed by exciting a 3p electron to the empty 4s,4p states from where it can recombine with the core hole under emission of a valence band electron or vice versa. The kinetic energy of this electron is increased relative to that of the 'normal' $M_{2,3}M_{4,5}M_{4,5}$ electron energy by the difference in energy between the valence band (maximum in density of states) and the lowest empty 4s,4p states. This energy

difference is about 4 eV for the oxides [77], which agrees well with the energy difference of the two transitions.

The cause of the low energy transition at 44 eV is still a point of discussion. Most authors suggest a cross-transition ($Fe_{M_{2,3}}Fe_{M_{4,5}}O_{L_{2,3}}$) to be responsible for this feature [67,68,72,73]. Ramsey and Russell [77], however, reject this since they did not find an increase in intensity for this transition at low oxygen exposures of a clean Fe(110) crystal. This increase is expected because the density of oxygen 2p states strongly increases for the first 10 L of oxygen exposure [78]. Therefore they suggest that this transition is caused by a change in the d-band structure of the iron due to charge transfer from iron to oxygen. The correct energy can be calculated for this change. This transition is mainly expected for high oxygen exposures [77]. Other authors, however, do report an increase in the 44 eV feature also for exposures <10L [66,69,70]. Thus, in my opinion, best evidence is found for the cross-transition explanation for this feature. According to Seo et al. [60] this transition is strongly present in Fe_2O_3 (α,γ) and FeOOH.

Based on the explanation of the three features building the Fe $M_{2,3}VV$ peak as given above it is difficult to understand why the 44 eV feature is (nearly) absent for FeO and Fe_3O_4 while the metallic ($M_{2,3}M_{4,5}M_{4,5}$ at 47 eV) feature is dominantly present, as is reported by Seo et al. [60]. This can not be explained by differences in the valence band spectra because they are basically the same for all iron oxides [79]. So the cause should be found either in a difference in the 3p core level or in a difference in the co-ordination of the iron ions in the different oxides.

Though there is a small increase in binding energy of the Fe 3p electrons going from Fe^0 to Fe^{3+} [80] any effect due to this change should also be expected for the auto-ionisation feature. However, this change is not found. An other argument is that an increasing binding energy for the Fe 3p electrons should result in an increasing energy for the transition going from Fe^0 to Fe^{3+}. Then a difference in energy opposite to what is reported (44 eV for Fe^{3+} and 47 eV for Fe^0) is expected. So it is unlikely that differences in the 3p core level are responsible for the 'behaviour' of the 47 eV peak.

An effect of the co-ordination of the metal ions on the transition as found for Ti and V [64,65] is not likely. Because, if there is an effect of octahedrically or tetrahedrically co-ordinated Fe(II) or Fe(III) species (no effect is reported for the core level XPS spectra [80]) there should be a difference between FeO and Fe_3O_4 in the $M_{2,3}VV$ spectra. However, the difference between the spectra of both oxides as determined by Seo et al. [60] is very small. Assuming influence from the co-ordination a difference is expected because, based on the position of the different iron ions in the crystal lattice, a Fe $M_{2,3}VV$ spectrum of Fe_3O_4 should be the sum of one third of a FeO spectrum (accounting for the Fe(II) ions, which are all octahedrically co-ordinated both in FeO and in Fe_3O_4) and two thirds of a γ-Fe_2O_3 spectrum. Strictly, the 'γ-Fe_2O_3' part of the sum should consist partly of γ- and partly of α-Fe_2O_3 spectrum to get the correct ratio of both types of co-ordination for the Fe(III) ions but the $M_{2,3}VV$ spectra for both α- and γ-Fe_2O_3 are practically the same. A good summary of the co-ordination of the iron ions in the different oxides is given by Wandelt [79].

A possible explanation for the presence of a 47 eV peak in the FeO and Fe_3O_4 spectra of Seo et al. [60] might be that metallic iron was present on their surfaces. Though they used

'bulk' oxides for their experiments they sputtered the surfaces in order to remove surface contaminants (and different surface oxides). It may be that the surface was partly reduced (which is, in this case, practically the same as preferentially sputtering of oxygen) by the Ar^+ ion bombardment. The ratio of the O KLL and Fe $L_{2,3}VV$ for the different oxides also indicates sub-stoichiometric amounts of oxygen. This could also explain why many authors who find FeO or Fe_3O_4 on their surfaces using different techniques observe a Fe $M_{2,3}VV$ peak just exhibiting the 44 and 51 eV features. For example Leibbrandt et al. [82] determined the stoichiometry of iron oxide on Fe(100) and Fe(100)-Pt surfaces to be $Fe_{1-x}O$ whereas the 47 eV peak is absent in their spectra. Van Pruissen et al. [30-33] did not observe the metallic iron peak on oxidised Cu(111)-Fe and Cu(110)-Fe surfaces although he had evidence for $Fe_{1-x}O$, Fe_3O_4 and Fe_2O_3 on these surfaces. However, Miyano et al. [67] observed a 47 eV peak on oxidised Fe(100), but their oxygen exposure (200 L) is not sufficient for saturation at 300K [59]. Sakisaka et al. [68] and Smentkovski and Yates [66] report a likewise observation after annealing of an oxidised (350 L at 300 K) iron surface at 773 K though their O KLL/Fe $L_{2,3}VV$ ratio decreased from 2.2 to 0.55, suggesting the presence of metallic iron at or near the surface.

4.3 Oxidation of one monolayer of Fe on Cu(100).

4.3.1 Peak shape synthesis.

Because of the origin of the peak shape of the iron $M_{2,3}VV$ peak as described in section 4.2 it was decided to synthesise the spectra with three peaks. The basic peak shape chosen is a mixed Gaussian/Lorentzian function which is much used in XPS analysis [40]. The main advantage of this function is the flexibility of the peak shape. The function is a product function with four parameters:

$$I(E) = \frac{h}{[1+M\cdot(E-E^0)^2/\beta^2]\cdot\exp\{(1-M)\cdot\ln 2\cdot(E-E^0)^2/\beta^2\}} \qquad (1)$$

where h represents the peak height, M indicates the ratio of the Lorentzian and Gaussian contribution, β is roughly the half-width-at-half-maximum and E^0 is the energy of the peak maximum. For either a pure Gaussian or Lorentzian β is exactly equal to the half-width-at-half-maximum, but for a mixed lineshape the true halfwidth is somewhat smaller [40]. Fitting the iron $M_{2,3}VV$ peak with three peaks thus results in 12 principally free parameters. Because the spectra as used for the fits were already subject to two steps of data handling this amount of free parameters is undesirable. So it was decided to reduce the number of free parameters to three: the height of the peaks. As the rest of the parameters must be fixed, a reasonable choice had to be made for the values. Since Coster-Kronig transitions are very fast processes they result in a relatively broad energy distribution of the emitted electrons and thus in a broad peak. All three of the transitions are in a way Coster-Kronig transitions so it seems reasonable to assume that they result in more or less the same peak shape (β and M). These values were determined by fitting one peak to the Fe $M_{2,3}VV$ peak obtained from a Cu(100) surface containing 16 ML of Fe (as was expected no Cu $M_{2,3}VV$ is visible). Fitting was done by minimisation of χ^2. The parameters M and β resulting from this fit, which is shown in Fig. 1, were respectively 0.5 and 3.6 eV. As is visible in Fig. 1 this peak shape has

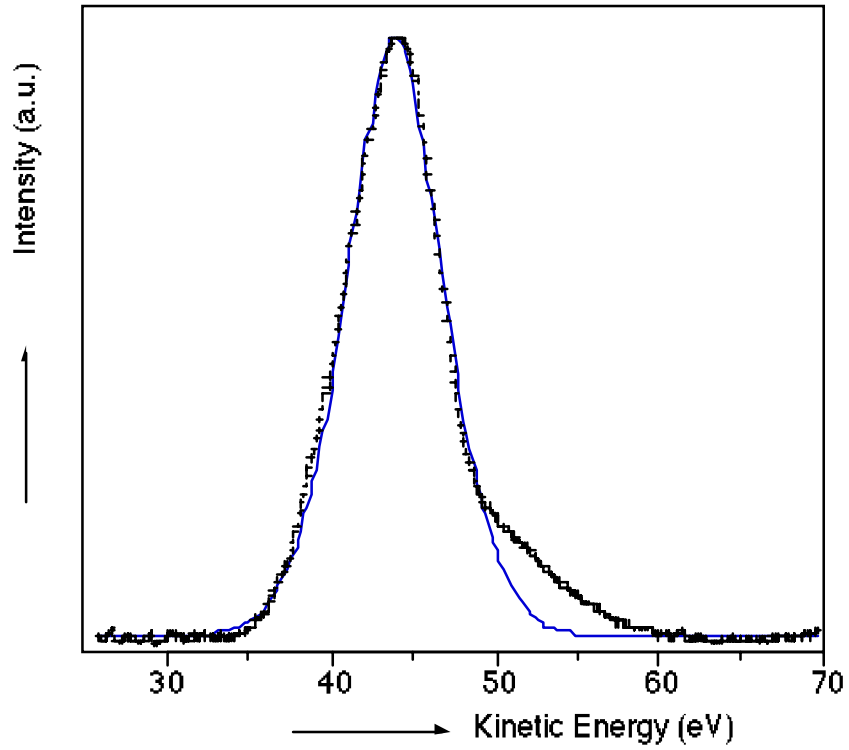

Figure 1 *The iron $M_{2,3}VV$ spectrum of 16 ML of Fe on Cu(100) after background removal (+). The line represents a best fit to the spectrum using one peak and E^0=43.7 eV, β=3.6 eV and M=0.5.*

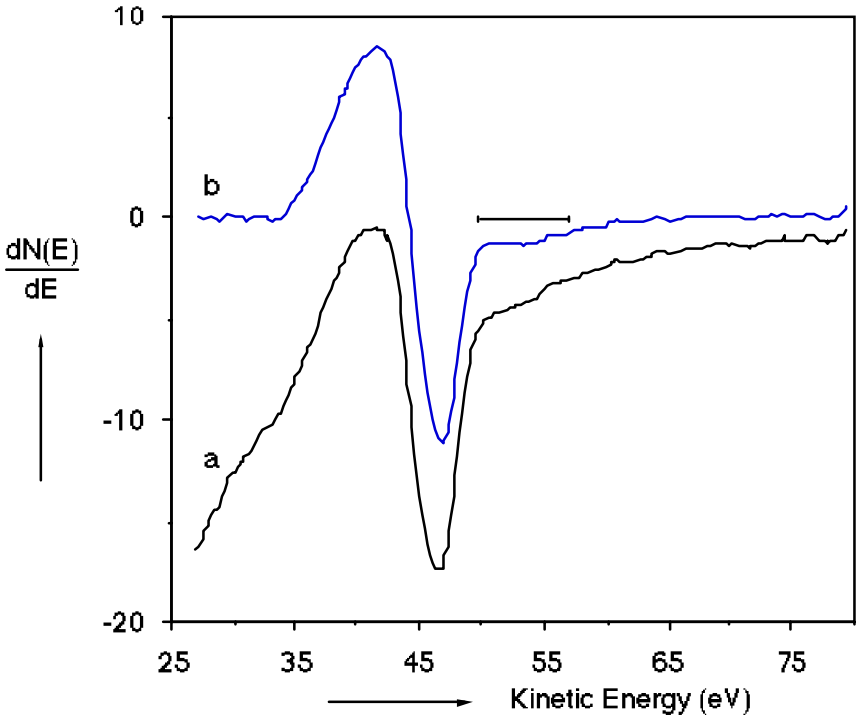

Figure 2 *The numerical derivative of a 16 ML on Cu(100) spectrum before (a) and after (b) background subtraction. The bar indicates the position of the (metallic) auto-ionisation peak.*

two major deficiencies: it doesn't account for the asymmetric shape and the relatively large tail at the high energy side of the peak. This 'tail' is probably caused by the auto-ionisation process, which is also found for metallic iron. The energy of this peak is higher than that of the auto-ionisation peak in the oxides. That this difference is not mentioned in literature is probably due to the fact that the energy of the peak is hard to determine in the derivative spectra as can be seen in Fig. 2, which shows the (numerical) derivative of the Fe $M_{2,3}VV$ peak of Fig. 1. The derivative of the original spectrum is also shown to make clear that this feature is no artefact of the background subtraction. The higher energy of this auto-ionisation peak for the metal is probably due to a higher energy of the empty 4s,4p states compared to the oxides. This peak is omitted in the fitting procedure of the spectra used in this chapter because, due to the large overlap between this relatively small auto-ionisation peak and the copper $M_{2,3}VV$ peak, subtraction of the Cu $M_{2,3}VV$ peak will probably influence the magnitude of the metallic auto-ionisation peak. This omission may lead to an overestimation of the oxidic auto-ionisation peak as long as there is a relative large contribution of the metallic peak.

The remaining parameters to choose are the peak positions. Regarding the origin of the peaks large differences in energy of both 'oxidic' peaks are not expected for Fe^{2+} and Fe^{3+}. Also a change in the energy of the Fe $M_{2,3}M_{4,5}M_{4,5}$ upon oxidation is not expected as I believe this peak to represent only metallic iron. So the peak position of the metallic peak is kept at 43.7 eV (46.3 eV in dN/dE mode), a result from the fit shown in Fig. 1. The peak positions of the cross-transition and auto-ionisation peak were determined by fitting the Fe $M_{2,3}VV$ spectra of oxidised surfaces containing 0.19-2.7 ML of Fe (on Cu(100)). These values appeared to be independent of the amount of Fe on the surface and were 41.4±0.3 and 48.4±0.3 eV (respectively 44.0 and 51.0 eV in dN/dE mode).

Thus the peak synthesis is done with three peaks with the same shape (i.e. β and M) as the metallic Fe $M_{2,3}M_{4,5}M_{4,5}$ peak and with the peak positions of metallic iron and of the two oxide peaks as determined from peaks of different amounts of γ-Fe_2O_3 on Cu(100).

4.3.2 Results and discussion.

In Fig. 3 some Fe $M_{2,3}VV$ peaks of a Cu(100) surface containing 1.0 ML of iron and different amounts of oxygen are presented. The oxygen coverage (θ_O) was determined by calibrating the oxygen signal to that of the known amount oxygen of an oxygen saturated Cu(100) surface, which is 0.52±0.05 ML [51]. In order to ease comparison of the spectra as used for analysis in this chapter with spectra published elsewhere both the integral and the differentiated spectra are given in respectively Fig. 3a and 3b. The peaks in Fig. 3a were obtained from the measured spectra by subtracting a background following the method of Peacock [47] and a subsequent subtraction of a Cu $M_{2,3}VV$ peak as measured on a clean Cu(100) surface. This procedure is described in full detail in chapter 9. Note the good baseline on both sides of the peaks, indicating a good reliability of data handling upto this point. The intensities of the spectra are corrected for day to day changes of the beam current using the intensity of the background at 44 eV as internal reference [48]. It was judged a better standard for these spectra than the intensity at 80 eV as described chapter 9 because of a (smoothly) changing background during oxidation. The spectra in Fig. 3b were obtained by smoothing and numerical differentiation of the spectra in Fig. 3a. In Fig. 3b three vertical lines are drawn to guide the eye at respectively 43, 46 and 51 eV. Features at energies above

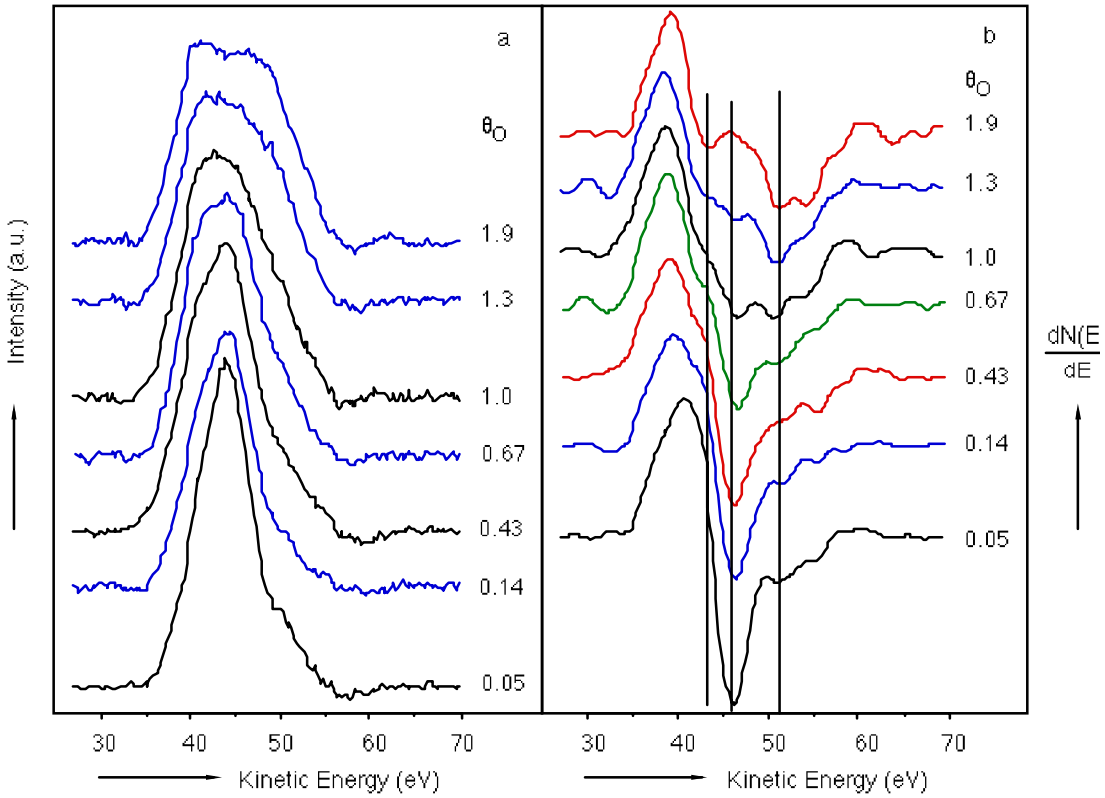

Figure 3 *Some iron $M_{2,3}VV$ Auger spectra of a Cu(100) surface containing one monolayer of iron and different amounts of oxygen, as N vs. E spectra from which both the background and the Cu $M_{2,3}VV$ peak are removed (a) and their derivatives (b).*

51 eV are due to imperfect subtraction of the Cu $M_{2,3}VV$ peak which is enhanced by the differentiation. It is obvious from Fig. 3 that a strong shape change occurs upon oxidation from the beginning. It is also clear from Fig. 3b that peak-to-peak heights are difficult to determine from the derivative spectra of these peaks and therefore an other method of quantification is required.

Some of the fits on the 1.0 ML Fe spectra with different amounts of oxygen are shown in Fig. 4. The quality of the fits in Fig. 4 is representative for all fits. Though the quality of the fits could be improved by allowing more free parameters this only resulted in a rearrangement in the contribution of the three peaks of about 10% of the total peak area. So the influence of this improvement on the trends as observed is small.

The results of the peak synthesis of spectra of one monolayer of iron on Cu(100) containing different amounts of oxygen are shown in Fig. 5. In this figure the absolute areas of the three peaks and the sum of them are plotted as function of the amount of oxygen at the surface.

A slight increase in the total area of the Fe $M_{2,3}VV$ peak upon oxidation is visible in Fig. 5. A decrease could be expected when the spreading of the Fe atoms over a layer of increasing thickness during oxidation is taken into account. This causes an attenuation of the signal of part of the iron atoms due to the small inelastic mean free path of electrons of this energy. The actual increase of the area of the $M_{2,3}VV$ peak is probably caused by an increasing excitation cross-section of the Fe 3p electrons with an increasing amount of

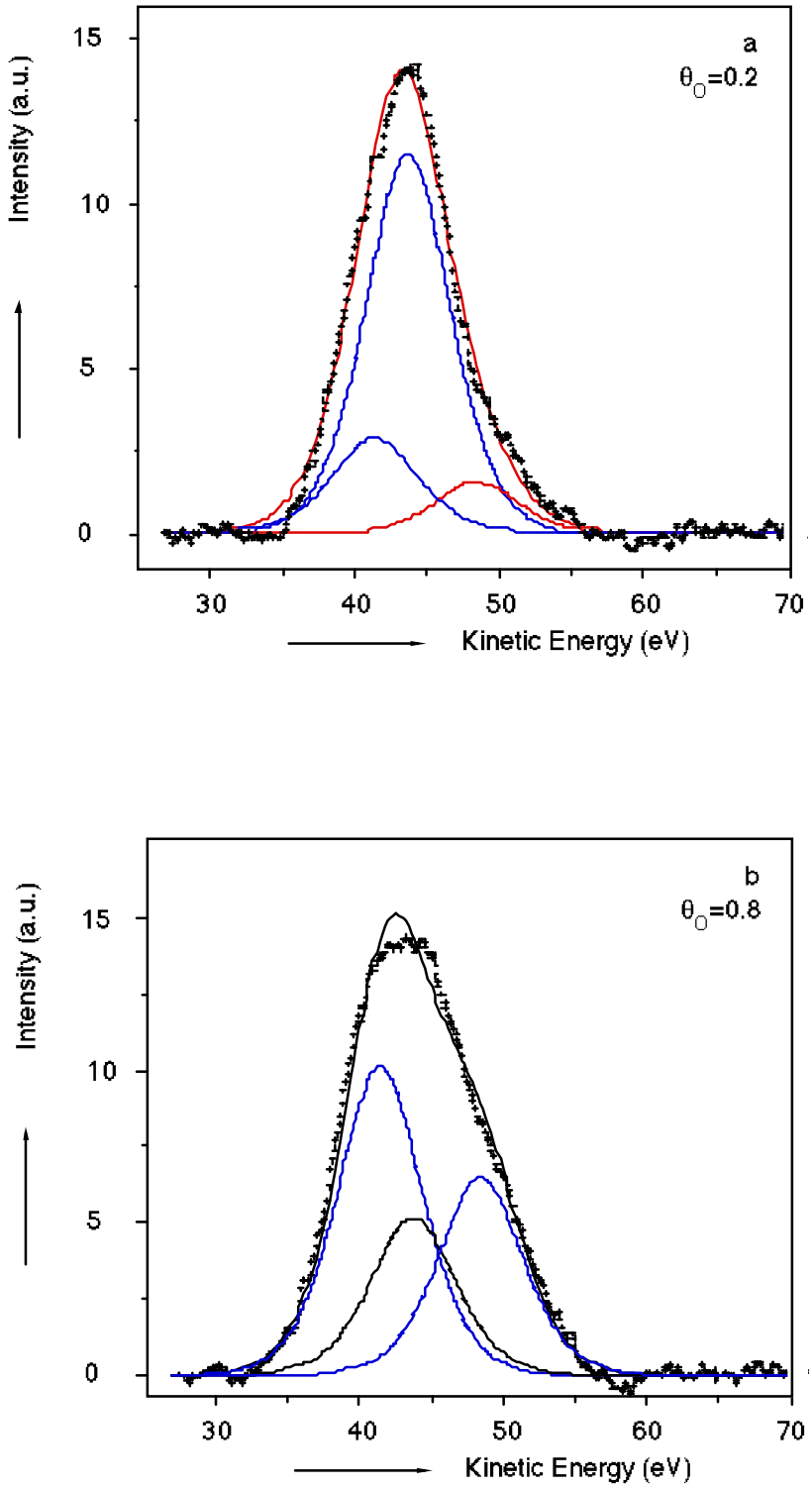

Figure 4 *Some fits of iron $M_{2,3}VV$ spectra of one monolayer of iron on Cu(100) containing 0.2 ML (a), 0.8 ML (b), 1.2 ML (c) and 1.5 ML (d) of oxygen. The + represent the original spectra, the dotted lines are the individual contributions of the three peaks and the bold line is the sum of the three peaks.*

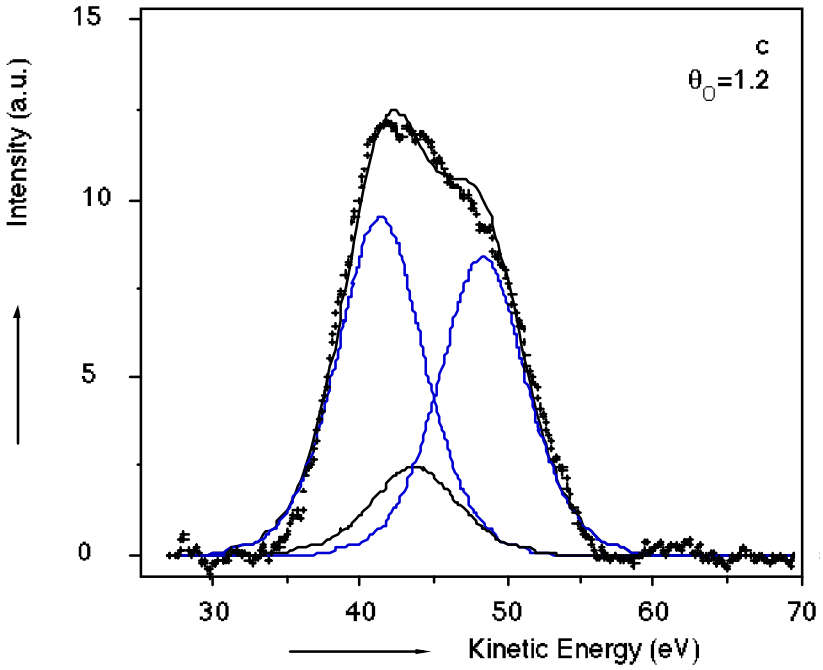
c
θ_O=1.2
Intensity (a.u.)
Kinetic Energy (eV)
0
5
10
15
30
40
50
60
70

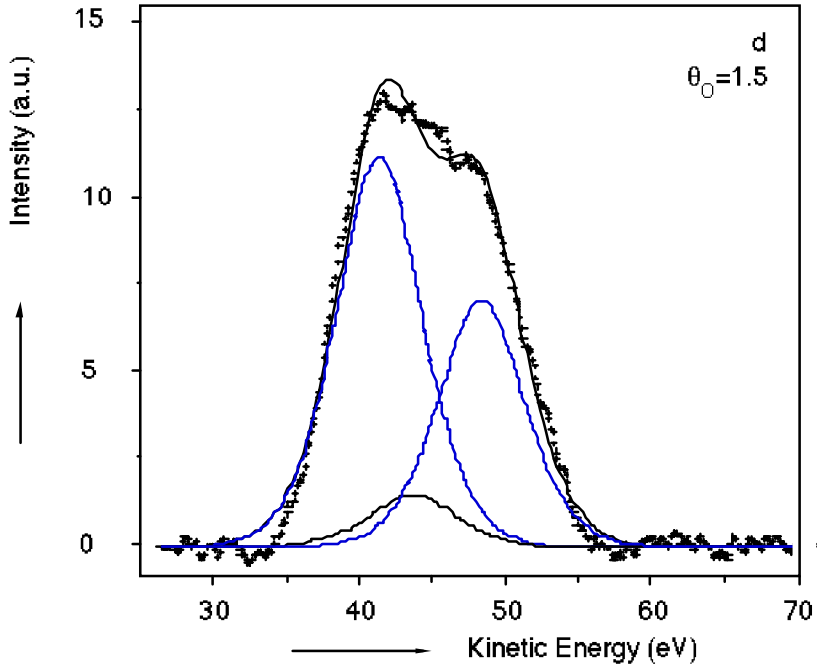
d
θ_O=1.5
Intensity (a.u.)
Kinetic Energy (eV)
0
5
10
15
30
40
50
60
70

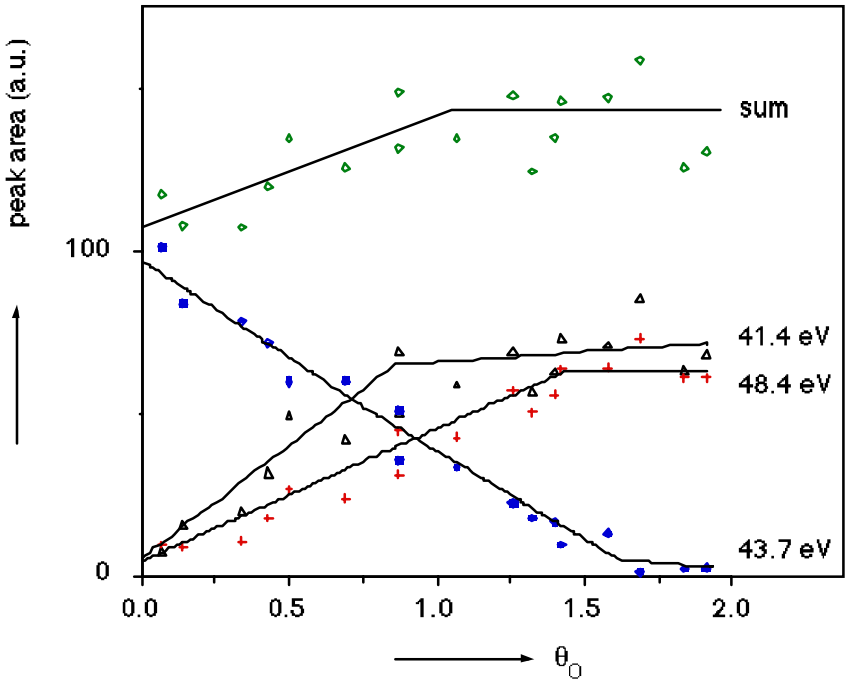

Figure 5 *Individual areas and the sum of them resulting from the fit of the Fe $M_{2,3}VV$ spectra of one ML of Fe as function of the amount of oxygen adsorbed on the surface. The lines are drawn to guide the eye.*

oxygen. This increasing excitation cross-section is also observed with APS [72] and EELS [67]. Ramsey and Russell [77], however, report a decrease in the $M_{2,3}VV$ feature upon oxidation. This apparent decrease is probably due to their use of the second derivative for the analysis which is questionable for quantitative analysis of overlapping peaks.

Regarding the area of the (metallic) 43.7 eV peak as function of θ_O two things are remarkable: an apparently linear decrease and the disappearance of the peak at the value at which θ_O is sufficient to oxidise all iron to Fe^{3+}. This means that either metallic iron is present until all iron is oxidised to Fe^{3+}, in other words iron must be oxidised directly to Fe^{3+}, or Fe^{2+} contributes to this peak. A consecutive oxidation of iron to Fe^{2+} and then to Fe^{3+} can be ruled out. Because then, due to an in that case necessary contribution of Fe^{2+} to the 43.7 eV peak, a sharper decrease in the 43.7 eV peak area is expected for $\theta_O>1$. Based on the lines in Fig. 5 oxidation of Fe to (initially) coexisting Fe^{2+} and Fe^{3+} cannot be ruled out. The origin of the Fe $M_{2,3}VV$ peak, however, does not suggest any reasons for the presence of a $M_{2,3}M_{4,5}M_{4,5}$ peak for Fe^{2+} and an absence for Fe^{3+}. So the first explanation seems more plausible. Also there may be an influence of the underlying copper on the oxidation state of the iron or on the $M_{2,3}VV$ peak. It seems good to note here that also in the derivative spectra the metallic peak remains visible at least upto $\theta_O=1.3$ (Fig. 3b).

Furthermore it is obvious that both oxidic peaks increase with the amount of oxygen. The intensity of the cross-transition peak increases initially at a higher rate with θ_O than the auto-ionisation peak. However, the slope decreases strongly somewhere between $\theta_O=0.5$ and $\theta_O=0.8$ whereas the auto-ionisation peak increases upto $\theta_O=1.5$. At this point the contribution of both oxidic peaks is nearly the same. The initial growth of the low energy

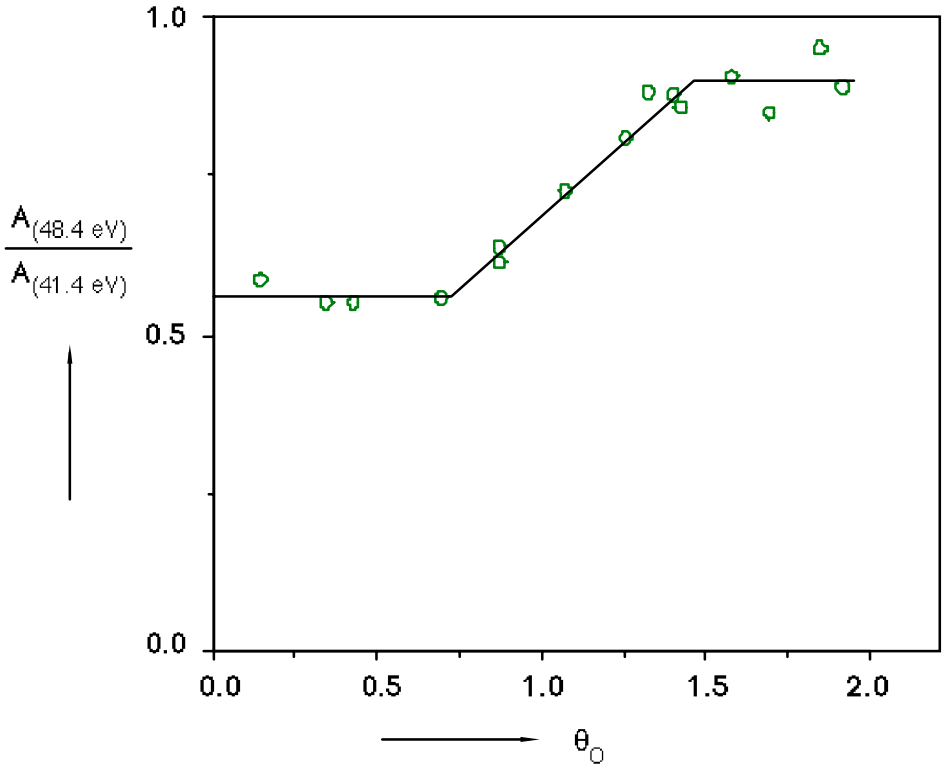

Figure 6 *The ratio of the auto-ionisation and the cross-transition peak areas as function of the amount of oxygen. The lines are drawn to guide the eye.*

peak agrees with the observation of others [66,69,70]. But it disagrees with the observation of Ramsey and Russell [77], who didn't observe an increase of the low energy peak for oxygen exposures below 10 L, but this was based on second derivative spectra. So at least for the Cu(100) + 1 ML Fe surface their argument against the low energy peak as caused by a cross-transition concerning O 2p electrons is not valid. The strong increase in intensity of this transition can then be ascribed to a strong increase of the number of O 2p electrons in the valence band which is independent of the kind of oxide [79].

The ratio of the areas of the high and low energy peaks as function of the amount of oxygen gives more interesting information about this system, as can be seen in Fig. 6. This ratio is constant at 0.6 upto θ_O=0.7 then increases apparently linearly to 0.9 for θ_O>1.5. The changing ratio may be explained by the presence of two kinds of oxygen on the iron surface. Jansson and Morgen [70] already suggested this for the oxidation of polycrystalline iron based on factor analysis of both the Fe $M_{2,3}VV$ and the O KLL spectra. Also, using ellipsometry evidence was found for a different kind of oxygen adsorbing initially on Fe(100) [59] and on Cu(100)-Fe [77]. Now the suggestion arises that the low energy peak is caused by 'surface' oxygen which is differently bound to the iron than 'bulk' oxygen. This is difficult to prove for the Cu(100)-Fe surfaces because the bulk/surface ratio depends on the unknown corrugation of the surface and this effect can hardly be ruled out because of the small sampling depth. An other possible explanation is that Fe^{2+} and Fe^{3+} have a different ratio for both transitions. In that case initially Fe^{2+} is formed (may be together with Fe^{3+})

upto θ_O=0.6-0.7 when Fe^{3+} starts forming at the expense of Fe^{2+} (and Fe^0). This agrees with the second possible explanation given for the behaviour of the 43.7 eV peak, however, the argument against it remains.

The change in the ratio stops at the very moment that all iron could be oxidised to Fe^{3+}, i.e. θ_O=1.5. The other half monolayer of oxygen adsorbing after this point does not seem to have influence on the Fe $M_{2,3}VV$ spectra and therefore can probably be ascribed to oxygen bound to the Cu surface. This agrees well with the disappearance of the 43.7 eV peak at θ_O=1.5.

4.4 Conclusions.

It is not possible to distinguish between the different iron oxides based on the presence or absence of either the cross-transition or the metallic peak Fe $M_{2,3}VV$ peak. On the contrary the presence of a (large) peak at 43.7 eV (46.3 eV in dN/dE mode) in the iron $M_{2,3}VV$ spectrum is a strong indication of the presence of metallic iron in the surface region. Support for this can be found in literature (section 4.2) and in the analysis of the $M_{2,3}VV$ peak during oxidation of one monolayer of iron on Cu(100) (section 3 of this chapter).

On oxidising one monolayer of iron on Cu(100) the iron is first oxidised completely to Fe_2O_3 before oxygen adsorbs on the Cu(100) (-Fe_2O_3) interface. The iron is not consecutively oxidised to Fe^{2+} and Fe^{3+} but either at once to Fe^{3+} or to initially coexisting Fe^{2+} and Fe^{3+}.

A difference in the ratio of the cross-transition and the auto-ionisation peak between initially and finally adsorbing oxygen is observed. This might be due to a different effect of surface and bulk oxygen on the Fe $M_{2,3}VV$ transition. Since this is not understood completely more investigations on the development of the Fe $M_{2,3}VV$ peak upon oxidation would be interesting.

5

The interaction of Cu(100)-Fe surfaces with oxygen studied with photoelectron spectroscopy. I

Mg K_α excited photoemission.

Abstract

The oxidation of Cu(100)-Fe surfaces was studied using XPS. Surfaces containing 0 - 10 ML were oxidised at room temperature exposing 2 Pa·s of oxygen. For all surfaces evidence for Fe_2O_3 was found. Only for surfaces containing more than 5 ML a clear metallic Fe $2p_{3/2}$ was observed. This means that more oxygen could be adsorbed than observed in chapter 3 and 4.

The analysis of the change of the 2p peak shape of a surface containing 1 ML of Fe as function of the amount of oxygen showed that oxidation proceeds via an intermediate containing both Fe^{2+} and Fe^{3+}.

5.1 Introduction.

In this chapter XPS is used to obtain more information on the Cu(100)-Fe-O system. The sensitivity of the Fe 2p peak for the oxidation state gives the possibility to determine the type of iron oxide independently from stoichiometric calibrations. Neglecting a possible influence of the substrate and extrapolating to bulk iron the results presented in chapter 3 and 4 seem to contradict the results reported by Leibbrandt et al. [55] who found $Fe_{0.95}O$ after oxidation of Fe(100) at 300K. The amount of oxygen found by them was, however, equal to that found for oxidised Cu(100) surfaces containing more than 2 ML of iron [82]. The results presented in chapter 3 and 4 also conflict with conclusions reported by Kishi et al. [35] though they used oxygen exposures obviously too small to produce oxygen saturated surfaces.

The XPS results will also be used to verify the direct oxidation from Fe^0 to Fe^{3+} as proposed in chapter 4.

5.2 Results and discussion.

Surfaces containing 0-10 ML of iron were oxidised exposing 2 Pa·s of oxygen at room temperature. In Fig. 1 the oxygen 1s signal is plotted versus the iron 2p signal. The line drawn in Fig.1 is the least squares fit through all points. The intensities are corrected for the differences in X-ray beam intensity assuming that the sum of the Cu 2p, Fe 2p and O 1s multiplied by their respective relative sensitivity factors (rsf's) is a good representation the beam intensity. The rsf's used were taken from the Phi handbook [53]. These rsf's are obtained with a Phi Omnifocus III lens in front of the hemispherical analyser. So it must be realised that the conditions are different and thus the rsf's may be wrong. Multiplying the corrected intensities with their rsf's (as was done) in principle results in mole fractions ($X_x=rsf_x \cdot I_x/\Sigma rsf_i \cdot I_i$), however this requires correct rsf's and a homogeneous sample. Errors in the rsf's influence the absolute numbers but, within certain limits, not the linearity in Fig.1. So the slope is not used here to calculate the stoichiometry. In any case, the intercept is equal to the signal of 0.5 ML of oxygen on Cu(100) within experimental error and this confirms the 0.5 ML of oxygen present in excess of the oxygen bound to the iron as reported before [82]. However, at iron coverages (exceeding 3 ML) still more oxygen can be adsorbed. This is not expected based on previous results and it will be discussed later.

Since for the eye there seemed no difference between the Fe 2p spectra of surfaces containing different amounts of iron (up to 3 ML), fits to the spectra are compared. The spectra were fitted with 4 peaks representing the Fe $2p_{3/2}$, the Fe $2p_{1/2}$ the satellite of the Fe $2p_{3/2}$ and an extra peak to take account for the asymmetry of the Fe $2p_{3/2}$ peak. The satellite of the Fe $2p_{1/2}$ is omitted because it appeared to be weak compared to the noise and also the possible asymmetry of the Fe $2p_{1/2}$ did not seem to influence the fit. The fits were performed by minimisation of χ^2 of four mixed Gaussian/ Lorentzian functions with fixed width (FWHM of 3.8 eV for all peaks except the asymmetry function which appeared to give the best results with 5 eV) and Gauss/Lorentz ratio of 0.5. An example of a fit is shown in Fig. 2 which gives the fit results for a Fe 2p peak taken of a surface containing 1.5 ML of iron on Cu(100) after exposure of 2 Pa·s of oxygen. In table I the results of the fits are reported averaged for 6 spectra (0.5 - 3 ML) because the fits showed no trends due to different θ_{Fe}. Both the position of the $2p_{3/2}$ after oxidation (shifted 3.9 ± 0.2 eV to higher binding energy in respect to the metal $2p_{3/2}$ peak [83]) and the presence of a satellite at 8 eV higher binding energy [79] indicate

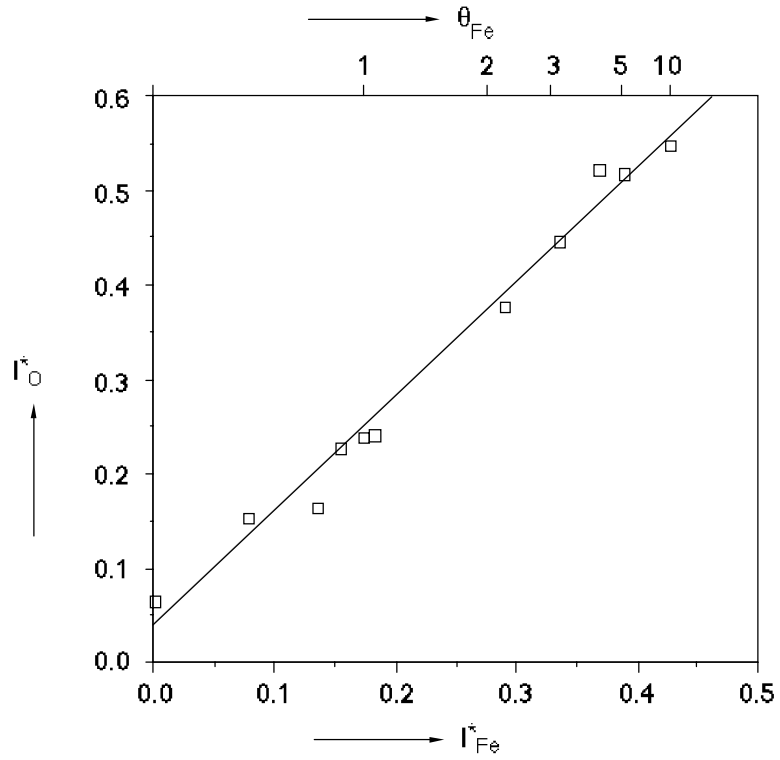

Figure 1 *The relative O 1s signal as function of the relative Fe 2p signal after 2 Pa·s of oxygen obtained on Cu(100) surfaces containing different amounts of iron.*

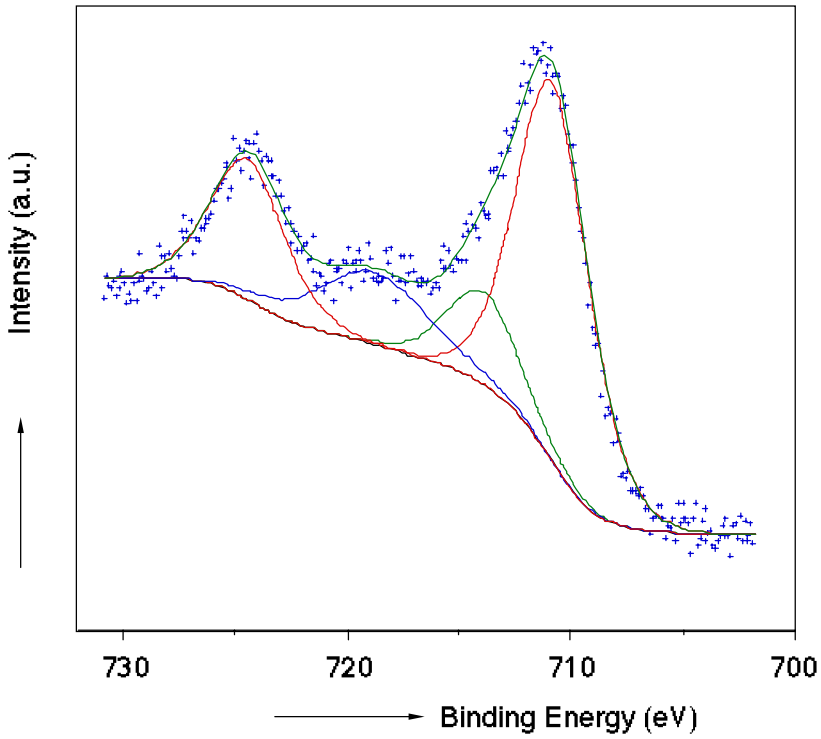

Figure 2 *A Fe 2p spectrum of Cu(100) + 1.5 ML Fe after 2 Pa·s of oxygen. The background and the four peaks resulting from the fit as described in the text are also shown.*

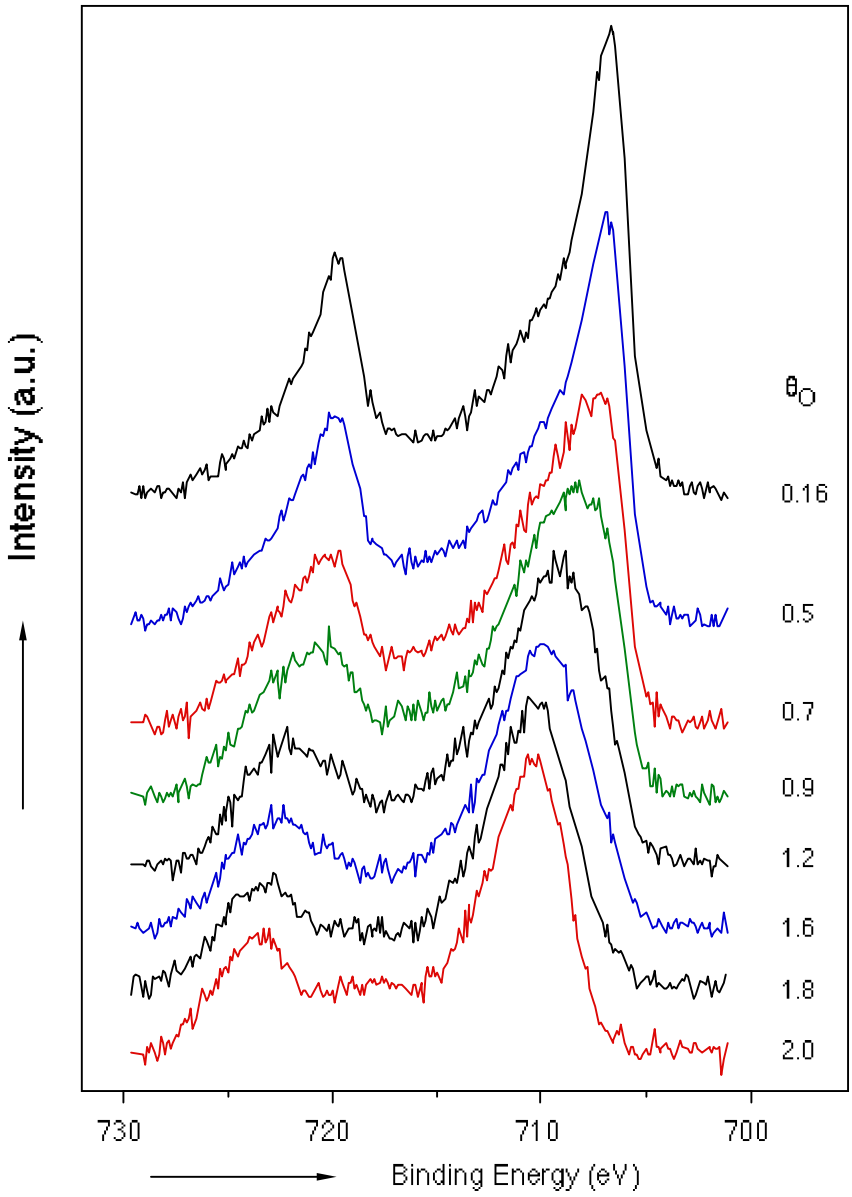

Figure 3 *Some Fe 2p spectra after background subtraction of a step by step oxidation of Cu(100) + 1 ML Fe.*

the presence of Fe_2O_3 at the surface under these conditions. This proof for formation of Fe_2O_3 during the oxidation of Cu(100) containing up to 3 ML of iron is, unlike the other determinations, independent of calibrations of amounts of iron and oxygen.

In order to be able to follow the development of the oxide on the surface, Cu(100) + 1 ML Fe was oxidised step by step. The oxygen pressures and exposure times were chosen such as to obtain reasonable changes in the amount of oxygen adsorbed on the surface in a reasonable time. Fig. 3 shows the change in the Fe $2p_{3/2}$ peak during oxidation after background subtraction. The oxygen coverage of the fresh prepared surface is due to the presence of oxygen adsorbed during evaporation. From Fig. 3 it is clear that the iron peak starts changing immediately and that after adsorption of a certain amount of oxygen the final Fe_2O_3 peak shape is reached, whereas still more oxygen can be adsorbed on the surface. This

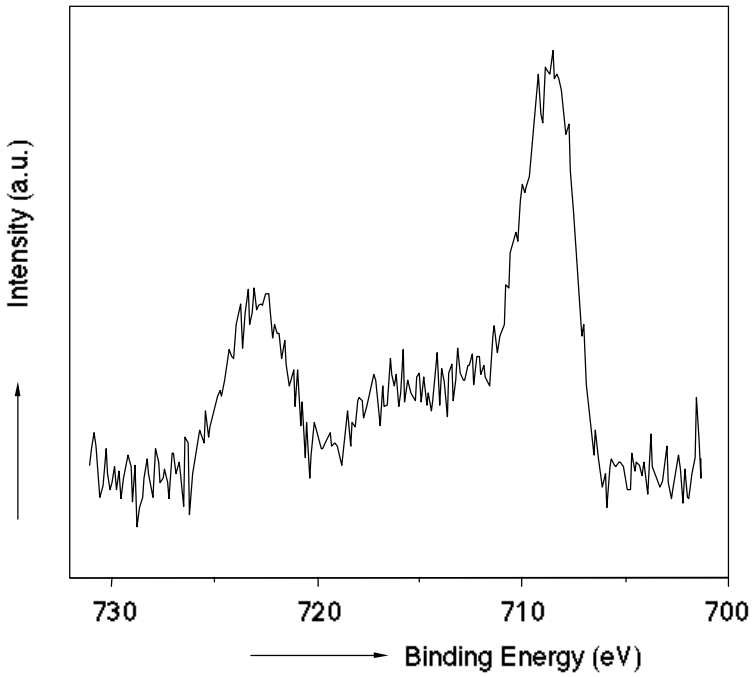

Figure 4 *The sum of the Fe^{2+} 2p spectra resulting from the spectrum decomposition of the Fe 2p spectra obtained during a step by step oxidation of Cu(100) + 1 ML Fe as described in the text.*

Table I. Mean characteristics of the Fe 2p peak shape of oxidised surfaces containing 0 - 3 ML of iron.

peak	position (eV)	FWHM (eV)	relative contribution
$2p_{3/2}$	710.24 ± 0.17	3.8	0.516 ± 0.014
asymmetry	713.3 ± 0.3	3.8	0.124 ± 0.017
satellite	718.2 ± 0.3	5.0	0.156 ± 0.017
$2p_{1/2}$	723.8 ± 0.2	3.8	0.204 ± 0.005

agrees with the 'excess' oxygen which adsorbs on the copper after oxidation of the iron. Since a linear decrease of the metallic Fe $M_{2,3}VV$ peak with increasing amount of oxygen suggested immediate formation of Fe^{3+} out of Fe^0 [46] it was tried to verify this by decomposing the intermediate spectra with the first (in principle oxygen free, though containing 0.16 ML of oxygen) and the last (completely oxidised to Fe_2O_3) spectrum by means of a linear fit. However, a sum of the sharp Fe^0 $2p_{3/2}$ and the more broad Fe^{3+} $2p_{3/2}$ result in a clear double peak which is never found in the real spectra. To resolve this the spectra were composed using a linear combination of the Fe^0 and Fe^{3+} spectra. It was judged from the background on the high and the low energy side of the difference spectrum whether the choice of the weights might be correct. The resulting difference spectra resembled each other strongly. Since no clear trends were visible in these 'rest' spectra only the sum of them (to reduce noise) is shown in Fig. 4. The peak shape and position of this spectrum suggest the presence of Fe^{2+} though the $2p_{3/2}$ is too narrow (3 eV instead of 3.8 eV, but also Kurtz and Henrich report small FWHM

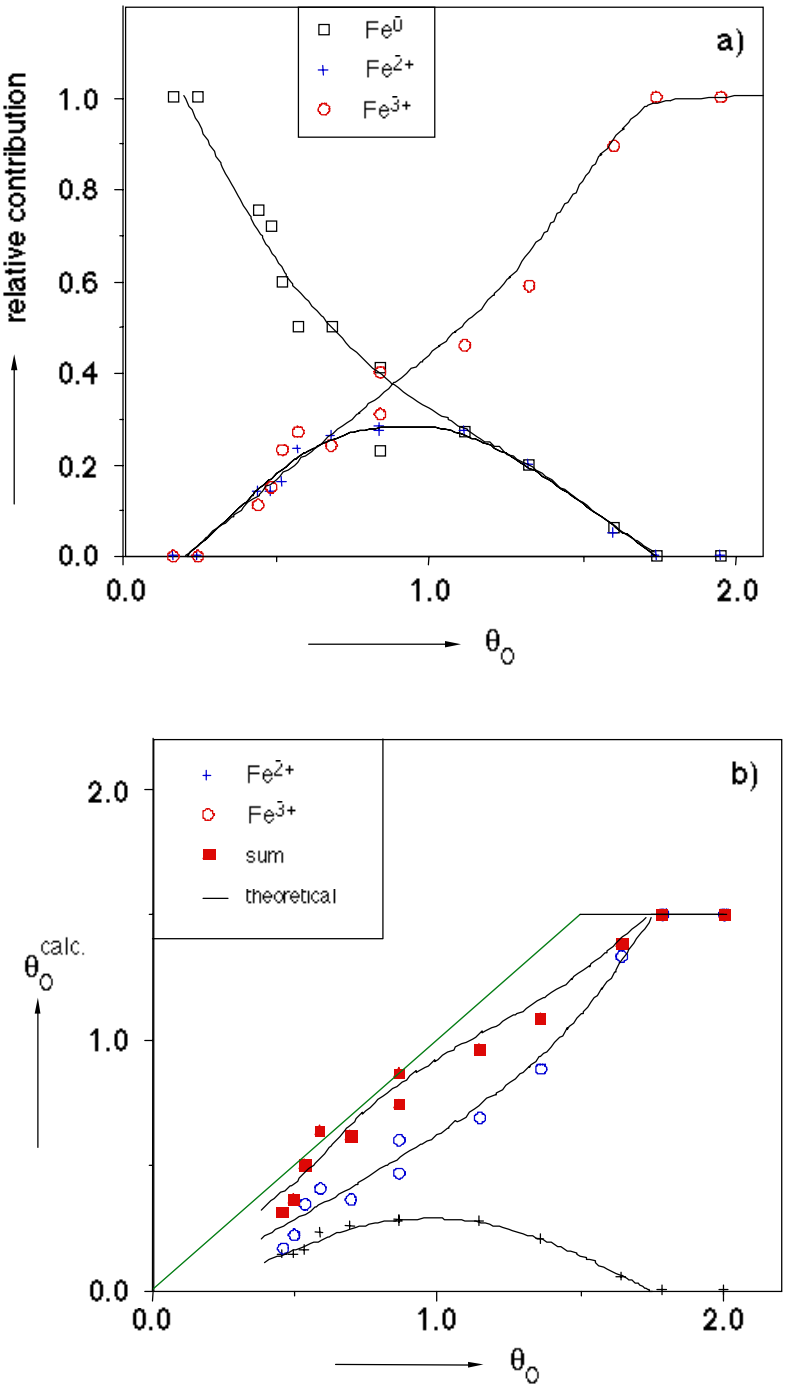

Figure 5 *The partial contribution of Fe^0, Fe^{2+} and Fe^{3+} to the Fe 2p spectra of the step by step oxidation of Cu(100) + 1 ML Fe as function of the amount of oxygen (a) and the amount of oxygen calculated from the number of iron ions as function of θ_O calculated from the O 1s (b). The broken lines drawn are to guide the eye.*

values for Fe^{2+} [84]). In Fig. 5a the results of the decomposition are shown giving the relative contribution of the Fe^0, Fe^{2+} and Fe^{3+} as function of the amount of oxygen. It may be clear that a discussion of a linear decrease of the Fe^0 contribution is not really sensible since the 'Fe^0' peak already contained a Fe^{2+} and a Fe^{3+} contribution. However, the contribution of the Fe^{2+} and the Fe^{3+} peaks seems to increase together first and later the Fe^{2+} contribution

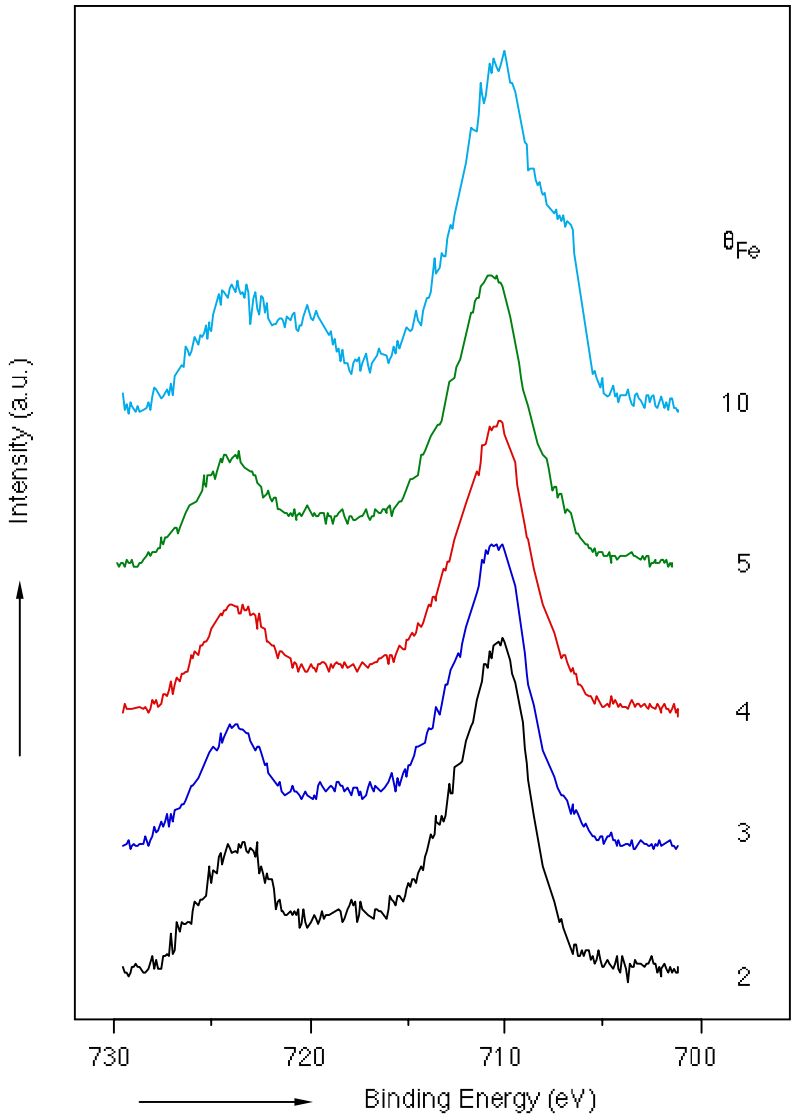

Figure 6 *The Fe 2p spectra after background subtraction of oxidised surfaces containing 2, 3, 4, 5 and 10 ML of Fe on Cu(100).*

decreases down to zero. So it can be concluded that the Fe_2O_3 is formed via an intermediate phase containing both Fe^{2+} and Fe^{3+}.

A possible falsification of the decomposition method above may come from the amount of iron ions in relation to the amount of oxygen to be present at the surface. In order to check this the amount of oxygen bound to Fe^{2+} and Fe^{3+} (on the same 1 ML Fe on Cu(100) surface) is calculated assuming the oxygen present as O^{2-}, and θ_O=2.0 ML at the end of the oxidation. The result is shown in Fig. 5b. The solid line drawn in Fig. 5b represents the theoretical amount of oxygen bound to iron assuming all iron is oxidised before oxygen adsorbs on the copper surface. The data for small θ_O are omitted because the Fe^0 peak already contains a contribution of the Fe^{2+} and Fe^{3+} which can not be accounted for in the calculation. However, the influence of this decreases with a decreasing contribution of Fe^0 to the peak. For high oxygen coverages the discrepancy is of course due to the adsorption of the excess oxygen, which does not necessarily has to start abruptly. The most important conclusion from Fig. 5b is that the amount

of oxygen calculated from the iron ions (as present according to the decomposition that resulted in the peak of Fig. 4) never exceeds the total amount of oxygen as calculated from the O 1s peak.

An other interesting point arises when Fig. 5a is compared with Fig. 6 in chapter 4. Fig. 6 from chapter 4 shows the ratio of the contribution of the cross-transition and the auto-ionisation features to the electron excited Fe $M_{2,3}VV$ peak as function of θ_O for the oxidation of 1 ML Fe on Cu(100). The value of θ_O at which the Fe^{2+} contribution stops increasing (in Fig. 5a) seems to coincide with that where the ratio between the cross-transition and the auto-ionisation starts to change. Since there was no direct proof for the existence of Fe^{2+} during the oxidation, this change in the ratio was ascribed to the presence of a kind of surface oxygen [46]. Now it is known that Fe^{2+} is probably present during the oxidation, the changing ratio can be explained from a changing ratio of the number of Fe^{2+} and Fe^{3+} ions. This also means that Fe^{2+} and Fe^{3+} may indeed exhibit a different $M_{2,3}VV$ peak shape as suggested by Seo et al. [60], but that it should be found in the ratio of both oxide features of the Fe $M_{2,3}VV$ peak. However, a surface oxygen effect on the ratio can not be excluded.

From Fig. 1 it was clear that the amount of oxygen after saturation still increases when more than 3 ML of iron is deposited. This means that more than 2 ML of iron (or 2.3 ML of iron when the 0.5 ML excess oxygen is included) can be oxidised. Since the Cu $2p_{3/2}$ peak (E_{kin}=320 eV, imfp~8 Å) is still clearly present up to θ_{Fe}=5 any metallic iron present should be visible in the Fe 2p spectra (E_{kin}=530 eV, imfp~10 Å). However, comparison of the Fe 2p spectra taken of oxidised surfaces containing 2, 3, 4, 5 and 10 ML iron (Fig. 6) shows that only for the 10 ML spectrum the metallic $2p_{1/2}$ and $2p_{3/2}$ are strongly present. For the other spectra the metallic Fe $2p_{3/2}$ peak may be present as a shoulder at ~707 eV, but very weakly. These findings agree with the amount of oxygen still increasing for θ_{Fe}>3 ML (Fig. 1), but do not fit in a model of only 2.3 ML of iron that can be oxidised to Fe_2O_3. The difference may come from an error in the micro-balance (though this is highly unlikely because the error must exceed 25%) or from differences in the structure of the iron film before oxidation influencing the mass-transport in the oxide layer. In principle even at 10 ML the iron is expected to be present as flat fcc iron on Cu(100) [20]. However, both the temperature and contamination out of the gas may influence the growth. Though the difference in evaporation conditions between the experiments presented in this chapter and chapter 3 and 4 seem to be small, this may be the cause. Especially the difference in oxygen contamination after evaporation (θ_O • 0.16 in this study against θ_O • 0.05 in chapters 3 and 4) may be responsible for a different growth of the iron. The structure of the iron on the surface is very important for the amount of iron that can be oxidised [61].

Closer examination of the 10 ML (but also for those of 25 and 44 ML) shows that only Fe^{3+} and Fe^0 contributions are present. Though a shift of 0.2 eV to lower binding energy of the Fe^{3+} spectrum is necessary in order to synthesise the spectrum out of a Fe^{3+} and Fe^0 spectrum a Fe^{2+} contribution appears to be absent. Apparently the type of iron oxide formed is Fe_2O_3 and independent of the amount of Fe deposited on the Cu(100) surface.

5.3 Conclusions.

The shape of the Fe 2p peak after exposure of 2 Pa·s of oxygen to Cu(100)-Fe surfaces shows the presence Fe_2O_3 independent of the amount of iron. Quantitative analysis of the amounts of Fe and O agrees with this, though more oxygen could be adsorbed during these

experiments than expected based on experiments described in chapters 3 and 4. Also the presence of 0.5 ML of excess oxygen for $\theta_{Fe} \leq 2$ ML is confirmed by these experiments.

During the oxidation of 1 ML of iron on Cu(100) first both Fe^{2+} and Fe^{3+} are formed. Later Fe^{2+} disappears as does the Fe^{0} in favour of Fe^{3+}. Combining this observation with the Fe $M_{2,3}VV$ peak shape analysis [46] suggests Fe^{2+} and Fe^{3+} might exhibit a different $M_{2,3}VV$ peak shape. This difference must then be found in a different ratio of the contribution of the two oxide features composing the $M_{2,3}VV$ iron oxide peak.

6

The interaction of Cu(100)-Fe surfaces with oxygen studied with photoelectron spectroscopy. II

He I and He II excited photoemission.

Abstract

The valence band structure of Cu(100)-Fe surfaces is studied for different amounts of iron and oxygen using He I and He II radiation for excitation. Interesting changes in the Cu 3d structure occur that may be due to changes in the structure of the top layer of the Cu substrate. The shape of the valence band after 2 Pa·s of oxygen confirms the presence of Fe_2O_3 on these surfaces. Stepwise oxidation showed a direct increase of the O 2p level, whereas the Fe 3d band near the Fermi edge initially did not change much. This may be the cause of the apparently invisible oxygen occurring during the adsorption of the first ML as seen by $\delta\Delta$ determined by ellipsometry.

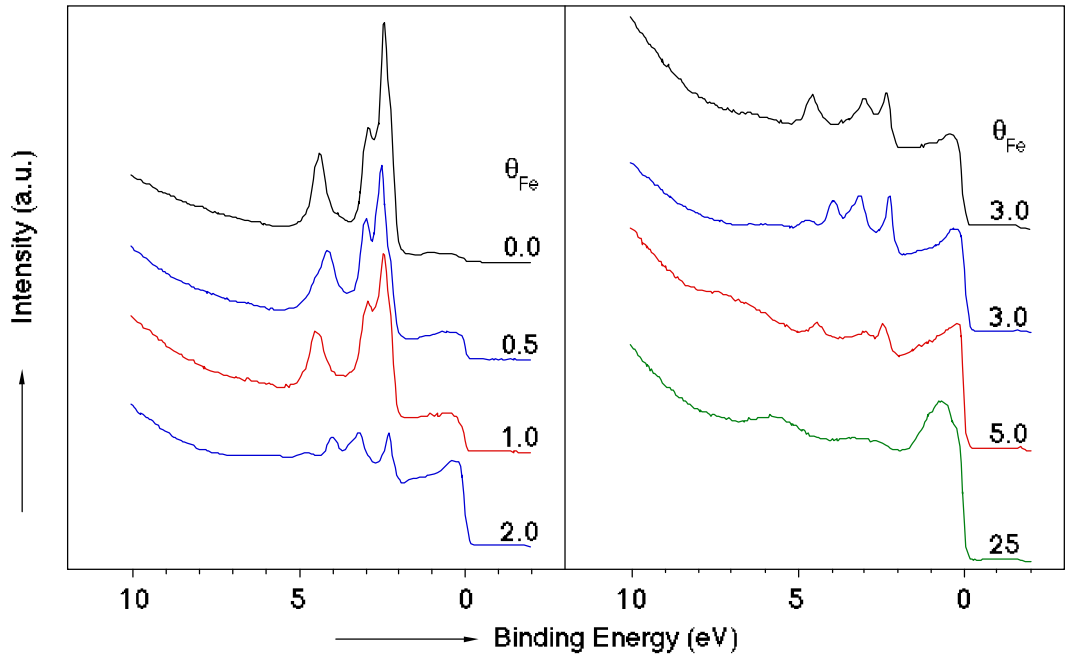

Figure 1 *He I photoemission spectra of freshly prepared Cu(100)-Fe surfaces.*

6.1 Introduction.

Knowledge of the valence band and conduction band structure of surfaces is of great importance for a better understanding of physical and chemical events occurring in or at the surface. The electronic structure near the Fermi level is responsible for the optical properties of the material and for the reactivity towards other materials. From this point of view the Cu/Fe system is very interesting because both metals have a different band structure, a different crystal structure at room temperature, and an endothermic heat of mixing indicating a bad interaction.

This chapter deals with the change in the valence band of the Cu(100)-Fe surface containing different amounts of iron due to interaction with oxygen. He I and He II results are compared because the excitation cross-sections of the O 2p and the Cu/Fe 3d change differently upon changing the energy of the photons.

6.2 Results and discussion.

In Fig. 1 He I photoemission spectra of surfaces containing different amounts of iron are shown. With increasing iron coverage two main changes in the valence band structure occur. Near the Fermi level the copper 4s band is overshadowed by a growing iron 3d band, while on the other hand, as could be expected, the copper 3d band structure decreases with growing iron layer thickness. The iron 3d band is already clearly visible for 0.5 ML Fe whereas for 2 Å (≈1 ML Fe) on polycrystalline copper the difference was much smaller [37,38]. Those spectra, however, were excited with Mg K_α radiation which may explain the difference.

On examining the structure of the copper 3d band (the peaks between 2 and 5 eV) another difference seems to exist for the different surfaces. This difference that consists of changes in the peak maxima and intensities, is at least partly due to the highly angular dependence of the

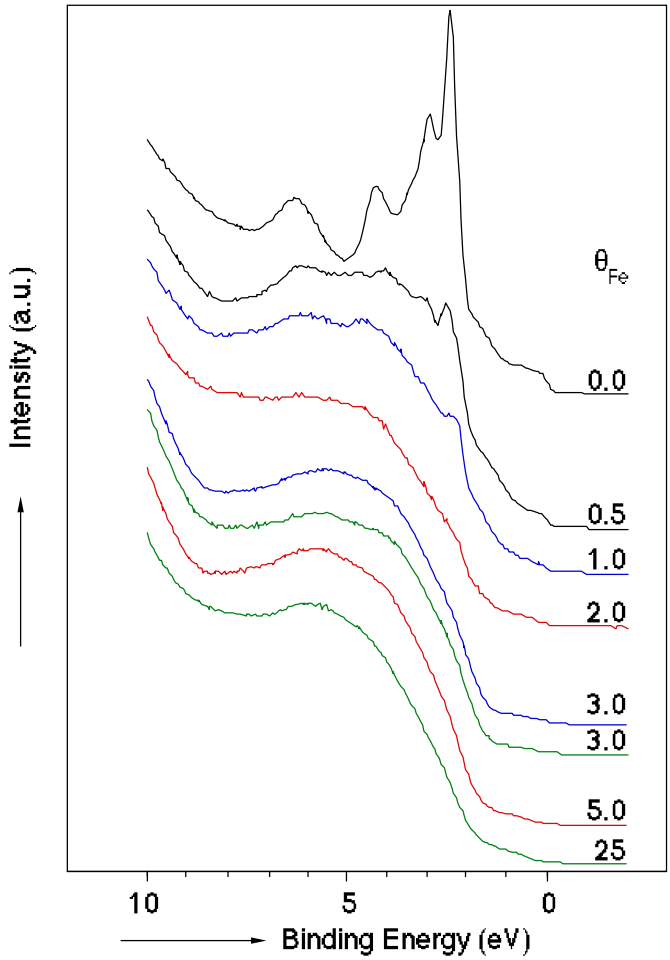

Figure 2 He I photoemission spectra of Cu(100)-Fe surfaces after 2 Pa·s of oxygen.

copper 3d band structure of monocrystalline surfaces [87, 88]. Since the sample had to be moved in order to clean and to evaporate new iron and because it was difficult to place the crystal in exactly the same position, the Cu 3d structure often reproduced badly when a new surface was prepared. As an example, 2 spectra of two different separately prepared surfaces containing 3 ML of iron are shown in Fig. 1. The difference is found in the copper 3d band structure. Similarly different spectra were obtained for clean Cu(100), though they are not shown here. Therefore discussion considering the copper 3d part of these spectra has to be done carefully. Spectra taken before and after oxidation can be compared with each other without this problem since sample movements were not carried out in that case.

The changes in the He I photoemission spectra due to oxidation up to saturation can be seen in Fig. 2. The amount of oxygen used was 2 Pa·s, which is sufficient to reach saturation within a few percent [82]. In all spectra, but those of pure Cu and 'bulk' iron, the copper 3d band structure seems to vanish into the iron oxide band structure. Closer examination learns that the band at 2.4 eV decreases mostly due to oxidation with respect to the other copper 3d features. This can only partly be caused by the screening of the copper 3d electrons by the iron oxide layer since the inelastic mean free path of those electrons is high with respect to the amount of oxide (at least when 0.5 ML Fe is present). A good indication for this is that the Cu 3d band is still visible after the evaporation of 5 ML of iron. Possibly the decrease is caused by

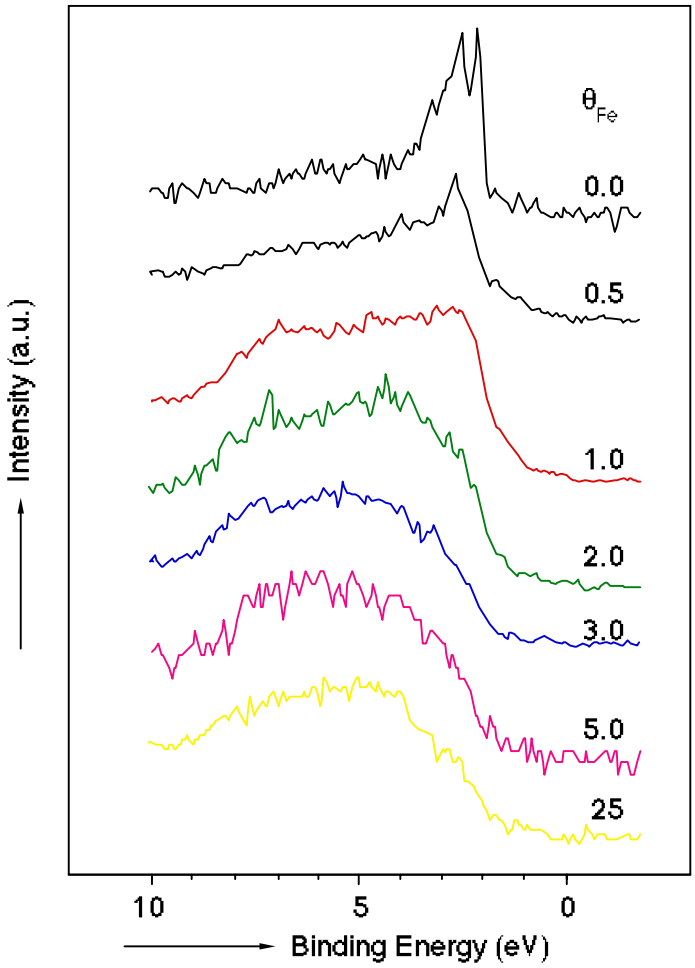

Figure 3 *He II photoemission spectra of Cu(100)-Fe surfaces after 2 Pa·s of oxygen.*

an electronic interaction between the iron oxide and the copper surface but it may also be caused by a slight deformation of the surface. In fact, also for the oxidised surface without iron a decrease of the most intense peak (at ~2.4 eV) in respect to the peak at 3 eV of about 25% can be observed. It is known from calculations [89] and experiments [9, 90] that 0.5 ML of oxygen on Cu(100) (which is the saturation value of this surface [51]) induces a missing row reconstruction of the surface. However, the change in the ratio between the 2.4 and 3 eV peak with increasing Fe coverage (Fig. 1) suggests the presence of an electronic interaction since iron grows epitaxially on Cu(100) for the first several ML. Against this can be said that the interaction cannot be very strong since the heat of mixing is positive. On the other hand there must be some electronic interaction because bulk like fcc iron is not stable at 300 K. The stress caused by this anomaly may be enough to change the above mentioned ratio if the 2.4 eV peak is mainly influenced by structural changes surface region.

Other important observations in Fig. 2 are that the Fe 3d states near the Fermi level have disappeared completely due to the formation of an insulating oxide and that the O 2p band and the Fe 3d band form a broad apparently featureless band. The shoulder near the Fermi level, characteristic for the Fe^{2+} [79] containing compounds is apparently absent. However, Wandelt [79] reported the shoulder in Al K_α excited valence band spectra of Fe_xO and Fe_3O_4, which does not necessarily indicate an absence or presence in the Fe^{3+} and Fe^{2+} valence band spectra

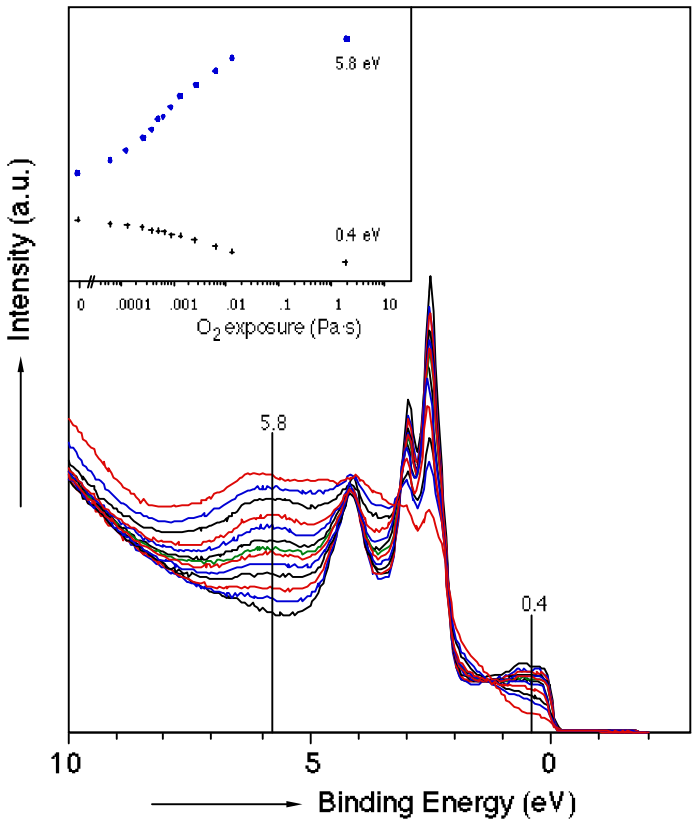

Figure 4 *He I photoemission spectra of a stepwise oxidation of 0.5 ML Fe on Cu(100). The insets give the intensity of the spectra at the binding energies of 0.4 and 5.8 eV indicated by vertical dashed lines.*

excited with He I radiation. Nevertheless, valence band spectra of Fe_xO excited with hν=30eV [79] and Fe_3O_4 excited with He I and He II [91] exhibit the shoulder whereas Fujimori et al. [92] reported the absence of this shoulder in Fe_2O_3 spectra excited with a wide range of photon energies starting with 21.2 eV. In fact the He I spectrum reported by them is quite similar to those observed by us for 3 and 25 ML of Fe on Cu(100). This seems to be an other confirmation that the Cu(100)-Fe surfaces contain Fe_2O_3 after exposure to 2 Pa·s oxygen at room temperature. Further evidence for this can be found in Fig. 3 which shows the He II excited valence band spectra of the same surfaces as reported in Fig. 2. Also in the He II spectra no shoulder near the Fermi level is visible. The other trends are the same as in the He I spectra but for the background which is much higher in the He I spectra due to the lower kinetic energy of those electrons in respect to the He II excited electrons.

The effect of oxidation on the valence band of Cu(100)-Fe surfaces was also studied after various exposures and thus containing different amounts of oxygen. Although it would have been favourable to know the absolute amount of oxygen for the different spectra, only the exposure could be used. Reason for this was that a small displacement of the sample was necessary in order to place the sample in the right position for the Mg anode. As explained before, this displacement results in changes in the spectra which are clearly less desirable. In Fig. 4-6 the spectra of step-by-step oxidation of surfaces containing respectively 0.5 ML, 3 ML and bulk like iron (25 ML Fe) are shown. During O_2 exposure the He discharge lamp was stopped

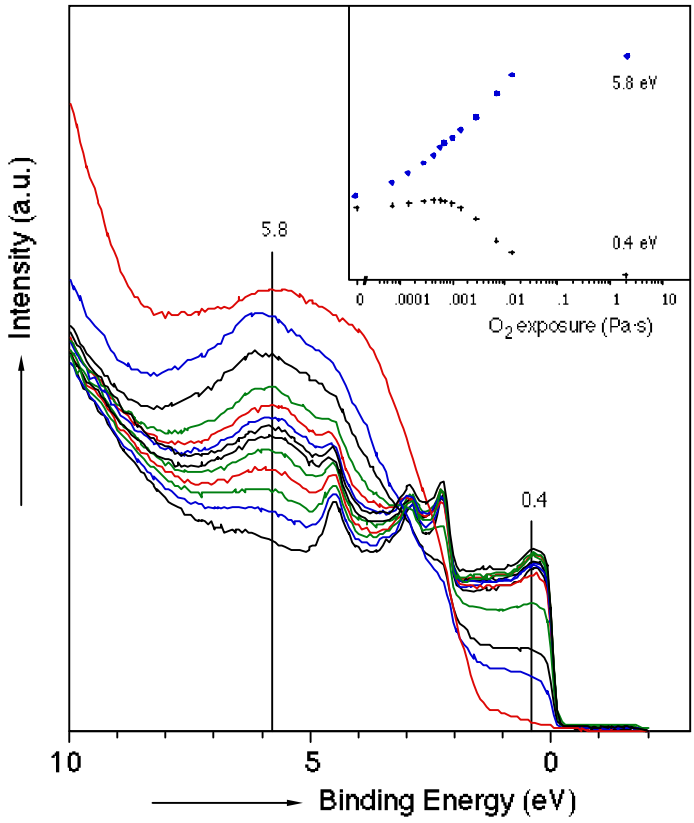

Figure 5 *As Fig. 4 for 3 ML of Fe.*

only for the final exposure (2 Pa·s, and in this case only the discharge was stopped, not the He flow) in order to acquire lamp conditions as similar as possible. However, a small drift in the photon flux due to small pressure variations can not be excluded and may influence the absolute values of the spectra. To show the development of the O 2p band and the decrease of the Fe 3d band near the Fermi level more clearly, an inset representing the intensity of the valence band spectra at 5.8 and 0.4 eV is given in every figure. The vertical dashed lines indicate these two energies.

In all spectra an immediate formation of the O 2p becomes visible when the oxidation starts. In fact, for 3 ML and bulk like iron the O 2p is already visible in the first spectrum due to small contamination occurring during deposition. This direct growth of the O 2p band is in agreement with what is reported for bulk iron by Brundle [78]. It also appears to agree with what is seen in the analysis of the Fe $M_{2,3}VV$ peak shape of 1 ML of iron on Cu(100) during oxidation [46]: the low energy Fe oxide peak ascribed to a $Fe_{M2,3}Fe_{M4,5}O_{L2,3}$ cross-transition increases first and fast with increasing amount of oxygen. The coincidence of this immediate increase of the O 2p feature (whereas other changes in the valence band occur slower) and the same initially fast growth of the low energy iron oxide Auger peak seems to give further evidence for the Auger feature being indeed a cross-transition. The suggestion given by Ramsey and Russel [77] that this Auger feature is due to changes in the 3d band structure of iron is clearly contradicted by the change of the iron 3d band in the UPS spectra which appears to happen slow for the first mPa·s.

The initially slow change in the intensity of the Fe 3d band near the Fermi level is strange regarding the fact that each adsorbed oxygen atom may be expected to take up 2 electrons out

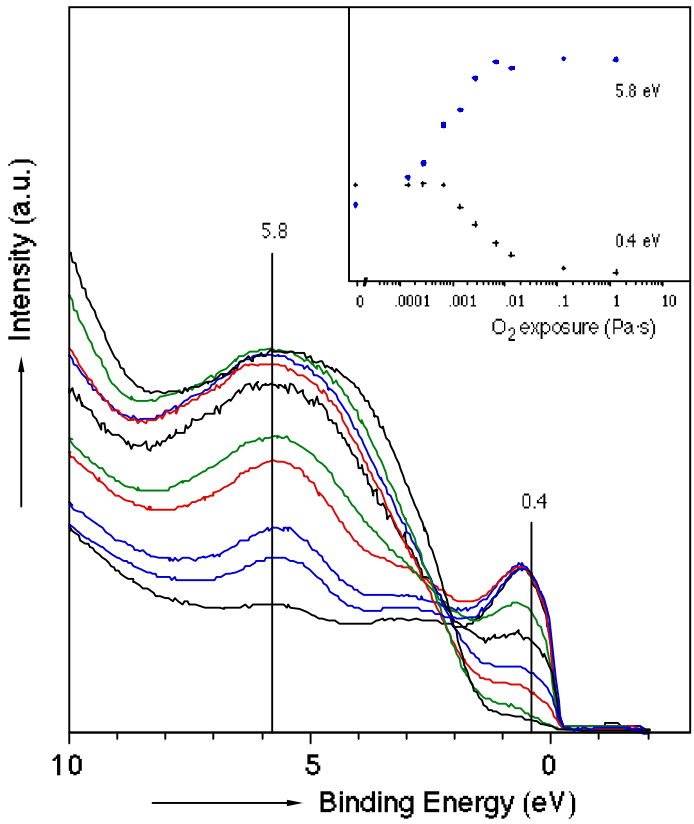

Figure 6 *As Fig. 4 for bulk like Fe (25 ML).*

of this band inducing a fast decrease of Fe 3d electrons and thus a fast decrease of this band. Though the oxygen 2p may be more intense because the 2p orbital already contains 4 electrons and is thus 'highly visible' with and without the 2 extra electrons, the removal of the two electrons out of the 3d band near the Fermi level is also expected to move these states to a higher binding energy. Apparently this does not happen (or at least not completely) for the first amount of oxygen. This may explain the 'invisible' oxygen as found with ellipsometry [82] without contradiction by the nearly linear decrease of the metallic Fe $M_{2,3}VV$ peak [46] and the metallic Fe 2p peak [93] in the peak shape analysis as function of the amount of oxygen.

The relatively slow decrease of the 3d band is near the Fermi level is less clear in the spectra of the surface containing 0.5 ML of Fe (Fig. 4) than for the other two surfaces studied because the amount of oxygen in respect to the amount of iron is higher at lower exposure for this surface since the initial sticking probability is the same for all iron containing Cu(100) surfaces [82].

7

The interaction of CO and H_2 with oxidised Cu(100)-Fe surfaces.

The interaction of oxidised Cu(100)-Fe surfaces containing 0.1 - 2.0 ML of iron with H_2 and CO has been studied. Surfaces containing more than 0.8 or 0.6 ML of iron which are oxidised at 300 K are inert to respectively CO and H_2 at 630 K and pressures up to 0.2 Pa. CO can remove only oxygen bound to copper and when bare copper sites are available. Hydrogen also requires uncovered copper for reaction but then all oxygen can be removed.

Further oxidation at 630 K induces the iron oxide formed at 300 K to reorganise in such a way that free copper sites are formed and both H_2 and CO can react with oxygen from the surface.

7.1 Introduction.

This chapter deals with the reduction of oxidised Cu(100)-Fe surfaces with CO and H_2. The reactivity of both gases with oxidised copper-iron surfaces prepared on Cu(111) and Cu(110) has been studied by Van Pruissen et al. [29,32,34]. For Cu(111)-Fe surfaces they report that CO can remove only oxygen bound to copper - under the reaction conditions used - unless γ-Fe_2O_3 was present initially. γ-Fe_2O_3 could be reduced to Fe_3O_4. On Cu(110)-Fe surfaces all oxygen bound to copper could be removed and a small part of the oxygen of the $Fe_{0.95}O$ present on these surfaces. Using hydrogen it was possible to reduce both copper-iron surfaces completely. On Cu(111) they determined that the reaction rate was of half order in the hydrogen pressure. This is different from the first order which is found for the kinetics of the hydrogen interaction with both oxidised copper and iron surfaces [34,59,94]. Vink et al. [59] determined that the dissociation of H_2 is the rate determining step in the reduction of iron oxide on Fe(100) with hydrogen. The half order dependence of the reaction rate of p_{H_2} means that the hydrogen dissociation can not be the rate determining step in the reduction and they ascribed it to the presence of single iron atoms in the copper surface or to small clusters of iron atoms which facilitate hydrogen dissociation.

7.2 Results and Discussion.

Oxidised Cu(100)-Fe surfaces were prepared by evaporating 0.1 - 2.0 ML of iron and exposing the Cu(100)-Fe surface to oxygen until saturation was reached at room temperature. As described in chapter 3 - 6, the oxygen present at the surface occurs in two forms, as Fe_2O_3 and as half a monolayer of oxygen bound to copper and/or the Fe_2O_3-Cu interface. The total amount of oxygen is then $0.5+1.5\cdot\theta_{Fe}$. On heating the crystal to temperatures at which CO and H_2 were to be exposed (i.e. 630 K) the amount of oxygen present at the surface decreased according to AES measurements. No relationship between the amount of remaining oxygen and θ_{Fe} could be found, though the remaining amount of oxygen was always larger than $1.5\cdot\theta_{Fe}$. No change in the Fe $M_{2,3}VV$ peak shape was observed after heating, which means that no metallic iron was present. When reduction of this surface proceeds in the reverse order with respect to oxidation, reduction should go via an intermediate containing Fe^{3+}, Fe^{2+} and Fe^0 to Fe^0. The metallic iron produced in this process should either contribute to the Fe $M_{2,3}VV$ peak or dissolve in the Cu. Since both changes are not observed there is no reason to expect the stoichiometry of the iron oxide to change from Fe_2O_3 upon heating. As oxygen is not expected to desorb from these surfaces the oxygen probably diffuses into the bulk of the crystal, where it is undetectable for AES. On surfaces containing less than 0.2 ML of iron this happened at a high rate: ca. 30 min. after the start of the heating the oxygen signal had decreased to 75% of the original signal. However, since ellipsometry has a depth sensitivity which is at least one order of magnitude larger than that of AES it is expected that the oxygen is still visible with $\delta\Delta$.

The use of the parameter $\delta\Delta$ in this chapter is slightly different from that used in the rest of this thesis. In this chapter $\delta\Delta$ represents the change in Δ, i.e. $\Delta^0-\Delta$ where Δ^0 is the value of Δ of the Cu(100)-Fe surface after iron evaporation, oxidation at room temperature and heating the crystal to the temperature at which the reaction was to take place. This means that any changes in Δ due to oxidation and heating of the surface are not included in $\delta\Delta$.

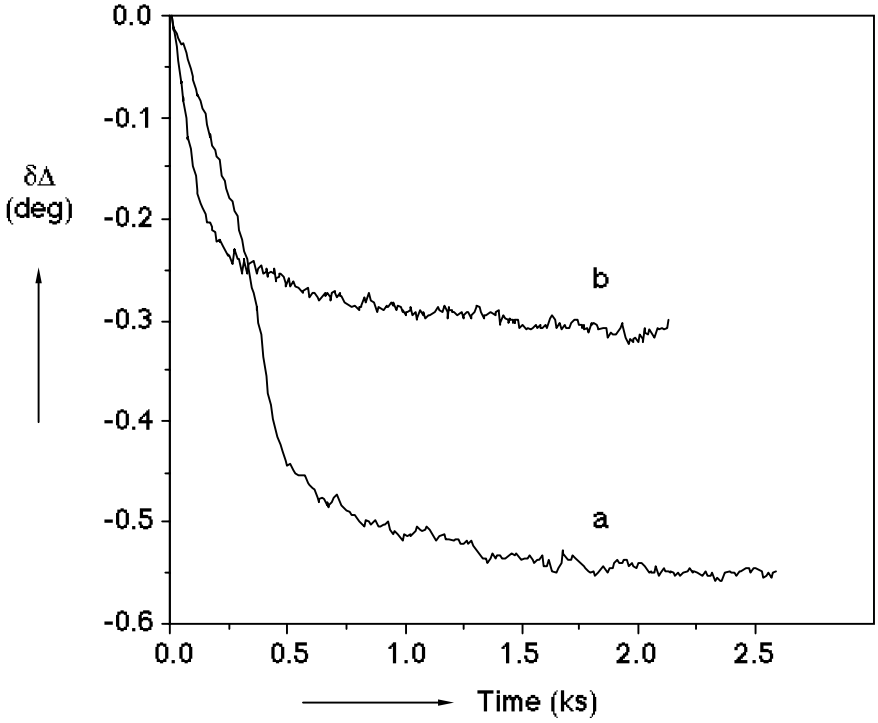

Figure 1 *The change in Δ as function of the CO exposure of two Cu(100) surfaces containing 0.2 ML of iron oxidised at 300 K. The CO pressure was 0.02 Pa and the crystal temperature 630 K. The difference between curve (a) and (b) is explained in the text.*

7.2.1 Interaction with CO.

The reactivity of these surfaces towards CO was studied at 630 K and pressures up to 0.1 Pa. For surfaces containing more than 0.8 ML of iron no change in Δ was observed. Surfaces containing less iron showed a decrease in δΔ. The total change in δΔ seemed to be smaller for high than for low iron coverages and thus more oxygen could be removed from a surface with small iron coverages. However, these reduction curves did not reproduce very well. The irreproducibility of these results is probably caused by small differences during the preparation which is reflected in the oxygen distribution before the reduction. Since AES measurements revealed that all iron remained at the surface and that at least $1.5 \cdot \theta_{Fe}$ oxygen was present after the CO exposures the oxygen removed was probably connected to copper. From oxidation experiments it appeared that the Fe is first oxidised before oxygen adsorbs on the copper interface. This indicates, as could be expected from (bulk) thermodynamic data, that oxygen is preferentially bound to Fe. These observations suggest that CO can not reduce the Fe_2O_3 on these surfaces. This is different from what happens on Cu(111)-Fe and Cu(110)-Fe surfaces. On these surfaces it appeared to be possible to reduce the iron oxide partly [29,32]. The lack of reactivity (under these conditions) of surfaces containing more than 0.8 ML of iron can be explained assuming that CO requires free copper sites before it can react with oxygen bound to copper. This is also the case for oxidised Cu(100) surfaces without Fe [95]. The absence of an iron oxide free surface for $\theta_{Fe} \geq 0.8$ was also found in previous experiments with different amounts of iron on Cu(100) at 300 K. These showed that the contribution of oxygen adsorbed on Cu(100) to the change in Δ due to oxidation was negligible for $\theta_{Fe} > 0.8$ [82].

In Fig. 1 two reduction curves of two freshly prepared surfaces containing 0.2 ML of iron are shown as function of time. The pressure was 0.02 Pa for both experiments. Though the total change in $\delta\Delta$ due to the reduction is different for both reductions, it must be mentioned that the shape of the curves is identical at the end of the reaction. When curve (b) is shifted down by 0.25° in Δ and in time by ca. 500 s both curves are overlap each other within experimental error. A similar behaviour was observed for the CO interaction with oxygen adsorbed on pure Cu(100) [95] and could be explained with a model of competitively adsorbed O-atoms and CO molecules of which the reaction to CO_2 is rate limiting. The slow start of the reaction (curve (a)) is then due to a lack of free sites on which CO can adsorb. On the surface of curve (b) free sites were already present at the start of the CO exposure, allowing a fast reaction from the beginning. The amount of oxygen as determined with AES confirms this mechanism since on the surface of curve (a) more oxygen (0.2 ML) was present than on that of curve (b) after heating to 630 K. Apparently the oxygen has disappeared from the 'bare' copper surface.

Although oxygen disappears from the surface as seen by AES and probably migrates into the bulk upon heating this does not explain why it is not possible to remove it with CO as seen by $\delta\Delta$. On pure copper single crystals it has always been possible to remove all of the oxygen even when it had penetrated into the bulk [34,58,96]. Apart from desorption, which is highly unlikely, one explanation is that the migration of oxygen in copper is so fast that it disappears from the "sight" of the ellipsometer. In principle it is possible to calculate the depth sensitivity of an ellipsometer from the refractive indices of the components, the angle of incidence and the wavelength of the light used. However, the refractive index of a solution of oxygen in copper (with an unknown concentration profile) is unknown. So it is impossible to make an exact calculation of the depth sensitivity. Based on the refractive index of copper and an angle of incidence of 0° an indication of the order of magnitude can be obtained using $\lambda/(4\pi k)$, where k is the imaginary part of the refractive index. The result is 140 Å. It seems not impossible that oxygen migrates fast enough at 630 K to reach even greater depths in the ca. 1 hour needed for temperature equilibration, AES measurements and outlining the ellipsometer. As the presence of iron (oxide) enables the oxygen to penetrate the bulk at temperatures at which it is stable on clean Cu single crystal surfaces it also might enhance the mobility of oxygen in the bulk. Alternatively dissolved oxygen may remain in the copper near surface region below the iron oxide, where its stability is enhanced.

To get some more information about the reactivity of these surfaces towards CO a surface containing 0.8 ML of iron was oxidised again at 630K after oxidation at 300K. It should be realised that the extra oxygen adsorbed must be present mostly as penetrated into the copper since no indication for changes in the oxidation state of iron could be found after this oxidation. Fig. 2 shows four consecutively obtained reduction curves of one surface for which the oxidation and reduction was repeated, curve (a) to (d). The fourth reduction of an other surface with the same θ_{Fe} is also shown (curve (e)). Curves (a), (b) and (d) are obtained using 0.05 Pa, (c) at 0.02 and (e) at 0.1 Pa. The arrows in Fig. 2 indicate the change in Δ due to the oxidation at 630 K before and between the different reductions: arrow 1 before reduction (a), arrow 2 between (a) and (b) etc. During the reduction of curve (a) more oxygen could be removed than was adsorbed at 630 K (arrow 1). Thus part of the oxygen which was adsorbed at 300 K is also removed. During the other 3 reductions all oxygen adsorbed at 630 K could be removed with CO. It is remarkable that the shape of the curve changes after the first reduction. However, the shape of the curves resembles strongly those of the CO-reductions of oxidised

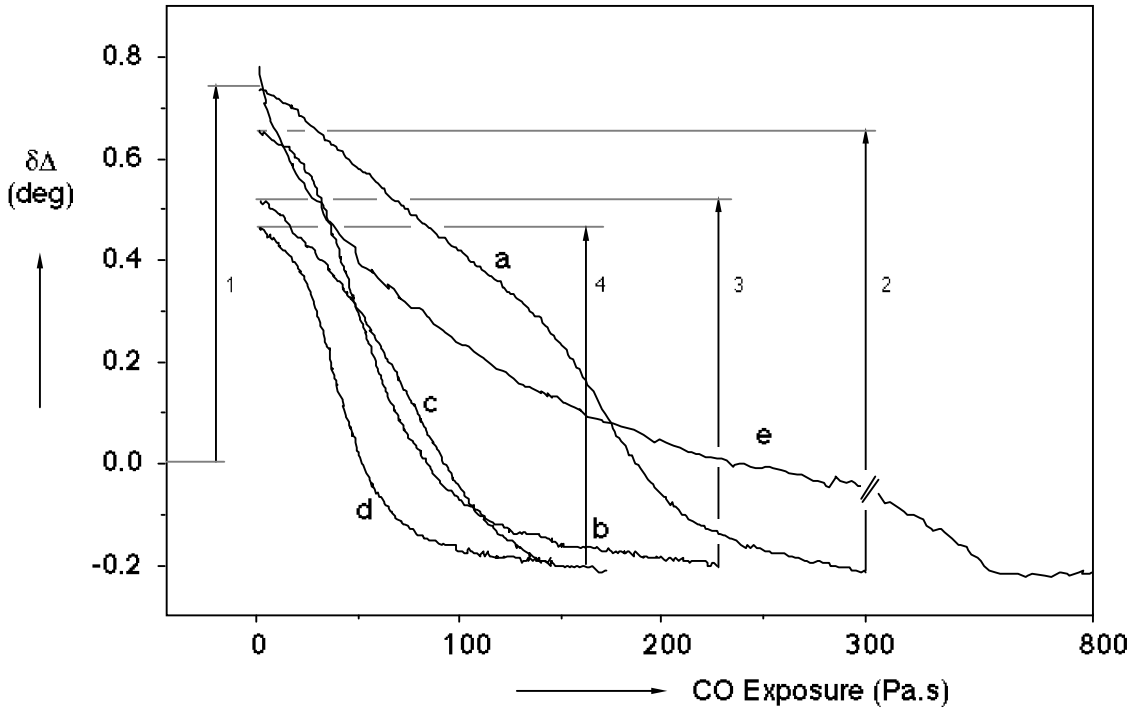

Figure 2 *The change in Δ as function of the CO exposure of a Cu(100) surface containing 0.8 ML of iron oxidised at 300 K and reoxidised at 630 K. Curves (a) to (d) are taken consecutively on one surface; the first arrow indicates the change in Δ due to the first oxidation at 630 K, the second arrow represents the second oxidation performed after the reduction (a) and before reduction (b) etc. Reduction curve (e) is the fourth reduction observed on a new prepared surface.*

Cu(100)-Fe surfaces [32] and oxidised Cu(100) surfaces [95]. For those surfaces a model of the reaction mechanism was given which explains the shape of the curves. This model is based on two competitive events: the formation of free sites (needed for CO adsorption) by the reaction of adsorbed CO and oxygen and the refilling of those sites by subsurface oxygen. Which of both processes is rate determining depends on the temperature, which influences the reaction constants of the CO_2 formation and of the refilling of the surface sites with subsurface oxygen, the CO adsorption equilibrium constant and the CO pressure. A difficulty occurring on these surfaces is the irreproducibility of the reduction curves which is probably due to a changing surface structure, i.e. a change of the iron oxide clusters and thus of the amount of 'free' copper surface and a change in the oxygen distribution in the crystal. Van Pruissen et al. could obtain reproducible results on Cu(111)-Fe surfaces after 3 oxidation-reduction cycles [29] but because of a much higher iron content of their surfaces and their preparation method their surfaces were in a much more stable state than the surfaces used in this study. However, though all curves as determined on the Cu(100)-Fe surfaces can be fitted with the model, the number of free parameters must be too large to draw any conclusions from this small data set.

Both the qualitative agreement of the reaction kinetics with that of pure copper surfaces and the fact that reaction is possible after oxidation at 630 K indicates that the surface must change under influence of oxygen. Apparently the iron oxide reorganises leaving free copper surface. The iron oxide is expected to remain at the surface thus to create free surface three dimensional clusters must be formed at the surface. The LEED pattern of these surfaces is similar to that observed after oxidation at 300 K [82] though a bit more diffuse.

7.2.2 Interaction with hydrogen.

Several surfaces containing 0-1.3 ML of iron were (after complete oxidation at 300 K) exposed to hydrogen at pressures varying between 0.01 and 0.2 Pa at a crystal temperature of 630 K. For surfaces with θ_{Fe}>0.6 ML no reaction was observed. Surfaces containing less iron could be reduced completely. As for the CO reduction experiments the interaction of these surfaces with hydrogen reproduced badly. However, in contrast to the CO reduction all oxygen could be removed as seen with AES. Although one would expect the change in the parameter Δ to be as large as upon oxidation (but of opposite sign), the change in Δ due to the removal of oxygen is different, i.e. smaller, than that during oxidation of the surface at 300 K. This can be explained by two effects: the first is the already mentioned migration of oxygen into the bulk out of "sight" of the ellipsometer and the second is the reorganisation of the compounds in the surface region: e.g. cluster formation and diffusion of iron into the copper substrate. In the CO experiments the final situation consisted of iron oxide on a copper surface, here we are left with metallic iron. However, the effect of changes in the distribution of the surface compounds (or even surface morphology) is difficult to predict or to determine. Both the dissolution of iron and oxygen are enhanced at high temperatures and could therefore be inhibited at low temperatures but in that case no reaction with H_2 occurs. A change in the iron distribution, however, can be seen with AES which shows that both the ratio of the Fe/Cu $M_{2,3}VV$ and the Fe $L_{2,3}M_{2,3}V$ / Cu $L_{2,3}VV$ peaks had decreased strongly compared to that directly after evaporation. This indicates that the iron migrates into the crystal at these temperatures. The migration is also observed in some of the other experiments on Cu(100)-Fe surfaces and by Van Pruissen et al. on Cu(111)-Fe and Cu(110)-Fe [29,32]. The effect of this changed distribution of the iron on Δ is expected to be small with respect to the change in Δ due to oxidation. So the explanation based on the oxygen migration is preferred.

Fig. 3 shows some reduction curves of surfaces containing small amounts (θ_{Fe}<0.3) of iron. The change in Δ is initially fast which may be ascribed to the reaction of hydrogen with oxygen bound to copper and slows down after some time where the reduction of iron oxide takes place. Since not all iron segregates upon reoxidation (at least at low temperature) and there seems to be a large difference in reactivity of surfaces oxidised at high and at low temperature as will be discussed later, a new surface had to be prepared after each reduction. The difficulty to prepare exactly reproducible surfaces makes the determination of the order of the reaction in the H_2 pressure impossible.

Conclusions here must be restricted to the observation that the reactivity of these surfaces towards H_2 decreases with increasing θ_{Fe} and since the coverage at which no reaction is observed is nearly the same as for the CO reduction it may be concluded that on these systems a copper surface free of iron oxide is required for the reaction (probably H_2 dissociation).

For surfaces containing more than 0.6 ML of iron the initial reactivity towards H_2 was too small to be detected at the reaction conditions used in this study. So some experiments were performed to examine whether it is possible to activate the surface and to elucidate the reasons of the inactivity.

A simple oxidation at 630 K (after a normal room temperature oxidation) appeared to be sufficient to activate a surface containing 0.8 ML Fe for reduction with H_2. As on the surfaces with a low iron coverage all oxygen could be removed (according to AES) and the iron diffused into the bulk of the copper crystal. Apparently oxidation at elevated temperatures has an important influence on the surface as seen by the hydrogen molecules. Apart from the effects

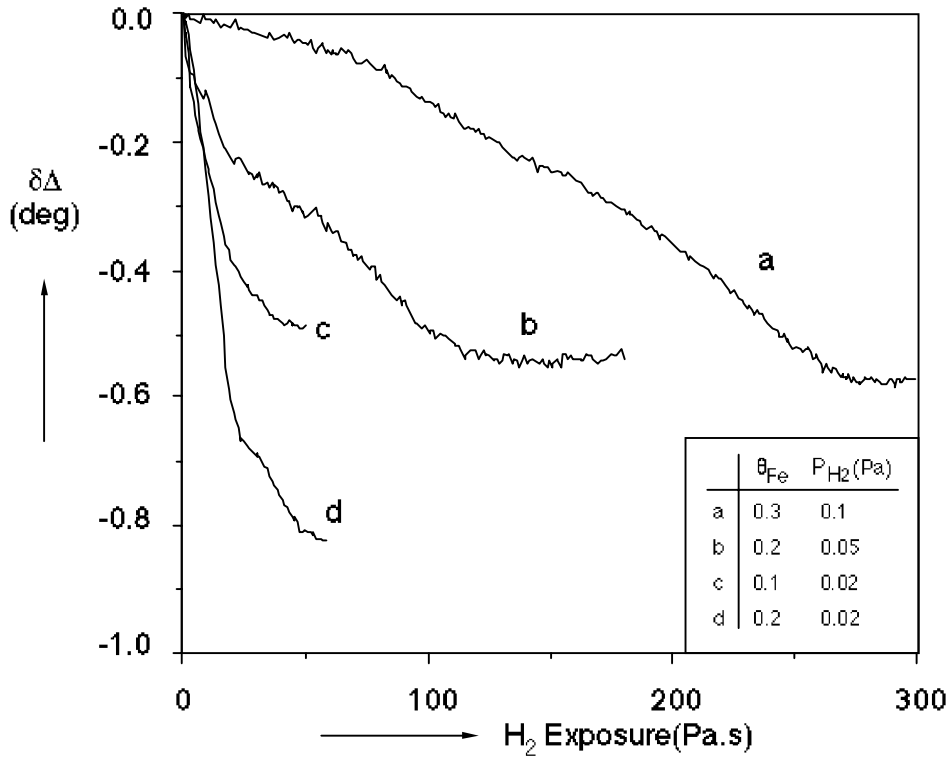

Figure 3 *The change in Δ as function of the H_2 exposure of Cu(100) surfaces containing different amounts of iron oxidised at 300 K. The crystal temperature was 630 K.*

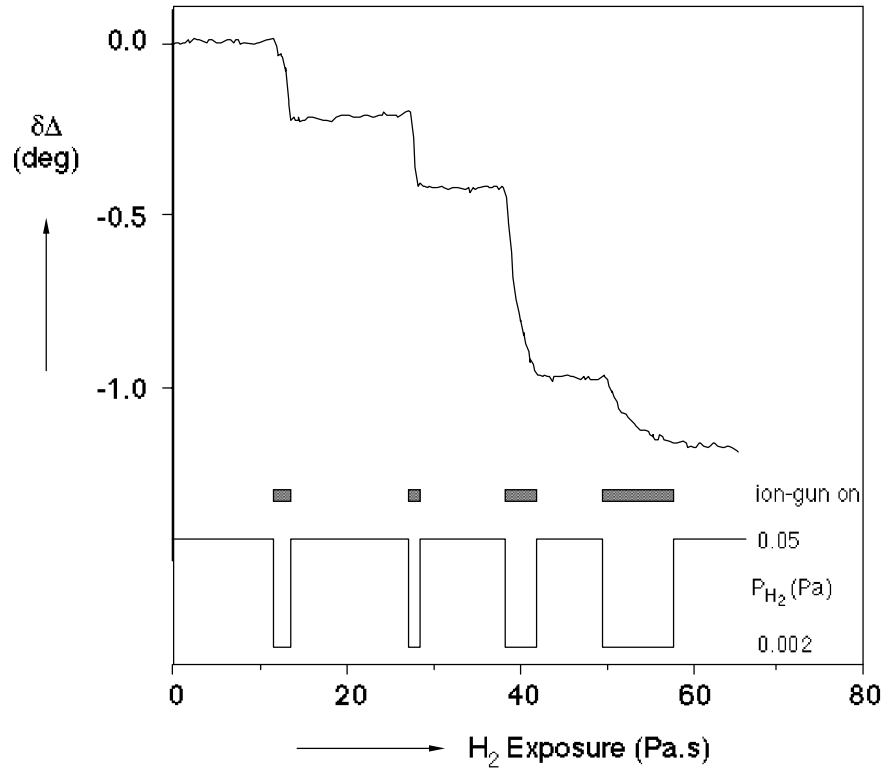

Figure 4 *The change in Δ as function of the H_2 exposure of a Cu(100) surface containing 1.0 ML of iron oxidised at 300 K. The crystal temperature was 630 K. The H_2 pressure is given in the lower part of the figure and the dotted rectangles indicate the periods during which the ion gun was switched on.*

of oxidation at high temperature on the structure of the of the iron oxide layer as was already indicated in the discussion of the CO reduction experiments, also defects in the iron oxide structure may be created. A second experiment which may give more information about this possibility was performed: 0.5 ML Fe was evaporated onto a surface already containing 1.0 ML of iron which was partly oxidised at 300 K and exposed to H_2. This surface did not show any reactivity towards H_2 at 530 K. This low temperature was used in the hope to keep the metallic iron at the surface. Although this experiment was meant to induce surface defects this is either not possible or the wrong type of defects was created.

In a third experiment the reduction of the surface (1 ML Fe) was initiated by 'activated' H_2. To perform this experiment the ion-gun was switched on at $2 \cdot 10^{-3}$ Pa with the rear end of the crystal directed to the ion beam and the front grid of the Retarding Field Analyser was kept at a potential 100 V above the acceleration voltage of the ion-gun. The reaction was monitored with the ellipsometer. Fig. 4 shows the results of the experiment with the activated H_2. It is clear that the reaction is very fast when the ion-gun is switched on and stops completely when it is turned off (note the higher pressure when the gun is off: 0.05 Pa). It may be remarked here that in a similar experiment performed on an oxidised Fe(100) surface ($\delta\Delta$=7°) the reaction rate was increased by a factor 500 when turning on the ion-gun. With this difference in reactivity in mind one should expect to see reactivity (if there is any) in the experiment when the ion-gun is turned off and the pressure is increased by a factor 25. However, the surface remains inert. Also here, reduction was possible after a high temperature reoxidation of a (ion-gun assisted) reduced surface.

The experiments described above strongly indicate that on these surfaces copper sites free of iron oxide (but not necessarily free of oxygen) are required for reaction of hydrogen with oxygen on the surface and that the surface of the iron oxide is not able to adsorb or dissociate H_2 in reasonable amounts. Apparently the iron oxide is stabilised by the underlying copper. This might be due to a higher affinity of iron than of copper towards oxygen. Whereas on pure (oxidised) iron surfaces surface defects can be created at low cost by migration of oxygen into the (iron) bulk this may be less favourable when copper is present directly under the iron oxide layer.

7.3 Conclusions.

1. The Cu(100)-Fe surfaces as prepared in this study are not very stable at high temperatures. Iron, but not iron oxide, dissolves into the copper crystal.
2. CO reacts only with oxygen bound to copper.
3. The reaction mechanism seems the same as for iron free Cu(100) though the iron oxide blocks the surface for CO adsorption and thus for reaction.
4. Hydrogen requires copper surface free of iron oxide for reaction and then all oxygen can be removed.
5. Iron oxide on Cu(100) is more stable towards H_2 than iron oxide on bulk iron.
6. Iron oxide probably forms three dimensional clusters upon oxidation at 630 K.

8

The interaction of CO with Cu(100)-Fe surfaces

Abstract

The interaction of CO with Cu(100)-Fe surfaces containing 0 to 1.7 ML of Fe was studied with ellipsometry and Auger electron spectroscopy. Only reversible molecular adsorption was observed. Dissociation was not observed at temperatures up to 620 K and pressures up to 0.1 Pa. Apparently fcc iron (100) surfaces do not dissociate CO under these conditions.

Depending on the iron coverage and the pre treatment of the surface a fast and a slow adsorption stage is observed. The fast adsorption only occurs on surfaces containing iron clusters or on surfaces completely covered with iron whereas slow adsorption occurs only on surfaces on which bare copper surface is present. During the slow adsorption stage iron carbonyl-like species are formed, iron clusters are broken up in single iron atoms or both processes occur together.

Since the Cu(100)-Fe surfaces are not thermo-stable it was not possible to determine the heat of adsorption.

8.1 Introduction.

The interaction of CO with pure iron and iron alloys has already been subject of several studies [6,29,97-99]. The motivation of these studies is, besides the fundamental interest in these systems, also their importance for the Fischer-Tropsch synthesis. The reason to investigate iron alloys is that the common used iron catalysts quickly deactivate due to the formation of iron carbides [100]. The use of iron alloys can probably prevent the formation of carbides. Nickel-iron surface alloys were investigated by Vreeburg [98]. Copper-iron surface alloys were investigated by Van Pruissen et al. [29], Gijzeman et al. [97] and Boellaard [99] and are also the subject of this paper. On Cu-Fe alloy surfaces Van Pruissen et al. observed both molecular and dissociative adsorption. Reversible molecular adsorption was observed after an initial saturation of the surface by equal amounts of carbon and oxygen due to dissociation of CO. The amount of molecularly absorbed CO did not increase when more than about four monolayers of iron were deposited, but one should remember that the iron is spread over several layers implying an unknown surface concentration. For Cu(111)-Fe they found a heat of adsorption of 70±15 kJ/mol, independent of the coverage and iron content [29]. This ΔH_{ad} is lower than the initial ΔH_{ad} found by Vink et al. [6] on a Fe(100) surface containing 0.25 ML of C and O: 100±5 kJ/mol. And it is somewhat higher than ΔH_{ad} on Cu(100) which is 50-70 kJ/mol [5]. Boellaard et al. studied CO adsorption on alumina supported Cu-Fe catalysts. They observed CO induced iron segregation, irreversible CO adsorption on the iron sites and iron carbide formation (at elevated temperatures) due to dissociation of iron.

The composition of Cu(100)-Fe surfaces is quite different from the surfaces prepared by Van Pruissen et al. As mentioned in chapter 1, the use of an evaporation source (at room temperature) initially gives epitaxial iron islands on the copper surface followed by a layer-by-layer growth (4 - 11 ML), instead of a mixture of iron and copper. According to Wuttig et al. [13] the presence of CO during evaporation induces a longer region of layer-by-layer growth. This effect is already found for CO pressures of $7 \cdot 10^{-8}$ Pa indicating a strong interaction of the few adsorbed CO molecules since no adsorption could be detected at this pressure. The copper/iron surfaces are not stable, even at room temperature slow changes occur [7-11,20]. It will be clear that this reorganisation of the surface atoms will have a great influence on the properties of the surface towards CO-adsorption.

In this chapter the interaction of CO with Cu(100)-Fe surfaces and the effect of temperature induced surface changes on the interaction is studied. A possible explanation for the adsorption mode and the unexpected non-dissociative adsorption of CO on these surfaces will be given. The technique used to study the CO adsorption is ellipsometry.

8.2 Experimental.

The amount of CO adsorbed was determined with ellipsometry. For some experiments it was interesting to observe changes in CO coverage with changing temperature. However, temperature dependent measurements had to be corrected for a reversible change in Δ (and Ψ) due to a small displacement of the crystal caused by the temperature change. Within the temperature range used, this artificial change in Δ was linearly proportional to the temperature. Changes in the iron distribution in the surface layers due to temperature enhanced migration appeared to have no influence on $\delta\Delta$ because after cooling down Δ came back to its original

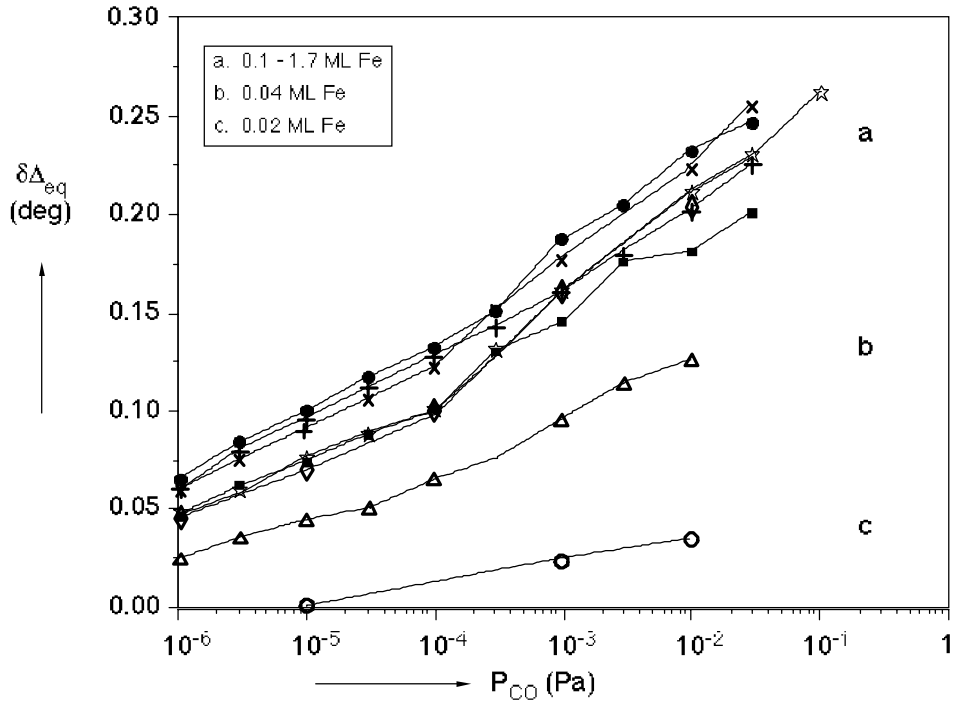

Figure 1 *Isotherms (T = 298 K) of CO adsorptions on Cu(100) surfaces containing different amounts of iron: 0.02 ML (o), 0.04 ML (•), 0.1 ML (■), 0.3 ML (+), 0.6 ML (●), 0.8 ML (x), 1.0 ML (•) and 1.7 ML (☆).*

value within 0.01°. All the ellipsometry data used in this paper are corrected for the artificial changes due to the temperature.

8.3 Results.

The CO-adsorption isotherms of freshly prepared Cu(100)-Fe surfaces containing 0.02 - 1.7 ML Fe taken at 300 K are shown in Fig. 1. The isotherms were obtained by continuously exposing CO at increasing pressures. After each pressure rise sufficient time was waited to determine $\delta\Delta$ at the equilibrium coverage ($\delta\Delta_{eq}$). After desorption $\delta\Delta$ returned to zero and with AES no carbon and oxygen could be detected. Saturation of the surfaces with CO is obviously not reached for the pressures used. Unfortunately higher pressures than 0.1 Pa could not be used due to the possible formation of $Ni(CO)_4$ in the stainless steel UHV system in combination with exposure times of hours required to reach equilibrium. In fact these long exposures needed were the reason that most of the experiments in Fig. 1 were already stopped before reaching 0.1 Pa.

On this kind of surfaces the heat of adsorption (ΔH_{ad}) and the dependence of ΔH_{ad} both θ_{Fe} and θ_{CO} are highly interesting. To determine ΔH_{ad} adsorption isotherms must be collected at different temperatures. However, the Cu(100)-Fe surfaces are not thermo-stable. The influence of the instability on the adsorption behaviour was checked by exposing CO to surfaces which were previously heated to a certain temperature. The heating procedure consisted of a fast heating to the temperature mentioned after which the crystal was directly allowed to cool down. Due to the large sample holder the cooling process was slow. This means that the crystal was 15-30 min. at a temperature near to the one mentioned. However, important here is not the

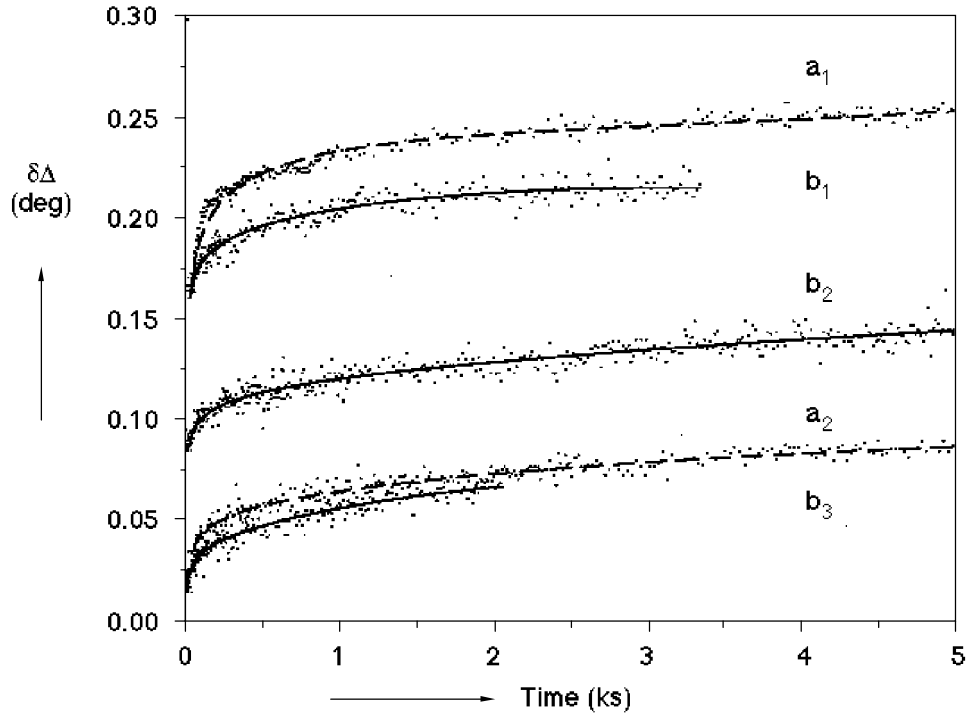

Figure 2 *The change in Δ as function of the time for CO pressures of 0.01 Pa at room temperature for Cu(100)-Fe surfaces containing (a) 0.8 ML Fe and (b) 1.0 ML Fe, annealed at different temperatures. a_1: not annealed, a_2: annealed at 500 K, b_1: annealed at 330 K, b_2: annealed at 380 K and b_3: annealed at 620 K.*

exact time of the heat treatment (since the equilibrium situation is far from what we want) but a change in surface composition. Some adsorptions after different heat treatments are shown in Fig. 2. In this figure δΔ is plotted against the time of CO exposure (P_{CO} = 0.01 Pa). All adsorptions are performed at room temperature. Curves a_1 and a_2 represent the adsorption on a surface containing 0.8 ML of iron. Curve a_1 is taken on a fresh prepared surface and a_2 for a surface which has been heated to 500 K. The curves b_1-b_3 are taken on a surface containing 1.0 ML Fe. The curve of a fresh prepared surface is not shown but it closely overlaps the curve of the fresh prepared θ_{Fe}=0.8 surface (a_1). The curves b_1, b_2 and b_3 are obtained on surfaces previously heated to respectively 330, 380 and 620 K. It is clear that a the total amount of CO adsorbed on these surfaces decreases with a more severe heat treatment of the surface. Of course this makes the determination of ΔH_{ad} at temperatures above 300 K impossible. The use of lower temperatures, however, is not possible in the UHV system used and also adsorption of CO on the Cu(100) surface could disturb the experiment in that case [102].

As already mentioned the time scale of the adsorption experiments is large. Therefore an adsorption experiment is shown in more detail in Fig. 3. In this figure the change in Δ due to the CO adsorption on a Cu(100) + 1.0 ML Fe surface is shown as function of time. Also the temperature during the experiment is shown. Though not really important here, the surface had been heated for 30 min. at 380 K which is the reason why the equilibrium coverage is smaller than expected from Fig. 1. Directly after the beginning of the CO exposure (P_{CO} = 0.01 Pa) δΔ rises quickly to approximately 0.09°, after which δΔ continues increasing slowly to the equilibrium coverage of approximately 0.16°. In the experiment shown in Fig. 3 the system was evacuated before the equilibrium coverage at room temperature was reached. As expected,

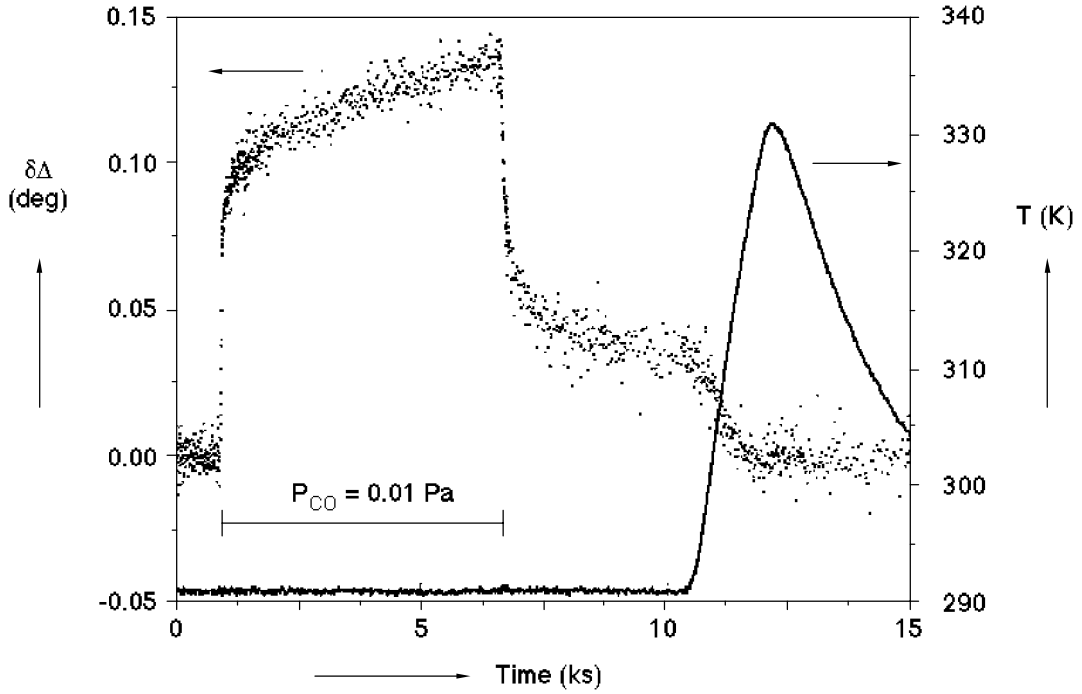

Figure 3 *The change in Δ and the temperature during a CO adsorption (at P_{CO} = 0.01 Pa) and desorption on a Cu(100) surface containing 1.0 ML of iron. The surface was annealed at 380 K before the measurement.*

evacuation results in a direct and fast decrease of the CO coverage until the last 0.04° which only desorbs very slowly. However, a temperature rise of only some 40 degrees causes the CO to desorb completely, δΔ returns to zero and no carbon or oxygen contamination could be detected with AES.

8.4 Discussion.

The adsorption of CO on Cu(100)-Fe surfaces appears to be reversible and molecular since all CO desorbs and no dissociation products could be found within the detection limit which is about 0.02 ML for oxygen. Even when CO is exposed at high temperatures (up to 620 K) and at 0.1 Pa no carbon or oxygen contamination could be detected afterwards.

This reversible molecular adsorption is in strong contrast with the behaviour of CO on pure Fe surfaces [6], Cu(111)-Fe and Cu(110)-Fe surfaces [29,97] and Ni(111)-Fe surfaces [56] since on all these surfaces CO dissociates. The lack of dissociation on the Cu(100)-Fe surfaces at low temperatures is probably be due to the (100)-fcc structure in which the iron is present on the surface. Gijzeman [103] calculated for the Ni(111)-Fe surface that dissociation probably only occurs on iron clusters consisting of three atoms which are not all three neighbours but bend under an angle of 120°. These clusters can not exist on the fcc-(100) surface. Dissociation can occur on the bcc surfaces without hexagonal symmetry because of the more open structure of these surfaces, and on the Cu(110)-Fe surfaces of Gijzeman et al. [97] due to the presence of bcc iron on these surfaces.

When the isotherms taken on Cu(100)-Fe surfaces are compared with those taken on Cu(111)-Fe and Cu(110)-Fe surfaces [29,97] the difference seems to consist mainly of a larger change in Δ on Cu(100)-Fe surfaces than on those of refs. [29,97] ($\delta\Delta_{max}$•0.29° as compared to

0.08°). However, on the surfaces described in [29,97] adsorption took place on a surface saturated with the dissociation products of CO. This may be the explanation that on the Cu(100)-Fe surfaces significantly more CO adsorbs. For clean Fe(110) Gijzeman et al. [97] saw a decrease in the amount of CO adsorbed with an increasing oxygen coverage. A second explanation may be that before performing the CO adsorption experiments the surfaces used in [29,97] were oxidised and reduced at high temperatures (~600 K) to remove contamination. However, the high temperature also induces segregation of copper atoms [9,11]. This implies that the number of iron atoms in the surface layer is unknown and could be smaller than on Cu(100)-Fe surfaces.

The most striking observation from Fig. 1, however, is that the amount of CO adsorbed at a given pressure increases with θ_{Fe} until θ_{Fe} reaches 0.1. For higher iron coverages the isotherms overlap within experimental error. Though at 0.1 Pa saturation of the surface with CO obviously is not reached yet it is remarkable that at iron coverages much smaller than 1 ML the same amount of CO can be adsorbed. To be able to say more about this it is required to know more about the amount of CO adsorbed on the surface. An approximation of the absolute coverage can be given by using the absolute coverage of CO on Fe(110) as calculated by Gijzeman et al. [97]. For clean Fe(110) they found a saturation coverage of $\delta\Delta$=0.38°, which corresponds with $6.2 \cdot 10^{18}$ molecules per m^2 [25]. Assuming a linear sensitivity of Δ for θ_{CO} (which is done implicitly but with success for CO-adsorption on Fe, Ni, Ni(111)-Fe, Cu(111)-Fe and Cu(110)-Fe [6,29,56,97,101]) and transferability of the results for CO on Fe(110) to Cu(100)-Fe (which is correct for oxygen on Cu(100)-Fe [82]) 1 ML of adsorbed CO results in a change in Δ of 1°. A more direct determination of the absolute coverage was done by turning on the electron gun (2500 eV, 3 μA) during the desorption. This resulted in an oxygen and carbon contamination of about 40% of the value calculated using $\delta\Delta$, which is a reasonable agreement realising that low energy electron bombardment not necessarily leads to dissociation, but also induces desorption. Using this calibration it appears that the equilibrium coverage of CO at 0.01 Pa on 0.1 ML Fe is about 0.2 ML. Disregarding Fe enhanced adsorption of CO on Cu the average number of CO molecules bound to one Fe atom exceeds unity. In fact in the case of θ_{Fe}=0.01 and θ_{Fe}=0.04 at P_{CO}=0.01 Pa the ratio is about 2. Iron enhanced CO adsorption on Cu is not very likely under these circumstances. On catalysts this type of adsorption was suggested only for high pressures (1 kPa) [99]. An explanation for the high CO/Fe ratio may be the formation of iron carbonyl like species ($Fe(CO)_n$).

The assumption of a linear change in $\delta\Delta$ with θ_{CO} on these surfaces may not hold due to the different types of adsorbed CO. However, on Ni and Fe single crystal surfaces the change in Δ due to one CO molecule is the same. This indicates that the dipole of the CO molecule and the induced dipole in the surface are the same on both metals. There is no reason to expect this to be different on the Cu(100)-Fe surfaces as long as the CO/Fe ratio is smaller than unity (no dissociation occurs and a different ΔH_{ad} probably does not influence the dipole much, since also for Ni and Fe the difference in ΔH_{ad} is about 40 kJ/mol. As soon as the ratio CO/Fe exceeds unity one may expect the sensitivity to decrease since the dipoles probably weaken due to mutual interaction. In that case the number of CO molecules adsorbed is even larger than determined assuming linearity. Another cause for non linearity may be the a change in the dielectric constant due to reorganisation of the surface induced by adsorbed CO. This, however, is unlikely because it should also influence Ψ and, moreover reorganisation caused by heating did not show any effect on both Δ and Ψ.

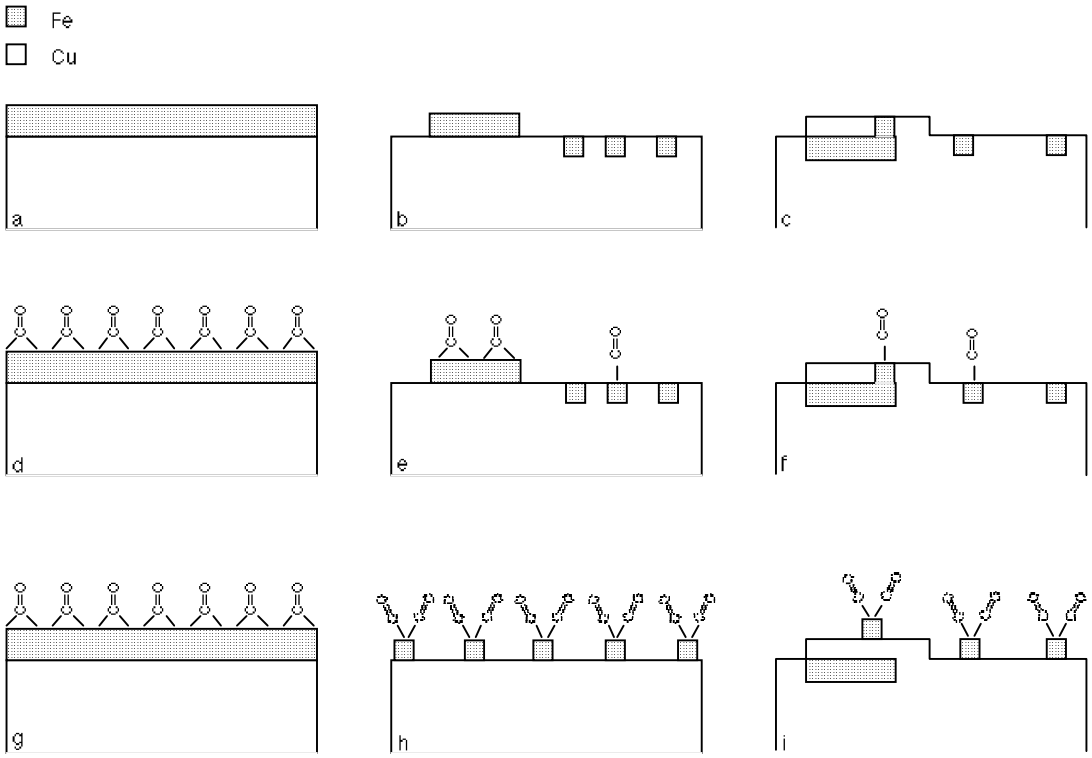

Figure 4 *A schematic model for the CO adsorptions on Cu(100)-Fe surfaces. a) represents a surface which is completely covered by Fe, b) shows a surface with both Fe clusters and dissolved iron atoms and c) gives the effect of a severe heat treatment at more than 500 K. d), e) and f) show what happens during a short exposure of CO and g), h) and i) show the results of prolonged exposure until equilibrium coverage.*

Supposing this carbonyl formation actually happens, one might expect to find some effects of it in the adsorption kinetics. Indeed, in the adsorption curves of Fig. 2 and Fig. 3 a fast and a slow stage can be observed. Since CO adsorption is usually a fast process [97] (with a initial sticking probability close to unity) there seems to be some evidence here for the existence of two different adsorption processes on this surface. The initial fast CO adsorption is probably similar to the molecular adsorption on other surfaces [6,29,97,98], whereas the slow stage may be caused by the carbonyl formation.

For a better understanding of what might happen on the surface during the experiments the discussion will be continued using a simple model based on the known growth behaviour of Fe on Cu(100). In the regime of θ_{Fe} as used ($0.01 < \theta_{Fe} < 1.7$) the iron is present after evaporation as clusters of at most 2 layers height and partly dissolved in the Cu surface layer (Fig. 4a for high θ_{Fe} and Fig. 4b for $\theta_{Fe} \bullet 0.1$) [9-13,20,102,105]. The structure of the iron is fcc. The effect of a heat treatment is that Cu atoms migrate over the iron clusters and depending on the time and temperature the Fe clusters are more or less buried. Though for these surfaces the equilibrium situation will be that the iron is completely dissolved in the copper crystal another 'extreme' will be found before. The maximum solubility of iron in the surface layers will be reached. The maximum solubility is probably below the bulk solubility of Fe in copper which is 4% [106]. The top layer of a Cu(100)-Fe surface after a short heating to 620 K might look like Fig. 4c. Since only the top layer is interesting for the CO adsorption the deeper buried iron is not really important in this figure.

It is worthwhile now to consider the circumstances under which both stages are found separately or together. Slow adsorption alone is found for all surfaces after a heat treatment to

more than 500 K and for freshly prepared surfaces with θ_{Fe}<0.05. Fast adsorption without a following slow stage is found only for θ_{Fe}=1.7. A combination of both processes is found on all other surfaces. A heat treatment always resulted in a decrease of extent of the fast adsorption.

Apparently fast adsorption only occurs on surfaces containing enough iron to present iron islands to the carbon monoxide (Fig. 4d-4e). After the fast adsorption the CO starts to adsorb on the single atoms dissolved in the surface layer. This can happen only for surfaces not completely covered with iron. These surfaces can be formed either by the deposition of small (< 0.1 ML) amounts of iron (Fig. 4b) or by a heat treatment of surfaces with a higher iron content (Fig. 4c). In either case the fast adsorption can be pictured as shown in Fig. 4d-4e for doubly co-ordinated CO and by the slow adsorption as shown in Fig. 4e-4f for singly co-ordinated CO. Of course it can not be excluded that already in the fast stage adsorption on these sites occurs. In this way on-top adsorption is required, which is also observed by Boellaard et al. on Cu/Fe catalysts [99]. The formation of iron carbonyl like species, $Fe(CO)_x$ ($2 \leq x \leq 5$), is now relatively easy. The iron can be lifted out of the surface maybe helped by a second CO molecule (Fig. 4h-4i), a process that costs less energy when the iron is surrounded by Cu atoms than by Fe atoms (CO induced iron segregation is even energetically favourable, -87 kJ/mol [105]). This process is slower than the first (normal) adsorption because the activation barrier should be higher.

It may be suggested that part of the slow adsorption stage is due to the formation of extra sites created by CO induced iron segregation from deeper layers. Segregation of Fe in the Cu/Fe system induced by the adsorption of CO is observed in Cu/Fe catalysts [99]. Adsorption experiments on heat treated surfaces never gave evidence for iron segregation. The Fe/Cu MVV ratio was checked before and after adsorption but no difference could be detected. Heating and cooling down under 0.1 Pa CO did not change these observations. However, in the case of the experiments on catalysts [99] both the CO pressure and the exposure are 4 orders of magnitude higher. Under those pressures even CO adsorption on Cu(100) is observed [102].

An other process which is may happen during the slow adsorption stage is the break up of the Fe clusters caused by the CO. This can, of course, only occur when enough space is available. This process is shown in Fig. 4h. CO induced cluster break-up is observed before [107]. In the UHV system used there was no experimental way either to prove or disprove this possibility.

For surfaces on which there is no space for the formation of carbonyl like species or cluster break-up (Fig. 4g) no slow adsorption is expected and found.

8.5 Conclusions.

1. Cu(100)-Fe surfaces show only molecular CO adsorption.
2. In contrast to Cu(111)-Fe and Cu(110)-Fe surfaces, CO does not dissociate on Cu(100)-Fe surfaces with iron coverages up to 1.7 ML, pressures up to 0.1 Pa and temperatures up to 620 K, which may be due to the square fcc structure of the iron on these surfaces.
3. The amount of molecularly adsorbed CO does not increase when a quantity of more than about 0.1 ML of iron is deposited.
4. Besides the initial fast adsorption of CO on the Fe islands, CO also adsorbs on Fe atoms dissolved in the surface layer causing a slow increase of the CO coverage. Since the amount of adsorbed CO exceeds θ_{Fe} for θ_{Fe}ε0.1 probably also carbonyl like species are formed in this stage.

5. After annealing the fast adsorption of CO on the Fe islands is obstructed by Cu atoms covering the Fe islands. The CO adsorption on annealed Cu(100)-Fe surfaces is therefore limited to single Fe atoms dissolved in the surface layer.

9

Low Energy Auger Electron Spectroscopy of clean and oxidised Cu(100) and Fe/Cu(100) surfaces.

Abstract

The background subtraction method for undifferentiated Auger spectra proposed by Peacock is shown to be reliable for the low energy Fe and Cu $M_{2,3}VV$ peaks. This is illustrated by the good results obtained for spectra of clean and oxidised Cu(100), Cu(100) containing 0 - 5 ML of Fe and oxidised surfaces. This variety of surfaces made it possible to test the method on spectra with overlapping peaks of different heights and on spectra in which the peak shape changed.

The spectra of the unoxidised Cu(100)/Fe surfaces could be described by weighted sum of the pure Cu and Fe $M_{2,3}VV$ peaks. The background intensity at energies higher than the Cu peak could be used as an internal calibration factor for the spectra. These results are used to calculate the inelastic mean free paths for the Cu and Fe $M_{2,3}VV$ electrons. These values were 0.36 ± 0.07 and 0.44 ± 0.09 nm respectively.

For the oxidised surfaces the Fe (oxide) peak could be extracted by a simple subtraction of a pure Cu $M_{2,3}VV$ peak. This Cu peak apparently did not change shape upon oxidation.

9.1 Introduction.

Auger Electron Spectroscopy is one of the most used techniques in surface science to determine the composition of the surface of many types of (conducting) samples. However, in some cases analysis of spectra is hampered by the overlap of peaks of different elements or by a change in peak shape. Both problems often occur in studies of low energy Auger peaks of transition metal (alloy) surfaces. The low energy Auger transitions contain valuable information about the composition of the top layers or the chemical compounds present at the surface e.g. Fe oxides [60], formation of vanadium and titanium nitrides [64,65], Fe/Cr alloys and Fe/Cu and Fe/Ni surface alloys and their oxides [32,52,108].

In the traditional analysis of AES data differentiated spectra are used. However, peak shape changes are a source of errors in quantification of these spectra and it is more difficult to analyse the change of shape. A second problem can occur in the derivative mode when the peaks are situated on a strongly changing background as is the case for features below 300 eV when using a Retarding Field Analyser (RFA). Labohm [44] solved this problem by developing a reasonably accurate correction method based on a linear approximation of the background. When using the peak area in the undifferentiated background subtracted spectrum, peak shape changes are of no influence any more but in practise the peaks as measured are on top of a background which has to be subtracted first. This procedure is not straightforward.

Most methods described in literature other than those that use a non-physical polynomial, spline or other fits as background, use a basic background of the form

$$B(E)=\frac{A_1}{E^{m_1}} \qquad (1)$$

which is based on models of the inelastic scattering of electrons and the generation of secondary electrons [47,75,109,110]. These models predict m_1 to be approximately unity. The parameters A_1 and m_1 of Eq (1) are fitted to the high energy side of the peak and subtracted. The next step in the procedure depends on the further use of the spectrum. If the spectrum is to be used for Auger fine-structure analysis both a second electron cascade (caused by the Auger electrons) has to be subtracted and a deconvolution with the instrument function has to be performed. The latter requires quite a lot of computation time and the determination of the instrument response function [111-113].

On the other hand if the spectrum is to be used for quantitative analyses, subtraction of a step of the form

$$S(E)=\frac{A_2}{E^{m_2}}\int_E^{E^T} N_A(E')dE' \qquad (2)$$

is relatively convenient and accurate [47]. $N_A(E)$ is the number of Auger electrons with energy E, E^T is the energy threshold at the high energy side of the peak and A_2 and m_2 are the parameters of the second cascade to be fitted at the low energy side of the peak.

The form of the background as described by both Eqn (1) and Eqn (2) requires the presence of linear regions in the log(N(E)) versus log(E) plots above and below the Auger features. These regions should be used to fit the values of m_1, m_2 and A_1.

Tougaard [76] proposed a more complicated method for background subtraction based on a more physical theory (taking into account the depth distribution and the scattering cross sections of the elements) that was proved to be valid for XPS and X-ray excited Auger

transitions. He also claims that the method is useful for electron excited Auger spectra after subtraction of the electron cascade due to other than the Auger electrons. However, the method becomes more complicated than for XPS because of the depth dependence of excitation probability of the exciting beam. Because of the relative simplicity of the use of Eqn (3) it was decided to use the method of Peacock.

According to Bender [110] a successful background subtraction method should satisfy the following criteria. The method should be:

1 accurate and reproducible;
2 universal: applicable to all kinds of elements in all kinds of compounds;
3 based on first principles and be independent of the fitting parameters;
4 not too much dependent on the choice of the input parameters;
5 fast from the computational point of few;
6 sensitive for small peaks;
7 able to distinguish peaks superimposed on the inelastic tail of peaks of other elements.

In this chapter it is shown that the method described by Peacock [47] in a slightly adapted form is successful in the background subtraction of low energy Auger features and satisfies the last two criteria, though some care is needed when small peaks are superimposed on the inelastic tails of other peaks. To test the reliability of the method the $M_{2,3}VV$ spectra of clean Cu(100), Cu(100) + Fe and the oxidised Cu and Cu/Fe surfaces were analysed. The spectra of these surfaces give a good opportunity to test the method because the Cu and Fe $M_{2,3}VV$ peaks (44 and 58 eV respectively) overlap slightly and the Fe $M_{2,3}VV$ peak exhibits a strong shape change upon oxidation. The procedure was used to calculate an Auger signal versus amount of Fe plot (AST - plot) from which a reasonable inelastic mean free path (imfp) for the Cu and Fe $M_{2,3}VV$ electrons can be calculated assuming monolayer growth for the first monolayer.

9.2 Results and discussion.

The Auger spectra were used for data analysis without any smoothing after sampling from the LIA. An energy range of 70 - 80 eV was used in all spectra to fit Eqn (1). A larger region expanding to higher energies gave the same results but required a longer sampling time. After subtraction of this basic background the inelastic tail under the peaks can be calculated by the iterative procedure described by Peacock [47]. Because of the small linear range in the log N(E) versus log E plot at very low energies (below 40 eV) the region to fit m_2 of Eqn (2) had to be chosen carefully. In most cases convergence within a few percent was reached after 5 iterations. Unless mentioned otherwise 5 iterations were used in the background calculations.

A typical spectrum in the Cu $M_{2,3}VV$ region obtained from a clean Cu(100) surface and the background calculated from the first 3 iterations are shown in Fig. 1. The fourth and fifth iteration are not visibly different from third on this scale and were thus omitted in this figure. The reproducibility of the peak shape and position was good and independent of small changes

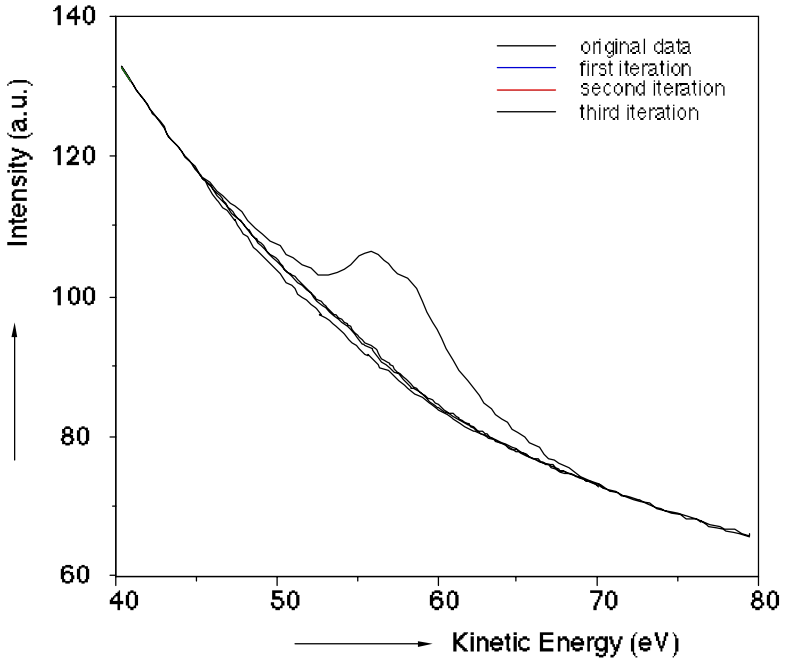

Figure 1 *Original Cu $M_{2,3}VV$ spectrum and three iterations of the background calculation.*

Table 1. Fit parameters of several Cu and Fe $M_{2,3}VV$ spectra of fresh and oxidised Cu(100) surfaces containing 0-5 ML Fe.

Surface	Region to fit m_2 (eV)	m_2	No. of it.	Cu $M_{2,3}VV$ area	Fe $M_{2,3}VV$ area
Cu(100)	40.0 - 45.0	2.0	5	254	-
Cu(100) + θ= 0.52 O_{ad}	40.0 - 45.0	2.0	5	232	
Cu(100) + 0.25 ML Fe	30.0 - 34.0	1.7	2	219	59.3
Cu(100) + 1.0 ML Fe	30.0 - 34.0	1.6	5	114	236
Cu(100) + 2.0 ML Fe	30.0 - 34.0	1.6	5	55.1	413
Cu(100) + 5.0 ML Fe	30.0 - 34.0	1.8	5	-	520
Cu(100) + 0.25 ML Fe oxidised	27.0 - 31.0	1.8	2	163	-
Cu(100) + 1.0 ML Fe oxidised	27.0 - 31.0	2.0	5	116	-

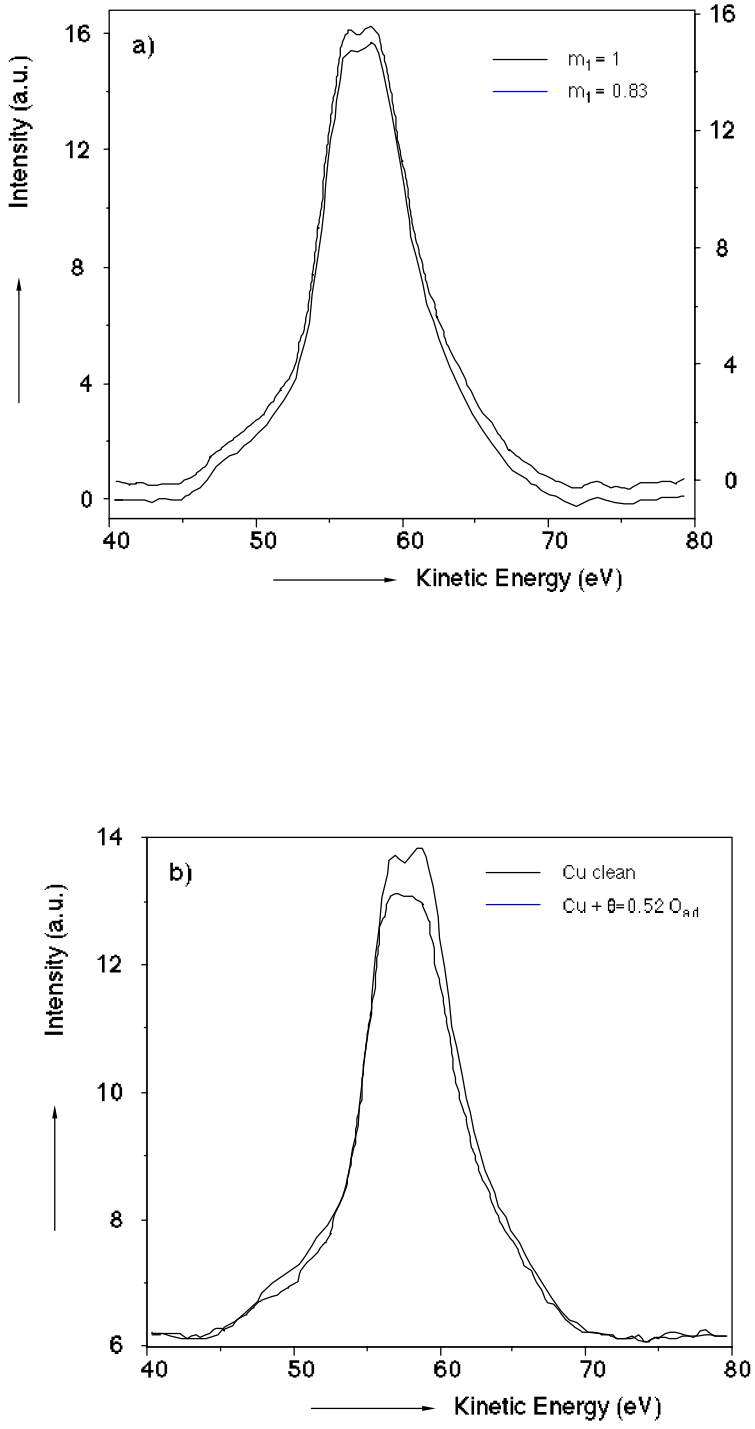

Figure 2 *(a) Influence of the two different basic backgrounds on the peak shape and area. The difference in peak area is 0.5%. (b) Cu $M_{2,3}VV$ spectra of a clean Cu(100) surface and an oxygen covered Cu(100) surface (θ_O = 0.52 ± 0.05).*

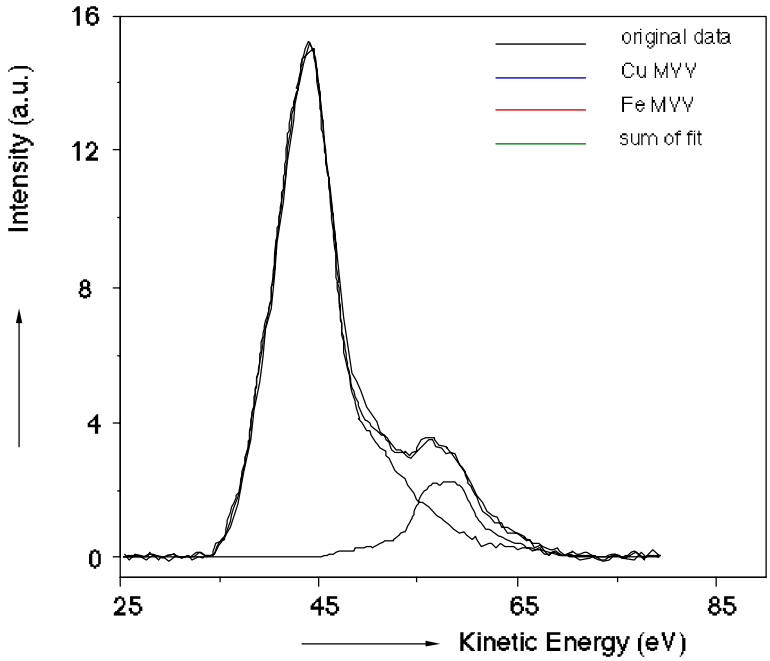

Figure 3 *Fit of a Cu $M_{2,3}VV$ and a Fe $M_{2,3}VV$ spectrum onto a spectrum of a Cu(100) with 2.0 ML Fe.*

in the instrumental configuration due to the sample movements which are required for cleaning, Fe evaporation and ellipsometry. Since it is sometimes convenient to use an offset in the output from the LIA, the high energy side of the spectra should be fitted to the expression

$$B(E) = C + \frac{A_1}{E^{m_1}} \qquad (3)$$

where C is the offset. This equation cannot be linearised with respect to its parameters. Because experience shows that m_1 is always close to unity I fitted one spectrum (taken without offset, C=0) to Eqns. 1 and 2 (A_1, m_1, A_2 and m_2 variable) and fitted the same spectrum with Eqns. 3 and 2 (C, A_1, A_2 and m_2 variable and m_1=1). Fig. 2a shows the result for the Cu $M_{2,3}VV$ peaks using the two procedures. The difference in the peak areas is smaller than 1%. This result is consistent with the observation of Sickafus [75] that deviations in the fit parameters of Eqn (1) are corrected by the parameters in the second step of the background subtraction (Eqn (2)).

An amount of adsorbed oxygen corresponding to θ=0.52 ± 0.05, which is the saturation value of adsorbed O at Cu(100) [51], apparently had no influence on background, peak shape and peak position. This can be seen in Fig. 2b which shows the $M_{2,3}VV$ peak of a clean and an oxidised Cu(100) surface and in Table 1 which lists the important fit parameters for the two spectra. Both spectra were normalised to the background intensity at 79 eV. This normalisation procedure will be discussed in more detail later. The difference in area between the two peaks is caused by screening of the Cu atoms by the adsorbed oxygen.

So far it has been shown that the method used for background subtraction does indeed give reliable results for Cu(100) and Cu(100)/O. The peak shape and position of Cu does not change after oxidation, a result that will be used later.

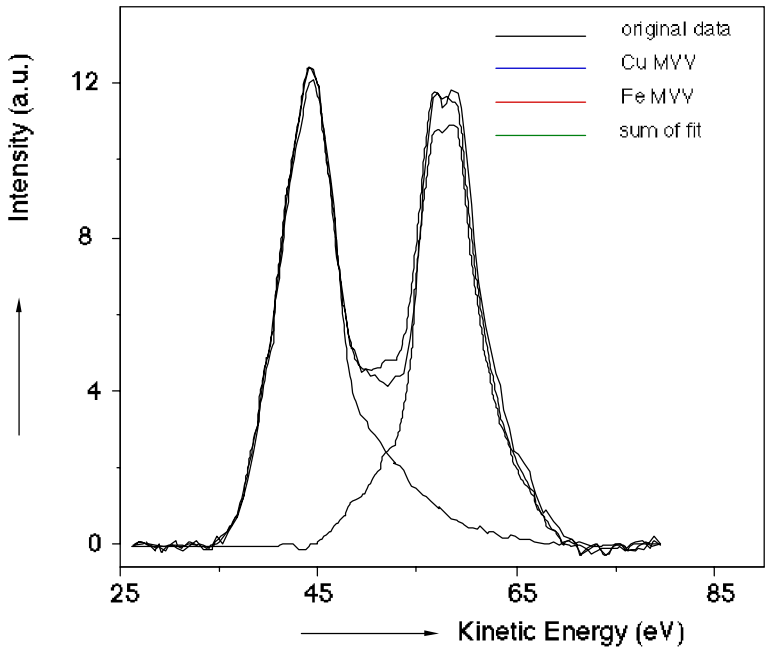

Figure 4 *Fit of a Cu $M_{2,3}VV$ and a Fe $M_{2,3}VV$ spectrum onto a spectrum of a Cu(100) with 1.0 ML Fe.*

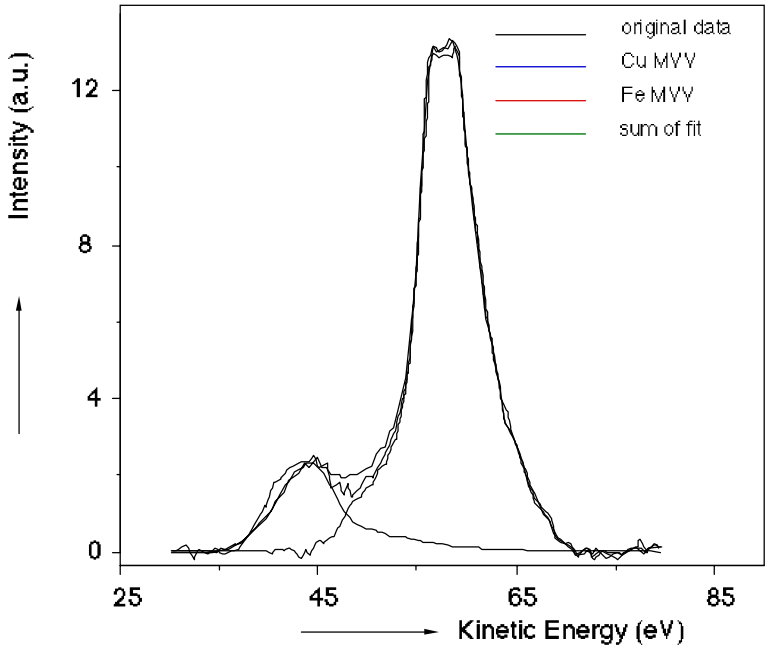

Figure 5 *Fit of a Cu $M_{2,3}VV$ and a Fe $M_{2,3}VV$ spectrum onto a spectrum of a Cu(100) with 0.25 ML Fe.*

A more complicated spectrum is obtained from the copper-iron system. Figs. 3 and 4 show the $M_{2,3}VV$ spectra of 2.0 and 1.0 monolayer of Fe on Cu(100) after background subtraction. A monolayer of Fe, as used here, contains the same number of atoms per unit area as the Cu(100) surface. This assumption is based on the epitaxial growth mode of Fe on Cu(100) [16]. Background subtraction from these spectra works satisfactory, as can be seen in Figs. 3 and 4. In Table 1 it can be seen that the fit procedure gave the same m_2 values for these surfaces and that 5 iterations were used. The separate Fe and Cu peaks calculated with the least squares fit of the pure Cu and Fe $M_{2,3}VV$ peaks and the sum of both are also shown in the Figs. 3 and 4.

The quality of the least squares fits of the two pure metal peaks onto the overlapping Fe and Cu peaks (Figs. 3 and 4) also indicates that the background subtraction method is quite reliable. It furthermore indicates that within the accuracy of the method no change in the peak shape occurs. This means that the $M_{2,3}VV$ spectrum of the bimetallic surface can be represented by the weighted sum of the two $M_{2,3}VV$ spectra of both constituents.

For surfaces containing small amounts of Fe (< 0.5 ML) some problems in the background determination occurred. These problems arise from a change in the background due to the presence of Fe causing the linear region at the low energy side of the $M_{2,3}VV$ peaks in the log(N) versus log(E) plot to shift to lower energies. Sometimes the linear region was very small or even absent. This often resulted in an extraordinary low value for m_2 compared to spectra of surfaces containing more Fe and either a strong apparent deformation of the Cu peak or no convergence in the iterative process. So analysis of the spectra with small amounts of Fe had to be done very carefully. Good results could be obtained by changing the region in which m_2 was fitted or by stopping the iteration after 2 or 3 steps. One should realise that convergence is not reached in this case. The peak shape of the Cu peak was used as criterion, assuming that the shape is independent of the amount of Fe on the surface. This assumption seems to be valid because at larger amounts of Fe no change was observed. The final result is given in Fig. 5.

A still more complicated case for background subtraction is presented by the spectra of oxidised Cu-Fe surfaces, where the Fe peak splits into two peaks. In Figs. 6a and 7a the spectra of the oxidised surfaces containing 0.25 and 1.0 ML Fe are shown. As with the spectra of the unoxidised surfaces background subtraction of spectra with high amounts of Fe worked without complications. With low amounts of Fe the same kinds of problems occurred as for the unoxidised surfaces. These problems could be 'solved' in the same way, i.e. subtraction of a copper peak (which does not change upon oxidation) should result in a reasonable spectrum for oxidised iron. Figs. 6b and 7b show the Fe (oxide) $M_{2,3}VV$ peak . The quality of the baseline in these spectra which were obtained after subtraction of a pure Cu $M_{2,3}VV$ peak normalised to the high energy flank of the peak, indicates that the procedure is working correctly. It also supports the earlier results that no change in the peak shape and position of the Cu $M_{2,3}VV$ peak due to the presence of iron and oxygen occurs within the accuracy of the instrument and the background subtraction method. Now the iron oxide peak can be separated from the Cu peak and it is possible to analyse the iron oxide peak in more detail as is done in chapter 4.

As a simpler application of these results the extraction of the inelastic mean free path (imfp) for the Cu and Fe Auger electrons from the data will be considered. Because the electron gun

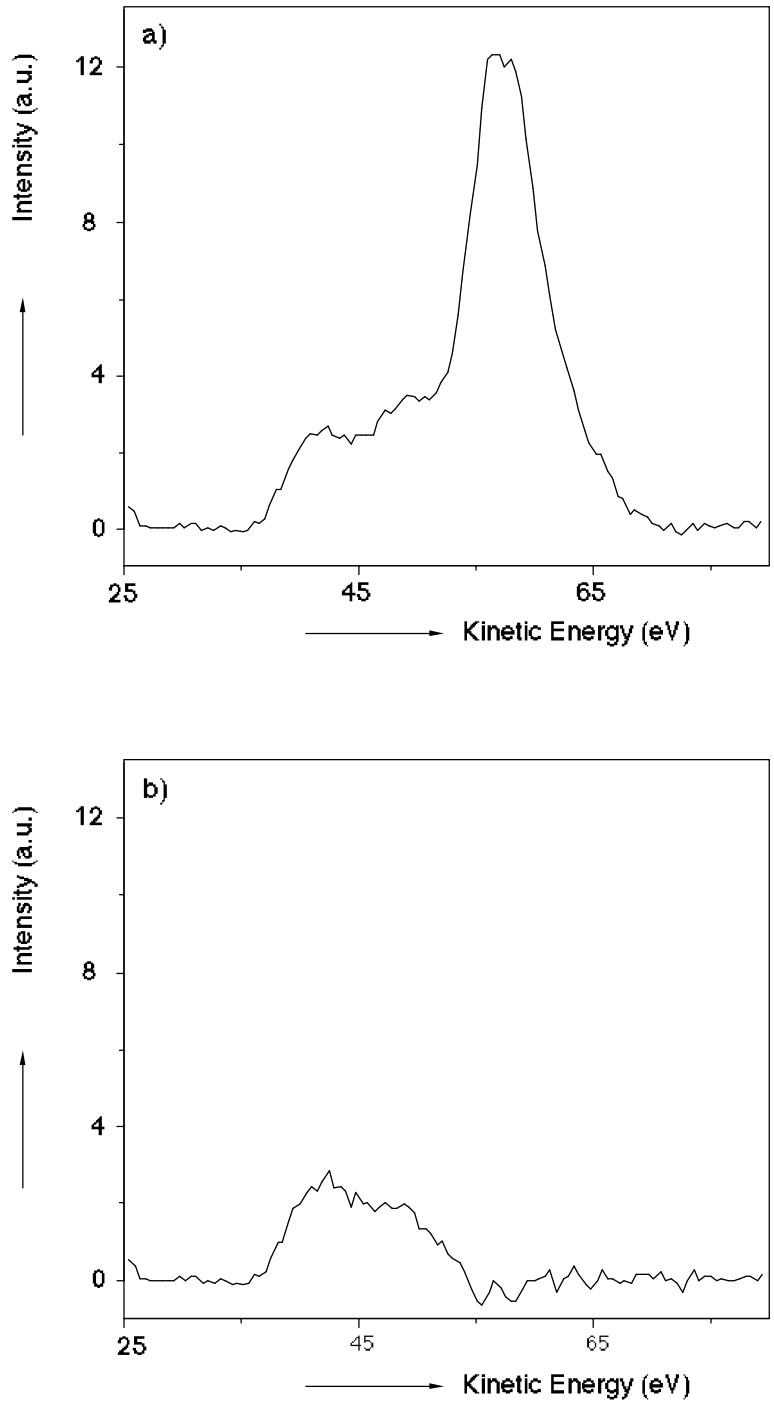

Figure 6 *Spectrum of an oxidised Cu(100) surface containing 0.25 ML Fe (a) and the spectrum after subtraction of the Cu $M_{2,3}VV$ peak (b).*

power supply was not emission stabilised a (preferably internal) calibration method had to be found. Langeron et al. [48] showed that the peak height/background ratio at the energy of the peak position only depends on the surface composition and the primary beam energy.

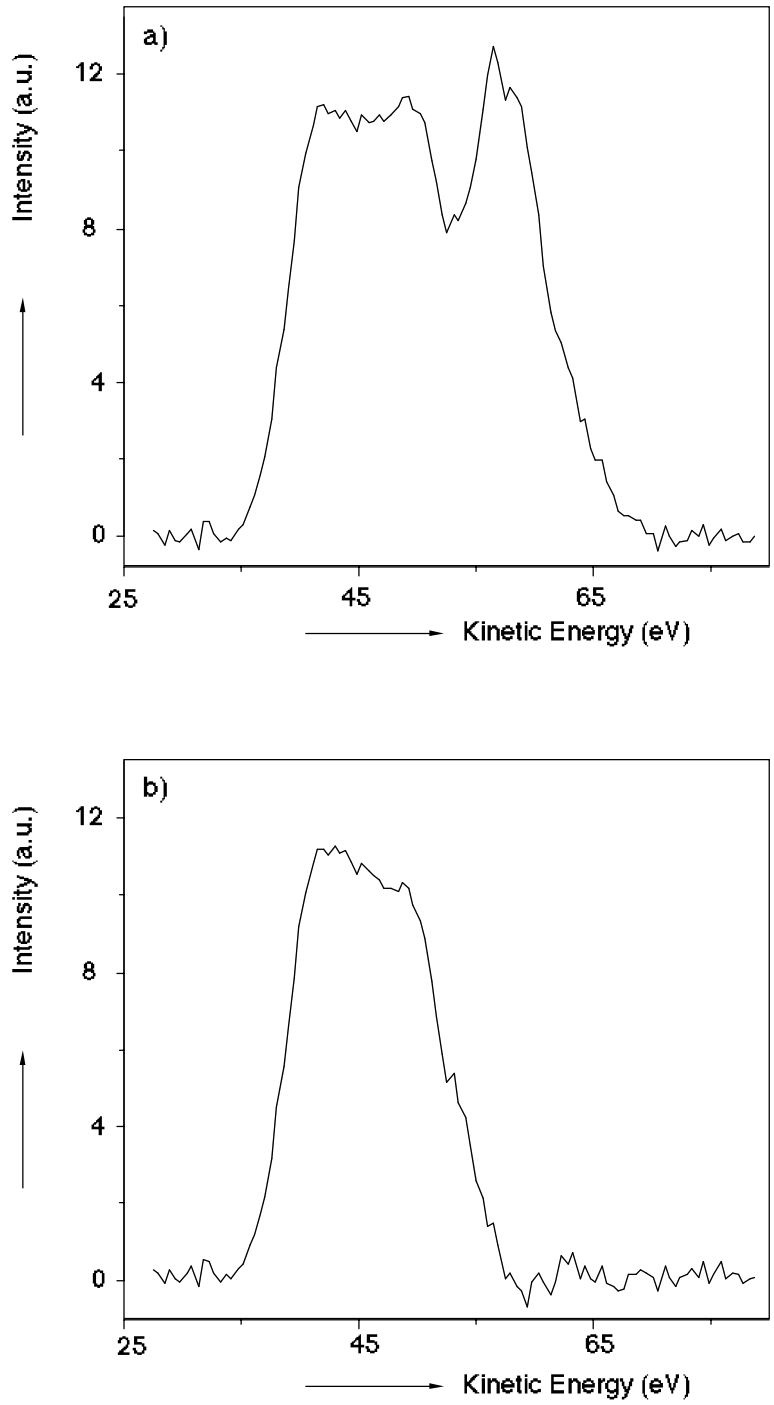

Figure 7 *Spectrum of an oxidised Cu(100) surface containing 1.0 ML Fe (a) and the spectrum after subtraction of the Cu $M_{2,3}VV$ peak (b).*

Therefore it was checked whether it is possible to use the background intensity at a higher energy than the Auger feature as a calibration factor. A point at higher energy was chosen because the shape of the background in that region appeared to be independent of changes in

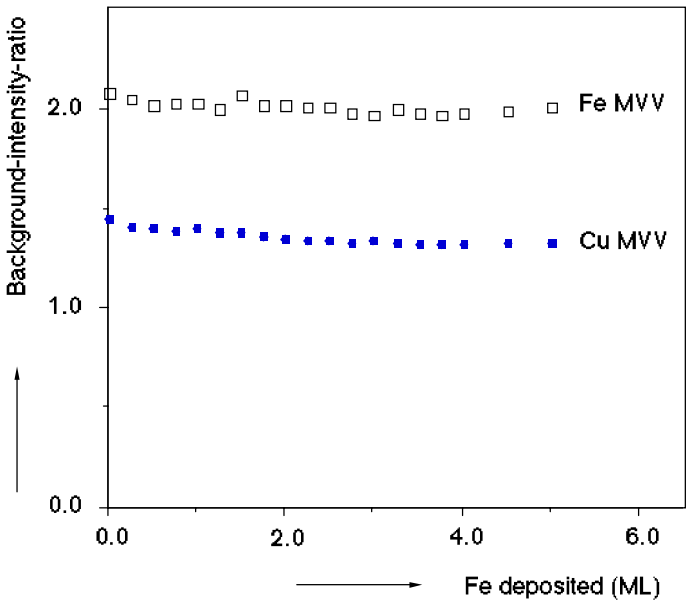

Figure 8 *The ratios of the background intensity under the Auger peaks and the intensity at 79 eV for the Fe and the Cu $M_{2,3}VV$ peaks during the evaporation.*

the amount of Fe or O at the surface. Instead of the Auger peak height used the peak area was used because the latter is less sensitive to peak shape changes. In Fig. 8 the ratios of the background intensity at the peak position (as calculated with the procedure described above) and the background at 79 eV are plotted for both the Fe and the Cu peaks against the amount of Fe deposited. The constant ratios during the complete experiment confirm the validity of both the background subtraction method and the use of the background intensity at 79 eV as internal calibration factor.

The area of the Cu and Fe peaks for surfaces containing 0 - 5 ML of Fe are plotted against the amount of Fe in Fig. 9. The calibration method described above is used to calculate the data in Fig. 9. Now it is possible to calculate the imfp of the Cu and Fe $M_{2,3}VV$ peaks from the initial slope of the curves in Fig. 9. This requires an assumption about the growth mode of Fe on Cu(100). Most authors find proof for a monolayer by monolayer growth [8,21,26]. Glatzel et al. [16] were the first to suggest a bi-layer by bi-layer growth mode. This was based on breakpoints in a high energy Fe $L_{2,3}M_{2,3}V$/ (Fe $L_{2,3}M_{2,3}V$ + Cu $L_{2,3}VV$) versus time of evaporation plot calibrated with Rutherford back scattering. Landskron et al. [17] observed breakpoints in the high energy Fe $L_{2,3}VV$ (703 eV) versus evaporation time plot at 3 and 6 ML. They ascribed these breakpoints to a reconstruction of the surface. Though the most significant results to determine the growth mode should be expected when the imfp's have almost the same length as the interlayer spacing of the layers (the larger the ratio between the inter-layer-spacing and the imfp the larger the change in the slope before and after the breakpoints) the results shown in Fig. 9 exhibit no clear breakpoints. While the Fe curve can be fitted reasonably well for both monolayer and bi-layer growth, the Cu curve can be fitted significantly better for monolayer growth. Part of the inconsistency of these results and the results mentioned in literature may be due to the strong temperature dependence of Cu segregation/interlayer mixing as reported by Steigerwald et al. [19]. They also observed some evidence for what may be bi-layer growth: half of the Cu atoms remained exposed at the

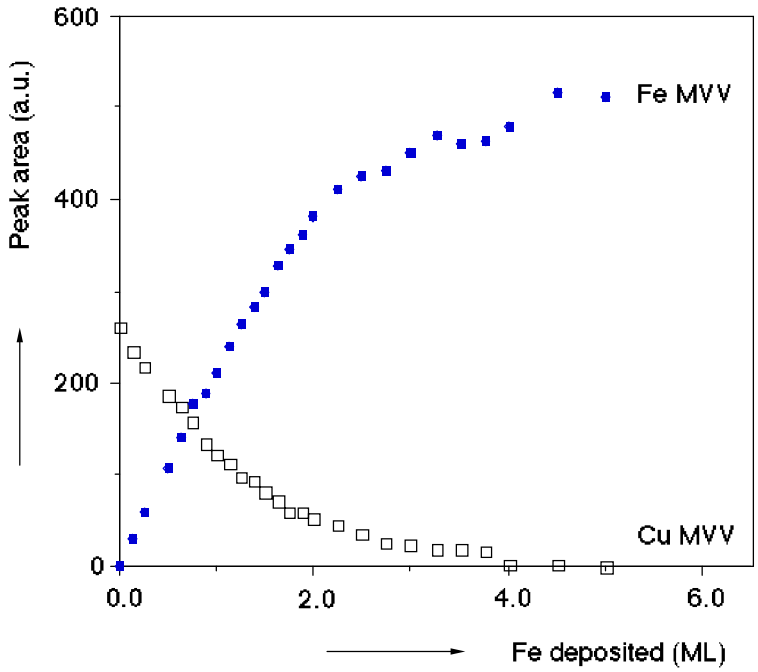

Figure 9 *Peak area of the Cu $M_{2,3}VV$ and the Fe $M_{2,3}VV$ peak as function of the amount of Fe evaporated.*

surface after evaporation of 1.0 ML of Fe at 295 K. But after evaporation at slightly higher temperatures even more Cu atoms remained exposed at the surface. The imfp's calculated from the monolayer fits are 0.36 ± 0.07 and 0.44 ± 0.09 nm for Cu $M_{2,3}VV$ and Fe $M_{2,3}VV$ electrons respectively. These imfp's are corrected for the effective angle of detection of an RFA ($\cos\theta = 0.74$) [114] and agree well with values given in literature [43].

9.3 Conclusions.

1 The background subtraction method supposed by Peacock gives good results in the analysis of the (low energy) Cu and Fe $M_{2,3}VV$ Auger spectra. Peak overlap and peak shape changes due to oxidation do not influence the quality of the results. Still some care is required in analysing spectra with small peaks superimposed on inelastic tails of peaks of other elements.

2 The combined Cu-Fe $M_{2,3}VV$ spectra can be described by a simple linear fit of the $M_{2,3}VV$ peaks of the pure metals in the complete composition range. For oxidised surfaces the Fe peaks can be separated by simply subtracting the copper peak from the observed spectra.

3 The background intensity at energies slightly higher than the Cu peak can be used as internal calibration factor. This is used to normalise the peak area's.

4 The inelastic mean free paths of the Cu and Fe $M_{2,3}VV$ electrons are found to be 0.36 ± 0.07 and 0.44 ± 0.09 nm respectively.

10

Conclusion

As was expected the reactivity of the Cu(100)-Fe surfaces exhibits many differences with clean copper and iron surfaces. Most of the differences described in this thesis concern the iron (oxide) on the surface. Since the surfaces nearly always consisted of an iron (oxide) layer on top of the Cu(100) surface the interaction between the copper surface and the iron (oxide) must be responsible for the different reactivity of the iron. The growth of fcc iron instead of bcc iron on Cu(100) already indicated a good interaction. Also the iron oxide formed on the Cu(100) surface (for θ_{Fe}<2 ML) appeared to have a good interaction with the copper as could be concluded from the LEED pattern that was observed for Cu(100)+0.8 ML Fe after saturation with oxygen (chapter 3). This LEED pattern exhibited a strong contraction. An other indication for this good interaction is the very low reactivity of the oxidised surfaces towards H_2 and CO (chapter 7) when the surfaces are completely covered with iron oxide.

For oxidation at room temperature no differences in initial oxidation rate were observed with ellipsometry for surfaces containing more than 0.19 ML of iron. This means that the oxidation probably proceeds via a precursor mechanism since the oxygen is initially bound to the iron on the surface (chapter 3-6). A precursor mechanism is also observed on pure copper single crystal surfaces [115].

Analysis of the Fe $M_{2,3}VV$ Auger spectra obtained during the oxidation of 1 ML of Fe on Cu(100) made it possible to exclude a successive oxidation of the iron from Fe^0 to Fe^{2+} to Fe^{3+} (chapter 4). Repetition of the same experiment using XPS revealed the presence of both Fe^{2+} and Fe^{3+} during the oxidation until all iron was oxidised to Fe^{3+}. On all surfaces saturated with

oxygen at 300 K (θ_{Fe} • 16 ML) a top layer of Fe_2O_3 was found with AES (chapter 3 and 4), XPS (chapter 5) and UPS (chapter 6). As for oxidation at 300 K of Fe(100) the amount of oxygen adsorbing on Cu(100)-Fe surfaces is limited. Quantitative analysis of the AES spectra of oxygen saturated Cu(100)-Fe surfaces containing up to 16 ML of iron showed that somewhat more than 2 ML of Fe can be oxidised to Fe_2O_3 (on surfaces containing less than 2 ML Fe all iron is oxidised to Fe_2O_3 and 0.5 ML of oxygen adsorbs on the Cu(100) interface). The ellipsometric data confirmed these findings assuming the same sensitivity of Δ for oxygen as on pure iron (chapter 3). However, equivalent experiments in a different UHV system equipped with XPS showed evidence for a much thicker iron oxide layer. This difference can possibly be explained by differences in surface structure after iron evaporation: the oxygen contamination on these surfaces was ~4 times higher than on the surfaces used for the AES and ellipsometry experiments.

The formation of closed layer of Fe_2O_3 on the Cu(100)-Fe surfaces also seems to be contradicted by results of Leibbrandt et al. [61]. They used High Energy Ion Scattering - Shadowing and Blocking (HEIS-SB) to determine the stoichiometry of the iron oxide formed on Fe(100). They concluded that FeO_x (wüstite) was present on their surfaces based on the number of displaced Fe atoms as function of the number of oxygen atoms adsorbed. The difference between their results and those presented in this thesis might be due to the strong interaction between the copper substrate and the oxide which also seems to cause a very low reactivity of the oxidised (at 300 K) Cu(100)-Fe surfaces towards CO and H_2 (chapter 7). This low reactivity is probably due to both a very small number of defect sites in the iron oxide and the small mobility of ions in this oxide. So Cu(100)-Fe surfaces may stabilise a 'different' iron oxide than Fe(100) does. On the other hand, when the interaction of the iron oxide on Fe(100) with the underlying iron lattice is strong enough to displace one 'extra' layer of iron atoms without oxidising them this exactly counts for the difference. Their argument against this is that for higher oxygen contents the number of displaced iron atoms still indicates FeO_x. However, those oxygen contents were obtained at 473 K and also on the Cu(100)-Fe surfaces strong indications for a different oxide structure were indirectly found in reduction experiments (chapter 7).

CO-adsorption on the Cu(100)-Fe surfaces appeared to be non dissociative and reversible. Apparently the close packed square symmetry of the fcc-Fe(100) surface is not able to dissociate CO though the interaction with the iron is strong enough to break iron clusters into single atoms and to form iron carbonyl like species on the surface. The hypothesis that CO breaks iron clusters and forms carbonyl like species is based on the number of CO molecules adsorbing per iron atom and the observation of a fast ('normal' molecular adsorption) and a slow (cluster breaking and carbonyl formation) adsorption stage.

The detailed analysis of the Fe $M_{2,3}VV$ Auger peak obtained during oxidation (chapter 4) was made possible by using an unconventional non-derivative data acquisition method and by using a background subtraction method that was originally developed for high energy AES spectra obtained with a cylindrical mirror analyser, for low energy AES spectra (chapter 9). Combination of the results of this analysis with XPS results (and a literature study into the origin of the Fe $M_{2,3}VV$ peak shape) indicated that it is difficult to determine the type of iron oxide from the $M_{2,3}VV$ peak shape.

Samenvatting

De interesse van veel wetenschappers voor systemen bestaande uit twee metalen komt voort uit het feit dat het samenvoegen van twee metalen vaak resulteert in het ontstaan van nieuwe eigenschappen. Het bestuderen van deze systemen en hun (nieuwe) eigenschappen verschaft meer inzicht in materie in het algemeen. Van veel directer belang voor de samenleving is dat deze nieuwe eigenschappen kunnen leiden tot nieuwe producten of verbeteringen aan bestaande producten.

Net als voor zuivere metalen geldt voor metaallegeringen dat bulk- en oppervlakte-eigenschappen verschillen. Dit uit zich zowel op het fysische als het chemische vlak. Met name de (chemische) reactiviteit van metaaloppervlakken is van belang voor vele toepassingen. Hierbij kan worden gedacht aan corrosie en aan heterogene katalyse. In beide gevallen kan gekozen worden voor een combinatie van bepaalde metalen om de gewenste eigenschappen te combineren.

Om de chemische reactiviteit van oppervlakken goed te kunnen bestuderen is het wenselijk om met goed gedefinieerde oppervlakken en omstandigheden te kunnen werken. Dat is de reden dat het in dit proefschrift beschreven onderzoek is uitgevoerd aan een éénkristaloppervlak onder ultra hoog vacuum condities. Een monokristallijn oppervlak is de basis voor een goed gedefinieerd oppervlak en het vacuum garandeert dat het oppervlak lang genoeg schoon blijft om de gewenste reacties gecontroleerd uit te kunnen voeren en achteraf de oppervlaktesamen-steling te kunnen bepalen. Omdat gewerkt wordt onder goed gedefinieerde omstandigheden ligt het voor de hand om de reactiviteit ten opzichte van betrekkelijk eenvoudige moleculen als O_2, CO en H_2 te bestuderen. Overigens zijn dit belangrijke reactanten in veel processen en de reacties blijken nog complex genoeg te zijn. De genoemde omstandigheden vormen een model-situatie die grote verschillen vertoont met de praktijk. Toch blijkt dit 'model' één van de betere mogelijkheden om een relatie te leggen tussen oppervlaktereactiviteit enerzijds en structuur op atomair niveau anderzijds[1].

De reden dat in dit proefschrift gekozen is voor het koper-ijzer-systeem is dat deze twee metalen een aantal punten verschillen. De belangrijkste verschillen zijn: de kristalstructuur bij kamertemperatuur (fcc voor Cu en bcc voor Fe), de oppervlaktespanning (van koper een stuk lager dan van ijzer) en de reactiviteit voor zuurstof en koolmonoxide (ijzeroxides zijn veel stabieler dan koperoxides, CO dissocieert op ijzer terwijl het op koper nauwelijks adsorbeert bij 300 K). Bovendien was al een en ander bekend over de reactiviteit van koper-ijzer-opper-vlakken. Van Pruissen [116] heeft de reactiviteit van Cu(111)-Fe en Cu(110)-Fe voor O_2, CO en H_2 uitgebreid bestudeerd. De bereiding van die oppervlakken gebeurde echter met behulp van $Fe(CO)_5$ ontleding. Dit resulteert in minder goed gedefinieerde oppervlakken dan met de opdampmethode zoals beschreven in dit proefschrift, omdat koolstof- en zuurstof-verontreinig-ingen bij hoge temperatuur verwijderd moesten worden. Voor een aantal waarnemingen zal dit verschil echter weing uitmaken.

De mogelijkheid om ijzer op te dampen in combinatie met de ruime hoeveelheid literatuur over de groei van ijzer op Cu(100) heeft de keus geleid tot het Cu(100)-Fe-systeem. Het bijzondere van het Cu(100)-Fe-oppervlak is dat het ijzer epitaxiaal (fcc) aangroeit terwijl bij kamertemperatuur nauwelijks menging optreedt. Overigens wordt het mengen in dit systeem gedreven door entropie en oppervlakte-energie aangezien de mengenthalpie van koper en ijzer positief is. Enige menging treedt wel op, zeker op monolaag-niveau en bij hogere

tempera-turen. Daarom zijn de meeste experimenten beschreven in dit proefschrift bij kamertemperatuur uitgevoerd.

In de hoofdstukken 3-6 wordt de interactie van de Cu(100)-oppervlakken, die (gedeeltelijk) met fcc-ijzer bedekt zijn, met zuurstof beschreven. In de verschillende hoofdstukken worden de resultaten van verschillende technieken beschreven en gecombineerd. Zo is in hoofdstuk 3 ellipsometrie, Auger-electronen-spectroscopie en lage-energie-electronen-diffractie toegepast om tot een model te komen voor de oxidatie van Cu(100)-Fe-oppervlakken met verschillende hoeveelheden ijzer. Hierbij worden voornamelijk uitspraken gedaan over het oppervlak na verzadiging met zuurstof. In hoofdstuk 4 wordt een poging gedaan de verandering van de piekvorm van de Fe-$M_{2,3}$VV-Auger-piek tijdens de oxidatie van 1 ML (monolaag) Fe te benutten om meer inzicht te krijgen in het verloop van de oxidatie. Literatuuronderzoek, de resultaten van de piekvorm-analyse en de XPS-resultaten (Fe 2p), die in hoofdstuk 5 gepresen-teerd worden, geven aan dat de Fe-$M_{2,3}$VV-piek niet echt geschikt is om (makkelijk) te kunnen waarnemen of er FeO, Fe_3O_4 danwel Fe_2O_3 aan het oppervlak aanwezig is. De analyse van de XPS-resultaten (hoofdstuk 5) geeft echter wel een goed inzicht in het verloop van de oxidatie. Verder bevestigen de XPS-resultaten het in hoofdstuk 3 beschreven model grotendeels en daar waar zij afwijken wordt een verklaring gesuggereerd. Tot slot wordt in hoofdtsuk 6 UPS gebruikt om nogmaals het oxide bij verzadiging te determineren en om te bestuderen of de veranderingen in de valentieband tijdens oxidatie in verband gebracht kunnen worden met initieel lagere gevoeligheid van de ellipsometer voor zuurstof.

De oxidatie van Cu(100)-Fe-oppervlakken blijkt te verlopen via een precursor-mechanisme. Dit kan worden afgeleid uit de initiële oxidatiesnelheid die niet afhankelijk blijkt te zijn van de hoeveelheid ijzer op het oppervlak. Zonder precursor-mechanisme mag namelijk verwacht worden dat voor $\theta_{Fe}<1$ een afname in de oxdatiesnelheid wordt waargenomen als θ_{Fe} afneemt omdat de initiële reactiekans voor adsorptie van O_2 op Cu(100) ongeveer twee ordes van grootte kleiner is dan op ijzer. Het ijzer op het oppervlak wordt eerst geoxideerd. Daarbij ontstaan in eerste instantie zowel Fe^{2+} als Fe^{3+}. Op oppervlakken met minder dan 2 ML ijzer wordt uiteindelijk alle ijzer geoxideerd tot Fe_2O_3, waarna een halve monolaag zuurstof op het koperoppervlak adsorbeert. Als meer dan 2 ML ijzer aanwezig is wordt 3.5 ML zuurstof opgenomen die gebonden wordt in de vorm van Fe_2O_3. Dit ijzeroxide ligt dan dus op een laagje metallisch (fcc-) ijzer. De mobiliteit van de ionen in het oxide dat gevormd is bij 300 K is kennelijk niet groot genoeg om verdere oxidatie te bewerkstelligen.

De reactiviteit van de geoxideerde oppervlakken voor CO en H_2, zoals beschreven in hoofdstuk 7, geeft vervolgens meer informatie over de structuur van het oxide. Voor oppervlakken waarvan de hoeveelheid ijzeroxide naar alle waarschijnlijkheid voldoende is om het koper geheel af te dekken is -indien de oppervlakken bij kamertemperatuur geoxideerd zijn- geen enkele reactiviteit ten opzichte van CO en H_2 waar te nemen voor drukken tot 0.2 Pa en bij een kristaltemperatuur van 630 K. Van oppervlakken met minder ijzer kan H_2 alle zuurstof verwijderen terwijl CO alleen reageert met de zuurstof die gebonden is aan koper. Voor alle oppervlakken geldt dat wanneer na de oxidatie bij 300 K ook nog zuurstof is geadsorbeerd bij 630 K, H_2 het oppervlak geheel kan reduceren terwijl CO alleen de zuurstof gebonden aan het koper verwijdert. Dit leidt tot een tweetal conclusies: Fe_2O_3 bevat te weinig defecten om reactief te zijn ten opzichte van H_2 en CO

onder genoemde omstandigheden en er is 'vrij' koper-oppervlak nodig om CO met zuurstof van het koper te laten reageren of om H_2 te dissociëren. De dan gevormde waterstofatomen kunnen het ijzeroxide wel reduceren.

Dat het fcc-ijzer op de Cu(100) oppervlakken unieke eigenschappen heeft blijkt ook uit de reactiviteit voor CO. De adsorptie van CO op Cu(100)-Fe (beschreven in hoofdstuk 8) blijkt moleculair en reversibel. Op alle ijzer-éénkristaloppervlakken dissocieert CO bij 350 K. Ook op de Cu-Fe-oppervlakken van Van Pruissen dissocieert het. Vreeburg et al. [56] neemt geen dissociatie waar op Ni(111)-Fe-oppervlakken mits de ensembles van ijzeratomen uit minder dan drie atomen bestaan. Ensembles die uit drie of meer atomen bestaan dissociëren wel CO. Ook op Ni(111) is het ijzer aanwezig in fcc-structuur. Kennelijk beschikt de vierkante symmetrie van het fcc-Fe(100) niet over adsorptie plaatsen met de juiste geometrie voor dissociatie. Er zijn wel sterke aanwijzingen dat de interactie tussen het ijzer en de CO sterk genoeg is om de ijzeratomen uit elkaar te trekken en zelfs carbonyl-achtige structuren te vormen. Dit is gebaseerd op de verhouding van het aantal ijzeratomen en het aantal geadsorbeerde CO-moleculen enerzijds en op twee duidelijk verschillende stadia in de 'adsorptie'-snelheid op verschillende oppervlakken anderzijds.

Een gedeelte van het werk beschreven in dit proefschrift was alleen mogelijk dankzij verbeteringen van de wijze waarop Auger-spectra worden verkregen en geanalyseerd. Automatisering en softwarematige data-analyse openden een weg om meer informatie uit de spectra te halen door niet-afgeleide spectra op te nemen en te analyseren. In hoofdstuk 2 wordt onder andere aandacht besteed aan de voordelen van deze onconventionele techniek en in hoofdstuk 9 wordt een methode beschreven waarmee spectra van hun achtergrond ontdaan kunnen worden. Het succes van de methode blijkt uit de analyse van de Fe-$M_{2,3}$VV-piek zoals die is beschreven in hoofdstuk 4.

Reactivity of Cu(100)-Fe surfaces

De reactiviteit van Cu(100)-Fe oppervlakken.
(met een samenvatting in het Nederlands)

PROEFSCHRIFT

TER VERKRIJGING VAN DE GRAAD VAN DOCTOR AAN DE RIJKSUNIVERSITEIT TE UTRECHT OP GEZAG VAN DE RECTOR MAGNIFICUS, PROF. DR. J.A. VAN GINKEL INGEVOLGE HET BESLUIT VAN HET COLLEGE VAN DECANEN IN HET OPENBAAR TE VERDEDIGEN OP MAANDAG 28 FEBRUARI 1994 DES NAMIDDAGS TE 2.30 UUR.

door

Hans-Peter den Daas

GEBOREN OP 8 DECEMBER 1965 TE MEPPEL

promotor : Prof. Ir. J.W. Geus
co-promotor : Dr. O.L.J. Gijzeman
(Beiden verbonden aan de Faculteit der Scheikunde van de Rijksuniversiteit te Utrecht)

CIP-GEGEVENS KONINKLIJKE BIBLIOTHEEK, DEN HAAG

Daas, Hans-Peter den

Reactivity of Cu(100)-Fe surfaces / Hans-Peter den Daas. -
Utrecht : Universiteit Utrecht, Faculteit Scheikunde
Proefschrift Universiteit Utrecht. - Met lit. opg. - Met
samenvatting in het Nederlands.
ISBN 90-393-0110-7
Trefw.: ijzer ; reactiviteit / fysische chemie

Voorwoord

Het in dit proefschrift beschreven werk is grotendeels uitgevoerd in de werkgroep oppervlaktechemie (thans onderdeel van de vakgroep Anorganische chemie, toen ik in dienst kwam onderdeel van de vakgroep Fysische en Colloïdchemie en gedurende mijn hele onderzoeksperiode deel van het Debye Instituut) en voor een gedeelte bij het Dipartimento di Fysica, Università dell'Aquila (It.).

Iedereen die, op zijn eigen manier, heeft bijgedragen aan het tot stand komen van dit proefschrift wil ik hier graag bedanken:

Mijn promotores John Geus en Onno Gijzeman, de technici Ad Mens en Kees Rietveld met hun onmisbare steun op het lab, de studenten Joep van Giezen, Manon Jeurissen, Chloé Laszlo en Erwin Voogt (de laatste ook nog 3 maanden als collega), mijn collegae in de groep Ruud Balkenende, Robert-Jan Vreeburg, Wijnand van Kooten en Rob van Wijk en de audio-visuele dienst onder leiding van Jan den Boesterd. Ook voor de steun van Jan Verhoeven (AMOLF), met name aan het begin van mijn onderzoek en in de voorbereidingsfase, ben ik zeer erkentelijk.

Furthermore I am very grateful to Luca Lozzi, Maurizio Passacantando, Pietro Picozzi and Sandro Santucci who are responsible for my enjoyable and productive 6 months visit to their laboratory in l'Aquila and the grant of the EC Human Capital and Mobility Programme offered to me by the INFM. Last (but no least) I would like to thank Maurizio De Crescenzi (Dipartimento di Fysica, Università di Roma II and Dipartimento di Fysica, Università di Camerino) for introducing me to the l'Aquila group during my one month visit to his lab in Rome, October 1990.

Contents

This thesis is based on the following papers:

Chapter 3 Oxidation of ultra thin iron layers on Cu(100). Composition of the oxide films.
H. den Daas, O.L.J. Gijzeman and J.W. Geus, Surf. Sci. **285** (1993) 15.

Chapter 4 Oxidation of one monolayer of iron on Cu(100) studied with AES peak shape analysis.
H. den Daas, O.L.J. Gijzeman and J.W. Geus, Surf. Sci. **290** (1993) 26.

Chapter 5 The interaction of Cu(100)-Fe surfaces with oxygen studied with photoelectron spectroscopy I.
H. den Daas, M. Passacantando, L. Lozzi, S. Santucci and P. Picozzi, submitted to Surf. Sci.

Chapter 6 The interaction of Cu(100)-Fe surfaces with oxygen studied with photoelectron spectroscopy II.
H. den Daas, M. Passacantando, L. Lozzi, S. Santucci and P. Picozzi, submitted to Surf. Sci.

Chapter 7 The interaction of CO and H_2 with oxidised Cu(100)-Fe surfaces.
H. den Daas, O.L.J. Gijzeman and J.W: Geus, Appl. Surf. Sci. **68** (1993) 557.

Chapter 8 The interaction of CO with Cu(100)-Fe surfaces. H. den Daas, E.H. Voogt, O.L.J. Gijzeman and J.W. Geus, accepted for publication in Surf. Sci.

Chapter 9 Low Energy Auger Electron Spectroscopy of clean and oxidised Cu(100) and Cu(100)-Fe surfaces.
H. den Daas, O.L.J. Gijzeman and J.W. Geus, Surf. and Interface Anal. **18** (1992) 397.

Related papers:

'Structural and electronic studies of clean and oxidised thin Fe films on polycrystalline copper.', S. Di Nardo, M. Passacantando, P. Picozzi, S. Santucci, L. Lozzi, M. De Crescenzi and H. den Daas, Surf. Interface Anal. **18** (1992) 98.

'Extended energy loss fine structure and X-ray photoelectron spectroscopy studies of clean and oxidised Fe thin films on polycrystalline copper.', S. Di Nardo, M. Passacantando, P. Picozzi, S. Santucci, L. Lozzi, M. De Crescenzi and H. den Daas, Surf. Interface Anal. **19** (1992) 478.

1

Introduction

1.1 Bimetallic surfaces and their reactivity.

In recent literature quite a lot of work dedicated to Cu-Fe surfaces can be found. The reasons that authors give for their investigations depend on their field of interest but can basically be reduced to the fact that the properties of the Cu-Fe system cannot be described by a simple addition of the bulk properties of both metals. Of course this observation is not restricted to the Cu-Fe system.

So the first reason to study bimetallic systems is the fundamental question which (new) properties are induced when two metals are put together. Answers to this question result in a better understanding of matter in general. Sometimes the new properties can be made profitable to mankind and that is where applied research comes in. So the second reason to study bimetallic systems is that the understanding of these systems can improve existing applications or lead to new applications.

As for the pure metals, in bimetallic systems differences exist between bulk and surface properties. These differences are not only interesting from a physical point of view (for example crystalline and electronic structure, magnetic properties, or surface composition compared to bulk composition) but also from a chemical point of view. One may be curious to know what the reactivity of a bimetallic surface is compared to that of the single constituents.

On the more practical side the interaction of surfaces with gases may be disastrous when one thinks of corrosion, but also very worthwhile because, for example, in heterogeneous

catalysis metals (or metal compounds) are often used to produce desirable products. In principle catalysts are used to enhance chemical reactions in order to permit (industrial) processes to be carried out under better (= cheaper) conditions. Since present day requirements in industry ask for a more careful use of reactants, catalysts with a better performance must be developed. This means higher selectivity for the desired product without loosing activity or reducing the lifetime of the catalyst. This requires a good understanding of the mechanisms of the reactions taking place on the surface of the catalyst. Though the differences between catalysts and model surfaces like single crystals are huge, the study of model systems is a convenient way to get a better insight in processes occurring on the surface. Campbell states it even stronger in his review paper on bimetallic surface chemistry [1]: "The well-defined bimetallic surfaces offered for first time an ability to correlate surface chemical reactivity with atomic level surface structure."

When studying the reactivity of well-defined surfaces it is sensible to use relatively simple molecules like oxygen, carbon monoxide and hydrogen. However, even these simple molecules can result in complicated processes. Furthermore, because oxygen is an element involved in many surface processes both the reactivity of surfaces towards molecular oxygen and the reactivity of oxygen adsorbed (or incorporated in the surface in some way) towards gases other than oxygen is an important subject. Information about the interaction of CO and H_2 can be used to get more information about structure and composition of oxidised surfaces. And, on the other hand, it can give an indication of what kind of sites are involved in the interaction. The same can be said for the interaction of CO with unoxidised surfaces.

1.2 Cu-Fe surfaces.

For this thesis the most important differences between copper and iron are the crystal structure at room temperature, the surface free energy and the reactivity towards oxygen and carbon monoxide. These and other properties of both metals are listed in Table 1.

Many studies have been done on the Cu-Fe system [7-28]. Several of them concern the magnetic properties of these surfaces [22-28], or in close relation to that, the structure of iron grown on copper single crystal surfaces [7-13]. Also the chemical reactivity of the Cu-Fe surfaces has been subject of quite a number of studies [29-37].

The growth of iron on Cu(100) has been studied with a large number of techniques. Though some discussion still exists about details in the growth mechanism, all authors agree about the formation of an fcc iron layer when iron is evaporated at or below 300 K. Since the discussion concerns mostly the exact number of monolayers at which the growth mode changes and the exact temperature at which those changes happen, just an outline of the growth without mentioning many numbers or temperatures will be given.

Evaporating iron at room temperature initially gives epitaxial iron islands on the copper surface followed by a layer-by-layer growth (4 - 11 ML) [7-13]. According to Wuttig et al. [13] the presence of CO during evaporation induces a longer region of layer-by-layer growth. This effect is already found for CO pressures of $7 \cdot 10^{-8}$ Pa. The copper/iron surfaces are not stable, even at room temperature slow changes occur [7-11]. The Cu(100)-Fe system has been studied with STM by Brodde et al. [9] and by Chambliss et al. [10]. They report an iron induced diffusion of copper atoms starting at room temperature. This is confirmed by an ion-scattering spectroscopy study [12]. Brodde et al. [9] also found that annealing the surfaces

Table 1. Some properties of copper and iron.

	copper	**iron**
Bulk		
molecular weight (g/mol)	63.546	55.847
density (g/cm^3 298 K)	8.92	7.86 (bcc)
melting point (K)	1356	1808
$T_{transition}$ (K) bcc⁄fcc [2]	--	T < 1180 bcc T > 1223 fcc
nearest neighbour (Å)	2.55	2.48 (bcc)
refractive index [3]	0.25 + 3.6i	2.87 + 3.36i
ΔG_f oxides (kJ/mol, 298 K) [4]	Cu_2O -198.3 CuO -168.8	FeO -283.7 Fe_3O_4 -1159.1 Fe_2O_3 -849.5
surface		
γ (ergs/cm^2) [5]	1670 (1320 K)	2150 (1673 K)
ΔH_{ads} for CO (kJ/mol) (at θ_{CO}=0, 300 K)	69.4 [5] Cu(100)	100 ± 5 [6] Fe(100)*)
s_0 oxygen (300 K)	0.01	1

*) on most Fe single crystal surfaces CO dissociates at 300 K

causes an extensive migration of copper atoms. The copper atoms even seem to cover the iron islands.

Van Pruissen et al. [29-34] studied the reactivity of Cu(111)-Fe and Cu(110)-Fe surfaces quite extensively. However, the use of iron pentacarbonyl to deposit iron on the copper surfaces results in less well-defined surfaces as one might desire. The possibility to deposit iron on the surface by means of evaporation and the relative good knowledge of the growth of iron on the Cu(100) plane led to the choice to study the reactivity of the Cu(100)-Fe surfaces. Direct comparison with the work of Van Pruissen is thus impossible, but a simple heat treatment of the surface should take away most of the differences caused by the two preparation methods and leave differences caused by the different copper planes.

1.3 Scope of this thesis.

The central theme of this thesis is how oxygen reacts with the well-defined Cu(100)-Fe surfaces and what the composition of the surface is after the reaction. The influence of the iron coverage on the interaction and the composition is taken into account. Since the oxidation of iron can result in different kinds of iron oxide, much attention is paid to the oxide formed and to the intermediates that exist during the reaction. Chapter 3 describes the results of the oxidation of Cu(100)-Fe surfaces studied with Auger electron spectroscopy (AES), ellipsometry and low energy electron diffraction (LEED). In chapter 4 a more detailed analysis of the Fe $M_{2,3}VV$ Auger transition during oxidation is given. Chapter 5 and 6 are dedicated to photo-emission results (XPS and UPS respectively).

The reactivity of the oxidised surfaces to hydrogen and carbon monoxide is also a matter of interest since it tells more about the structure of the oxide (surface). In chapter 7 the study of this reactivity is described.

The formation of fcc iron on the Cu(100) surfaces opens the possibility to study this type of iron at temperatures where bulk fcc iron is unstable. The interaction of carbon monoxide with iron is probably influenced by the structure of the iron on an atomic level. Chapter 8 deals with the interesting features of the interaction CO with Cu(100)-Fe surfaces.

The results described in chapter 4 could only be obtained after an improvement in data acquisition and analysis of the AES spectra. Chapter 2 gives, besides a general description of the techniques used in this thesis, also a description and discussion of a better method for data acquisition of AES spectra. The necessary changes in the data analysis are described in chapter 9.

2

Experimental

2.1 Introduction. Ultra high vacuum.

The interest in solid-gas (or solid-vacuum) interfaces has been increasing rapidly during the last three decades. On one hand this is due to the practical importance of these interfaces in daily life (read: 'industrial purposes') as found in heterogeneous catalysis, micro-electronics and corrosion, and on the other hand it is due to the possibility of studying these interesting interfaces under appropriate conditions: ultra high vacuum (UHV). The reason UHV is appropriate for these studies is twofold: First, many surface sensitive analytical techniques require pressures below 10^{-6} Pa because they use low energy charged or neutral particles as probes (for electrons typically energies up to 10^{3} eV are used). The mean free path of these particles in vacuum depends on the energy and the pressure. Second, since the interest often concerns clean surfaces or surfaces containing known amounts of hetero atoms/compounds, the partial pressure of contaminating compounds must be below a certain level to be able to maintain the surfaces in the desired condition during a reasonable time interval. In practice this means that in UHV systems base pressures in the 10^{-8} Pa range are maintained. Development and improvement of adequate pump systems and welding technology during the last decades make these pressures now readily obtainable.

Besides vacuum technology many techniques were developed to study surface composition and structure (both electronic and geometric) of different kinds of samples. Apart from giving different types of information some techniques are destructive, some non-

destructive and others enhance or influence chemical processes on the surfaces. Thus special care is required in choosing the proper techniques and in interpreting the data correctly. As all techniques have their own special qualities several of them are required to get proper insight in the surface (-processes).

In order to get information about the reactivity, composition and structure of Cu(100)-Fe (oxide) surfaces AES, ellipsometry, LEED, XPS and UPS are used in combination. Since all these techniques are well described in the literature [38-42], only features of the techniques that are of special interest for the studies described in this thesis will be explained in greater detail in the next sections. More attention is paid towards data acquisition and analysis for AES because the procedures as used in this thesis differ from the common procedures.

Finally a description of the UHV-systems used in this thesis and the methods for sample preparation will be given.

2.2 Auger electron spectroscopy.

Auger electron spectroscopy (AES) uses the electrons resulting from the Auger decay process [40]. The energy of an Auger electron depends on the energy of the orbitals involved and thus is characteristic for an element. Due to the small inelastic mean free path (imfp) of the Auger electrons (ca. 3 - 15Å for energies between 40 and 1000 eV) the information depth is reduced to about 2 - 10 atomic layers [43]. Thus AES gives (quantitative) information about the atomic composition of the top layers of the surface.

Since in AES the (core) holes required for the Auger process are usually created by high energy (ca. 2 - 5 keV) electrons the number of so called secondary electrons is much higher than in the case of X-ray induced holes. These secondary electrons are the result of a number of inelastic scattering processes in the surface region. In the spectra the electrons of interest are thus superimposed on a background which is at least one order of magnitude higher in number. In the past the most convenient way to make the data accessible was to detect the derivative (or second derivative depending on the analyser) using a phase sensitive amplifier (lock-in-amplifier) and a x-y recorder. In this way small signals can be 'separated' from a large background with relatively high signal-to-noise levels. An other 'advantage' of this procedure is that a slowly changing background can be (must be) neglected. Correction methods have been developed for steep backgrounds [44].

Nowadays, the availability of cheap personal computers (a 80286 can do the job) and 14 bit or more analogue-to-digital converters eliminates all reasons not to use more sophisticated methods. However, the peak-to-peak heights of the differentiated Auger spectra are still used by many scientists to determine the surface composition. It is relatively easy to compare the spectra with those of Auger handbooks and to use relative sensitivity factors to calculate the chemical composition of the surface. This presupposes the same peak shape for both the sample and the elemental standard used. Identical conditions are required in both cases: modulation amplitudes and all other instrument specific functions have to be the same. Although, even then, it can be dangerous to use the differentiated spectra for quantitative analysis. Both the overlap of peaks of different elements and a change in peak shape can cause errors in quantification. To illustrate this argument the results obtained from differentiated spectra are compared with results obtained using the original N(E) vs. E spectra and a background subtraction as described in chapter 9.

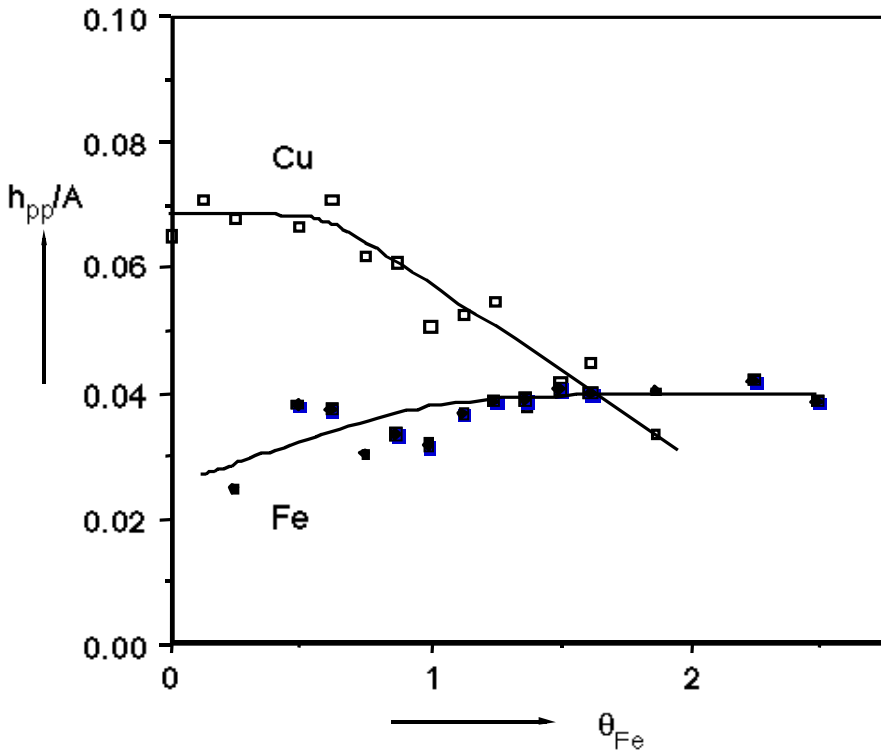

Figure 1 *The ratio of the peak-to-peak height and the peak area of the Cu and Fe $M_{2,3}VV$ peaks during evaporation of iron on Cu(100). Lines are drawn to guide the eye.*

Fig. 1 shows the ratio of the peak-to-peak height (h_{pp}) and the peak area (A) of the Fe and the Cu $M_{2,3}VV$ peaks obtained during the evaporation of Fe on Cu(100) as function of θ_{Fe} (the same spectra were used to obtain Fig. 8 in chapter 9). The differentiated spectra were obtained by means of numerical differentiation of the original spectra. It is clear that h_{pp}/A is not constant with changing peak intensities. A constant h_{pp}/A is expected when the peak shape does not change. For the metallic Cu(100)-Fe system no shape change of the $M_{2,3}VV$ peaks is observed within experimental error for both the Fe and the Cu $M_{2,3}VV$ peak [45]. So the changing h_{pp}/A must be due to effects of the overlap of both peaks. In that case one should expect the deviations to be largest for θ_{Fe} values for which one of both peaks is small in respect to the other. In fact this is the case. A similar effect is visible in Fig. 2. In this figure h_{pp}/A of the Cu and Fe $M_{2,3}VV$ peaks is given as function of the amount of oxygen on a Cu(100) surface containing one monolayer (ML) of iron. (The same spectra were used in Fig. 5 in chapter 4.) Here the decrease of h_{pp}/A for the Cu $M_{2,3}VV$ peak is caused by the increasing overlap with the Fe $M_{2,3}VV$ peak. The h_{pp}/A for the Fe $M_{2,3}VV$ peak decreases fast during the adsorption of the first ML of oxygen because most of the shape change in the Fe $M_{2,3}VV$ peak occurs during this part of the oxidation [46]. Quantitatively the derivative spectra are deluding in the described cases. In the last case it is also difficult to extract useful information about the oxidation.

To show that in some cases there is no difference in both methods, results of the analysis of the O KLL and Fe the LMM peaks obtained during the oxidation of Fe(100) are presented in Fig. 3. The ratio of the O and Fe peak areas is given as function of the ratio of the h_{pp} of the O $KL_{2,3}L_{2,3}$ (515 eV) and the Fe $L_3M_{4,5}M_{4,5}$ (705 eV) peaks. The straight line is the

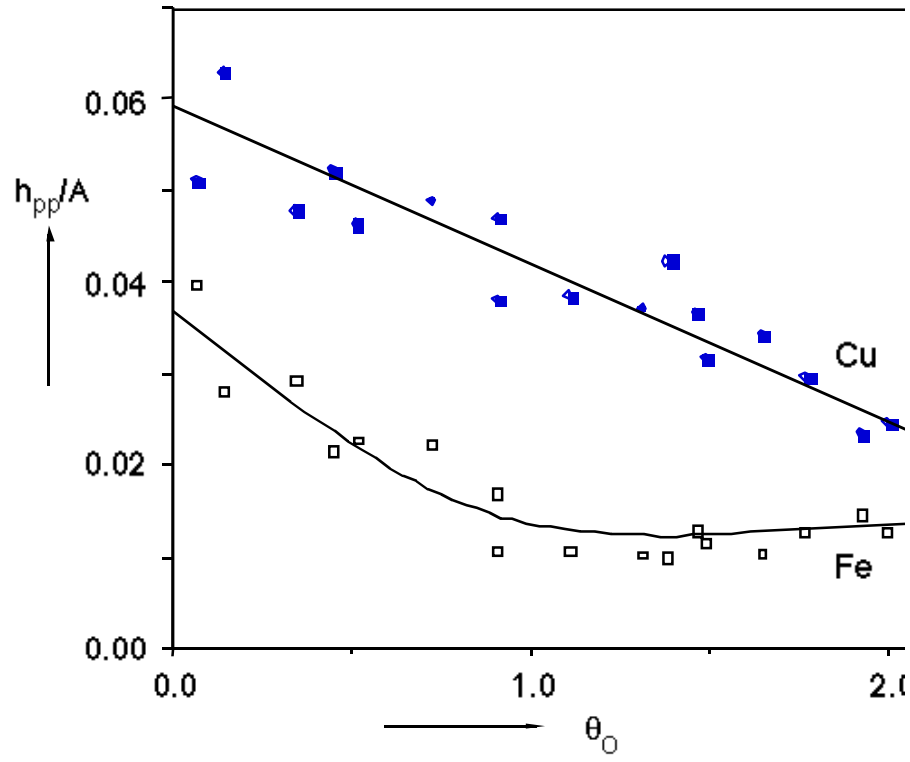

Figure 2 *The ratio of the peak-to-peak height and the peak area of the Cu and Fe $M_{2,3}VV$ peaks during oxidation of one monolayer of iron on Cu(100). The lines are drawn to guide the eye.*

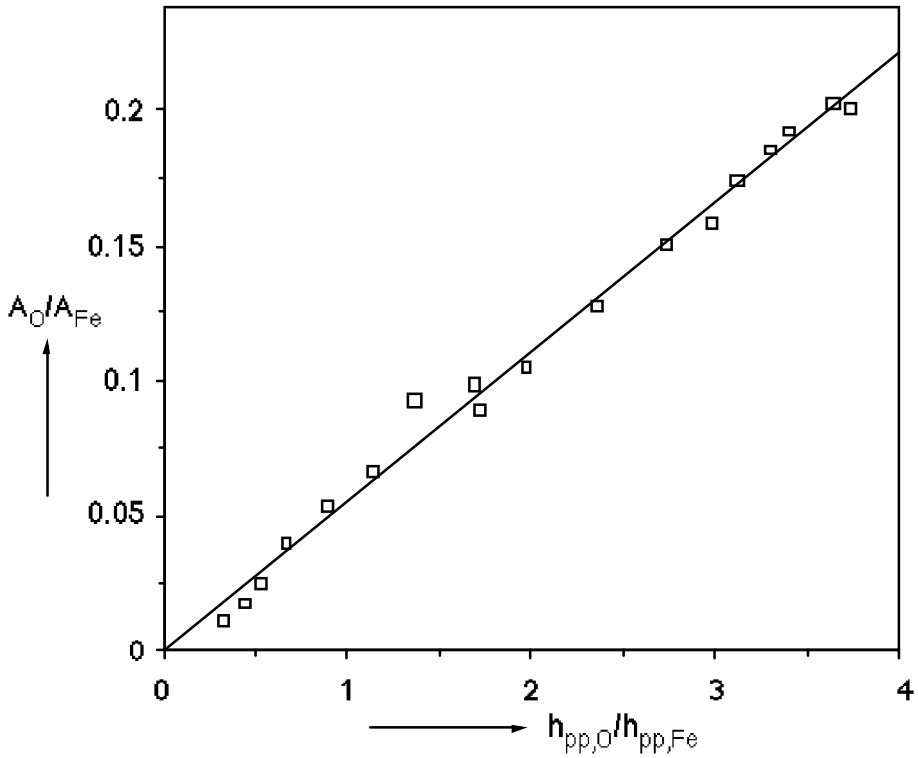

Figure 3 *The ratio of the O KLL and the Fe LMM peak area plotted against the ratio of the peak-to-peak height of the largest peaks during oxidation of Fe(100).*

linear fit through the points. The line indicates that both methods give the same results in quantification. One remark must be made: a possible shape change of the Fe $L_3M_{4,5}M_{4,5}$ peak might be invisible in the spectra used since they were obtained using a modulation amplitude of 8 V_{pp} (section 2.2.1 of this chapter gives more details about data acquisition).

It may be clear now that for reasons of accuracy it is better to collect (and use) the N(E) vs. E spectra. The use of this kind of spectra, however, introduces an other problem: background subtraction. In chapter 9 a method is described that appeared to give satisfactory backgrounds. Unless stated otherwise the AES spectra in this thesis were collected and handled as described in the next sections.

2.2.1 Instrumentation and data acquisition.

The AES spectra were produced by exciting the top-layer atoms using an electron beam perpendicular to the surface with an energy of 2500 eV and a beam current of 1-3 μA. For the subtraction of a good background on the high energy part of the AES spectra a higher primary beam energy (5 keV) would have favourable but the electron gun did not admit that. The lower limit of the intensity of the beam current was determined by the sensitivity of the detection system.

A 4 grid retarding field analyser (RFA, also used as LEED optics) with an on-axis electron gun was used to analyse the energy of the emitted electrons. The angle of acceptance of the RFA was 120°, the resolution 0.3%. The often used bias voltage of 200 V on the collector was not necessary because of a soot coating on the collector. The production of extra secondary electrons on the grids was prevented by a carbon coating which was evaporated on the grids. The retarding field was controlled by a computer. The voltage could be changed in steps of 60 mV from 0 to 2000 V. The step width used was 120 mV for the MVV region (20 - 80 eV) and 240 mV for the other parts of the spectrum.

A lock-in-amplifier (LIA) was used to obtain the first derivative of the I versus E spectra. A modulation frequency of 2.4 kHz was used. The spectra in the MVV region were collected with a peak-to-peak modulation amplitude of 0.7 V_{pp}, the sulphur LMM and the carbon KLL with 4.0 V_{pp} and the other spectra with a modulation amplitude of 8.0 V_{pp}. The output of the LIA was sampled either by integrating for 500 ms or by adding 10 samples from an analogue-to-digital converter at each energy step. The settings given above were chosen to compromise between the signal to noise ratio, the resolution and the time needed to collect a spectrum. Usually two scans were collected and added in order to check for drift and to increase the signal to noise ratio.

2.2.2 Data analysis.

The Fe $M_{2,3}VV$, Cu $M_{2,3}VV$ and O KLL peaks were extracted from the spectra by means of a background subtraction method proposed by Peacock [45,47]. Areas of the Fe $L_{2,3}M_{2,3}V$ and Cu $L_{2,3}VV$ peaks were calculated after subtraction of a linear background because the use of a primary beam energy of 2500 eV in combination with the long region in the spectrum containing Auger features for these surfaces (470 - 950 eV) makes it very difficult to use a more sophisticated method. The validity of this method for quantitative use was checked by using the peak-to-peak heights from numerically differentiated spectra.

Because of day to day changes in the electron gun emission it was necessary to correct the peak areas for changes in the beam current. For the $M_{2,3}VV$ spectra this could done by using the height of the background at 79 eV as internal standard [45, 48, 49] but for the high energy peaks a more complicated method had to be used. Since the surfaces only contained copper, iron and oxygen the sum of the Cu $L_{2,3}VV$, Fe $L_{2,3}M_{2,3}V$ and O $KL_{2,3}L_{2,3}$ peak areas multiplied by their relative sensitivity factors (RSF's) was taken to represent the beam current. The RSF's have to be used because the three components have different cross sections and inelastic mean free paths (imfp). The RSF's ($f_{Fe,Cu}$ and $f_{O,Cu}$) were determined relative to the Cu $L_{2,3}VV$ peak. The RSF of Fe was determined from the Fe $L_{2,3}M_{2,3}V$ intensity of 16 ML of Fe on the Cu(100) surface. The Fe $L_{2,3}M_{2,3}V$ intensity of this surface is the same as Cu $L_{2,3}VV$ intensity from the clean Cu surface. The RSF of Fe $L_{2,3}M_{2,3}V$ relative to Cu $L_{2,3}VV$ ($f_{Fe,Cu}$) could now be taken to be unity. To check the reliability of this number the imfp of the I_{Fe} vs. θ_{Fe} plot (ASt-plot) is calculated assuming a perfect first monolayer (the influence of a slightly imperfect first monolayer on the calculation is expected to be negligible). The resulting imfp is 1.2 ± 0.2 nm, which is in good agreement with calculations of Tanuma et al. [50]. As the preparation of a pure oxygen surface is impossible, the signal of the known saturation value of oxygen on Cu(100) (0.52±0.05 ML [51]) and an imfp of 1.0 nm for the O $KL_{2,3}L_{2,3}$ electrons were used to calculate the RSF. This appeared to be $f_{O,Cu} = 1.4 \pm 0.2$. When also the O $KL_1L_{2,3}$ and the O KL_1L_1 peak areas are included $f_{O,Cu}$ becomes unity. Here should be noted that the magnitude of the RSF depends sensitively on the background procedure. Thus the values mentioned here are useful only for the data handling as performed in this thesis. An other important point here is that the corrected intensities (f_xI_x/Sf_iI_i) do not necessarily represent mole fractions because that interpretation requires a homogeneous distribution of the atoms in the surface layers. Though in some special cases the error in the so determined mole fraction is small [52], mole fractions are not useful in the work presented here.

2.3 Photoelectron spectroscopy.

Photoelectron spectroscopy uses the electrons emitted from an atom by means of photon-excitation. In this thesis only Mg K_α (1253.6 eV) X-rays (XPS) and He I and II (respectively 21.2 and 40.8 eV) ultra violet radiation (UPS) are used. With the use of X-ray excitation is easy to determine the different elements present in the surface. The depth sensitivity of both UPS and XPS as used in this thesis is similar to that of AES. The usefulness comes from the possibility to determine the chemical surrounding of the element because the core levels are sensitive to this. Due to the low energy of the UV radiation for He I and He II UPS is especially (if not only) suitable for the study of the valence band. Since the valence band of multiple element systems often consists of overlapping contributions of those elements more information can in some cases be obtained using different excitation energies. This is due to different excitation cross-sections that change differently with changing excitation energy. The energy of the structures in the valence band can sometimes be used to discriminate between oxidation states of the component.

2.3.1 Instrumentation and data acquisition.

The X-ray photoelectrons were excited by Mg K_α radiation produced by a fresh Mg/Al anode operated at 20 mA and 14 kV. Using a new anode and the relatively low current ensured the absence of the Al K_α induced Cu 2p ghosts which disturb -when present- the Fe 2p spectra. A hemispherical analyser was operated at a pass energy of 35.75 eV and steps of 0.1 eV were used to obtain the Fe 2p (736-699 eV), the Cu $2p_{3/2}$ (940-925 eV) and the O 1s (535-525 eV) spectra. A sample time of 500 ms/step was used and respectively 10, 2 and 10 scans were added to improve the signal to noise ratio. Shirley backgrounds (using 5 iterations) were used to obtain the Fe 2p and Cu $2p_{3/2}$ peaks; for the O 1s peak a second order polynomial was subtracted because the presence of Fe and Cu Auger peaks on both sides of the O 1s made the use of a Shirley background impossible.

The UPS spectra were collected using a He discharge lamp the same analyser as used for the XPS spectra. The analyser was operated at a pass energy of 4.25 V and steps of 0.025 and 0.10 V were used for respectively He I (21.2 eV) and He II (40.8 eV) photoemission spectra. Scans were sampled until a reasonable signal to noise ratio was obtained.

2.4 Ellipsometry.

Ellipsometry is a technique that uses photons to determine (the change in) optical properties of the surface. This means that changes in the electron distribution of the surface layer can be determined. These changes can be caused by chemical processes or by changes in the surface structure. Great advantages of ellipsometry over other techniques are first that the photons used (He-Ne laser, 632.8 nm, ca. 2 eV) do not influence reactions and can be used at all pressures, second that the sample depth is about two orders of magnitude larger than for AES meaning that also atoms migrated into the bulk can be detected to some extent and third that the complete instrument is situated outside the UHV.

The useful information is obtained from the change in the state of polarisation of the reflected beam. Analysis of this change results in two parameters Δ and Ψ. Values of Δ and Ψ can also be calculated for a surface when the composition and the refractive indices (or other physical properties that can be used to calculate the refractive indices) of the constituents are known [38,53]. For many bulk materials these data are readily available [54]. However, the optical properties of very thin films (up to a few ML) are different from bulk values and for the films studied in this thesis even bulk properties are unknown. This may seem rather distressing but fortunately an empirical calibration is possible.

For oxygen adsorption and the oxidation of several metal single crystal surfaces an absolute calibration has recently been done by means of nuclear reaction analysis (NRA) [51,55]. It appeared that on all metals that were examined the change in Δ was linear with the change in the amount of sorbed oxygen with an exception for 'chemisorbed' oxygen on Ni, Co and Fe. Thus reactions concerning oxygen can easily be followed using ellipsometry. Also adsorption of CO causes a change in Δ but in this case calibration (especially for linearity) is difficult. However, good results based on the assumption of linearity are reported in literature [6,29,58].

In oxidation experiments under mild conditions of metals such as Ni, Fe, Co and Cu, the change in Ψ is usually small with respect to that of Δ and not necessarily linear with the oxygen uptake. Therefore much more attention is paid to changes in Δ than to changes in Ψ.

Due to the set-up of the UHV system sample movement is required for performing the different techniques. This means that absolute Δ and Ψ values can be reproduced with an accuracy of only several tenths of degrees. However, when performing ellipsometry with a fixed sample position changes in Δ and Ψ can be determined with two orders of magnitude better accuracy. For this reason $\delta\Delta$ and $\delta\Psi$ are used. $\delta\Delta$ and $\delta\Psi$ represent Δ^0-Δ and Ψ^0-Ψ respectively where Δ^0 and Ψ^0 as used in this thesis are the Δ and Ψ values of the surface after evaporation of iron. *This means that the initial values of Δ and Ψ (Δ^0 and Ψ^0) are different for surfaces containing different amounts of iron.*

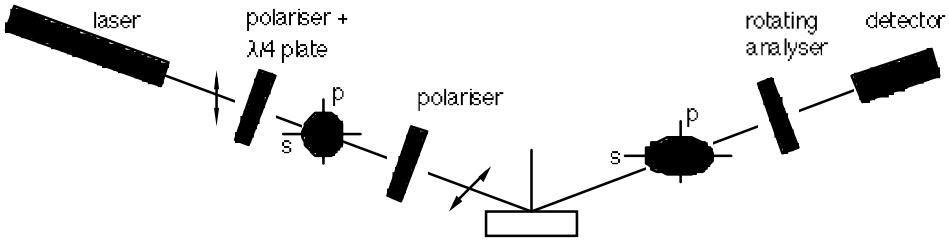

Figure 4 Experimental set-up of the ellipsometer.

2.4.1 Instrumentation and data acquisition.

Ellipsometry was performed in a configuration using a rotating analyser [38]. The set-up which is shown in Fig. 4 consists of a 10 mW He-Ne laser (λ=632.8 nm), a polariser and a quarter wave plate connected to each other (the axes making an angle of 45° in order to produce circular polarised light), a polariser to choose the desired angle of polarisation, the sample, a rotating analyser and finally a detector. Before and after the windows of the UHV system pin-holes were placed to stop unwanted reflections. The angle of incidence of the beam is 69.5°. The polariser/quarter wave plate assembly is used to enable a stepless change of the intensity. This is more convenient in respect to grey tone filters or pin-holes to reduce the intensity. The angle of the analyser is determined by means of an encoder plate connected to the polarisation filter which gives 1024 pulses per revolution on one channel and one 'master-pulse' per revolution on a second channel. An ADC converts the intensity as determined by the detector directly when a pulse is detected, starting each revolution at the master-pulse. The analyser rotates with about 5 Hz and usually the results of 8 revolutions are added before calculating Δ and Ψ. This procedure to determine a couple of Δ and Ψ values takes about 2.5 s. Since the time required to stabilise a desired reactant pressure is about 30 s the time needed to determine Δ and Ψ is not limiting for the experiments. In practice Δ and Ψ are determined every 5 s (and for slow changes even 10 or 30 s in order to reduce to amount of data).

Values that represent the intensity of the beam and the angle of the master-pulse with respect to the direction of the polarisation filter are required to determine Δ and Ψ. These values were determined before each experiment using light with an angle of polarisation of 90° with respect to the plane of incidence.

2.5 Experimental set-up.

2.5.1 The systems.

The UHV system used in Utrecht (chapters 3,4,7-9) was pumped by a turbomolecular pump (50 l/s), an ion-pump (200 l/s) and two titanium sublimation pumps. The base pressure was usually in the low 10^{-8} Pa range. To reach this pressure the system was baked by internal heating with lamps for two days. The system was equipped with an AES/LEED system, windows to perform ellipsometry, an electron beam evaporation source, an ion-gun, a Bayard-Alpert and a hot cathode pressure gauge and a rest-gas analyser. The pressure gauges could be read into the computer via the 4 ADC inputs of the LIA. To admit gases two gas inlet systems each containing the possibility to attach 4 lecture bottles were connected to the system by means of two leak-valves. Both systems could be pumped with the turbo pump separately from the main chamber. The crystal was mounted into a manipulator which could be moved in 3 orthogonal directions, rotated around the vertical axis (360°.) and tilted around a horizontal axis for 110°. The manipulator contained a heater with which the sample could be heated from 300 K to about 900 K. The temperature was determined by means of a chromel/alumel thermocouple pressed by force to the rear of the crystal. The crystal had to be moved to place it in the right positions to perform the different techniques. AES and LEED were performed with the crystal in the focus position of the LEED optics. For ellipsometry the position of the crystal was determined by the space required to let the beam pass through the windows and along the LEED optics without scattering.

The UHV system used in l'Aquila (chapters 5 and 6) was equipped with AES, LEED, XPS, UPS and an evaporation source which is in an other small chamber connected with the main system by means of a transport system. The complete system was pumped by an ion-pump (400 l/s).

2.5.2 The crystal.

The Cu(100) crystal was spark cut from a 5N copper rod within 0.5 deg of the [100] direction, mechanically polished and mounted in the manipulator. The cleaning procedure consisted of repeated Ar ion bombardment (600 V, 1-3μA/cm2) and annealing until no contamination could be detected with AES. In the end the crystal was annealed for 15 min. at 725 K. A sharp (1x1) LEED pattern could be observed after this procedure and cooled down to 300 K.

2.5.3 Gas handling.

The argon, oxygen, hydrogen and carbon monoxide used had purities of better than 5.0, 4.5, 4.5 and 4.5 respectively. During the experiments involving gas exposures the gas was admitted in the system while still pumping with the turbo pump (though with reduced pump speed) in order to establish a continuous refreshing of the gas inside the chamber.

2.5.4 Evaporation of iron.

The electron beam evaporation source was loaded with 4N iron and thoroughly degassed before use. A metal shield with three apertures was placed over the source to prevent the iron to cover the complete system. One is used for a mirror permitting to monitor the iron when evaporating, the second for a micro balance thickness monitor and the third was equipped with a shutter. The source was situated about 35 cm below the sample. The micro balance thickness monitor was calibrated for its position by means of a second monitor temporarily placed in the position of the sample. The calibration was performed for fluxes between 0.3 and 5 ML/min (at the position of the sample). The ratio between the fluxes determined by both monitors appeared to be independent of the flux for this range. When using the evaporation source all pumps were used. However, this could not prevent the pressure to rise to ca. 10^{-6} Pa. The oxygen contamination at the surface was usually lower than 5% of a ML and only few times could carbon be detected. Here must be mentioned that working with gases as CO and oxygen in the same chamber as where the evaporation source is used increases the amount of contamination in the iron (and the pressure during evaporation).

The amount of iron (and also of other components on the surface) is given in monolayers (ML), where one ML is equivalent to the number of atoms per unit area of the Cu(100) surface, i.e. $1.53 \cdot 10^{19}$ m^{-2}.

In l'Aquila the iron (purity better than 0.9999%) was evaporated from a electrically heated crucible. The flux was determined by means of a quartz micro balance thickness monitor placed at the same height as the sample. The iron was deposited at fluxes varying between 3 and 6 ML/min.

3

Oxidation of ultra thin iron layers on Cu(100) studied with AES and ellipsometry.

Abstract

The oxidation of Cu(100)-Fe surfaces containing 0-2.7 ML of Fe was studied at room temperature using Auger electron spectroscopy, ellipsometry and low energy electron diffraction. The initial oxidation rate was independent of θ_{Fe} which means that oxygen adsorption proceeds via a precursor mechanism. On all surfaces saturation of the oxidation occurred. For $\theta_{Fe}<2$ all iron was oxidised to $FeO_{1.43\pm0.07}$ (Fe_2O_3) and a surplus of $\theta_O=0.5$ was present, probably at the Cu-Fe_2O_3 interface. For iron coverages exceeding 2 ML the oxidation stopped after the uptake of 3.3±0.3 ML of oxygen. LEED experiments on a surface containing 0.8 ML of oxidised iron gave evidence for the formation of ordered domains of oxide in two (perpendicular) orientations. The distances of the spots indicate that a strong contraction of the oxide lattice takes place in order to match the Cu(100) lattice.

1 Introduction.

This chapter focuses on the reactivity of Cu(100) surfaces containing up to 2.7 ML Fe towards oxygen at room temperature and the composition and the structure of the surface after oxidation. The techniques used in this study are AES, ellipsometry and LEED.

The oxidation of Cu(111)-Fe and Cu(110)-Fe alloys was studied extensively by Van Pruissen et al. [30-34]. They prepared their alloys by decomposition of $Fe(CO)_5$ on clean Cu surfaces at elevated temperatures. The disadvantage of this procedure is the mixing of the Cu and Fe in the surface layers and a carbon and oxygen contamination at the surface. The exact amount of Fe deposited is unknown. On Cu(111) iron segregates upon oxidation and at high Fe contents γ-Fe_2O_3 is formed as determined from H_2 reduction experiments using ellipsometry. Also on Cu(110) iron oxide is formed at the surface. The stoichiometry on this surface was determined with LEED and AES and appeared to be $Fe_{0.95}O$ (wüstite).

The oxidation at room temperature of the Cu(100)-Fe system has been studied by Kishi and Nishioka [35] using XPS. The shifts of the Fe $2p_{3/2}$ peak after exposure of 750 L (0.1 Pa·s) O_2 to surfaces containing 0.3, 0.6 and 2.0 ML Fe were ascribed to FeO like species for the two lowest coverages and Fe_3O_4 like species for 2 ML of iron. So the type of oxide formed seems to depend on the amount of Fe present at the surface.

For Fe deposited on polycrystalline copper Di Nardo et al. [36,37] observed different Fe $2p_{3/2}$ peak positions for different Fe coverages after an oxygen exposure of 50 L (6.6 mPa·s). These exposures are too small to oxidise the Fe completely at room temperature, so it is hard to say from these experiments which kind of oxide is stable at room temperature.

3.2 Results.

3.2.1 Ellipsometry.

Cu(100) surfaces containing 0-2.7 ML Fe were exposed to oxygen. The O_2 pressure varied between $1 \cdot 10^{-6}$ and $1 \cdot 10^{-2}$ Pa and the crystal was kept at room temperature. In Fig. 1 $\delta\Delta$ and $\delta\Psi$ are plotted as function of the oxygen exposure for different Fe coverages (0-3 ML of Fe). For reasons of clearness not all oxidation curves are given, but the curves in Fig. 1 are representative for those of surfaces containing other amounts of iron. For all Fe coverages the reaction probability was first order in the oxygen pressure. The $\delta\Delta$ curves in Fig. 1a have an identical shape and the same initial slope. Though not visible on this scale, the $\delta\Delta$ curve of clean Cu(100) has a smaller initial slope. For all surfaces $\delta\Delta$ reaches its saturation value after 3-5 Pa·s (these values are also shown in Fig. 1a), whereas $\delta\Psi$ reaches its saturation value already after 0.2 Pa·s. The surface was taken to be saturated when the change in Δ could not be distinguished from drift, i.e. $|d\Delta/dt| < 0.05 \bullet\ hr^{-1}$. It is obvious that the value of $\delta\Delta$ at saturation increases with θ_{Fe}. The saturation value of $\delta\Psi$, however, decreases with θ_{Fe}. Therefore the saturation values $\delta\Delta_{sat}$ and $\delta\Psi_{sat}$ are plotted as function of θ_{Fe} in Fig. 2. The saturation values of 16 ML Fe on Cu(100) are also shown in Fig. 2. There is obviously no linear or other simple relationship between $\delta\Delta_{sat}$ and θ_{Fe}. The lines plotted in Fig. 2 represent the $\delta\Delta_{sat}$ and $\delta\Psi_{sat}$ values calculated according to a model that will be discussed together with the three indicated regions in section 3.4.2.2.

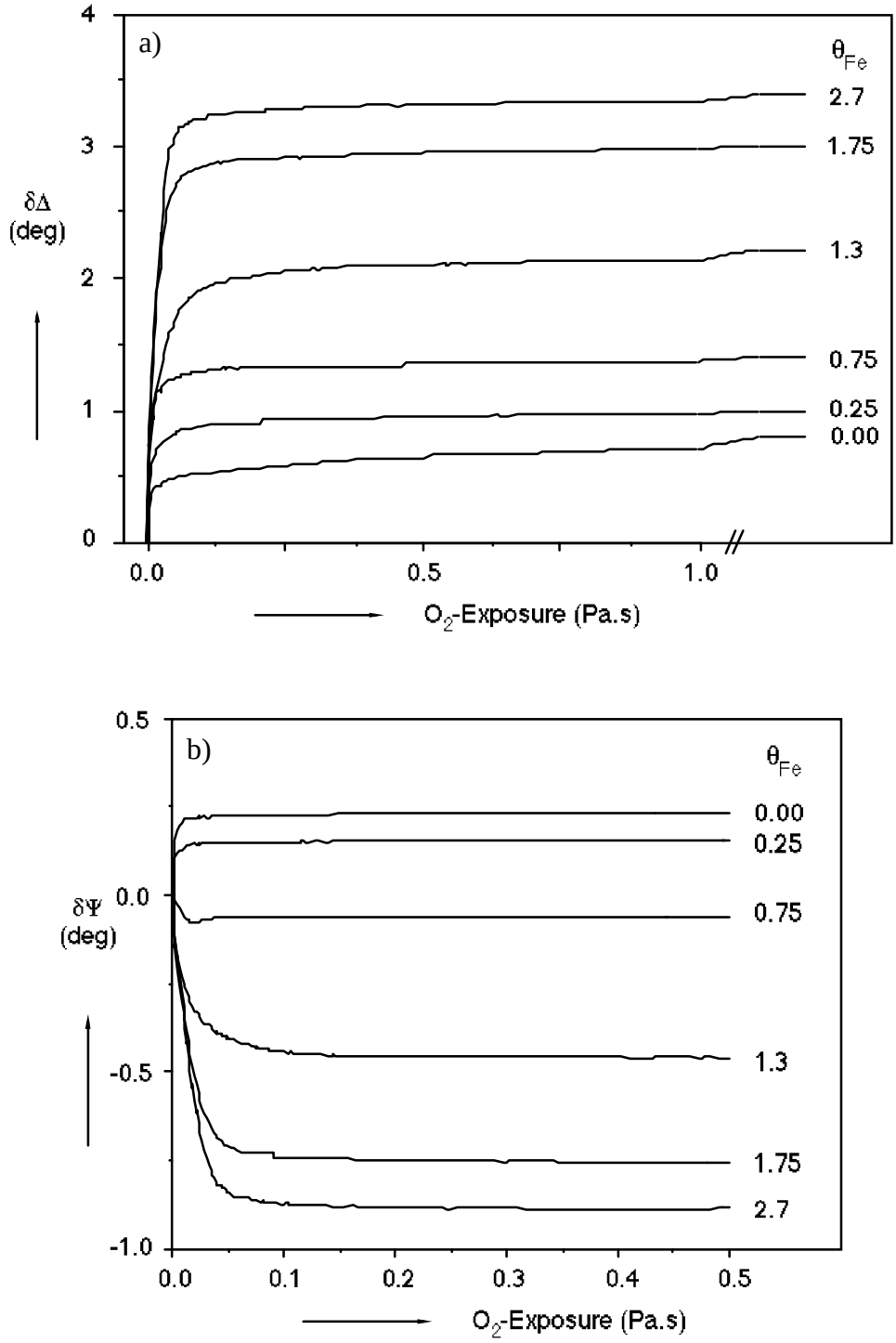

Figure 1 *The change in Δ (a) and Ψ (b) as function of the oxygen exposure for different coverages of iron on Cu(100) at 300K. The saturation values of δΔ of these surfaces are also given.*

3.2.2 AES.

The intensity of the O $KL_{2,3}L_{2,3}$ Auger peak at saturation ($f_{O,Cu} \cdot I_{O,sat}$) is plotted in Fig. 3 as function of the iron coverage. The saturation value of a surface containing 16 ML of Fe is given too. The drawn line is the best fit for $\theta_{Fe}<0.5$. The oxygen intensity does not vary linearly with θ_{Fe} at higher coverages. At $\theta_{Fe}>2$ ML the amount of oxygen is almost saturated.

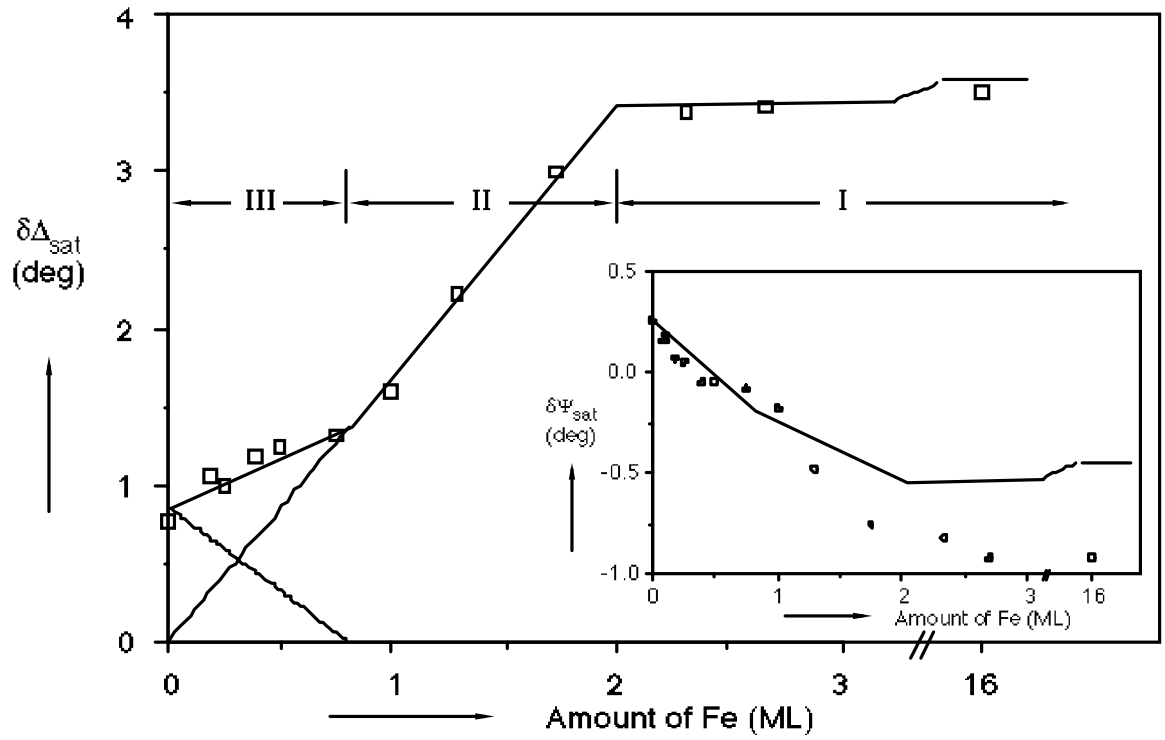

Figure 2 *The saturation value of $\delta\Delta$ as function of θ_{Fe} for oxidation of Cu(100)-Fe surfaces at room temperature. The meaning of the lines and regions is explained in the discussion. In the inset the saturation value of $\delta\Psi$ as function of θ_{Fe} is shown.*

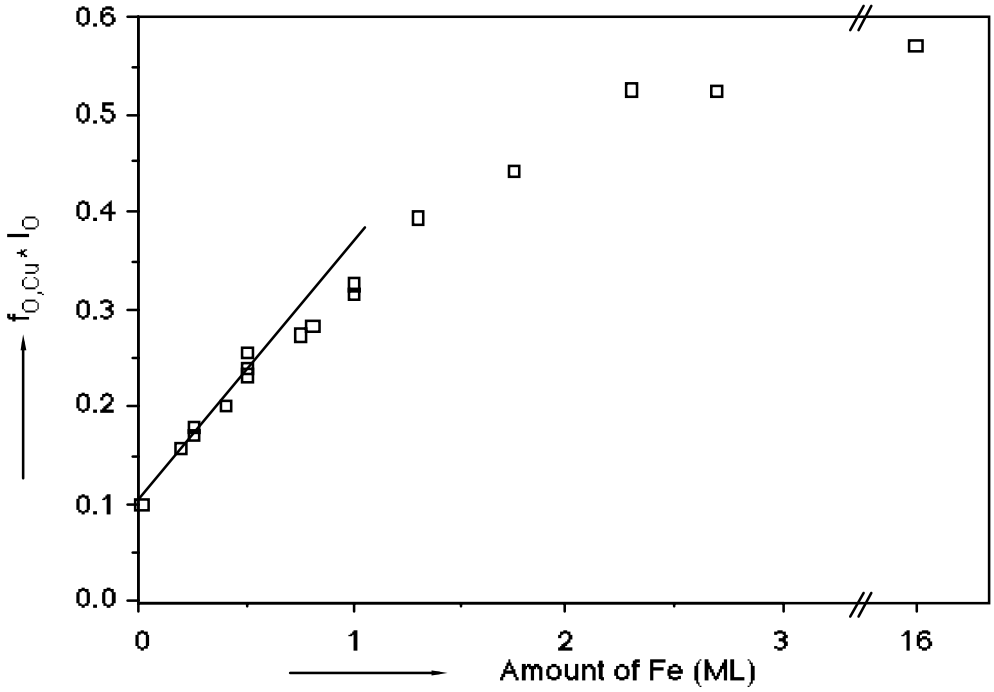

Figure 3 *The intensity of the O $KL_{2,3}L_{2,3}$ peak corrected for the relative sensitivity factor at saturation as function of θ_{Fe}. The line represents a linear fit through the data up to 0.5 ML.*

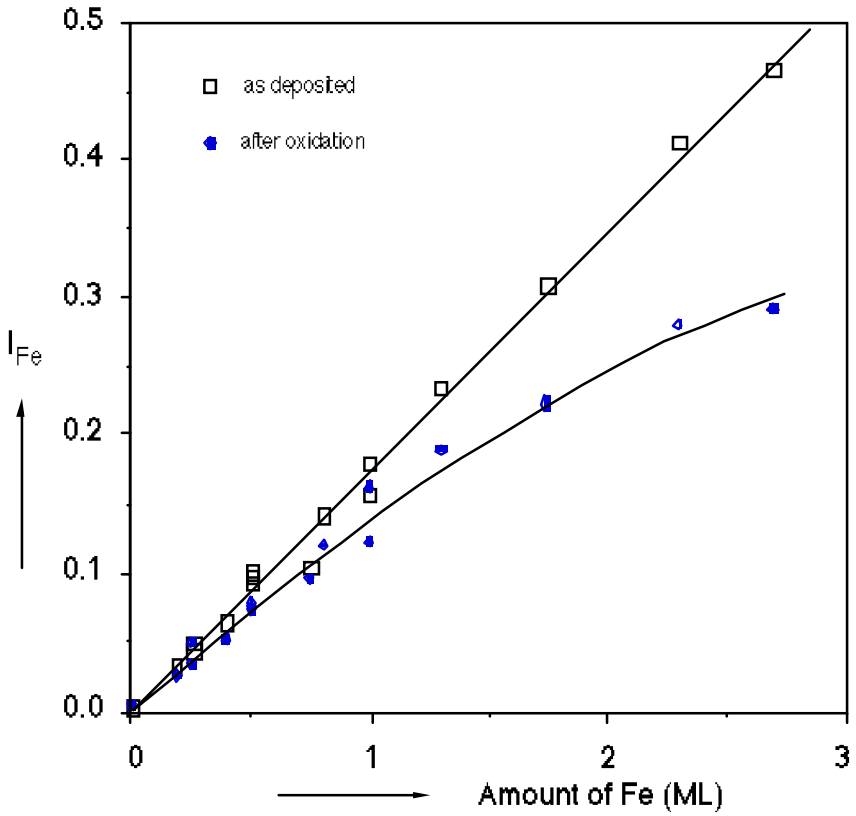

Figure 4 *The intensity of the Fe $L_{2,3}M_{2,3}V$ peak before and after oxidation as function of θ_{Fe}. The line through the points before oxidation is a linear fit, the line through the points after oxidation is to guide the eye.*

The deviation from linearity is also found for the Fe Auger intensity after oxidation. Fig. 4 shows I_{Fe} versus θ_{Fe} before and after oxidation. The line through the points taken before oxidation is a linear fit, the line through the points after oxidation is just to guide the eye. The decrease in signal after oxidation can be ascribed to screening of the Auger electrons due to the spreading of Fe atoms over more layers.

The Fe $M_{2,3}VV$ peaks from oxygen saturated surfaces containing different amounts of Fe were collected and compared in Fig. 5. Both the background and the Cu $M_{2,3}VV$ peak are removed from these spectra. To be able to compare the peak shape with the more frequently used derivative spectra the numerically differentiated spectrum of 2.3 ML Fe (oxidised until saturation) is shown in the inset.

3.2.3 LEED.

Fig. 6 shows the LEED pattern of a surface containing 0.8 ML Fe after oxidation at room temperature. Surfaces containing less Fe exhibited the same pattern but more diffuse. Also annealing at 600 K made the patterns more diffuse. The LEED-spots are arranged in two hexagons. The spots of one hexagon appear to be slightly elliptical with the axes parallel. The hexagons are rotated by 90° with respect to each other.

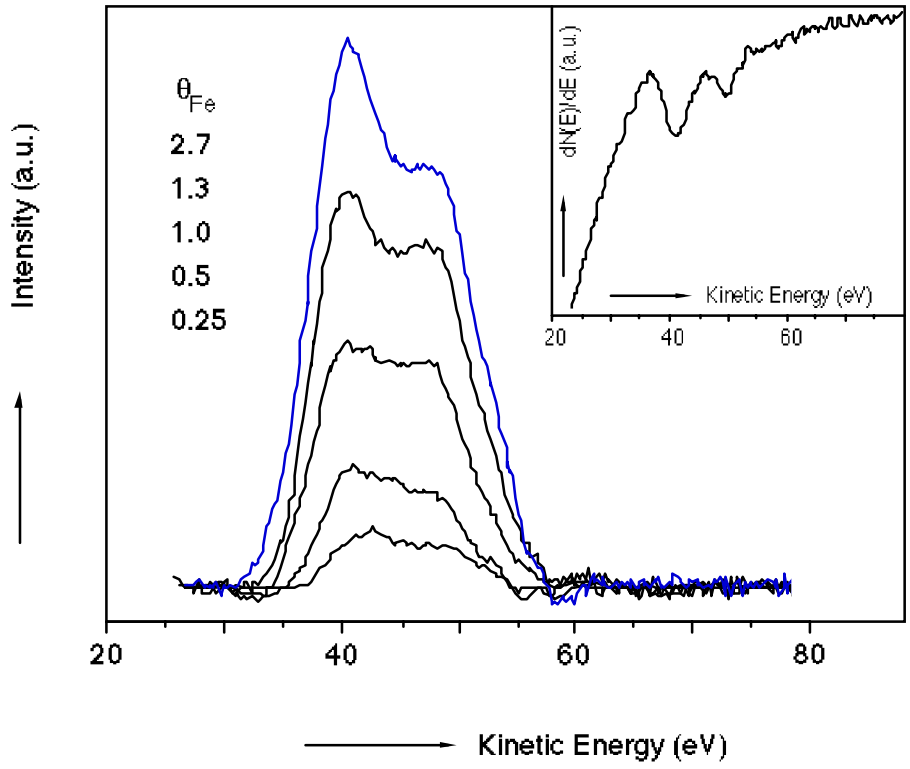

Figure 5 *The Fe $M_{2,3}VV$ peak of completely oxidised surfaces containing different amounts of iron. The inset shows the derivative of a Fe $M_{2,3}VV$ peak of a oxidised surface containing 2.3 ML of iron.*

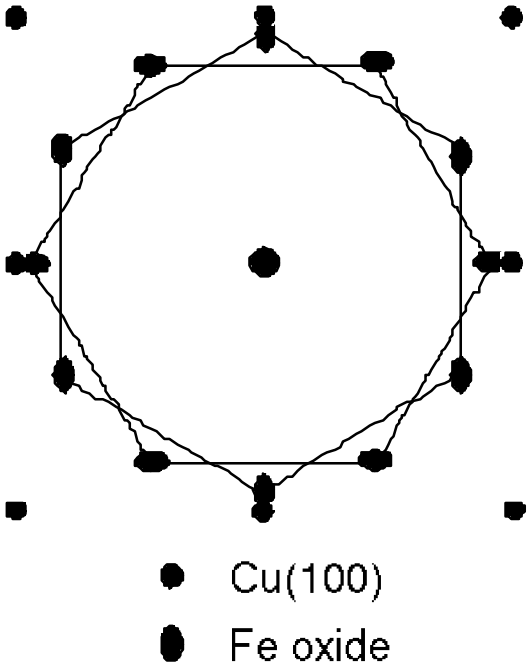

Figure 6 *The LEED pattern of a Cu(100) surface containing 0.8 ML of iron after oxidation until saturation. The beam energy was 119 eV.*

3.3 Discussion.

3.3.1 Oxidation mechanism.

In the curves of $\delta\Delta$ vs. the O_2-exposure of Fig. 1a no sharp changes in slope are visible. Also enlargement of the first 1 mPa·s of oxygen exposure does not reveal any changes. Such breakpoints were found by Van Pruissen et al. [30] for the oxidation of Cu(111)-Fe. They ascribed these breakpoints to a change from the oxidation of Fe to the oxygen adsorption on Cu. The value of $\delta\Delta$ at the breakpoint showed a linear relationship with the iron content of the surface. Breakpoints may be expected when free Cu surface sites are available after oxidation of all iron. Assuming an equal growth in three directions of the oxide coverages of more than 0.6 ML Fe can cover the surface completely. The calculation of this number is based on bulk atomic densities of fcc Fe and Fe_2O_3. The lack of these breakpoints in the oxidation curves with $\theta_{Fe}<0.6$ (though not shown in Fig. 1a, several curves for surfaces containing 0.19, 0.25, 0.40 and 0.50 ML of Fe were collected) may have two reasons. First of all Cu(111) has a smaller reactivity towards O_2 than Cu(100), implying a larger change in reaction rate going from oxidation of iron to adsorption of O_2 on Cu(111). The difference in sticking coefficient between clean Cu(100) and clean Cu(111) is about a factor 10 at $\theta_O=0$ [57,58]. So, if the sticking coefficients are about equal for oxygen on copper and iron sites, no changes would be visible. Second, the breakpoints may not be visible because $\delta\Delta$ has a different (i.e. smaller) sensitivity for oxygen adsorbed on Fe than on for oxygen on Cu.

So from Fig. 1a it is impossible to say much about the oxidation kinetics, apart from the slope at $\delta\Delta=0°$, which is independent of θ_{Fe} (for $\theta_{Fe}>0$). The initial slope of the oxidation curve of Cu(100) is much smaller. For this surface an initial sticking probability of 0.01 can be calculated. This agrees well with the results of Habraken et al. [57]. The slope of the other curves is about twice the value measured on Fe(100) [59]. As the sensitivity of $\delta\Delta$ for oxygen on Fe(100) is smaller for small amounts of oxygen than for larger amounts (a discussion on this will follow in the next section), it is hard to determine the absolute sticking probability of O_2 for the Cu(100)-Fe surfaces. Though, as the initial sticking probability is independent of θ_{Fe}, the oxygen adsorption should follow a precursor mechanism, as it does on Cu(100) [58].

3.3.2 Structure and stoichiometry.

3.3.2.1. AES.

From Fig. 3 it seems that the amount of oxygen adsorbed is not linearly dependent of the iron coverage. The deviation from linearity at $\theta_{Fe}>0.5$ may have two explanations: First there could be a change in the (mean) stoichiometry of the oxide. Second, the oxide may screen part of the O $KL_{2,3}L_{2,3}$ electrons due to the small inelastic mean free path (imfp) of the O $KL_{2,3}L_{2,3}$ Auger electrons relative to the thickness of the oxide layer.

A change in the stoichiometry is difficult to determine from the experiments as performed here. Although Seo et al. [60] claim that different iron oxides have different $M_{2,3}VV$ peak shapes this might not be the case as will be shown in chapter 4. Nevertheless Fig. 5 shows clearly that all peaks have the same features (two overlapping peaks) and the only difference is the relative contribution of both. No contribution of the metallic $M_{2,3}VV$ which lies in the

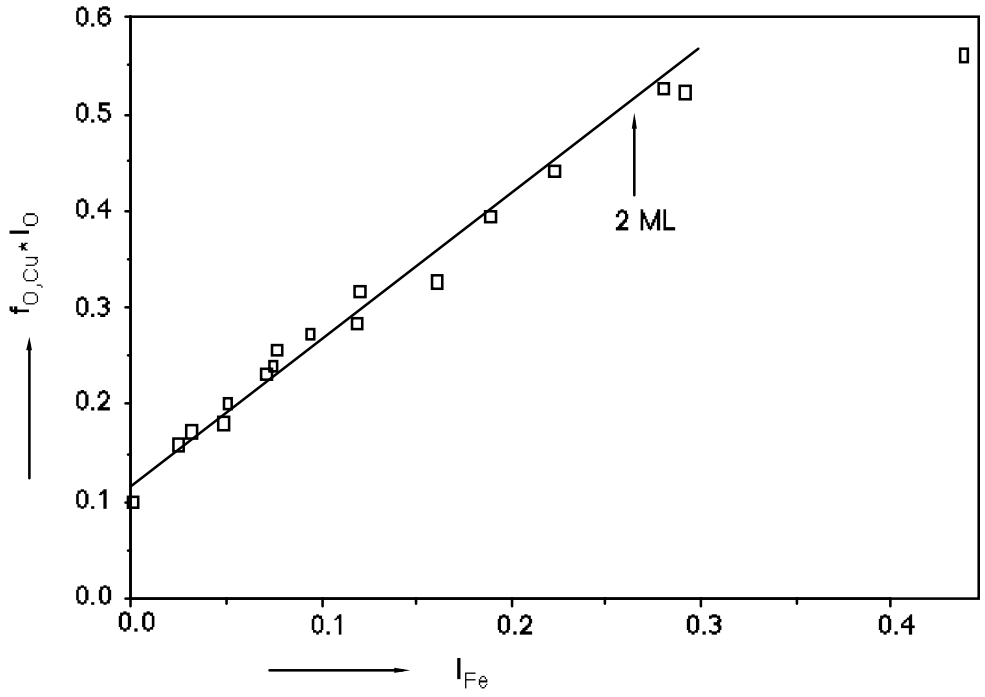

Figure 7 *The O $KL_{2,3}L_{2,3}$ intensity as function of the Fe $L_{2,3}M_{2,3}V$ intensity for surfaces oxidised to saturation. The line represents a linear fit through the points up to 1.75 ML of Fe. The arrow indicates the iron intensity calculated for 2.0 ML Fe.*

middle of the two oxidic peaks could be found. So metallic iron is certainly not present in the top layers.

The screening of part of the O $KL_{2,3}L_{2,3}$ electrons by the oxide layer was mentioned as a second reason for a deviation in linearity in Fig. 3. Fig. 4 shows clearly that the screening effect can not be neglected for Fe $L_{2,3}M_{2,3}V$ electrons in the oxide, at least not for iron coverages exceeding one half of a monolayer. Because the Fe $L_{2,3}M_{2,3}V$ electrons have a slightly larger imfp than the O $KL_{2,3}L_{2,3}$ electrons, I_O should be effected more by the screening. So it seems better to investigate the oxygen intensity as function of the iron intensity using for both signals the intensities corrected for the relative sensitivity factors. Therefore $f_{O,Cu} \cdot I_O$ is plotted against I_{Fe} (determined after oxidation; $f_{Fe,Cu} = 1$) in Fig. 7. The slope of the calculated line, which is also shown, is 1.43±0.07 (the error is based on the linear regression calculation) and the intercept is 0.12±0.02 which corresponds to a value of θ_O=0.5. The same oxygen/iron ratio can be calculated from the line drawn in Fig. 3. So the stoichiometry calculated from the oxygen intensities indicates the formation of Fe_2O_3. This is not consistent with the results of Kishi and Nishioka [35]. They determined FeO or Fe_3O_4 to be present depending on the amount of Fe at the surface. Their conclusions are based on the shape of the Fe $2p_{3/2}$ peak as measured with XPS. However, their surfaces were far from saturated with oxygen. In chapter 5 it will be shown that surfaces saturated with oxygen exhibit only the shape and position of a Fe 2p peak corresponding to Fe_2O_3. As the conclusions here are based on the amount of oxygen present at the surface at saturation relative to the amount of iron, the interpretation that only Fe_2O_3 is formed is preferred.

A deviation from linearity is also visible in Fig. 7. For $\theta_{Fe} \geq 2.3$ the oxygen intensity is almost constant, whereas the Fe intensity still increases.The constant oxygen intensity can be

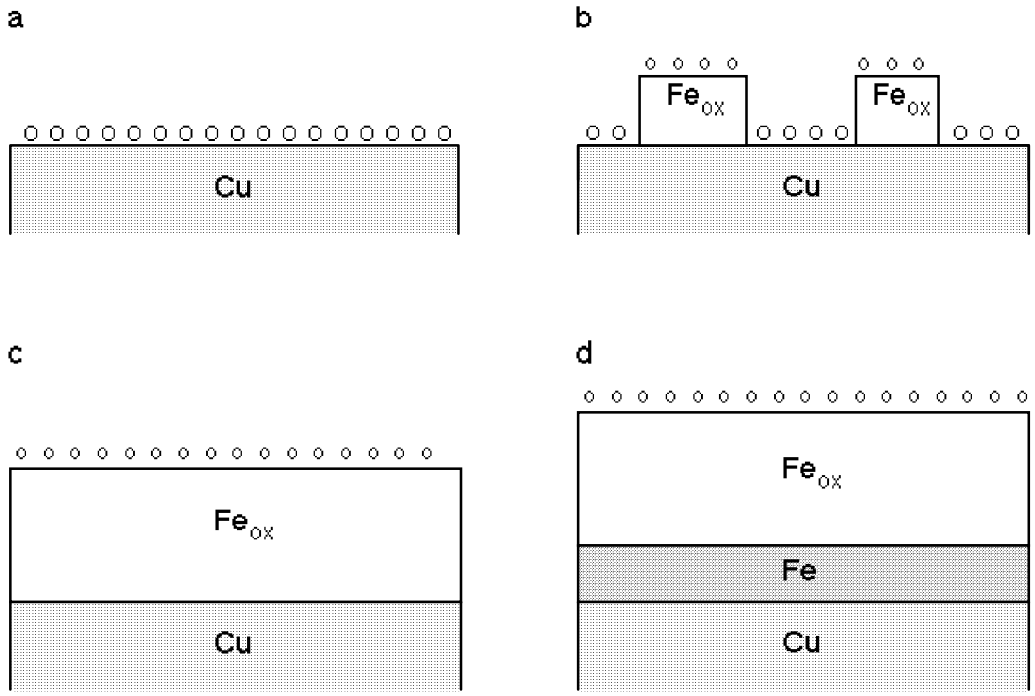

Figure 8 *A schematic model for the oxidised surfaces containing different amounts of Fe. a) $\theta_{Fe} = 0$, b) $0 \geq \theta_{Fe} \geq 0.8$, c) $0.8 \geq \theta_{Fe} \geq 2$ and d) $\theta_{Fe} > 2$.*

explained by a saturation of the oxygen adsorption comparable to that of room temperature oxidation of Fe(100) [55,59]. Based on the amount of oxygen 2 monolayers of iron can be oxidised at this saturation value. To highlight the value of θ_{Fe}=2 the place of I_{Fe} related to θ_{Fe}=2 in Fig. 7 is indicated by an arrow. The oxygen intensity calculated for θ_{Fe}=2 using the fit is not significantly different from the experimental values of surfaces containing 2.3, 2.7 and 16 ML of iron (the experimental points on the right side of the arrow in Fig. 7). So the oxidation of iron seems to stop when 2 ML of iron are oxidised.

An other important conclusion that can be drawn from Fig. 7 is that (at least up to 2 ML of Fe) there is a 'surplus' of oxygen of half a monolayer, the intercept of Fig. 7. For $\theta_{Fe} \geq 2$ this surplus is probably present at the Cu(100)-Fe_2O_3 interface as it is for θ_{Fe}=0, where it can be stabilised by the Cu atoms. In principle it could also be at the Fe_2O_3-vacuum interface or divided over both interfaces. But it is impossible to discriminate between these possibilities using AES. At higher iron coverages the surplus can also be interpreted as a change in stoichiometry (to the lower oxidation states) below the surface. However, this must be a small region very near to the Fe_2O_3-Fe interface because when the same amount of oxygen is spread over more (deeper) layers I_O should decrease.

So based on the AES results I come to a schematic model of the structure of the surface as given in Fig. 8. At zero coverage the saturated surface contains half a monolayer of oxygen on copper, Fig. 8a. For θ_{Fe}<2 all Fe is oxidised to Fe_2O_3 and a surplus of 0.5 ML of oxygen is present. This 'excess' oxygen is partly present at the iron free Cu(100) surface and partly connected to the iron oxide (for iron coverages too small to cover all of the Cu surface), Fig. 8b, or totally in contact with the iron oxide when the oxide layer covers the copper completely, Fig. 8c. At even higher Fe coverages (θ_{Fe}>2) a layer of metallic Fe is present between the Fe_2O_3 and the Cu surface, Fig. 8d. In this situation the thickness of the metallic Fe layer depends on θ_{Fe}, whereas the thickness of the oxide layer is independent of θ_{Fe}.

3.3.2.2. Ellipsometry.

In this section the ellipsometry results and their consistency with the model as proposed above will be discussed. In the behaviour of $\delta\Delta_{sat}$ as function of θ_{Fe} (Fig.2) three regions can be distinguished. These regions are numbered I, II and III from high to low θ_{Fe} (Fig. 2). For θ_{Fe}>2 ML (region I) $\delta\Delta_{sat}$ is about 3.5° which is the same value as that for fully oxidised Fe(100). From θ_{Fe}•0.8 to θ_{Fe}=2 (region II) $\delta\Delta_{sat}$ is proportional to θ_{Fe} and for $\theta_{Fe}\leq$0.8 (region III) $\delta\Delta_{sat}$ changes linearly with θ_{Fe} with an intercept at the saturation value of an iron free Cu(100) surface.

The saturation of the surface at $\delta\Delta$=3.5° for θ_{Fe}>2 ML (region I) can easily be explained realising that also for oxidation at room temperature of Fe(100) the surface saturates at this value [55,59]. At this oxygen coverage and for this temperature the oxidation stops because migration processes in the oxide layer become very slow [61]. The absolute amount of oxygen present on Fe(100) at $\delta\Delta$=3.5° is $5.1\pm0.4\cdot10^{19}$ m^{-2} [55] which equals θ_O=3.3±0.3 relative to the atomic density of Cu(100). This agrees well with the results of the AES experiments: oxidising 2 ML of Fe to Fe_2O_3 requires 3 ML of oxygen and adding the half monolayer excess oxygen 3.5 ML is required for saturation. So in this region the surface can be described by a layer of metallic Fe on the Cu(100) crystal surface with an iron oxide layer on top (Fig. 8d).

The proportional decrease of $\delta\Delta_{sat}$ with θ_{Fe} going from θ_{Fe}=2 to $\theta_{Fe}\approx$0.8 (region II) can be explained by a decrease of the amount of oxygen with θ_{Fe}. The least-squares fit through the four points is given by eq. (1).

$$\delta\Delta = -0.04\pm0.08 + (1.72\pm0.10)\cdot\theta_{Fe} \qquad (1)$$

When the sensitivity of $\delta\Delta$ for oxygen on Fe(100) as determined by means of nuclear reaction analysis (NRA) by Leibbrandt et al. [55] of 1.1 deg/ML (taken from Fig. 3 of the reference and recalculated to the atomic density of Cu(100)) is used, a stoichiometry can be calculated of $FeO_{1.56\pm0.09}$, which means Fe_2O_3. This constitutes an independent determination of the stoichiometry which agrees well with the AES results. Although this conclusion seems reasonable (and is in fact what I believe) a literal interpretation of an extrapolation to θ_{Fe}=0 following Eq. (1) is tantamount to a decrease of the thickness of the iron oxide in Fig. 8c to zero. This means that when all of a certain amount of Fe_2O_3 is removed $\delta\Delta$ becomes zero whereas at that point half a monolayer of oxygen is still present (the 'excess' oxygen found with AES). Apparently this half monolayer is not 'visible' to $\delta\Delta$. This means, however, that for oxygen on iron the change in Δ is not proportional to the actual coverage ($\delta\Delta = k\theta_O$). In fact, although Δ starts to change immediately upon oxygen exposure to Cu(100)-Fe or Fe(100), the resulting calibration curve is non-linear [59]. Initially the sensitivity for oxygen on Cu(100)-Fe is found to be 0.55±0.06 deg/ML, which is half the value for oxygen on Fe(100). Only at higher exposures (above about $\delta\Delta$=0.5°) a calibration curve of the type $\delta\Delta = a + k\theta_O$ is found [59]. This implies that for oxygen coverages above 1.0 ML ellipsometry does not 'see' all the oxygen present, but 'misses' exactly 0.5 ML. Since the oxygen in excess of 0.5 ML will be part of the iron oxide it seems reasonable to suppose that 'oxidic' oxygen is visible for the ellipsometer. Below this coverage some oxygen will be present on the surface and some will be present as 'oxidic' oxygen. The former will be invisible for the ellipsometer, the latter gives the its usual contribution. A

similar situation occurs for the chemisorption of oxygen on nickel as studied by ellipsometry [62]. So in the extrapolation procedure in region II of Fig. 2 an intercept is expected that corresponds to 0.5 ML of invisible oxygen, i.e. zero. This oxygen is most probably situated at the Fe_2O_3-vacuum interface. In Fig. 8b-d this oxygen is represented by small symbols.

Thus in region II the thickness of the oxide layer varies with θ_{Fe}, and an excess of oxygen is present situated on top of the oxide (Fig. 8c).

In the discussion above one major assumption has been made implicitly: the possible effect of the (changing) iron layer on $\delta\Delta$ and $\delta\Psi$ is ignored. Of course this is not realistic and the negative $\delta\Psi$ values in Figs. 1 and 2 seem to be in conflict with the oxidation of the pure metals. Both on copper and on iron $\delta\Psi$ is positive upon oxidation at 300 K (though very small in the case of iron). It should be realised, however, that in this case oxidation of a Cu-Fe surface influences the state of the surface (as seen with ellipsometry) in several ways. Starting with a given amount of iron both Δ and Ψ will change upon oxidation from their initial values due to the formation of iron oxide and due to the decreased amount of iron present between the copper and iron oxide layers. The $\delta\Delta$ and $\delta\Psi$ values would thus represent for instance the difference between a copper surface with 6 monolayers of iron and a copper surface with 4 monolayers of iron and two monolayers of iron oxidised to Fe_2O_3. The only way to account for this effect is to calculate Δ and Ψ for all surfaces and extract the observed values of $\delta\Delta$ and $\delta\Psi$ by a proper subtraction.

The calculations were based on the following assumptions: 1) the presence of the components in perfect flat layers, 2) bulk refractive indices of copper and iron can be used ($\tilde{n}_{Cu}$=0.13+ 3.55i and $\tilde{n}_{Fe}$=3.5+3.7i), 3) one monolayer of iron has the same thickness as the interlayer spacing of the Cu(100) planes (1.8 Å), 4) 1 ML of Fe results in a layer of iron oxide of 3.8 Å (bulk Fe_2O_3 density) and 5) the refractive index of the iron oxide is $\tilde{n}$=5.0+0i. The index of the oxide was adjusted as to match the calculated $\delta\Delta_{sat}$ values to the experimental values. First Δ^0 and Ψ^0 were calculated for surfaces containing different amounts of iron and next the Δ and Ψ values of the final oxidised situation as described by the model. Subtraction of the proper begin and end values results in the solid lines drawn in Fig.2. It is obvious that the calculated $\delta\Delta_{sat}$ values agree well with the experimental data whereas $(\delta\Psi_{sat})_{calc}$ shows a disagreement with the experiment. The latter is not so strange when is realised that the layers are not perfectly flat and that the refractive index of bulk (bcc) iron is used whereas thin (fcc) layers are present of which the index may be different from the bulk values. Both arguments have stronger effects on Ψ than on Δ (the negative sign of $\delta\Psi_{sat}$ is completely due to the decrease of the iron layer in favour of the oxide layer during oxidation).

When the thickness of the oxide layer becomes small, formation of clusters with free Cu surface in between can be expected. This probably happens for θ_{Fe}<0.8 (region III in Fig. 2). For the line drawn through the points of region III in Fig. 2 some extra assumptions have been used in the calculation: 1) the Cu surface covered by Fe_2O_3 is proportional to θ_{Fe} until complete coverage of the copper is reached, 2) oxygen adsorbed on iron oxide free parts of Cu(100) has its normal effect on $\delta\Delta$ and $\delta\Psi$ as does the oxygen in the iron oxide (the amount of invisible oxygen is then proportional to the Fe_2O_3 coverage with a maximum of θ_O=0.5 at total coverage) and 3) the expected changes in $\delta\Delta$ for both parts of the surface may be added. The change in the equations used to calculate Δ and Ψ for this particular problem is shown in

the appendix. In Fig. 2 the iron oxide part of $\delta\Delta_{sat}$ is represented by a dashed line and the Cu(100)-O part by a dotted line. Both lines add up to the calculated solid line through the experimental points. So this model can describe $\delta\Delta_{sat}$ for $\theta_{Fe}<0.8$ satisfactorily.

3.3.3 LEED.

The LEED pattern of 0.8 ML Fe oxidised to saturation resembles strongly the pattern observed by Simmons and Dwyer [63] for small amounts of oxygen on Fe(100). They explained the two hexagons by regions of oxide with two orientations. They proposed a stoichiometry of FeO but also Fe_3O_4 and γ-Fe_2O_3 have hexagonal symmetry in the close packed oxygen planes which can lead to the LEED pattern. The O-O distances of in the close packed planes of these oxides are 0.306, 0.297 and 0.295 nm respectively. The lattice parameter calculated from Fig. 6 is 0.27±0.02 nm, which results in a contraction of (10±8)% compared to the γ-Fe_2O_3 bulk lattice parameter. This means that the oxide lattice adjusts itself to the Cu(100) lattice distances though not completely. On Fe(100) the same happens. In that case a contraction of the lattice parameter of 4.5% is required and observed [63]. Furthermore from the diffuse spots it can be concluded that the surface is not highly ordered or the clusters are relatively small (but >50 Å). Both may be due to strains caused by the lattice mismatch.

Although the Cu(100) surface was expected to be covered completely by the iron oxide for this amount of Fe it is possible to see the Cu(100) spots in the LEED pattern in Fig. 6. Thus the coverage is not yet complete.

3.4 Conclusions.

1. The initial reaction rate for O_2 adsorption is independent of θ_{Fe} ($\theta_{Fe}\geq0.19$), which means that the reaction proceeds via a precursor mechanism.
2. For $\theta_{Fe}\leq2$ complete oxidation to Fe_2O_3 occurs and an extra amount of θ_O is probably present at the Fe_2O_3-Cu(100) interface.
3. For $\theta_{Fe}>2$ the oxidation stops when the equivalent of 2 ML of Fe is oxidised to Fe_2O_3, while the extra θ_O remains present.
4. The maximum amount of oxygen on these surfaces ($\theta_{Fe}>2$) is the same as on Fe(100) for room temperature oxidation.
5. For $\theta_{Fe}\leq0.8$ ML the oxide lattice is contracted in order to fit better to the Cu(100) lattice and clusters in two orientations rotated by 90• in respect to each other are present.

Appendix.

In this appendix it is shown that it is allowed to add the ellipsometric response (at least the parameter $\delta\Delta$) of a substrate with two adjacent overlayers A and B with complex refractive indices $\tilde{n}_A$ and $\tilde{n}_B$ depicted in Fig. 9. A simple geometric model is used because the (more sophisticated) effective medium approach is not suitable for oxides and the overlayer is assumed to consist of islands of different compounds. For each overlayer the usual ellipsometric equations hold for the amplitude reflection coefficient

$$R = \frac{r_{01} + r_{12}e^{-ix}}{1 + r_{01}r_{12}e^{-ix}} \qquad (A.1)$$

where

$$x = \frac{4\pi}{\lambda_0 \tilde{n}_0} d \left(\tilde{n}_1^2 - \tilde{n}_0^2 \sin^2\varphi_0\right)^{1/2} \qquad (A.2)$$

and r_{01} and r_{12} represent the amplitude reflection coefficients for the interface 0-1 and 1-2 respectively. The values of Δ and Ψ are then found from the relation

$$\tan\Psi e^{i\Delta} = \frac{R_p}{R_s} \qquad (A.3)$$

where the subscripts on R denote the amplitude reflection coefficients for light parallel (p) or perpendicular (s) to the plane of incidence. For the system shown in Fig. 9 each reflection coefficient R_s or R_p may be expressed as

$$R = f_A R_A + (1 - f_A) R_B \exp\left\{-i\frac{4\pi}{\lambda_0}(d_A - d_B)\cos\varphi_0\right\} \qquad (A.4)$$

where R_A is the reflection coefficient appropriate for a uniform layer of thickness d_A with complex refractive index $\tilde{n}_A$ and R_B has an analogous meaning. The fraction of the surface covered by layer is f_A and the exponential term accounts for the phase difference of the incoming light beam when it reaches the surface of A and B. Eq. (A.4) is essentially the statement that, in order to obtain the amplitude reflection coefficient of a surface, one must add the amplitudes of all reflected rays, taking proper account of their phase difference. This expression neglects those regions of the surface near to the contact between A and B where, strictly speaking, one should consider light rays entering layer A but leaving the surface through layer B. If the sizes of the different patches of A and B are large this contribution is expected to be negligible. The distance y between two emerging rays in Fig. 9 is $2d_A\tan\varphi_A$, which for $\varphi_0 = 70°$, $\mathrm{Re}(\tilde{n}_A)=1$ and d = 5 Å corresponds to 27 Å. Thus, if only two reflected rays contribute to the reflection coefficient the patch size of both A and B should be larger than 27 Å in order for this approximation to be valid. Using $\mathrm{Re}(\tilde{n}_A)=3.5$ which can be calculated for iron oxide on iron, the minimum island size decreases to 5.6 Å. As a LEED pattern is visible for $\theta_{Fe}<0.8$ this condition is probably met.

Now an exact calculation is possible using Eqs. (A.4), (A.1) and (A.3). The parameters used (d_A = 3Å, $\tilde{n}_A$ = 3.5 + 1.7i, d_B = 3.8Å, $\tilde{n}_B$ = 5.0 + 0i and $\varphi_0 = 70°$) were chosen so as to

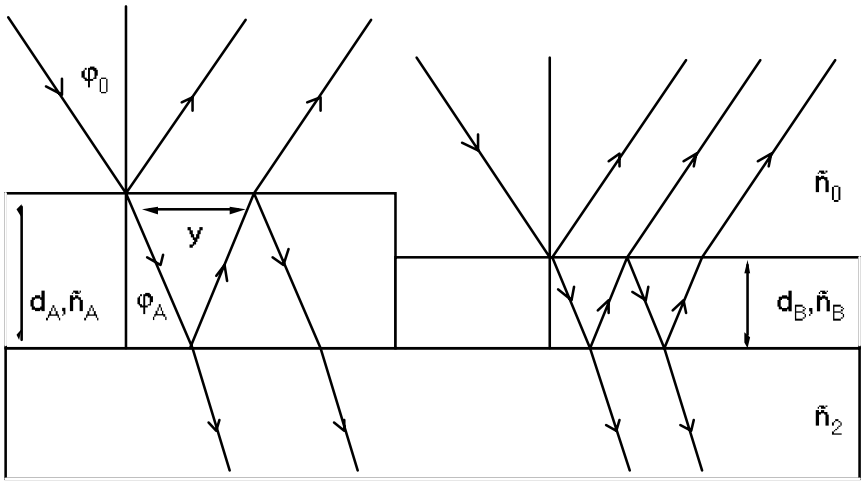

Figure 9 A schematic representation of the surface and the light rays during an ellipsometric experiment.

reflect the experimental $\delta\Delta_{sat}$ values in Fig. 2, but have no further significance. As can be seen in region III of Fig. 2 the calculation yields a linear relationship for both $\delta\Delta_{sat}$ and $\delta\Psi_{sat}$.

As the growth of iron oxide does probably not result in such well organised surfaces it is shown here that this is not very important for Δ and Ψ of thin layers on a substrate. In that case R can be expanded in Eq. (A.1) upto first order terms in x. This yields

$$R = r_{02}(1-i\beta x) \qquad (A.5)$$

where β is a function of r_{01}, r_{02} and r_{12}. Assuming just one kind of oxide present on the surface in clusters R can be given by

$$R = r_{02}\left\{1 - (1- f_A)\frac{4\pi i}{\lambda_0}d_A\cos\varphi_0 - f_A i\beta x_A\right\} \qquad (A.6)$$

The ratio R_p/R_s is then to first order in d_A

$$\tan\Psi e^{i\Delta} = \frac{r_{02\,p}}{r_{02\,s}}(1-f_A i\beta_p x_A + f_A i\beta_s x_A) \qquad (A.7)$$

and only dependent on $f_A d_A$ which means proportional to the volume of A present on the surface. So Δ and Ψ are not expected to be different for, say, two monolayers of iron on copper covering half of the crystal and one monolayer covering the total surface area. Calculations using the 'exact' Eq. (A.4) confirm this statement.

4

Oxidation of one monolayer of iron on Cu(100) studied with AES peak shape analysis.

Abstract

The peak shape of the iron $M_{2,3}VV$ Auger peak during the oxidation of one monolayer of iron on Cu(100) was studied. Peak shape analysis indicated that all iron is oxidised to Fe_2O_3 before oxygen adsorbs on the Cu(100) surface. Based on the results presented in this chapter the oxidation of iron probably proceeds at once from Fe^0 to Fe^{3+} though initially adsorbing oxygen causes a different ratio between the cross-transition and the auto-ionisation peak than later adsorbing oxygen.

4.1 Introduction.

Peak shape changes of Auger transitions due to changes in the chemical composition can be found for several elements. In most cases valence band electrons are involved in the transitions e.g. the KLL transition of carbon in graphite or carbides and the $M_{2,3}VV$ transition of the metals in titanium and vanadium nitrides and iron oxides. As the peak shape of these transitions is characteristic for a certain chemical state of the elements the shape can be used to identify the state and possibly the composition. For the examples given above this appears to be possible. Graphitic and carbidic carbon exhibit different C KLL peak shapes [40]. Dawson and Tzatzov showed the existence of a relationship between the shape of the Ti and V $M_{2,3}VV$ peaks and the amount of nitrogen present in the octahedral holes [64,65]. And for iron oxides the Fe $M_{2,3}VV$ peak shape is often used to determine which iron oxide is present at the surface [30-33,60,63,66-73].

Most peak shape analyses reported in literature are based on derivative (dN/dE or E·dN/dE) or even second derivative ($d^2N/(dE)^2$ or $E \cdot d^2N/(dE)^2$) spectra. Just a few authors use the integral (N vs. E) spectra [64,65]. Quantitative use of derivative spectra is dangerous a change of shape of the original peak also changes the peak-to-peak height in the derivative mode and the background in the low energy region (<100 eV) often changes strongly upon chemical or structural changes of the surface which thus influences the shape of the complete spectrum. So it seems better to collect N vs. E spectra and to remove the background [45,47,74-76] before performing a detailed analysis of the peak shape.

In section 2 of this chapter an overview of literature concerning the origin of the shape change of the Fe $M_{2,3}VV$ peak as caused by oxidation is given. In chapter 3 it was concluded from the high energy Auger peaks and from ellipsometric results that, for oxygen saturated surfaces containing less than 2 ML of iron, all the iron is oxidised to Fe_2O_3 and half a monolayer of oxygen is present at the Cu(100)-iron oxide interface. Since the composition at saturation is known, it is interesting to investigate the development of the Fe $M_{2,3}VV$ peak during oxidation. This is described in section 3 of this chapter.

4.2 Origin of the Fe $M_{2,3}VV$ peak shape change.

In literature there is a good agreement about the main features of the iron (oxide) $M_{2,3}VV$ peak. Because Auger spectra are usually recorded in the dN/dE (or E·dN/dE) mode the position of the negative going peak will be used here to identify the peak position. The main features of the Fe $M_{2,3}VV$ peak are found at 44, 47 and 51 eV. The energies mentioned in literature vary about 2 eV, but that is probably due to instrumental differences. The peak at 47 eV can be ascribed to the Fe $M_{2,3}M_{4,5}M_{4,5}$ super-Coster-Kronig transition and is found in spectra of surfaces (still) containing metallic iron and according to Seo et al. [60] in spectra of FeO and Fe_3O_4.

The high energy feature at 51 eV is generally ascribed to an auto-ionisation transition [67,68,77]. For this transition the 3p core hole is formed by exciting a 3p electron to the empty 4s,4p states from where it can recombine with the core hole under emission of a valence band electron or vice versa. The kinetic energy of this electron is increased relative to that of the 'normal' $M_{2,3}M_{4,5}M_{4,5}$ electron energy by the difference in energy between the valence band (maximum in density of states) and the lowest empty 4s,4p states. This energy

difference is about 4 eV for the oxides [77], which agrees well with the energy difference of the two transitions.

The cause of the low energy transition at 44 eV is still a point of discussion. Most authors suggest a cross-transition ($Fe_{M_{2,3}}Fe_{M_{4,5}}O_{L_{2,3}}$) to be responsible for this feature [67,68,72,73]. Ramsey and Russell [77], however, reject this since they did not find an increase in intensity for this transition at low oxygen exposures of a clean Fe(110) crystal. This increase is expected because the density of oxygen 2p states strongly increases for the first 10 L of oxygen exposure [78]. Therefore they suggest that this transition is caused by a change in the d-band structure of the iron due to charge transfer from iron to oxygen. The correct energy can be calculated for this change. This transition is mainly expected for high oxygen exposures [77]. Other authors, however, do report an increase in the 44 eV feature also for exposures <10L [66,69,70]. Thus, in my opinion, best evidence is found for the cross-transition explanation for this feature. According to Seo et al. [60] this transition is strongly present in Fe_2O_3 (α,γ) and FeOOH.

Based on the explanation of the three features building the Fe $M_{2,3}VV$ peak as given above it is difficult to understand why the 44 eV feature is (nearly) absent for FeO and Fe_3O_4 while the metallic ($M_{2,3}M_{4,5}M_{4,5}$ at 47 eV) feature is dominantly present, as is reported by Seo et al. [60]. This can not be explained by differences in the valence band spectra because they are basically the same for all iron oxides [79]. So the cause should be found either in a difference in the 3p core level or in a difference in the co-ordination of the iron ions in the different oxides.

Though there is a small increase in binding energy of the Fe 3p electrons going from Fe^0 to Fe^{3+} [80] any effect due to this change should also be expected for the auto-ionisation feature. However, this change is not found. An other argument is that an increasing binding energy for the Fe 3p electrons should result in an increasing energy for the transition going from Fe^0 to Fe^{3+}. Then a difference in energy opposite to what is reported (44 eV for Fe^{3+} and 47 eV for Fe^0) is expected. So it is unlikely that differences in the 3p core level are responsible for the 'behaviour' of the 47 eV peak.

An effect of the co-ordination of the metal ions on the transition as found for Ti and V [64,65] is not likely. Because, if there is an effect of octahedrically or tetrahedrically co-ordinated Fe(II) or Fe(III) species (no effect is reported for the core level XPS spectra [80]) there should be a difference between FeO and Fe_3O_4 in the $M_{2,3}VV$ spectra. However, the difference between the spectra of both oxides as determined by Seo et al. [60] is very small. Assuming influence from the co-ordination a difference is expected because, based on the position of the different iron ions in the crystal lattice, a Fe $M_{2,3}VV$ spectrum of Fe_3O_4 should be the sum of one third of a FeO spectrum (accounting for the Fe(II) ions, which are all octahedrically co-ordinated both in FeO and in Fe_3O_4) and two thirds of a γ-Fe_2O_3 spectrum. Strictly, the 'γ-Fe_2O_3' part of the sum should consist partly of γ- and partly of α-Fe_2O_3 spectrum to get the correct ratio of both types of co-ordination for the Fe(III) ions but the $M_{2,3}VV$ spectra for both α- and γ-Fe_2O_3 are practically the same. A good summary of the co-ordination of the iron ions in the different oxides is given by Wandelt [79].

A possible explanation for the presence of a 47 eV peak in the FeO and Fe_3O_4 spectra of Seo et al. [60] might be that metallic iron was present on their surfaces. Though they used

'bulk' oxides for their experiments they sputtered the surfaces in order to remove surface contaminants (and different surface oxides). It may be that the surface was partly reduced (which is, in this case, practically the same as preferentially sputtering of oxygen) by the Ar^+ ion bombardment. The ratio of the O KLL and Fe $L_{2,3}VV$ for the different oxides also indicates sub-stoichiometric amounts of oxygen. This could also explain why many authors who find FeO or Fe_3O_4 on their surfaces using different techniques observe a Fe $M_{2,3}VV$ peak just exhibiting the 44 and 51 eV features. For example Leibbrandt et al. [82] determined the stoichiometry of iron oxide on Fe(100) and Fe(100)-Pt surfaces to be $Fe_{1-x}O$ whereas the 47 eV peak is absent in their spectra. Van Pruissen et al. [30-33] did not observe the metallic iron peak on oxidised Cu(111)-Fe and Cu(110)-Fe surfaces although he had evidence for $Fe_{1-x}O$, Fe_3O_4 and Fe_2O_3 on these surfaces. However, Miyano et al. [67] observed a 47 eV peak on oxidised Fe(100), but their oxygen exposure (200 L) is not sufficient for saturation at 300K [59]. Sakisaka et al. [68] and Smentkovski and Yates [66] report a likewise observation after annealing of an oxidised (350 L at 300 K) iron surface at 773 K though their O KLL/Fe $L_{2,3}VV$ ratio decreased from 2.2 to 0.55, suggesting the presence of metallic iron at or near the surface.

4.3 Oxidation of one monolayer of Fe on Cu(100).

4.3.1 Peak shape synthesis.

Because of the origin of the peak shape of the iron $M_{2,3}VV$ peak as described in section 4.2 it was decided to synthesise the spectra with three peaks. The basic peak shape chosen is a mixed Gaussian/Lorentzian function which is much used in XPS analysis [40]. The main advantage of this function is the flexibility of the peak shape. The function is a product function with four parameters:

$$I(E) = \frac{h}{[1+M\cdot(E-E^0)^2/\beta^2]\cdot\exp\{(1-M)\cdot\ln 2\cdot(E-E^0)^2/\beta^2\}} \qquad (1)$$

where h represents the peak height, M indicates the ratio of the Lorentzian and Gaussian contribution, β is roughly the half-width-at-half-maximum and E^0 is the energy of the peak maximum. For either a pure Gaussian or Lorentzian β is exactly equal to the half-width-at-half-maximum, but for a mixed lineshape the true halfwidth is somewhat smaller [40]. Fitting the iron $M_{2,3}VV$ peak with three peaks thus results in 12 principally free parameters. Because the spectra as used for the fits were already subject to two steps of data handling this amount of free parameters is undesirable. So it was decided to reduce the number of free parameters to three: the height of the peaks. As the rest of the parameters must be fixed, a reasonable choice had to be made for the values. Since Coster-Kronig transitions are very fast processes they result in a relatively broad energy distribution of the emitted electrons and thus in a broad peak. All three of the transitions are in a way Coster-Kronig transitions so it seems reasonable to assume that they result in more or less the same peak shape (β and M). These values were determined by fitting one peak to the Fe $M_{2,3}VV$ peak obtained from a Cu(100) surface containing 16 ML of Fe (as was expected no Cu $M_{2,3}VV$ is visible). Fitting was done by minimisation of χ^2. The parameters M and β resulting from this fit, which is shown in Fig. 1, were respectively 0.5 and 3.6 eV. As is visible in Fig. 1 this peak shape has

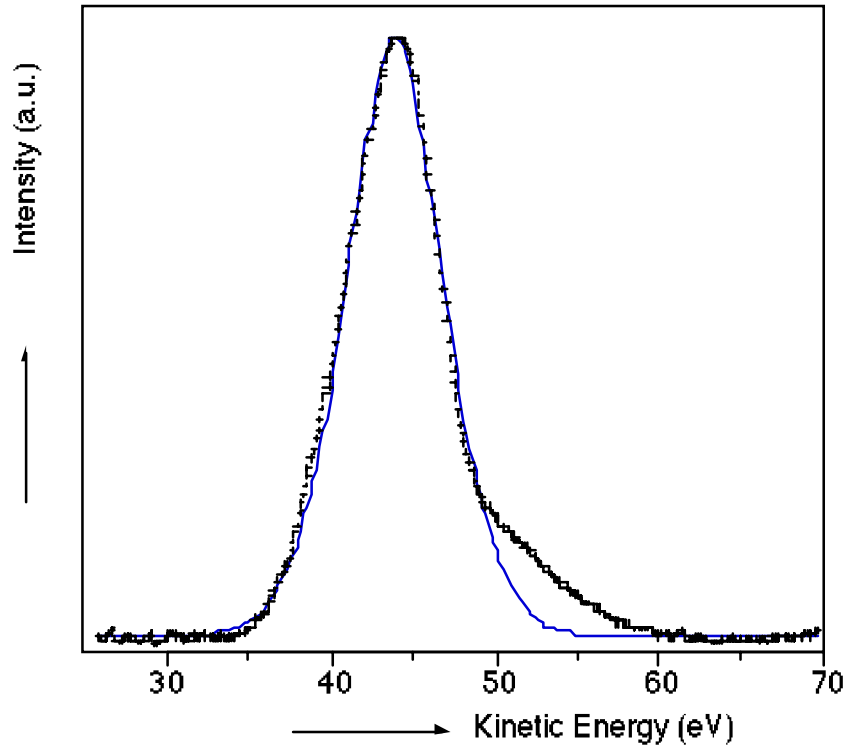

Figure 1 *The iron $M_{2,3}VV$ spectrum of 16 ML of Fe on Cu(100) after background removal (+). The line represents a best fit to the spectrum using one peak and E^0=43.7 eV, β=3.6 eV and M=0.5.*

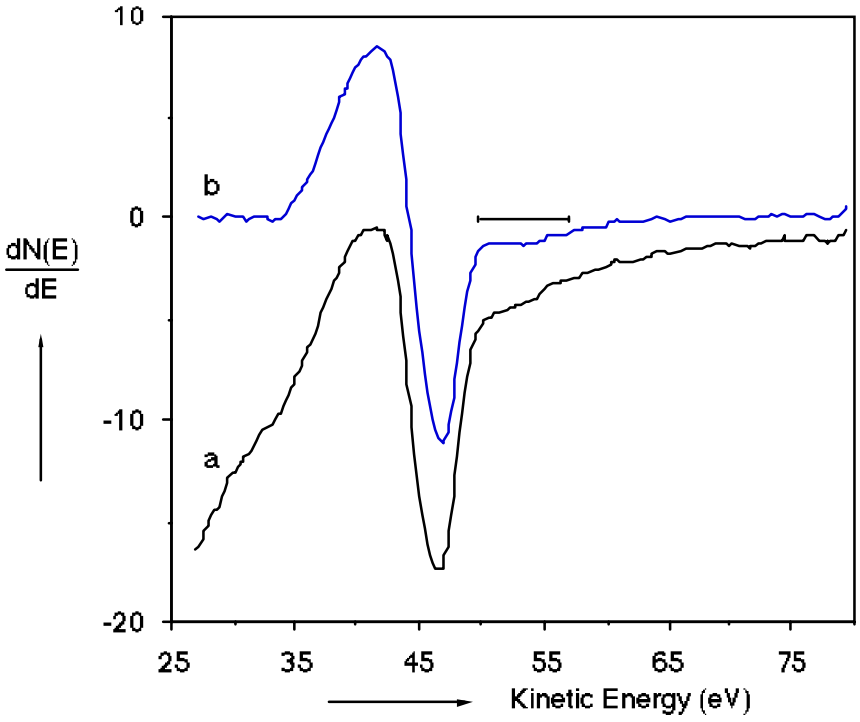

Figure 2 *The numerical derivative of a 16 ML on Cu(100) spectrum before (a) and after (b) background subtraction. The bar indicates the position of the (metallic) auto-ionisation peak.*

two major deficiencies: it doesn't account for the asymmetric shape and the relatively large tail at the high energy side of the peak. This 'tail' is probably caused by the auto-ionisation process, which is also found for metallic iron. The energy of this peak is higher than that of the auto-ionisation peak in the oxides. That this difference is not mentioned in literature is probably due to the fact that the energy of the peak is hard to determine in the derivative spectra as can be seen in Fig. 2, which shows the (numerical) derivative of the Fe $M_{2,3}VV$ peak of Fig. 1. The derivative of the original spectrum is also shown to make clear that this feature is no artefact of the background subtraction. The higher energy of this auto-ionisation peak for the metal is probably due to a higher energy of the empty 4s,4p states compared to the oxides. This peak is omitted in the fitting procedure of the spectra used in this chapter because, due to the large overlap between this relatively small auto-ionisation peak and the copper $M_{2,3}VV$ peak, subtraction of the Cu $M_{2,3}VV$ peak will probably influence the magnitude of the metallic auto-ionisation peak. This omission may lead to an overestimation of the oxidic auto-ionisation peak as long as there is a relative large contribution of the metallic peak.

The remaining parameters to choose are the peak positions. Regarding the origin of the peaks large differences in energy of both 'oxidic' peaks are not expected for Fe^{2+} and Fe^{3+}. Also a change in the energy of the Fe $M_{2,3}M_{4,5}M_{4,5}$ upon oxidation is not expected as I believe this peak to represent only metallic iron. So the peak position of the metallic peak is kept at 43.7 eV (46.3 eV in dN/dE mode), a result from the fit shown in Fig. 1. The peak positions of the cross-transition and auto-ionisation peak were determined by fitting the Fe $M_{2,3}VV$ spectra of oxidised surfaces containing 0.19-2.7 ML of Fe (on Cu(100)). These values appeared to be independent of the amount of Fe on the surface and were 41.4±0.3 and 48.4±0.3 eV (respectively 44.0 and 51.0 eV in dN/dE mode).

Thus the peak synthesis is done with three peaks with the same shape (i.e. β and M) as the metallic Fe $M_{2,3}M_{4,5}M_{4,5}$ peak and with the peak positions of metallic iron and of the two oxide peaks as determined from peaks of different amounts of γ-Fe_2O_3 on Cu(100).

4.3.2 Results and discussion.

In Fig. 3 some Fe $M_{2,3}VV$ peaks of a Cu(100) surface containing 1.0 ML of iron and different amounts of oxygen are presented. The oxygen coverage (θ_O) was determined by calibrating the oxygen signal to that of the known amount oxygen of an oxygen saturated Cu(100) surface, which is 0.52±0.05 ML [51]. In order to ease comparison of the spectra as used for analysis in this chapter with spectra published elsewhere both the integral and the differentiated spectra are given in respectively Fig. 3a and 3b. The peaks in Fig. 3a were obtained from the measured spectra by subtracting a background following the method of Peacock [47] and a subsequent subtraction of a Cu $M_{2,3}VV$ peak as measured on a clean Cu(100) surface. This procedure is described in full detail in chapter 9. Note the good baseline on both sides of the peaks, indicating a good reliability of data handling upto this point. The intensities of the spectra are corrected for day to day changes of the beam current using the intensity of the background at 44 eV as internal reference [48]. It was judged a better standard for these spectra than the intensity at 80 eV as described chapter 9 because of a (smoothly) changing background during oxidation. The spectra in Fig. 3b were obtained by smoothing and numerical differentiation of the spectra in Fig. 3a. In Fig. 3b three vertical lines are drawn to guide the eye at respectively 43, 46 and 51 eV. Features at energies above

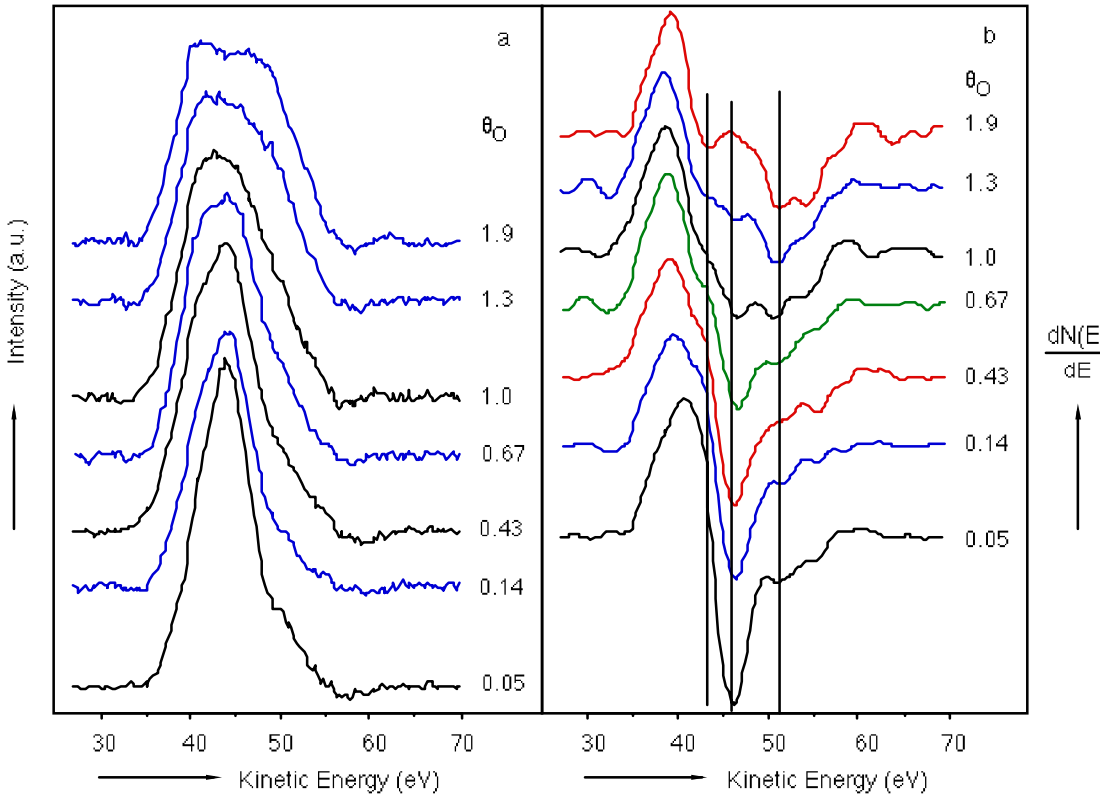

Figure 3 *Some iron $M_{2,3}VV$ Auger spectra of a Cu(100) surface containing one monolayer of iron and different amounts of oxygen, as N vs. E spectra from which both the background and the Cu $M_{2,3}VV$ peak are removed (a) and their derivatives (b).*

51 eV are due to imperfect subtraction of the Cu $M_{2,3}VV$ peak which is enhanced by the differentiation. It is obvious from Fig. 3 that a strong shape change occurs upon oxidation from the beginning. It is also clear from Fig. 3b that peak-to-peak heights are difficult to determine from the derivative spectra of these peaks and therefore an other method of quantification is required.

Some of the fits on the 1.0 ML Fe spectra with different amounts of oxygen are shown in Fig. 4. The quality of the fits in Fig. 4 is representative for all fits. Though the quality of the fits could be improved by allowing more free parameters this only resulted in a rearrangement in the contribution of the three peaks of about 10% of the total peak area. So the influence of this improvement on the trends as observed is small.

The results of the peak synthesis of spectra of one monolayer of iron on Cu(100) containing different amounts of oxygen are shown in Fig. 5. In this figure the absolute areas of the three peaks and the sum of them are plotted as function of the amount of oxygen at the surface.

A slight increase in the total area of the Fe $M_{2,3}VV$ peak upon oxidation is visible in Fig. 5. A decrease could be expected when the spreading of the Fe atoms over a layer of increasing thickness during oxidation is taken into account. This causes an attenuation of the signal of part of the iron atoms due to the small inelastic mean free path of electrons of this energy. The actual increase of the area of the $M_{2,3}VV$ peak is probably caused by an increasing excitation cross-section of the Fe 3p electrons with an increasing amount of

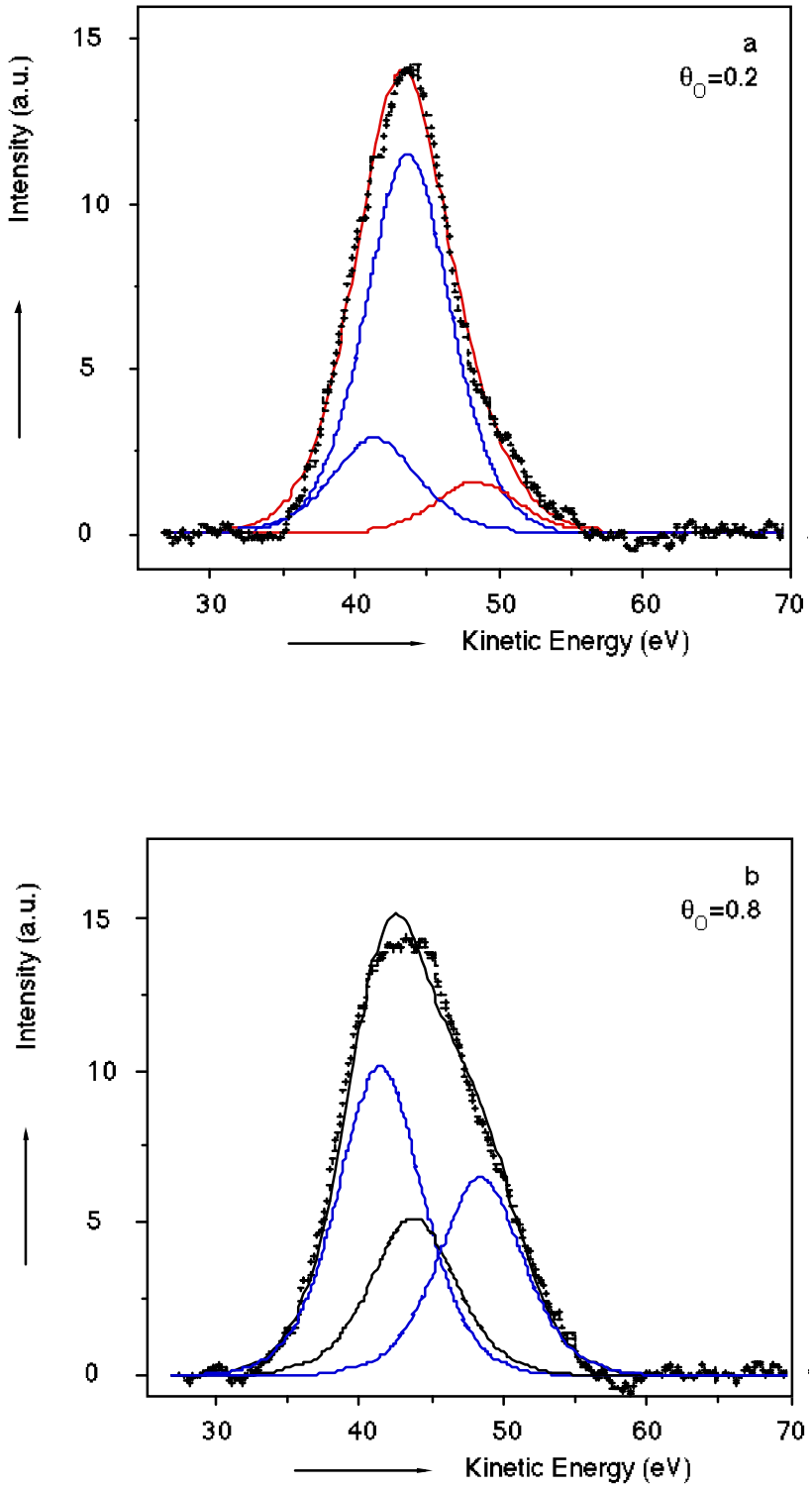

Figure 4 *Some fits of iron $M_{2,3}VV$ spectra of one monolayer of iron on Cu(100) containing 0.2 ML (a), 0.8 ML (b), 1.2 ML (c) and 1.5 ML (d) of oxygen. The + represent the original spectra, the dotted lines are the individual contributions of the three peaks and the bold line is the sum of the three peaks.*

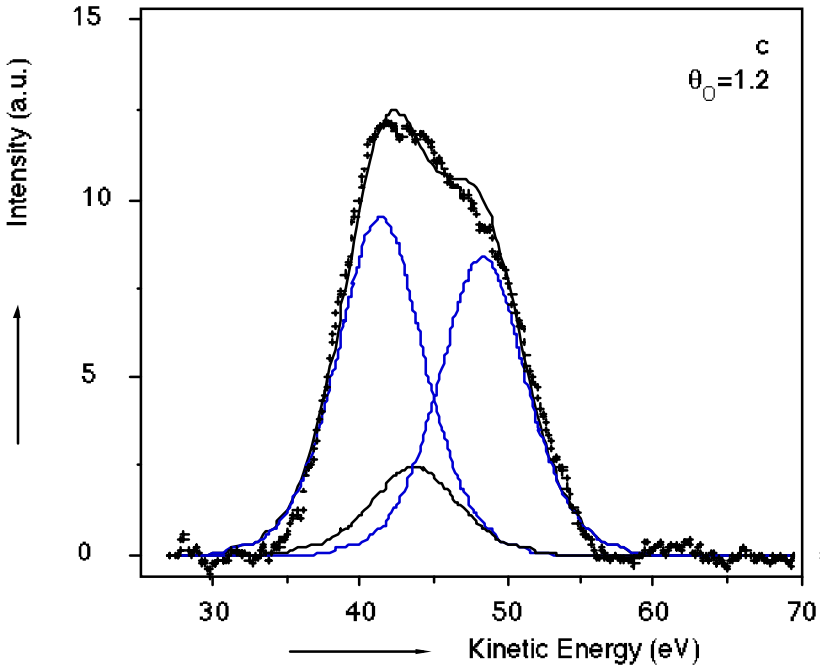
c
θ_O=1.2
Intensity (a.u.)
Kinetic Energy (eV)
0
5
10
15
30
40
50
60
70

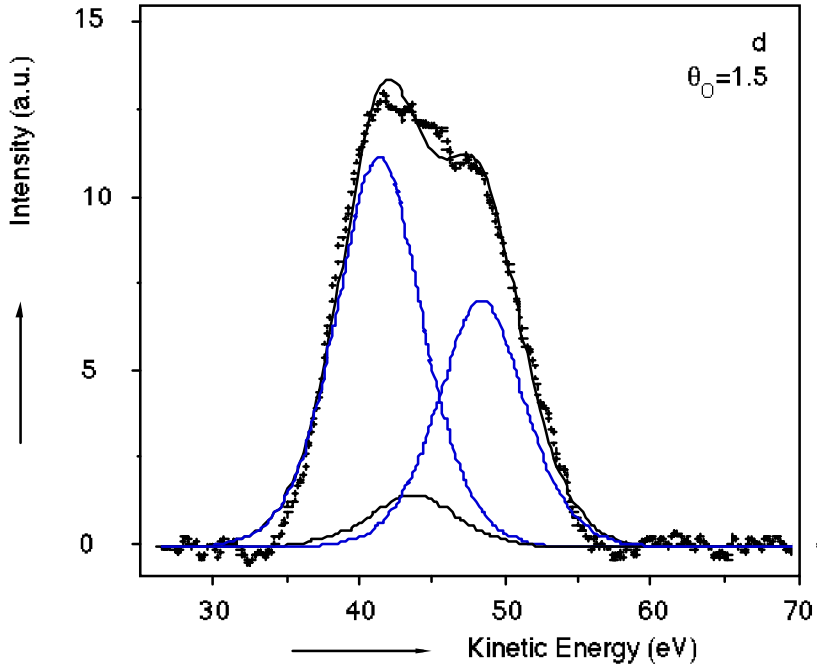
d
θ_O=1.5
Intensity (a.u.)
Kinetic Energy (eV)
0
5
10
15
30
40
50
60
70

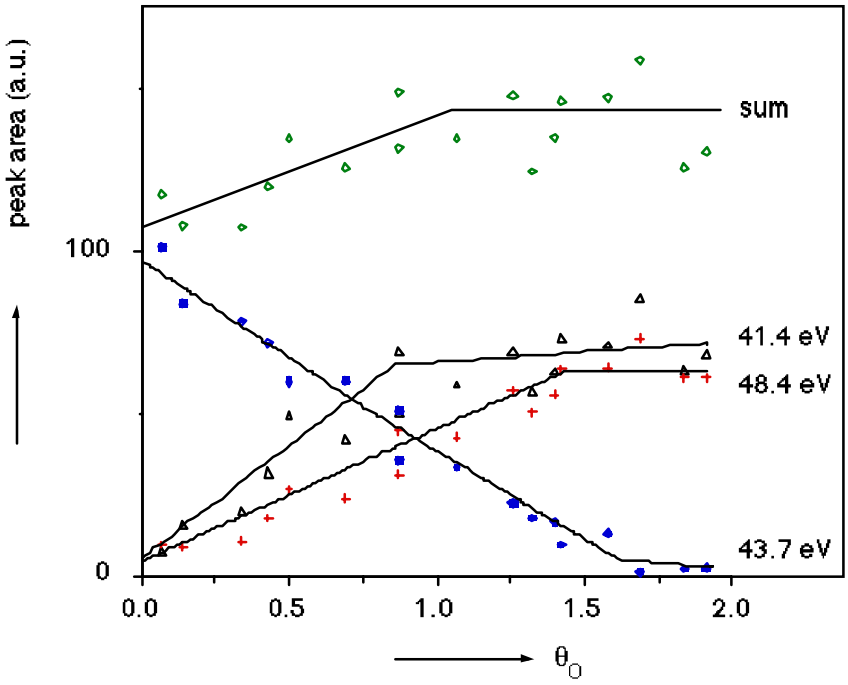

Figure 5 *Individual areas and the sum of them resulting from the fit of the Fe $M_{2,3}VV$ spectra of one ML of Fe as function of the amount of oxygen adsorbed on the surface. The lines are drawn to guide the eye.*

oxygen. This increasing excitation cross-section is also observed with APS [72] and EELS [67]. Ramsey and Russell [77], however, report a decrease in the $M_{2,3}VV$ feature upon oxidation. This apparent decrease is probably due to their use of the second derivative for the analysis which is questionable for quantitative analysis of overlapping peaks.

Regarding the area of the (metallic) 43.7 eV peak as function of θ_O two things are remarkable: an apparently linear decrease and the disappearance of the peak at the value at which θ_O is sufficient to oxidise all iron to Fe^{3+}. This means that either metallic iron is present until all iron is oxidised to Fe^{3+}, in other words iron must be oxidised directly to Fe^{3+}, or Fe^{2+} contributes to this peak. A consecutive oxidation of iron to Fe^{2+} and then to Fe^{3+} can be ruled out. Because then, due to an in that case necessary contribution of Fe^{2+} to the 43.7 eV peak, a sharper decrease in the 43.7 eV peak area is expected for $\theta_O>1$. Based on the lines in Fig. 5 oxidation of Fe to (initially) coexisting Fe^{2+} and Fe^{3+} cannot be ruled out. The origin of the Fe $M_{2,3}VV$ peak, however, does not suggest any reasons for the presence of a $M_{2,3}M_{4,5}M_{4,5}$ peak for Fe^{2+} and an absence for Fe^{3+}. So the first explanation seems more plausible. Also there may be an influence of the underlying copper on the oxidation state of the iron or on the $M_{2,3}VV$ peak. It seems good to note here that also in the derivative spectra the metallic peak remains visible at least upto $\theta_O=1.3$ (Fig. 3b).

Furthermore it is obvious that both oxidic peaks increase with the amount of oxygen. The intensity of the cross-transition peak increases initially at a higher rate with θ_O than the auto-ionisation peak. However, the slope decreases strongly somewhere between $\theta_O=0.5$ and $\theta_O=0.8$ whereas the auto-ionisation peak increases upto $\theta_O=1.5$. At this point the contribution of both oxidic peaks is nearly the same. The initial growth of the low energy

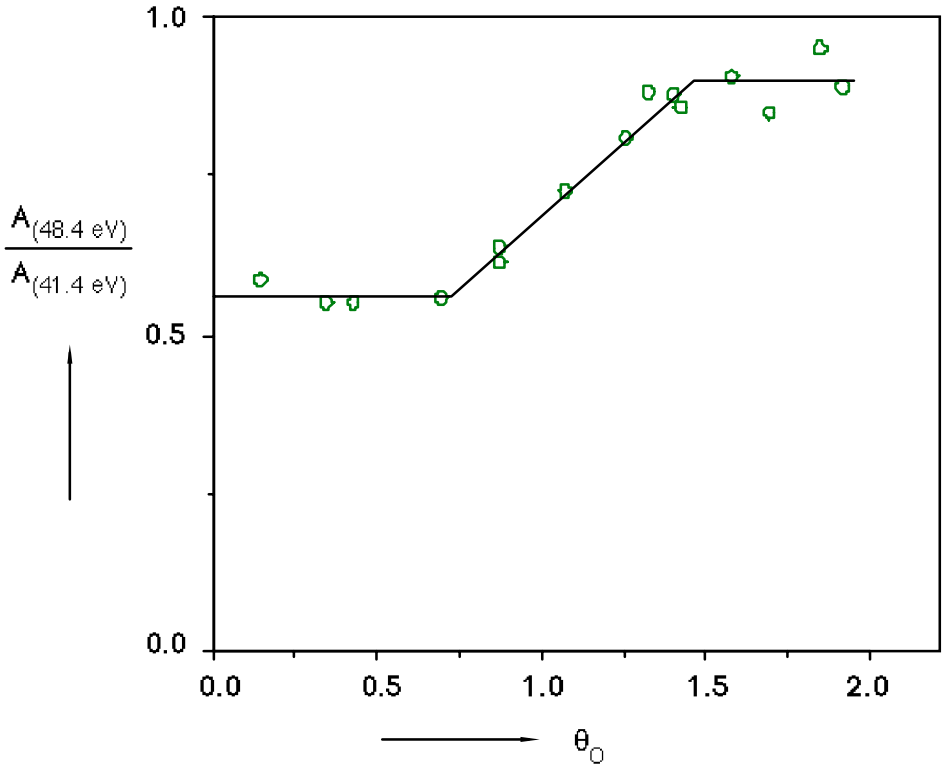

Figure 6 *The ratio of the auto-ionisation and the cross-transition peak areas as function of the amount of oxygen. The lines are drawn to guide the eye.*

peak agrees with the observation of others [66,69,70]. But it disagrees with the observation of Ramsey and Russell [77], who didn't observe an increase of the low energy peak for oxygen exposures below 10 L, but this was based on second derivative spectra. So at least for the Cu(100) + 1 ML Fe surface their argument against the low energy peak as caused by a cross-transition concerning O 2p electrons is not valid. The strong increase in intensity of this transition can then be ascribed to a strong increase of the number of O 2p electrons in the valence band which is independent of the kind of oxide [79].

The ratio of the areas of the high and low energy peaks as function of the amount of oxygen gives more interesting information about this system, as can be seen in Fig. 6. This ratio is constant at 0.6 upto θ_O=0.7 then increases apparently linearly to 0.9 for θ_O>1.5. The changing ratio may be explained by the presence of two kinds of oxygen on the iron surface. Jansson and Morgen [70] already suggested this for the oxidation of polycrystalline iron based on factor analysis of both the Fe $M_{2,3}VV$ and the O KLL spectra. Also, using ellipsometry evidence was found for a different kind of oxygen adsorbing initially on Fe(100) [59] and on Cu(100)-Fe [77]. Now the suggestion arises that the low energy peak is caused by 'surface' oxygen which is differently bound to the iron than 'bulk' oxygen. This is difficult to prove for the Cu(100)-Fe surfaces because the bulk/surface ratio depends on the unknown corrugation of the surface and this effect can hardly be ruled out because of the small sampling depth. An other possible explanation is that Fe^{2+} and Fe^{3+} have a different ratio for both transitions. In that case initially Fe^{2+} is formed (may be together with Fe^{3+})

upto θ_O=0.6-0.7 when Fe^{3+} starts forming at the expense of Fe^{2+} (and Fe^0). This agrees with the second possible explanation given for the behaviour of the 43.7 eV peak, however, the argument against it remains.

The change in the ratio stops at the very moment that all iron could be oxidised to Fe^{3+}, i.e. θ_O=1.5. The other half monolayer of oxygen adsorbing after this point does not seem to have influence on the Fe $M_{2,3}VV$ spectra and therefore can probably be ascribed to oxygen bound to the Cu surface. This agrees well with the disappearance of the 43.7 eV peak at θ_O=1.5.

4.4 Conclusions.

It is not possible to distinguish between the different iron oxides based on the presence or absence of either the cross-transition or the metallic peak Fe $M_{2,3}VV$ peak. On the contrary the presence of a (large) peak at 43.7 eV (46.3 eV in dN/dE mode) in the iron $M_{2,3}VV$ spectrum is a strong indication of the presence of metallic iron in the surface region. Support for this can be found in literature (section 4.2) and in the analysis of the $M_{2,3}VV$ peak during oxidation of one monolayer of iron on Cu(100) (section 3 of this chapter).

On oxidising one monolayer of iron on Cu(100) the iron is first oxidised completely to Fe_2O_3 before oxygen adsorbs on the Cu(100) (-Fe_2O_3) interface. The iron is not consecutively oxidised to Fe^{2+} and Fe^{3+} but either at once to Fe^{3+} or to initially coexisting Fe^{2+} and Fe^{3+}.

A difference in the ratio of the cross-transition and the auto-ionisation peak between initially and finally adsorbing oxygen is observed. This might be due to a different effect of surface and bulk oxygen on the Fe $M_{2,3}VV$ transition. Since this is not understood completely more investigations on the development of the Fe $M_{2,3}VV$ peak upon oxidation would be interesting.

5

The interaction of Cu(100)-Fe surfaces with oxygen studied with photoelectron spectroscopy. I

Mg K_α excited photoemission.

Abstract

The oxidation of Cu(100)-Fe surfaces was studied using XPS. Surfaces containing 0 - 10 ML were oxidised at room temperature exposing 2 Pa·s of oxygen. For all surfaces evidence for Fe_2O_3 was found. Only for surfaces containing more than 5 ML a clear metallic Fe $2p_{3/2}$ was observed. This means that more oxygen could be adsorbed than observed in chapter 3 and 4.

The analysis of the change of the 2p peak shape of a surface containing 1 ML of Fe as function of the amount of oxygen showed that oxidation proceeds via an intermediate containing both Fe^{2+} and Fe^{3+}.

5.1 Introduction.

In this chapter XPS is used to obtain more information on the Cu(100)-Fe-O system. The sensitivity of the Fe 2p peak for the oxidation state gives the possibility to determine the type of iron oxide independently from stoichiometric calibrations. Neglecting a possible influence of the substrate and extrapolating to bulk iron the results presented in chapter 3 and 4 seem to contradict the results reported by Leibbrandt et al. [55] who found $Fe_{0.95}O$ after oxidation of Fe(100) at 300K. The amount of oxygen found by them was, however, equal to that found for oxidised Cu(100) surfaces containing more than 2 ML of iron [82]. The results presented in chapter 3 and 4 also conflict with conclusions reported by Kishi et al. [35] though they used oxygen exposures obviously too small to produce oxygen saturated surfaces.

The XPS results will also be used to verify the direct oxidation from Fe^0 to Fe^{3+} as proposed in chapter 4.

5.2 Results and discussion.

Surfaces containing 0-10 ML of iron were oxidised exposing 2 Pa·s of oxygen at room temperature. In Fig. 1 the oxygen 1s signal is plotted versus the iron 2p signal. The line drawn in Fig.1 is the least squares fit through all points. The intensities are corrected for the differences in X-ray beam intensity assuming that the sum of the Cu 2p, Fe 2p and O 1s multiplied by their respective relative sensitivity factors (rsf's) is a good representation the beam intensity. The rsf's used were taken from the Phi handbook [53]. These rsf's are obtained with a Phi Omnifocus III lens in front of the hemispherical analyser. So it must be realised that the conditions are different and thus the rsf's may be wrong. Multiplying the corrected intensities with their rsf's (as was done) in principle results in mole fractions ($X_x=rsf_x \cdot I_x/\Sigma rsf_i \cdot I_i$), however this requires correct rsf's and a homogeneous sample. Errors in the rsf's influence the absolute numbers but, within certain limits, not the linearity in Fig.1. So the slope is not used here to calculate the stoichiometry. In any case, the intercept is equal to the signal of 0.5 ML of oxygen on Cu(100) within experimental error and this confirms the 0.5 ML of oxygen present in excess of the oxygen bound to the iron as reported before [82]. However, at iron coverages (exceeding 3 ML) still more oxygen can be adsorbed. This is not expected based on previous results and it will be discussed later.

Since for the eye there seemed no difference between the Fe 2p spectra of surfaces containing different amounts of iron (up to 3 ML), fits to the spectra are compared. The spectra were fitted with 4 peaks representing the Fe $2p_{3/2}$, the Fe $2p_{1/2}$ the satellite of the Fe $2p_{3/2}$ and an extra peak to take account for the asymmetry of the Fe $2p_{3/2}$ peak. The satellite of the Fe $2p_{1/2}$ is omitted because it appeared to be weak compared to the noise and also the possible asymmetry of the Fe $2p_{1/2}$ did not seem to influence the fit. The fits were performed by minimisation of χ^2 of four mixed Gaussian/ Lorentzian functions with fixed width (FWHM of 3.8 eV for all peaks except the asymmetry function which appeared to give the best results with 5 eV) and Gauss/Lorentz ratio of 0.5. An example of a fit is shown in Fig. 2 which gives the fit results for a Fe 2p peak taken of a surface containing 1.5 ML of iron on Cu(100) after exposure of 2 Pa·s of oxygen. In table I the results of the fits are reported averaged for 6 spectra (0.5 - 3 ML) because the fits showed no trends due to different θ_{Fe}. Both the position of the $2p_{3/2}$ after oxidation (shifted 3.9 ± 0.2 eV to higher binding energy in respect to the metal $2p_{3/2}$ peak [83]) and the presence of a satellite at 8 eV higher binding energy [79] indicate

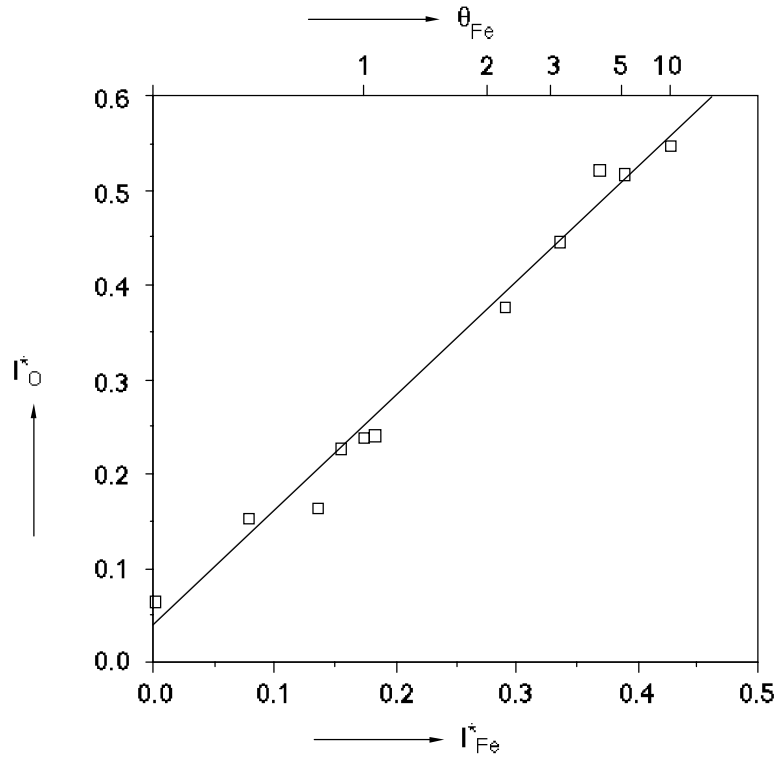

Figure 1 *The relative O 1s signal as function of the relative Fe 2p signal after 2 Pa·s of oxygen obtained on Cu(100) surfaces containing different amounts of iron.*

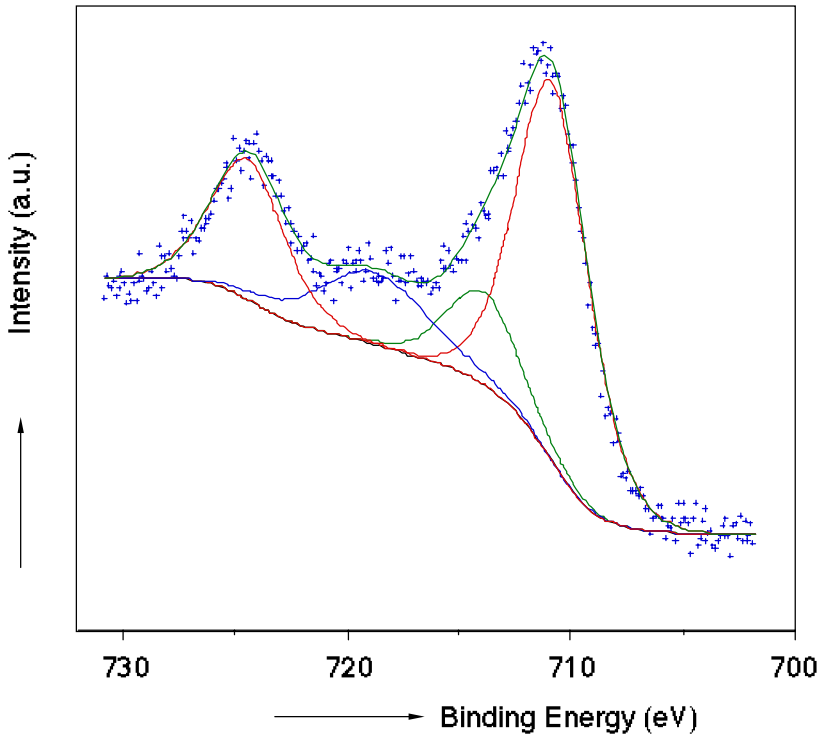

Figure 2 *A Fe 2p spectrum of Cu(100) + 1.5 ML Fe after 2 Pa·s of oxygen. The background and the four peaks resulting from the fit as described in the text are also shown.*

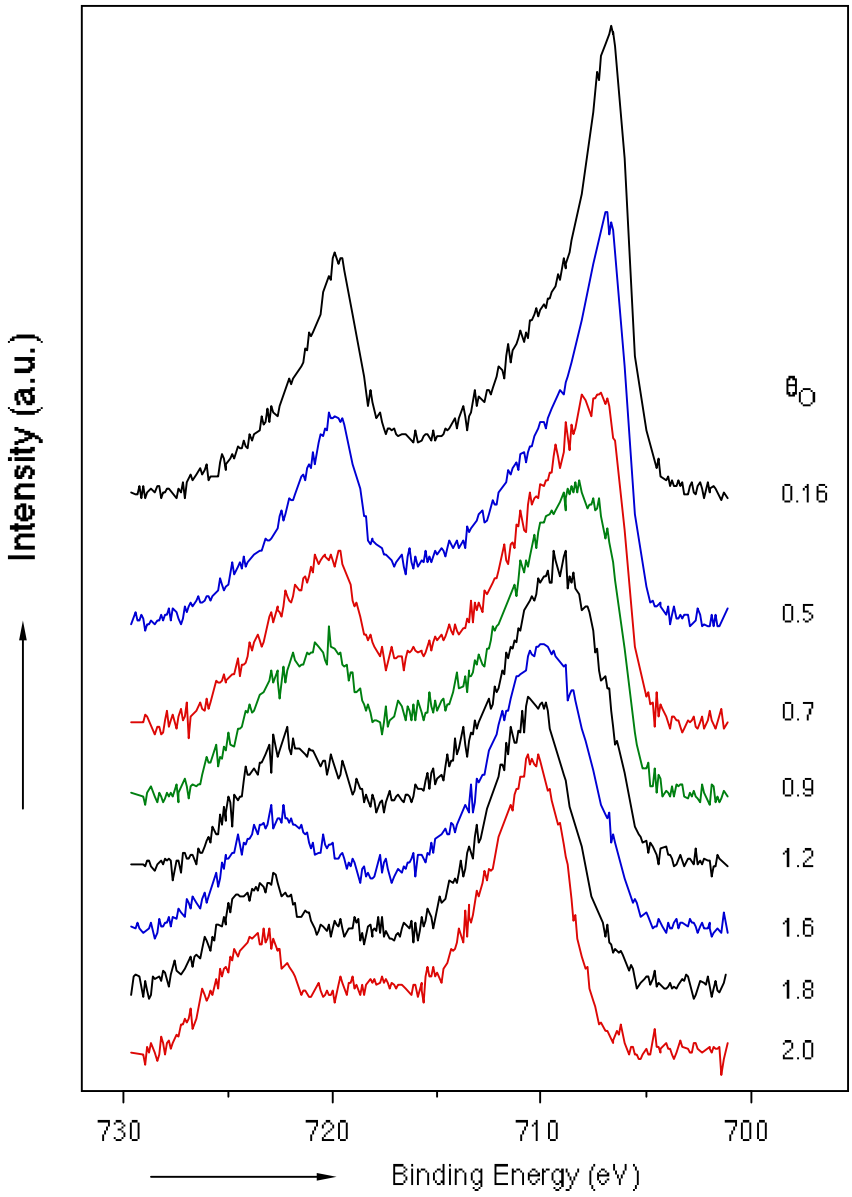

Figure 3 *Some Fe 2p spectra after background subtraction of a step by step oxidation of Cu(100) + 1 ML Fe.*

the presence of Fe_2O_3 at the surface under these conditions. This proof for formation of Fe_2O_3 during the oxidation of Cu(100) containing up to 3 ML of iron is, unlike the other determinations, independent of calibrations of amounts of iron and oxygen.

In order to be able to follow the development of the oxide on the surface, Cu(100) + 1 ML Fe was oxidised step by step. The oxygen pressures and exposure times were chosen such as to obtain reasonable changes in the amount of oxygen adsorbed on the surface in a reasonable time. Fig. 3 shows the change in the Fe $2p_{3/2}$ peak during oxidation after background subtraction. The oxygen coverage of the fresh prepared surface is due to the presence of oxygen adsorbed during evaporation. From Fig. 3 it is clear that the iron peak starts changing immediately and that after adsorption of a certain amount of oxygen the final Fe_2O_3 peak shape is reached, whereas still more oxygen can be adsorbed on the surface. This

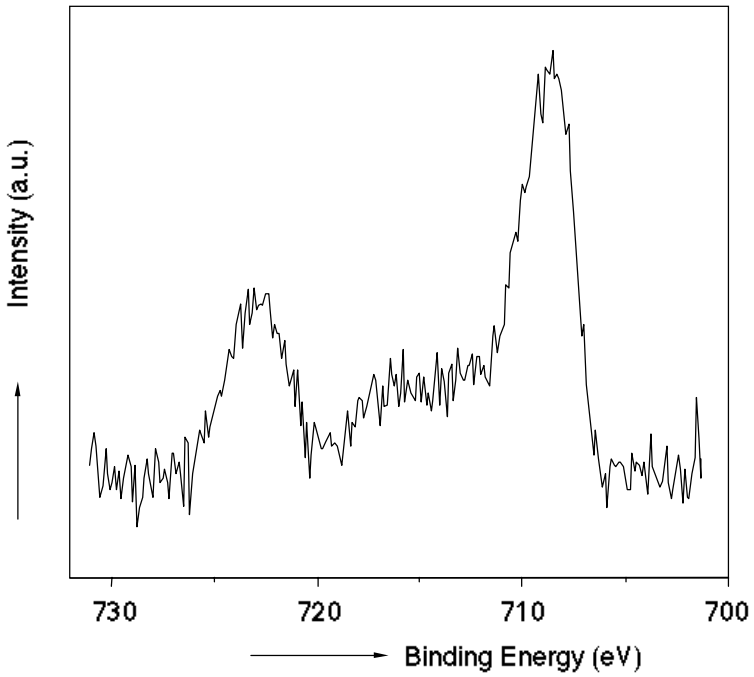

Figure 4 *The sum of the Fe^{2+} 2p spectra resulting from the spectrum decomposition of the Fe 2p spectra obtained during a step by step oxidation of Cu(100) + 1 ML Fe as described in the text.*

Table I. Mean characteristics of the Fe 2p peak shape of oxidised surfaces containing 0 - 3 ML of iron.

peak	position (eV)	FWHM (eV)	relative contribution
$2p_{3/2}$	710.24 ± 0.17	3.8	0.516 ± 0.014
asymmetry	713.3 ± 0.3	3.8	0.124 ± 0.017
satellite	718.2 ± 0.3	5.0	0.156 ± 0.017
$2p_{1/2}$	723.8 ± 0.2	3.8	0.204 ± 0.005

agrees with the 'excess' oxygen which adsorbs on the copper after oxidation of the iron. Since a linear decrease of the metallic Fe $M_{2,3}VV$ peak with increasing amount of oxygen suggested immediate formation of Fe^{3+} out of Fe^0 [46] it was tried to verify this by decomposing the intermediate spectra with the first (in principle oxygen free, though containing 0.16 ML of oxygen) and the last (completely oxidised to Fe_2O_3) spectrum by means of a linear fit. However, a sum of the sharp Fe^0 $2p_{3/2}$ and the more broad Fe^{3+} $2p_{3/2}$ result in a clear double peak which is never found in the real spectra. To resolve this the spectra were composed using a linear combination of the Fe^0 and Fe^{3+} spectra. It was judged from the background on the high and the low energy side of the difference spectrum whether the choice of the weights might be correct. The resulting difference spectra resembled each other strongly. Since no clear trends were visible in these 'rest' spectra only the sum of them (to reduce noise) is shown in Fig. 4. The peak shape and position of this spectrum suggest the presence of Fe^{2+} though the $2p_{3/2}$ is too narrow (3 eV instead of 3.8 eV, but also Kurtz and Henrich report small FWHM

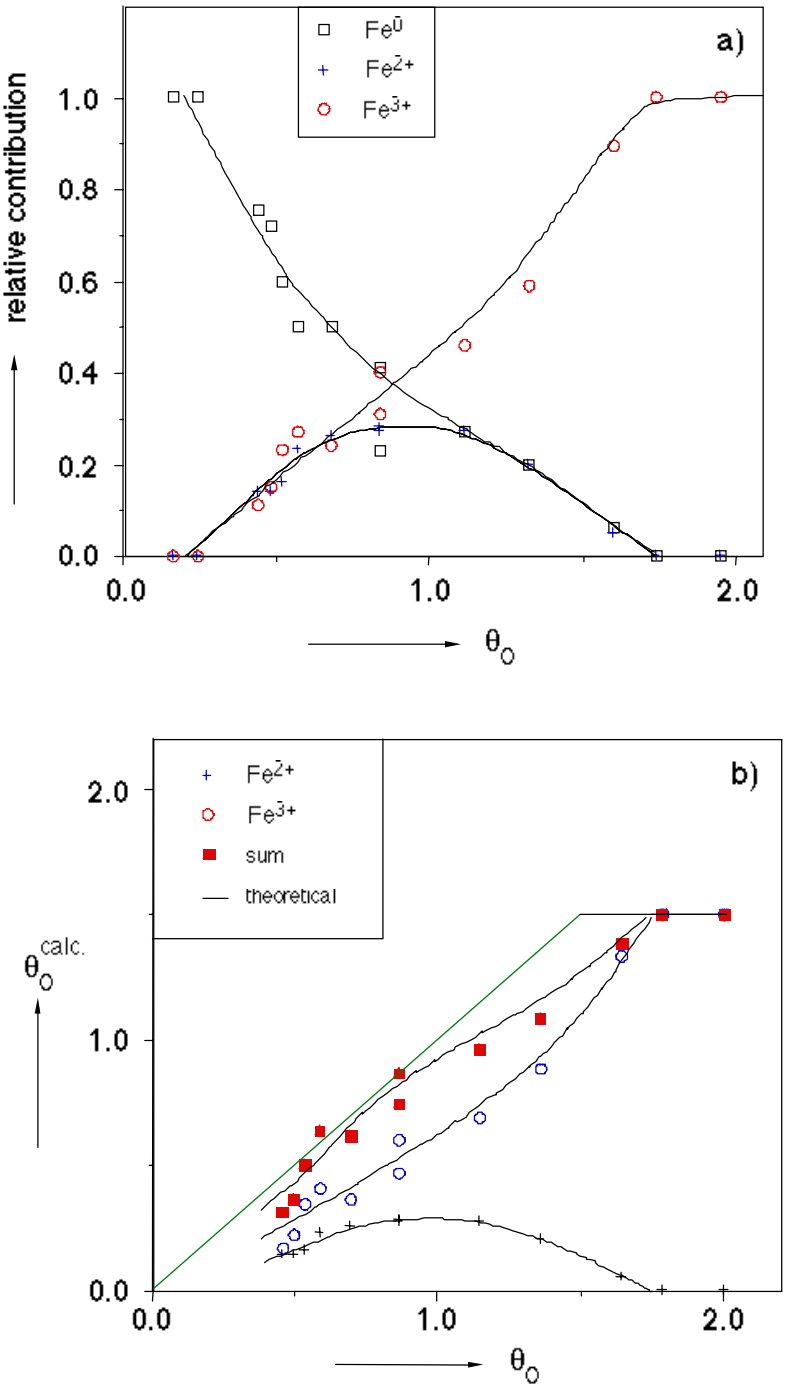

Figure 5 *The partial contribution of Fe^0, Fe^{2+} and Fe^{3+} to the Fe 2p spectra of the step by step oxidation of Cu(100) + 1 ML Fe as function of the amount of oxygen (a) and the amount of oxygen calculated from the number of iron ions as function of θ_O calculated from the O 1s (b). The broken lines drawn are to guide the eye.*

values for Fe^{2+} [84]). In Fig. 5a the results of the decomposition are shown giving the relative contribution of the Fe^0, Fe^{2+} and Fe^{3+} as function of the amount of oxygen. It may be clear that a discussion of a linear decrease of the Fe^0 contribution is not really sensible since the 'Fe^0' peak already contained a Fe^{2+} and a Fe^{3+} contribution. However, the contribution of the Fe^{2+} and the Fe^{3+} peaks seems to increase together first and later the Fe^{2+} contribution

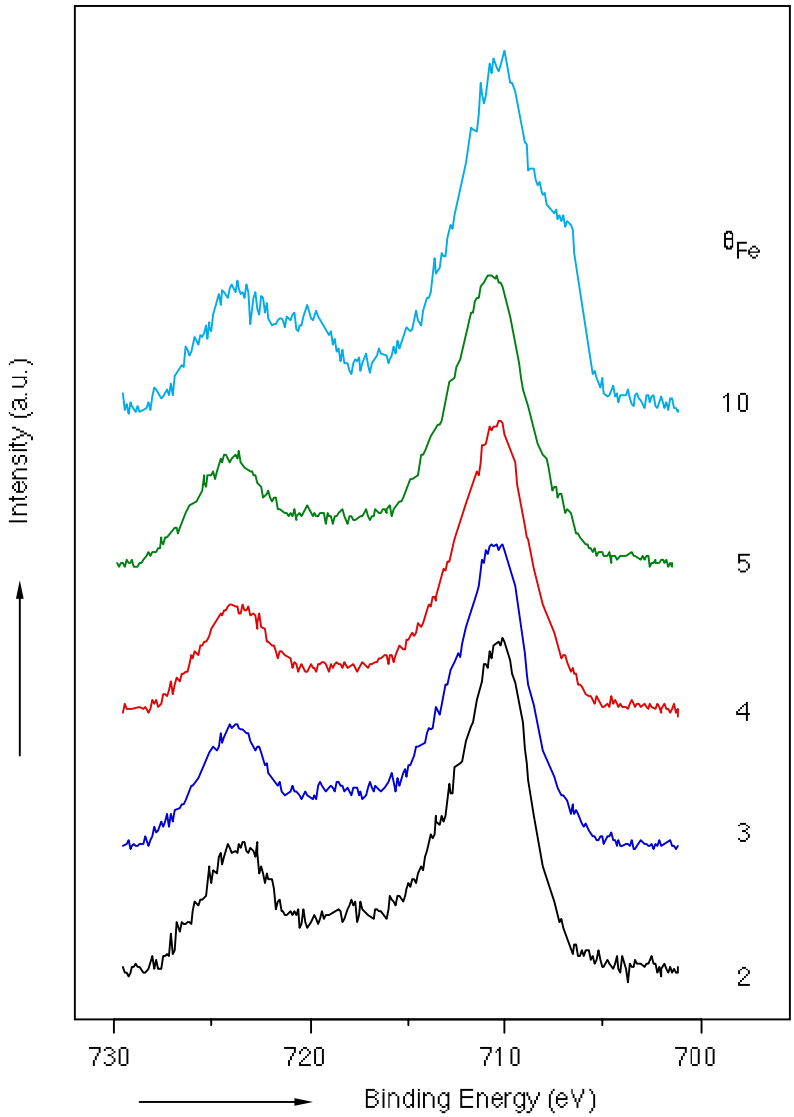

Figure 6 *The Fe 2p spectra after background subtraction of oxidised surfaces containing 2, 3, 4, 5 and 10 ML of Fe on Cu(100).*

decreases down to zero. So it can be concluded that the Fe_2O_3 is formed via an intermediate phase containing both Fe^{2+} and Fe^{3+}.

A possible falsification of the decomposition method above may come from the amount of iron ions in relation to the amount of oxygen to be present at the surface. In order to check this the amount of oxygen bound to Fe^{2+} and Fe^{3+} (on the same 1 ML Fe on Cu(100) surface) is calculated assuming the oxygen present as O^{2-}, and θ_O=2.0 ML at the end of the oxidation. The result is shown in Fig. 5b. The solid line drawn in Fig. 5b represents the theoretical amount of oxygen bound to iron assuming all iron is oxidised before oxygen adsorbs on the copper surface. The data for small θ_O are omitted because the Fe^0 peak already contains a contribution of the Fe^{2+} and Fe^{3+} which can not be accounted for in the calculation. However, the influence of this decreases with a decreasing contribution of Fe^0 to the peak. For high oxygen coverages the discrepancy is of course due to the adsorption of the excess oxygen, which does not necessarily has to start abruptly. The most important conclusion from Fig. 5b is that the amount

of oxygen calculated from the iron ions (as present according to the decomposition that resulted in the peak of Fig. 4) never exceeds the total amount of oxygen as calculated from the O 1s peak.

An other interesting point arises when Fig. 5a is compared with Fig. 6 in chapter 4. Fig. 6 from chapter 4 shows the ratio of the contribution of the cross-transition and the auto-ionisation features to the electron excited Fe $M_{2,3}VV$ peak as function of θ_O for the oxidation of 1 ML Fe on Cu(100). The value of θ_O at which the Fe^{2+} contribution stops increasing (in Fig. 5a) seems to coincide with that where the ratio between the cross-transition and the auto-ionisation starts to change. Since there was no direct proof for the existence of Fe^{2+} during the oxidation, this change in the ratio was ascribed to the presence of a kind of surface oxygen [46]. Now it is known that Fe^{2+} is probably present during the oxidation, the changing ratio can be explained from a changing ratio of the number of Fe^{2+} and Fe^{3+} ions. This also means that Fe^{2+} and Fe^{3+} may indeed exhibit a different $M_{2,3}VV$ peak shape as suggested by Seo et al. [60], but that it should be found in the ratio of both oxide features of the Fe $M_{2,3}VV$ peak. However, a surface oxygen effect on the ratio can not be excluded.

From Fig. 1 it was clear that the amount of oxygen after saturation still increases when more than 3 ML of iron is deposited. This means that more than 2 ML of iron (or 2.3 ML of iron when the 0.5 ML excess oxygen is included) can be oxidised. Since the Cu $2p_{3/2}$ peak (E_{kin}=320 eV, imfp~8 Å) is still clearly present up to θ_{Fe}=5 any metallic iron present should be visible in the Fe 2p spectra (E_{kin}=530 eV, imfp~10 Å). However, comparison of the Fe 2p spectra taken of oxidised surfaces containing 2, 3, 4, 5 and 10 ML iron (Fig. 6) shows that only for the 10 ML spectrum the metallic $2p_{1/2}$ and $2p_{3/2}$ are strongly present. For the other spectra the metallic Fe $2p_{3/2}$ peak may be present as a shoulder at ~707 eV, but very weakly. These findings agree with the amount of oxygen still increasing for θ_{Fe}>3 ML (Fig. 1), but do not fit in a model of only 2.3 ML of iron that can be oxidised to Fe_2O_3. The difference may come from an error in the micro-balance (though this is highly unlikely because the error must exceed 25%) or from differences in the structure of the iron film before oxidation influencing the mass-transport in the oxide layer. In principle even at 10 ML the iron is expected to be present as flat fcc iron on Cu(100) [20]. However, both the temperature and contamination out of the gas may influence the growth. Though the difference in evaporation conditions between the experiments presented in this chapter and chapter 3 and 4 seem to be small, this may be the cause. Especially the difference in oxygen contamination after evaporation (θ_O • 0.16 in this study against θ_O • 0.05 in chapters 3 and 4) may be responsible for a different growth of the iron. The structure of the iron on the surface is very important for the amount of iron that can be oxidised [61].

Closer examination of the 10 ML (but also for those of 25 and 44 ML) shows that only Fe^{3+} and Fe^0 contributions are present. Though a shift of 0.2 eV to lower binding energy of the Fe^{3+} spectrum is necessary in order to synthesise the spectrum out of a Fe^{3+} and Fe^0 spectrum a Fe^{2+} contribution appears to be absent. Apparently the type of iron oxide formed is Fe_2O_3 and independent of the amount of Fe deposited on the Cu(100) surface.

5.3 Conclusions.

The shape of the Fe 2p peak after exposure of 2 Pa·s of oxygen to Cu(100)-Fe surfaces shows the presence Fe_2O_3 independent of the amount of iron. Quantitative analysis of the amounts of Fe and O agrees with this, though more oxygen could be adsorbed during these

experiments than expected based on experiments described in chapters 3 and 4. Also the presence of 0.5 ML of excess oxygen for $\theta_{Fe} \leq 2$ ML is confirmed by these experiments.

During the oxidation of 1 ML of iron on Cu(100) first both Fe^{2+} and Fe^{3+} are formed. Later Fe^{2+} disappears as does the Fe^{0} in favour of Fe^{3+}. Combining this observation with the Fe $M_{2,3}VV$ peak shape analysis [46] suggests Fe^{2+} and Fe^{3+} might exhibit a different $M_{2,3}VV$ peak shape. This difference must then be found in a different ratio of the contribution of the two oxide features composing the $M_{2,3}VV$ iron oxide peak.

6

The interaction of Cu(100)-Fe surfaces with oxygen studied with photoelectron spectroscopy. II

He I and He II excited photoemission.

Abstract

The valence band structure of Cu(100)-Fe surfaces is studied for different amounts of iron and oxygen using He I and He II radiation for excitation. Interesting changes in the Cu 3d structure occur that may be due to changes in the structure of the top layer of the Cu substrate. The shape of the valence band after 2 Pa·s of oxygen confirms the presence of Fe_2O_3 on these surfaces. Stepwise oxidation showed a direct increase of the O 2p level, whereas the Fe 3d band near the Fermi edge initially did not change much. This may be the cause of the apparently invisible oxygen occurring during the adsorption of the first ML as seen by $\delta\Delta$ determined by ellipsometry.

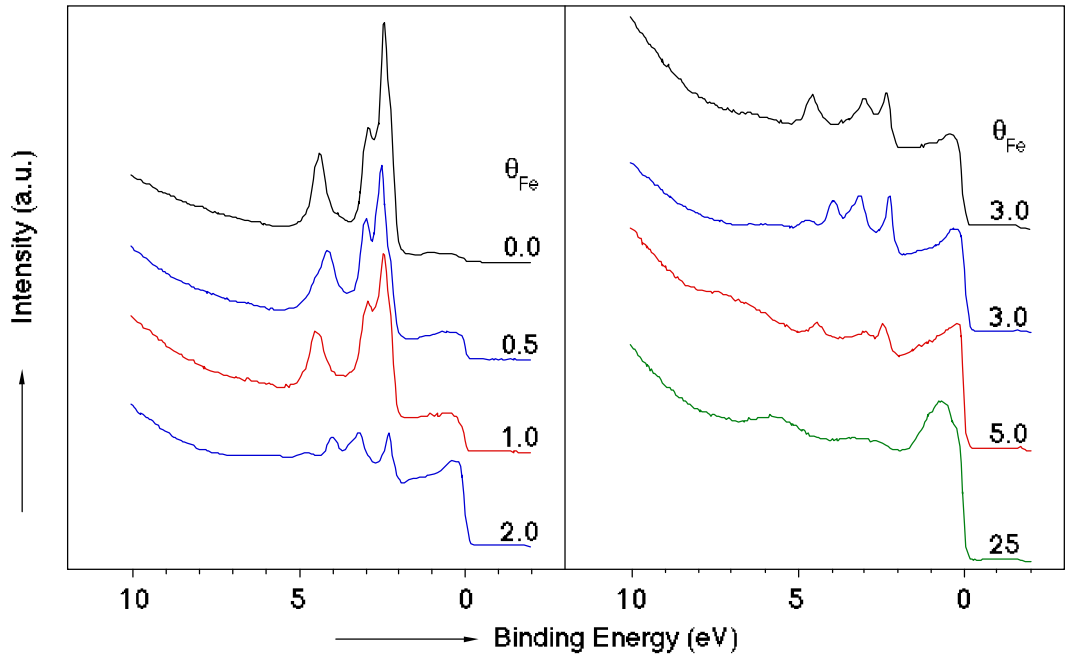

Figure 1 *He I photoemission spectra of freshly prepared Cu(100)-Fe surfaces.*

6.1 Introduction.

Knowledge of the valence band and conduction band structure of surfaces is of great importance for a better understanding of physical and chemical events occurring in or at the surface. The electronic structure near the Fermi level is responsible for the optical properties of the material and for the reactivity towards other materials. From this point of view the Cu/Fe system is very interesting because both metals have a different band structure, a different crystal structure at room temperature, and an endothermic heat of mixing indicating a bad interaction.

This chapter deals with the change in the valence band of the Cu(100)-Fe surface containing different amounts of iron due to interaction with oxygen. He I and He II results are compared because the excitation cross-sections of the O 2p and the Cu/Fe 3d change differently upon changing the energy of the photons.

6.2 Results and discussion.

In Fig. 1 He I photoemission spectra of surfaces containing different amounts of iron are shown. With increasing iron coverage two main changes in the valence band structure occur. Near the Fermi level the copper 4s band is overshadowed by a growing iron 3d band, while on the other hand, as could be expected, the copper 3d band structure decreases with growing iron layer thickness. The iron 3d band is already clearly visible for 0.5 ML Fe whereas for 2 Å (≈1 ML Fe) on polycrystalline copper the difference was much smaller [37,38]. Those spectra, however, were excited with Mg K_α radiation which may explain the difference.

On examining the structure of the copper 3d band (the peaks between 2 and 5 eV) another difference seems to exist for the different surfaces. This difference that consists of changes in the peak maxima and intensities, is at least partly due to the highly angular dependence of the

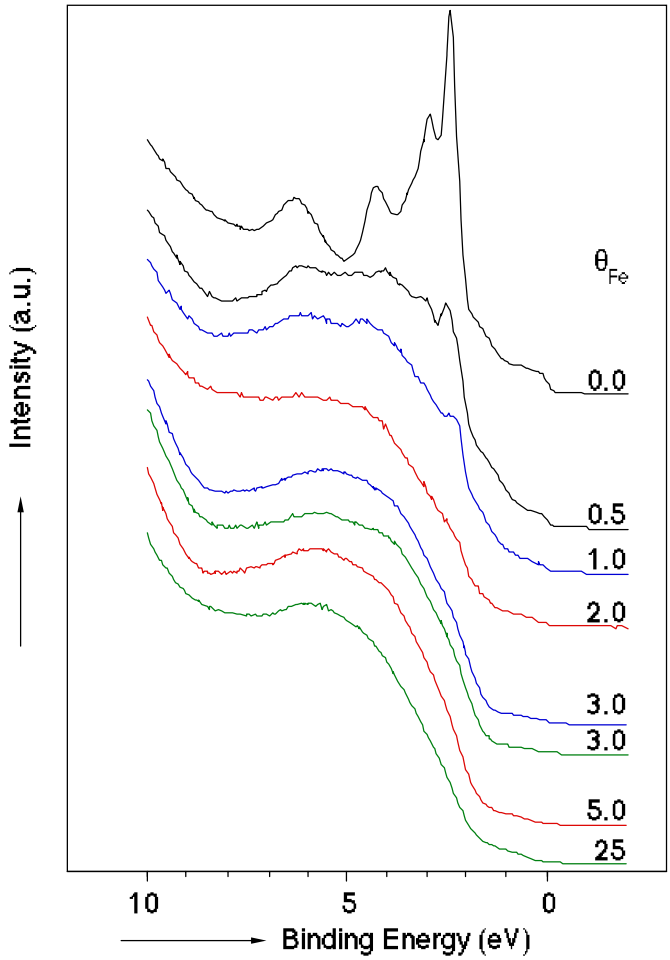

Figure 2 He I photoemission spectra of Cu(100)-Fe surfaces after 2 Pa·s of oxygen.

copper 3d band structure of monocrystalline surfaces [87, 88]. Since the sample had to be moved in order to clean and to evaporate new iron and because it was difficult to place the crystal in exactly the same position, the Cu 3d structure often reproduced badly when a new surface was prepared. As an example, 2 spectra of two different separately prepared surfaces containing 3 ML of iron are shown in Fig. 1. The difference is found in the copper 3d band structure. Similarly different spectra were obtained for clean Cu(100), though they are not shown here. Therefore discussion considering the copper 3d part of these spectra has to be done carefully. Spectra taken before and after oxidation can be compared with each other without this problem since sample movements were not carried out in that case.

The changes in the He I photoemission spectra due to oxidation up to saturation can be seen in Fig. 2. The amount of oxygen used was 2 Pa·s, which is sufficient to reach saturation within a few percent [82]. In all spectra, but those of pure Cu and 'bulk' iron, the copper 3d band structure seems to vanish into the iron oxide band structure. Closer examination learns that the band at 2.4 eV decreases mostly due to oxidation with respect to the other copper 3d features. This can only partly be caused by the screening of the copper 3d electrons by the iron oxide layer since the inelastic mean free path of those electrons is high with respect to the amount of oxide (at least when 0.5 ML Fe is present). A good indication for this is that the Cu 3d band is still visible after the evaporation of 5 ML of iron. Possibly the decrease is caused by

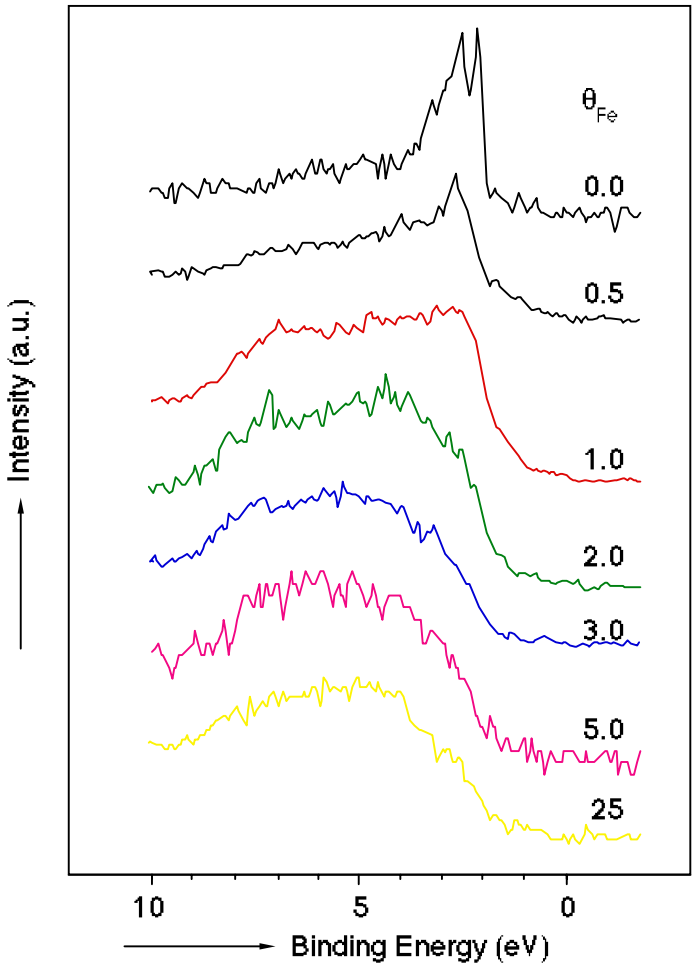

Figure 3 *He II photoemission spectra of Cu(100)-Fe surfaces after 2 Pa·s of oxygen.*

an electronic interaction between the iron oxide and the copper surface but it may also be caused by a slight deformation of the surface. In fact, also for the oxidised surface without iron a decrease of the most intense peak (at ~2.4 eV) in respect to the peak at 3 eV of about 25% can be observed. It is known from calculations [89] and experiments [9, 90] that 0.5 ML of oxygen on Cu(100) (which is the saturation value of this surface [51]) induces a missing row reconstruction of the surface. However, the change in the ratio between the 2.4 and 3 eV peak with increasing Fe coverage (Fig. 1) suggests the presence of an electronic interaction since iron grows epitaxially on Cu(100) for the first several ML. Against this can be said that the interaction cannot be very strong since the heat of mixing is positive. On the other hand there must be some electronic interaction because bulk like fcc iron is not stable at 300 K. The stress caused by this anomaly may be enough to change the above mentioned ratio if the 2.4 eV peak is mainly influenced by structural changes surface region.

Other important observations in Fig. 2 are that the Fe 3d states near the Fermi level have disappeared completely due to the formation of an insulating oxide and that the O 2p band and the Fe 3d band form a broad apparently featureless band. The shoulder near the Fermi level, characteristic for the Fe^{2+} [79] containing compounds is apparently absent. However, Wandelt [79] reported the shoulder in Al K_α excited valence band spectra of Fe_xO and Fe_3O_4, which does not necessarily indicate an absence or presence in the Fe^{3+} and Fe^{2+} valence band spectra

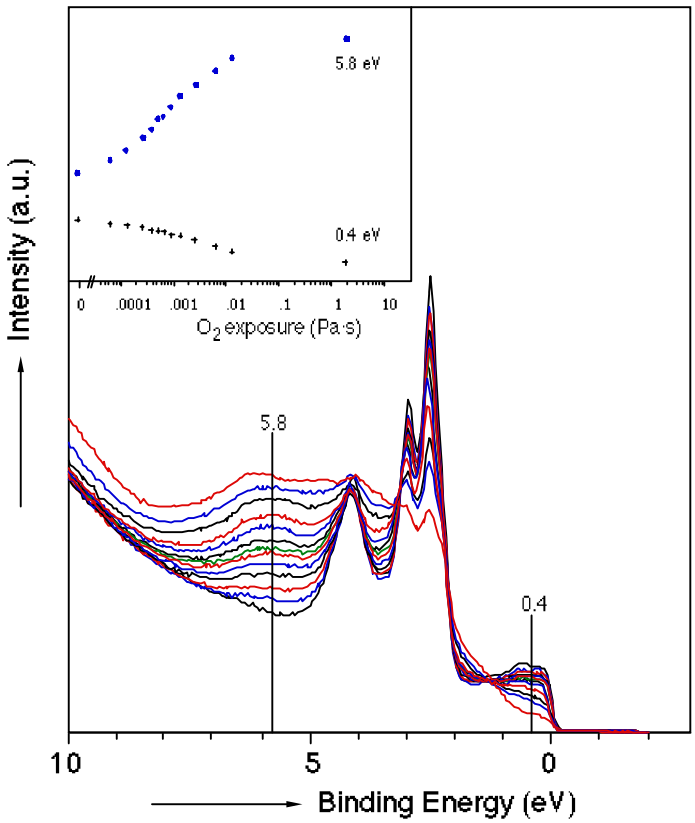

Figure 4 *He I photoemission spectra of a stepwise oxidation of 0.5 ML Fe on Cu(100). The insets give the intensity of the spectra at the binding energies of 0.4 and 5.8 eV indicated by vertical dashed lines.*

excited with He I radiation. Nevertheless, valence band spectra of Fe_xO excited with hν=30eV [79] and Fe_3O_4 excited with He I and He II [91] exhibit the shoulder whereas Fujimori et al. [92] reported the absence of this shoulder in Fe_2O_3 spectra excited with a wide range of photon energies starting with 21.2 eV. In fact the He I spectrum reported by them is quite similar to those observed by us for 3 and 25 ML of Fe on Cu(100). This seems to be an other confirmation that the Cu(100)-Fe surfaces contain Fe_2O_3 after exposure to 2 Pa·s oxygen at room temperature. Further evidence for this can be found in Fig. 3 which shows the He II excited valence band spectra of the same surfaces as reported in Fig. 2. Also in the He II spectra no shoulder near the Fermi level is visible. The other trends are the same as in the He I spectra but for the background which is much higher in the He I spectra due to the lower kinetic energy of those electrons in respect to the He II excited electrons.

The effect of oxidation on the valence band of Cu(100)-Fe surfaces was also studied after various exposures and thus containing different amounts of oxygen. Although it would have been favourable to know the absolute amount of oxygen for the different spectra, only the exposure could be used. Reason for this was that a small displacement of the sample was necessary in order to place the sample in the right position for the Mg anode. As explained before, this displacement results in changes in the spectra which are clearly less desirable. In Fig. 4-6 the spectra of step-by-step oxidation of surfaces containing respectively 0.5 ML, 3 ML and bulk like iron (25 ML Fe) are shown. During O_2 exposure the He discharge lamp was stopped

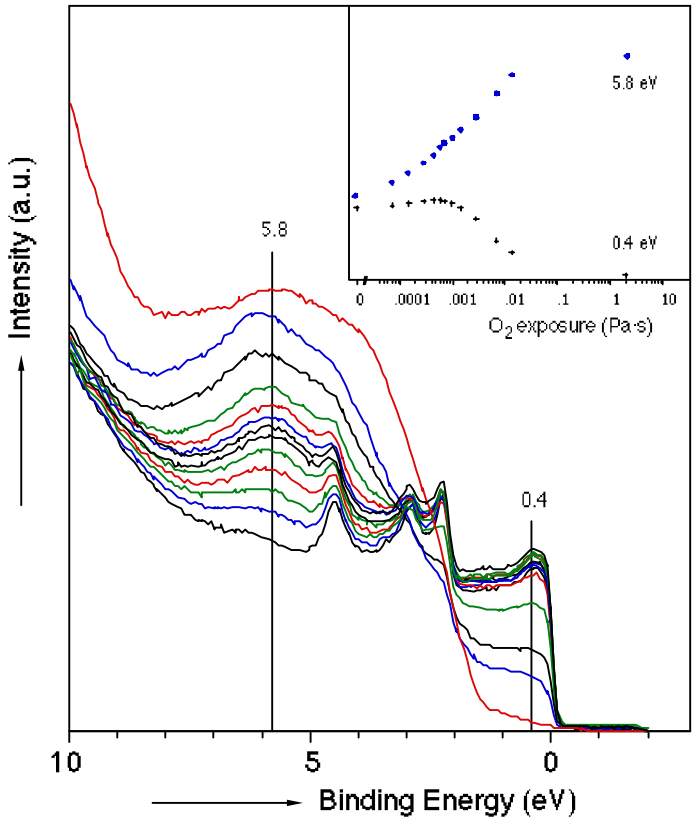

Figure 5 *As Fig. 4 for 3 ML of Fe.*

only for the final exposure (2 Pa·s, and in this case only the discharge was stopped, not the He flow) in order to acquire lamp conditions as similar as possible. However, a small drift in the photon flux due to small pressure variations can not be excluded and may influence the absolute values of the spectra. To show the development of the O 2p band and the decrease of the Fe 3d band near the Fermi level more clearly, an inset representing the intensity of the valence band spectra at 5.8 and 0.4 eV is given in every figure. The vertical dashed lines indicate these two energies.

In all spectra an immediate formation of the O 2p becomes visible when the oxidation starts. In fact, for 3 ML and bulk like iron the O 2p is already visible in the first spectrum due to small contamination occurring during deposition. This direct growth of the O 2p band is in agreement with what is reported for bulk iron by Brundle [78]. It also appears to agree with what is seen in the analysis of the Fe $M_{2,3}VV$ peak shape of 1 ML of iron on Cu(100) during oxidation [46]: the low energy Fe oxide peak ascribed to a $Fe_{M2,3}Fe_{M4,5}O_{L2,3}$ cross-transition increases first and fast with increasing amount of oxygen. The coincidence of this immediate increase of the O 2p feature (whereas other changes in the valence band occur slower) and the same initially fast growth of the low energy iron oxide Auger peak seems to give further evidence for the Auger feature being indeed a cross-transition. The suggestion given by Ramsey and Russel [77] that this Auger feature is due to changes in the 3d band structure of iron is clearly contradicted by the change of the iron 3d band in the UPS spectra which appears to happen slow for the first mPa·s.

The initially slow change in the intensity of the Fe 3d band near the Fermi level is strange regarding the fact that each adsorbed oxygen atom may be expected to take up 2 electrons out

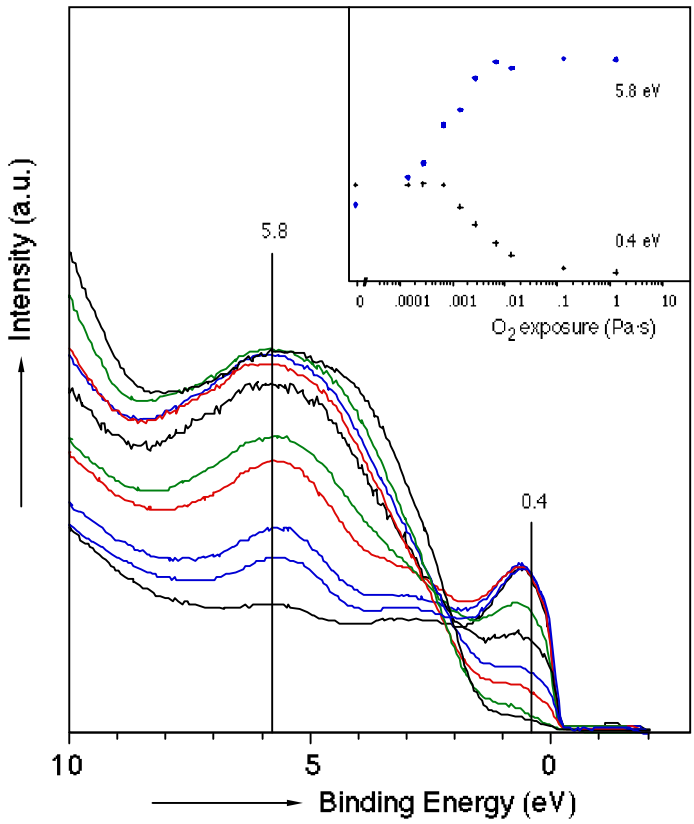

Figure 6 *As Fig. 4 for bulk like Fe (25 ML).*

of this band inducing a fast decrease of Fe 3d electrons and thus a fast decrease of this band. Though the oxygen 2p may be more intense because the 2p orbital already contains 4 electrons and is thus 'highly visible' with and without the 2 extra electrons, the removal of the two electrons out of the 3d band near the Fermi level is also expected to move these states to a higher binding energy. Apparently this does not happen (or at least not completely) for the first amount of oxygen. This may explain the 'invisible' oxygen as found with ellipsometry [82] without contradiction by the nearly linear decrease of the metallic Fe $M_{2,3}VV$ peak [46] and the metallic Fe 2p peak [93] in the peak shape analysis as function of the amount of oxygen.

The relatively slow decrease of the 3d band is near the Fermi level is less clear in the spectra of the surface containing 0.5 ML of Fe (Fig. 4) than for the other two surfaces studied because the amount of oxygen in respect to the amount of iron is higher at lower exposure for this surface since the initial sticking probability is the same for all iron containing Cu(100) surfaces [82].

7

The interaction of CO and H_2 with oxidised Cu(100)-Fe surfaces.

The interaction of oxidised Cu(100)-Fe surfaces containing 0.1 - 2.0 ML of iron with H_2 and CO has been studied. Surfaces containing more than 0.8 or 0.6 ML of iron which are oxidised at 300 K are inert to respectively CO and H_2 at 630 K and pressures up to 0.2 Pa. CO can remove only oxygen bound to copper and when bare copper sites are available. Hydrogen also requires uncovered copper for reaction but then all oxygen can be removed.

Further oxidation at 630 K induces the iron oxide formed at 300 K to reorganise in such a way that free copper sites are formed and both H_2 and CO can react with oxygen from the surface.

7.1 Introduction.

This chapter deals with the reduction of oxidised Cu(100)-Fe surfaces with CO and H_2. The reactivity of both gases with oxidised copper-iron surfaces prepared on Cu(111) and Cu(110) has been studied by Van Pruissen et al. [29,32,34]. For Cu(111)-Fe surfaces they report that CO can remove only oxygen bound to copper - under the reaction conditions used - unless γ-Fe_2O_3 was present initially. γ-Fe_2O_3 could be reduced to Fe_3O_4. On Cu(110)-Fe surfaces all oxygen bound to copper could be removed and a small part of the oxygen of the $Fe_{0.95}O$ present on these surfaces. Using hydrogen it was possible to reduce both copper-iron surfaces completely. On Cu(111) they determined that the reaction rate was of half order in the hydrogen pressure. This is different from the first order which is found for the kinetics of the hydrogen interaction with both oxidised copper and iron surfaces [34,59,94]. Vink et al. [59] determined that the dissociation of H_2 is the rate determining step in the reduction of iron oxide on Fe(100) with hydrogen. The half order dependence of the reaction rate of p_{H_2} means that the hydrogen dissociation can not be the rate determining step in the reduction and they ascribed it to the presence of single iron atoms in the copper surface or to small clusters of iron atoms which facilitate hydrogen dissociation.

7.2 Results and Discussion.

Oxidised Cu(100)-Fe surfaces were prepared by evaporating 0.1 - 2.0 ML of iron and exposing the Cu(100)-Fe surface to oxygen until saturation was reached at room temperature. As described in chapter 3 - 6, the oxygen present at the surface occurs in two forms, as Fe_2O_3 and as half a monolayer of oxygen bound to copper and/or the Fe_2O_3-Cu interface. The total amount of oxygen is then $0.5+1.5\cdot\theta_{Fe}$. On heating the crystal to temperatures at which CO and H_2 were to be exposed (i.e. 630 K) the amount of oxygen present at the surface decreased according to AES measurements. No relationship between the amount of remaining oxygen and θ_{Fe} could be found, though the remaining amount of oxygen was always larger than $1.5\cdot\theta_{Fe}$. No change in the Fe $M_{2,3}VV$ peak shape was observed after heating, which means that no metallic iron was present. When reduction of this surface proceeds in the reverse order with respect to oxidation, reduction should go via an intermediate containing Fe^{3+}, Fe^{2+} and Fe^0 to Fe^0. The metallic iron produced in this process should either contribute to the Fe $M_{2,3}VV$ peak or dissolve in the Cu. Since both changes are not observed there is no reason to expect the stoichiometry of the iron oxide to change from Fe_2O_3 upon heating. As oxygen is not expected to desorb from these surfaces the oxygen probably diffuses into the bulk of the crystal, where it is undetectable for AES. On surfaces containing less than 0.2 ML of iron this happened at a high rate: ca. 30 min. after the start of the heating the oxygen signal had decreased to 75% of the original signal. However, since ellipsometry has a depth sensitivity which is at least one order of magnitude larger than that of AES it is expected that the oxygen is still visible with $\delta\Delta$.

The use of the parameter $\delta\Delta$ in this chapter is slightly different from that used in the rest of this thesis. In this chapter $\delta\Delta$ represents the change in Δ, i.e. $\Delta^0-\Delta$ where Δ^0 is the value of Δ of the Cu(100)-Fe surface after iron evaporation, oxidation at room temperature and heating the crystal to the temperature at which the reaction was to take place. This means that any changes in Δ due to oxidation and heating of the surface are not included in $\delta\Delta$.

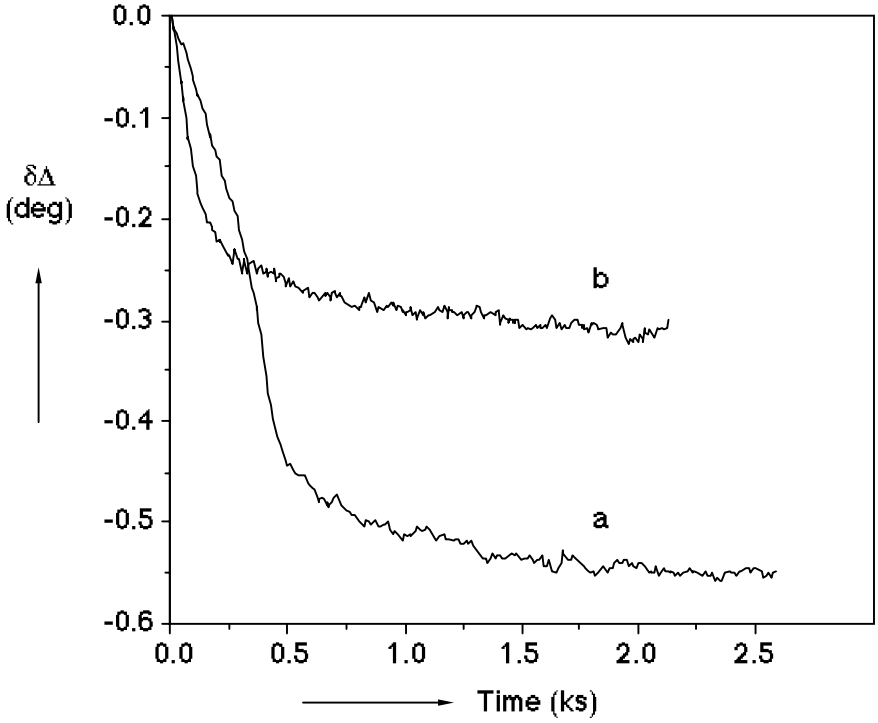

Figure 1 *The change in Δ as function of the CO exposure of two Cu(100) surfaces containing 0.2 ML of iron oxidised at 300 K. The CO pressure was 0.02 Pa and the crystal temperature 630 K. The difference between curve (a) and (b) is explained in the text.*

7.2.1 Interaction with CO.

The reactivity of these surfaces towards CO was studied at 630 K and pressures up to 0.1 Pa. For surfaces containing more than 0.8 ML of iron no change in Δ was observed. Surfaces containing less iron showed a decrease in δΔ. The total change in δΔ seemed to be smaller for high than for low iron coverages and thus more oxygen could be removed from a surface with small iron coverages. However, these reduction curves did not reproduce very well. The irreproducibility of these results is probably caused by small differences during the preparation which is reflected in the oxygen distribution before the reduction. Since AES measurements revealed that all iron remained at the surface and that at least $1.5 \cdot \theta_{Fe}$ oxygen was present after the CO exposures the oxygen removed was probably connected to copper. From oxidation experiments it appeared that the Fe is first oxidised before oxygen adsorbs on the copper interface. This indicates, as could be expected from (bulk) thermodynamic data, that oxygen is preferentially bound to Fe. These observations suggest that CO can not reduce the Fe_2O_3 on these surfaces. This is different from what happens on Cu(111)-Fe and Cu(110)-Fe surfaces. On these surfaces it appeared to be possible to reduce the iron oxide partly [29,32]. The lack of reactivity (under these conditions) of surfaces containing more than 0.8 ML of iron can be explained assuming that CO requires free copper sites before it can react with oxygen bound to copper. This is also the case for oxidised Cu(100) surfaces without Fe [95]. The absence of an iron oxide free surface for $\theta_{Fe} \geq 0.8$ was also found in previous experiments with different amounts of iron on Cu(100) at 300 K. These showed that the contribution of oxygen adsorbed on Cu(100) to the change in Δ due to oxidation was negligible for $\theta_{Fe} > 0.8$ [82].

In Fig. 1 two reduction curves of two freshly prepared surfaces containing 0.2 ML of iron are shown as function of time. The pressure was 0.02 Pa for both experiments. Though the total change in $\delta\Delta$ due to the reduction is different for both reductions, it must be mentioned that the shape of the curves is identical at the end of the reaction. When curve (b) is shifted down by 0.25° in Δ and in time by ca. 500 s both curves are overlap each other within experimental error. A similar behaviour was observed for the CO interaction with oxygen adsorbed on pure Cu(100) [95] and could be explained with a model of competitively adsorbed O-atoms and CO molecules of which the reaction to CO_2 is rate limiting. The slow start of the reaction (curve (a)) is then due to a lack of free sites on which CO can adsorb. On the surface of curve (b) free sites were already present at the start of the CO exposure, allowing a fast reaction from the beginning. The amount of oxygen as determined with AES confirms this mechanism since on the surface of curve (a) more oxygen (0.2 ML) was present than on that of curve (b) after heating to 630 K. Apparently the oxygen has disappeared from the 'bare' copper surface.

Although oxygen disappears from the surface as seen by AES and probably migrates into the bulk upon heating this does not explain why it is not possible to remove it with CO as seen by $\delta\Delta$. On pure copper single crystals it has always been possible to remove all of the oxygen even when it had penetrated into the bulk [34,58,96]. Apart from desorption, which is highly unlikely, one explanation is that the migration of oxygen in copper is so fast that it disappears from the "sight" of the ellipsometer. In principle it is possible to calculate the depth sensitivity of an ellipsometer from the refractive indices of the components, the angle of incidence and the wavelength of the light used. However, the refractive index of a solution of oxygen in copper (with an unknown concentration profile) is unknown. So it is impossible to make an exact calculation of the depth sensitivity. Based on the refractive index of copper and an angle of incidence of 0° an indication of the order of magnitude can be obtained using $\lambda/(4\pi k)$, where k is the imaginary part of the refractive index. The result is 140 Å. It seems not impossible that oxygen migrates fast enough at 630 K to reach even greater depths in the ca. 1 hour needed for temperature equilibration, AES measurements and outlining the ellipsometer. As the presence of iron (oxide) enables the oxygen to penetrate the bulk at temperatures at which it is stable on clean Cu single crystal surfaces it also might enhance the mobility of oxygen in the bulk. Alternatively dissolved oxygen may remain in the copper near surface region below the iron oxide, where its stability is enhanced.

To get some more information about the reactivity of these surfaces towards CO a surface containing 0.8 ML of iron was oxidised again at 630K after oxidation at 300K. It should be realised that the extra oxygen adsorbed must be present mostly as penetrated into the copper since no indication for changes in the oxidation state of iron could be found after this oxidation. Fig. 2 shows four consecutively obtained reduction curves of one surface for which the oxidation and reduction was repeated, curve (a) to (d). The fourth reduction of an other surface with the same θ_{Fe} is also shown (curve (e)). Curves (a), (b) and (d) are obtained using 0.05 Pa, (c) at 0.02 and (e) at 0.1 Pa. The arrows in Fig. 2 indicate the change in Δ due to the oxidation at 630 K before and between the different reductions: arrow 1 before reduction (a), arrow 2 between (a) and (b) etc. During the reduction of curve (a) more oxygen could be removed than was adsorbed at 630 K (arrow 1). Thus part of the oxygen which was adsorbed at 300 K is also removed. During the other 3 reductions all oxygen adsorbed at 630 K could be removed with CO. It is remarkable that the shape of the curve changes after the first reduction. However, the shape of the curves resembles strongly those of the CO-reductions of oxidised

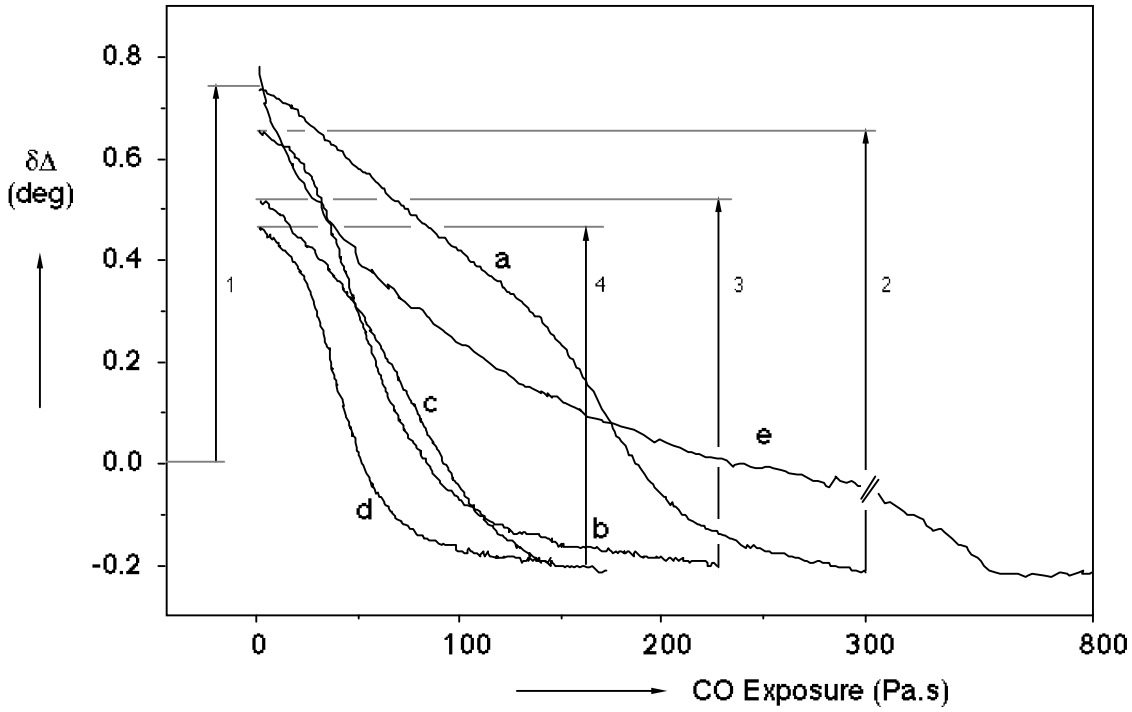

Figure 2 *The change in Δ as function of the CO exposure of a Cu(100) surface containing 0.8 ML of iron oxidised at 300 K and reoxidised at 630 K. Curves (a) to (d) are taken consecutively on one surface; the first arrow indicates the change in Δ due to the first oxidation at 630 K, the second arrow represents the second oxidation performed after the reduction (a) and before reduction (b) etc. Reduction curve (e) is the fourth reduction observed on a new prepared surface.*

Cu(100)-Fe surfaces [32] and oxidised Cu(100) surfaces [95]. For those surfaces a model of the reaction mechanism was given which explains the shape of the curves. This model is based on two competitive events: the formation of free sites (needed for CO adsorption) by the reaction of adsorbed CO and oxygen and the refilling of those sites by subsurface oxygen. Which of both processes is rate determining depends on the temperature, which influences the reaction constants of the CO_2 formation and of the refilling of the surface sites with subsurface oxygen, the CO adsorption equilibrium constant and the CO pressure. A difficulty occurring on these surfaces is the irreproducibility of the reduction curves which is probably due to a changing surface structure, i.e. a change of the iron oxide clusters and thus of the amount of 'free' copper surface and a change in the oxygen distribution in the crystal. Van Pruissen et al. could obtain reproducible results on Cu(111)-Fe surfaces after 3 oxidation-reduction cycles [29] but because of a much higher iron content of their surfaces and their preparation method their surfaces were in a much more stable state than the surfaces used in this study. However, though all curves as determined on the Cu(100)-Fe surfaces can be fitted with the model, the number of free parameters must be too large to draw any conclusions from this small data set.

Both the qualitative agreement of the reaction kinetics with that of pure copper surfaces and the fact that reaction is possible after oxidation at 630 K indicates that the surface must change under influence of oxygen. Apparently the iron oxide reorganises leaving free copper surface. The iron oxide is expected to remain at the surface thus to create free surface three dimensional clusters must be formed at the surface. The LEED pattern of these surfaces is similar to that observed after oxidation at 300 K [82] though a bit more diffuse.

7.2.2 Interaction with hydrogen.

Several surfaces containing 0-1.3 ML of iron were (after complete oxidation at 300 K) exposed to hydrogen at pressures varying between 0.01 and 0.2 Pa at a crystal temperature of 630 K. For surfaces with θ_{Fe}>0.6 ML no reaction was observed. Surfaces containing less iron could be reduced completely. As for the CO reduction experiments the interaction of these surfaces with hydrogen reproduced badly. However, in contrast to the CO reduction all oxygen could be removed as seen with AES. Although one would expect the change in the parameter Δ to be as large as upon oxidation (but of opposite sign), the change in Δ due to the removal of oxygen is different, i.e. smaller, than that during oxidation of the surface at 300 K. This can be explained by two effects: the first is the already mentioned migration of oxygen into the bulk out of "sight" of the ellipsometer and the second is the reorganisation of the compounds in the surface region: e.g. cluster formation and diffusion of iron into the copper substrate. In the CO experiments the final situation consisted of iron oxide on a copper surface, here we are left with metallic iron. However, the effect of changes in the distribution of the surface compounds (or even surface morphology) is difficult to predict or to determine. Both the dissolution of iron and oxygen are enhanced at high temperatures and could therefore be inhibited at low temperatures but in that case no reaction with H_2 occurs. A change in the iron distribution, however, can be seen with AES which shows that both the ratio of the Fe/Cu $M_{2,3}VV$ and the Fe $L_{2,3}M_{2,3}V$ / Cu $L_{2,3}VV$ peaks had decreased strongly compared to that directly after evaporation. This indicates that the iron migrates into the crystal at these temperatures. The migration is also observed in some of the other experiments on Cu(100)-Fe surfaces and by Van Pruissen et al. on Cu(111)-Fe and Cu(110)-Fe [29,32]. The effect of this changed distribution of the iron on Δ is expected to be small with respect to the change in Δ due to oxidation. So the explanation based on the oxygen migration is preferred.

Fig. 3 shows some reduction curves of surfaces containing small amounts (θ_{Fe}<0.3) of iron. The change in Δ is initially fast which may be ascribed to the reaction of hydrogen with oxygen bound to copper and slows down after some time where the reduction of iron oxide takes place. Since not all iron segregates upon reoxidation (at least at low temperature) and there seems to be a large difference in reactivity of surfaces oxidised at high and at low temperature as will be discussed later, a new surface had to be prepared after each reduction. The difficulty to prepare exactly reproducible surfaces makes the determination of the order of the reaction in the H_2 pressure impossible.

Conclusions here must be restricted to the observation that the reactivity of these surfaces towards H_2 decreases with increasing θ_{Fe} and since the coverage at which no reaction is observed is nearly the same as for the CO reduction it may be concluded that on these systems a copper surface free of iron oxide is required for the reaction (probably H_2 dissociation).

For surfaces containing more than 0.6 ML of iron the initial reactivity towards H_2 was too small to be detected at the reaction conditions used in this study. So some experiments were performed to examine whether it is possible to activate the surface and to elucidate the reasons of the inactivity.

A simple oxidation at 630 K (after a normal room temperature oxidation) appeared to be sufficient to activate a surface containing 0.8 ML Fe for reduction with H_2. As on the surfaces with a low iron coverage all oxygen could be removed (according to AES) and the iron diffused into the bulk of the copper crystal. Apparently oxidation at elevated temperatures has an important influence on the surface as seen by the hydrogen molecules. Apart from the effects

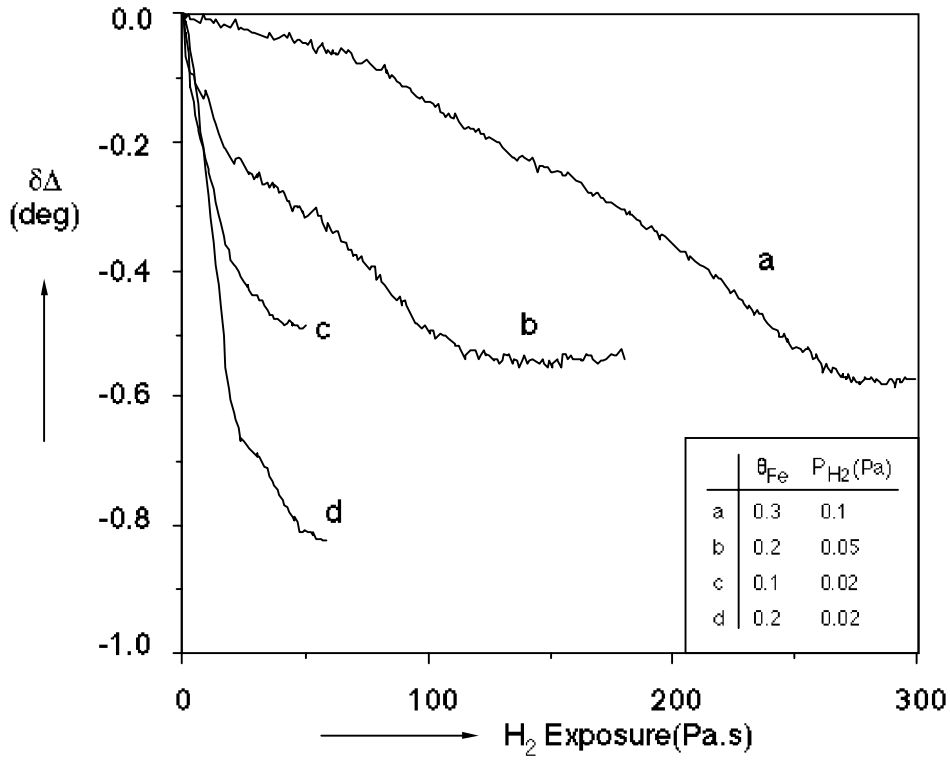

Figure 3 *The change in Δ as function of the H_2 exposure of Cu(100) surfaces containing different amounts of iron oxidised at 300 K. The crystal temperature was 630 K.*

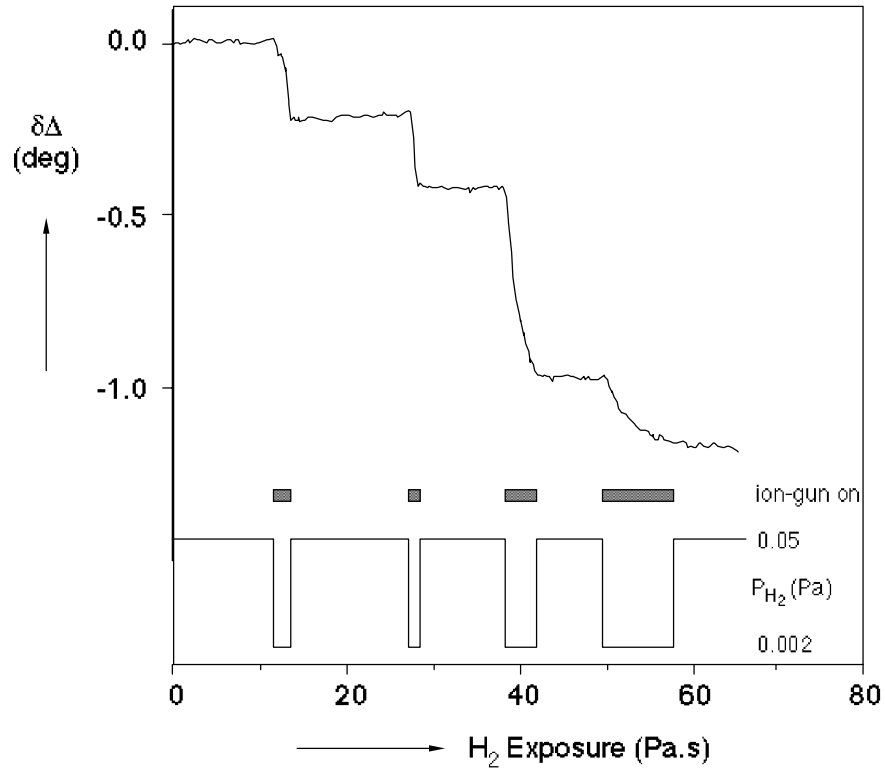

Figure 4 *The change in Δ as function of the H_2 exposure of a Cu(100) surface containing 1.0 ML of iron oxidised at 300 K. The crystal temperature was 630 K. The H_2 pressure is given in the lower part of the figure and the dotted rectangles indicate the periods during which the ion gun was switched on.*

of oxidation at high temperature on the structure of the of the iron oxide layer as was already indicated in the discussion of the CO reduction experiments, also defects in the iron oxide structure may be created. A second experiment which may give more information about this possibility was performed: 0.5 ML Fe was evaporated onto a surface already containing 1.0 ML of iron which was partly oxidised at 300 K and exposed to H_2. This surface did not show any reactivity towards H_2 at 530 K. This low temperature was used in the hope to keep the metallic iron at the surface. Although this experiment was meant to induce surface defects this is either not possible or the wrong type of defects was created.

In a third experiment the reduction of the surface (1 ML Fe) was initiated by 'activated' H_2. To perform this experiment the ion-gun was switched on at $2 \cdot 10^{-3}$ Pa with the rear end of the crystal directed to the ion beam and the front grid of the Retarding Field Analyser was kept at a potential 100 V above the acceleration voltage of the ion-gun. The reaction was monitored with the ellipsometer. Fig. 4 shows the results of the experiment with the activated H_2. It is clear that the reaction is very fast when the ion-gun is switched on and stops completely when it is turned off (note the higher pressure when the gun is off: 0.05 Pa). It may be remarked here that in a similar experiment performed on an oxidised Fe(100) surface ($\delta\Delta$=7°) the reaction rate was increased by a factor 500 when turning on the ion-gun. With this difference in reactivity in mind one should expect to see reactivity (if there is any) in the experiment when the ion-gun is turned off and the pressure is increased by a factor 25. However, the surface remains inert. Also here, reduction was possible after a high temperature reoxidation of a (ion-gun assisted) reduced surface.

The experiments described above strongly indicate that on these surfaces copper sites free of iron oxide (but not necessarily free of oxygen) are required for reaction of hydrogen with oxygen on the surface and that the surface of the iron oxide is not able to adsorb or dissociate H_2 in reasonable amounts. Apparently the iron oxide is stabilised by the underlying copper. This might be due to a higher affinity of iron than of copper towards oxygen. Whereas on pure (oxidised) iron surfaces surface defects can be created at low cost by migration of oxygen into the (iron) bulk this may be less favourable when copper is present directly under the iron oxide layer.

7.3 Conclusions.

1. The Cu(100)-Fe surfaces as prepared in this study are not very stable at high temperatures. Iron, but not iron oxide, dissolves into the copper crystal.
2. CO reacts only with oxygen bound to copper.
3. The reaction mechanism seems the same as for iron free Cu(100) though the iron oxide blocks the surface for CO adsorption and thus for reaction.
4. Hydrogen requires copper surface free of iron oxide for reaction and then all oxygen can be removed.
5. Iron oxide on Cu(100) is more stable towards H_2 than iron oxide on bulk iron.
6. Iron oxide probably forms three dimensional clusters upon oxidation at 630 K.

8

The interaction of CO with Cu(100)-Fe surfaces

Abstract

The interaction of CO with Cu(100)-Fe surfaces containing 0 to 1.7 ML of Fe was studied with ellipsometry and Auger electron spectroscopy. Only reversible molecular adsorption was observed. Dissociation was not observed at temperatures up to 620 K and pressures up to 0.1 Pa. Apparently fcc iron (100) surfaces do not dissociate CO under these conditions.

Depending on the iron coverage and the pre treatment of the surface a fast and a slow adsorption stage is observed. The fast adsorption only occurs on surfaces containing iron clusters or on surfaces completely covered with iron whereas slow adsorption occurs only on surfaces on which bare copper surface is present. During the slow adsorption stage iron carbonyl-like species are formed, iron clusters are broken up in single iron atoms or both processes occur together.

Since the Cu(100)-Fe surfaces are not thermo-stable it was not possible to determine the heat of adsorption.

8.1 Introduction.

The interaction of CO with pure iron and iron alloys has already been subject of several studies [6,29,97-99]. The motivation of these studies is, besides the fundamental interest in these systems, also their importance for the Fischer-Tropsch synthesis. The reason to investigate iron alloys is that the common used iron catalysts quickly deactivate due to the formation of iron carbides [100]. The use of iron alloys can probably prevent the formation of carbides. Nickel-iron surface alloys were investigated by Vreeburg [98]. Copper-iron surface alloys were investigated by Van Pruissen et al. [29], Gijzeman et al. [97] and Boellaard [99] and are also the subject of this paper. On Cu-Fe alloy surfaces Van Pruissen et al. observed both molecular and dissociative adsorption. Reversible molecular adsorption was observed after an initial saturation of the surface by equal amounts of carbon and oxygen due to dissociation of CO. The amount of molecularly absorbed CO did not increase when more than about four monolayers of iron were deposited, but one should remember that the iron is spread over several layers implying an unknown surface concentration. For Cu(111)-Fe they found a heat of adsorption of 70±15 kJ/mol, independent of the coverage and iron content [29]. This ΔH_{ad} is lower than the initial ΔH_{ad} found by Vink et al. [6] on a Fe(100) surface containing 0.25 ML of C and O: 100±5 kJ/mol. And it is somewhat higher than ΔH_{ad} on Cu(100) which is 50-70 kJ/mol [5]. Boellaard et al. studied CO adsorption on alumina supported Cu-Fe catalysts. They observed CO induced iron segregation, irreversible CO adsorption on the iron sites and iron carbide formation (at elevated temperatures) due to dissociation of iron.

The composition of Cu(100)-Fe surfaces is quite different from the surfaces prepared by Van Pruissen et al. As mentioned in chapter 1, the use of an evaporation source (at room temperature) initially gives epitaxial iron islands on the copper surface followed by a layer-by-layer growth (4 - 11 ML), instead of a mixture of iron and copper. According to Wuttig et al. [13] the presence of CO during evaporation induces a longer region of layer-by-layer growth. This effect is already found for CO pressures of $7 \cdot 10^{-8}$ Pa indicating a strong interaction of the few adsorbed CO molecules since no adsorption could be detected at this pressure. The copper/iron surfaces are not stable, even at room temperature slow changes occur [7-11,20]. It will be clear that this reorganisation of the surface atoms will have a great influence on the properties of the surface towards CO-adsorption.

In this chapter the interaction of CO with Cu(100)-Fe surfaces and the effect of temperature induced surface changes on the interaction is studied. A possible explanation for the adsorption mode and the unexpected non-dissociative adsorption of CO on these surfaces will be given. The technique used to study the CO adsorption is ellipsometry.

8.2 Experimental.

The amount of CO adsorbed was determined with ellipsometry. For some experiments it was interesting to observe changes in CO coverage with changing temperature. However, temperature dependent measurements had to be corrected for a reversible change in Δ (and Ψ) due to a small displacement of the crystal caused by the temperature change. Within the temperature range used, this artificial change in Δ was linearly proportional to the temperature. Changes in the iron distribution in the surface layers due to temperature enhanced migration appeared to have no influence on $\delta\Delta$ because after cooling down Δ came back to its original

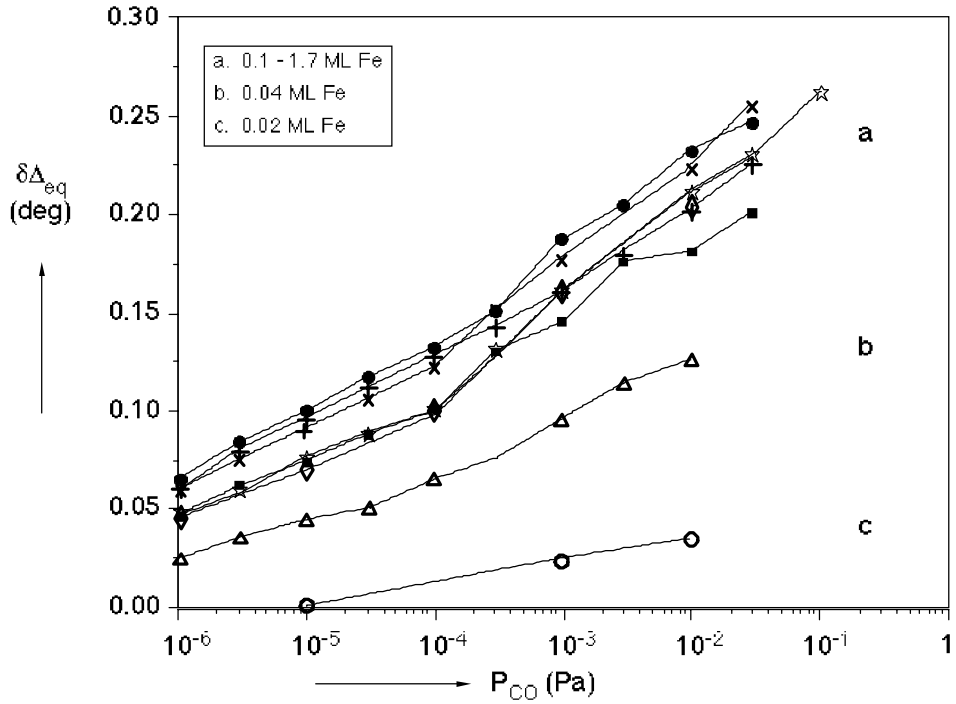

Figure 1 *Isotherms (T = 298 K) of CO adsorptions on Cu(100) surfaces containing different amounts of iron: 0.02 ML (o), 0.04 ML (•), 0.1 ML (■), 0.3 ML (+), 0.6 ML (●), 0.8 ML (x), 1.0 ML (•) and 1.7 ML (☆).*

value within 0.01°. All the ellipsometry data used in this paper are corrected for the artificial changes due to the temperature.

8.3 Results.

The CO-adsorption isotherms of freshly prepared Cu(100)-Fe surfaces containing 0.02 - 1.7 ML Fe taken at 300 K are shown in Fig. 1. The isotherms were obtained by continuously exposing CO at increasing pressures. After each pressure rise sufficient time was waited to determine $\delta\Delta$ at the equilibrium coverage ($\delta\Delta_{eq}$). After desorption $\delta\Delta$ returned to zero and with AES no carbon and oxygen could be detected. Saturation of the surfaces with CO is obviously not reached for the pressures used. Unfortunately higher pressures than 0.1 Pa could not be used due to the possible formation of $Ni(CO)_4$ in the stainless steel UHV system in combination with exposure times of hours required to reach equilibrium. In fact these long exposures needed were the reason that most of the experiments in Fig. 1 were already stopped before reaching 0.1 Pa.

On this kind of surfaces the heat of adsorption (ΔH_{ad}) and the dependence of ΔH_{ad} both θ_{Fe} and θ_{CO} are highly interesting. To determine ΔH_{ad} adsorption isotherms must be collected at different temperatures. However, the Cu(100)-Fe surfaces are not thermo-stable. The influence of the instability on the adsorption behaviour was checked by exposing CO to surfaces which were previously heated to a certain temperature. The heating procedure consisted of a fast heating to the temperature mentioned after which the crystal was directly allowed to cool down. Due to the large sample holder the cooling process was slow. This means that the crystal was 15-30 min. at a temperature near to the one mentioned. However, important here is not the

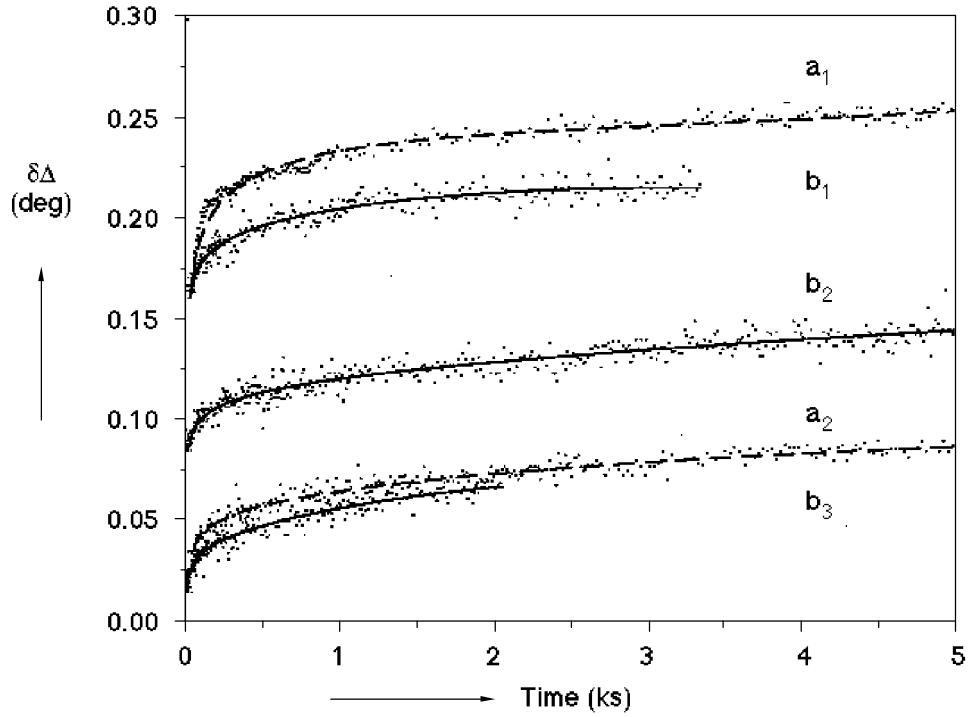

Figure 2 *The change in Δ as function of the time for CO pressures of 0.01 Pa at room temperature for Cu(100)-Fe surfaces containing (a) 0.8 ML Fe and (b) 1.0 ML Fe, annealed at different temperatures. a_1: not annealed, a_2: annealed at 500 K, b_1: annealed at 330 K, b_2: annealed at 380 K and b_3: annealed at 620 K.*

exact time of the heat treatment (since the equilibrium situation is far from what we want) but a change in surface composition. Some adsorptions after different heat treatments are shown in Fig. 2. In this figure δΔ is plotted against the time of CO exposure (P_{CO} = 0.01 Pa). All adsorptions are performed at room temperature. Curves a_1 and a_2 represent the adsorption on a surface containing 0.8 ML of iron. Curve a_1 is taken on a fresh prepared surface and a_2 for a surface which has been heated to 500 K. The curves b_1-b_3 are taken on a surface containing 1.0 ML Fe. The curve of a fresh prepared surface is not shown but it closely overlaps the curve of the fresh prepared θ_{Fe}=0.8 surface (a_1). The curves b_1, b_2 and b_3 are obtained on surfaces previously heated to respectively 330, 380 and 620 K. It is clear that a the total amount of CO adsorbed on these surfaces decreases with a more severe heat treatment of the surface. Of course this makes the determination of ΔH_{ad} at temperatures above 300 K impossible. The use of lower temperatures, however, is not possible in the UHV system used and also adsorption of CO on the Cu(100) surface could disturb the experiment in that case [102].

As already mentioned the time scale of the adsorption experiments is large. Therefore an adsorption experiment is shown in more detail in Fig. 3. In this figure the change in Δ due to the CO adsorption on a Cu(100) + 1.0 ML Fe surface is shown as function of time. Also the temperature during the experiment is shown. Though not really important here, the surface had been heated for 30 min. at 380 K which is the reason why the equilibrium coverage is smaller than expected from Fig. 1. Directly after the beginning of the CO exposure (P_{CO} = 0.01 Pa) δΔ rises quickly to approximately 0.09°, after which δΔ continues increasing slowly to the equilibrium coverage of approximately 0.16°. In the experiment shown in Fig. 3 the system was evacuated before the equilibrium coverage at room temperature was reached. As expected,

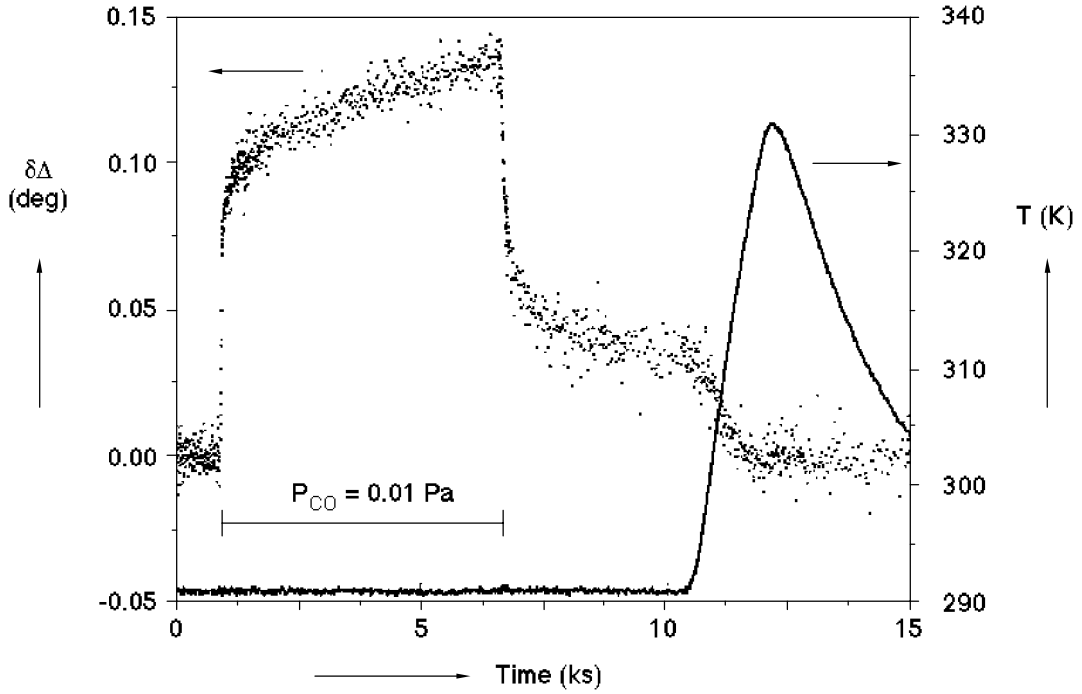

Figure 3 *The change in Δ and the temperature during a CO adsorption (at P_{CO} = 0.01 Pa) and desorption on a Cu(100) surface containing 1.0 ML of iron. The surface was annealed at 380 K before the measurement.*

evacuation results in a direct and fast decrease of the CO coverage until the last 0.04° which only desorbs very slowly. However, a temperature rise of only some 40 degrees causes the CO to desorb completely, δΔ returns to zero and no carbon or oxygen contamination could be detected with AES.

8.4 Discussion.

The adsorption of CO on Cu(100)-Fe surfaces appears to be reversible and molecular since all CO desorbs and no dissociation products could be found within the detection limit which is about 0.02 ML for oxygen. Even when CO is exposed at high temperatures (up to 620 K) and at 0.1 Pa no carbon or oxygen contamination could be detected afterwards.

This reversible molecular adsorption is in strong contrast with the behaviour of CO on pure Fe surfaces [6], Cu(111)-Fe and Cu(110)-Fe surfaces [29,97] and Ni(111)-Fe surfaces [56] since on all these surfaces CO dissociates. The lack of dissociation on the Cu(100)-Fe surfaces at low temperatures is probably be due to the (100)-fcc structure in which the iron is present on the surface. Gijzeman [103] calculated for the Ni(111)-Fe surface that dissociation probably only occurs on iron clusters consisting of three atoms which are not all three neighbours but bend under an angle of 120°. These clusters can not exist on the fcc-(100) surface. Dissociation can occur on the bcc surfaces without hexagonal symmetry because of the more open structure of these surfaces, and on the Cu(110)-Fe surfaces of Gijzeman et al. [97] due to the presence of bcc iron on these surfaces.

When the isotherms taken on Cu(100)-Fe surfaces are compared with those taken on Cu(111)-Fe and Cu(110)-Fe surfaces [29,97] the difference seems to consist mainly of a larger change in Δ on Cu(100)-Fe surfaces than on those of refs. [29,97] ($\delta\Delta_{max}$•0.29° as compared to

0.08°). However, on the surfaces described in [29,97] adsorption took place on a surface saturated with the dissociation products of CO. This may be the explanation that on the Cu(100)-Fe surfaces significantly more CO adsorbs. For clean Fe(110) Gijzeman et al. [97] saw a decrease in the amount of CO adsorbed with an increasing oxygen coverage. A second explanation may be that before performing the CO adsorption experiments the surfaces used in [29,97] were oxidised and reduced at high temperatures (~600 K) to remove contamination. However, the high temperature also induces segregation of copper atoms [9,11]. This implies that the number of iron atoms in the surface layer is unknown and could be smaller than on Cu(100)-Fe surfaces.

The most striking observation from Fig. 1, however, is that the amount of CO adsorbed at a given pressure increases with θ_{Fe} until θ_{Fe} reaches 0.1. For higher iron coverages the isotherms overlap within experimental error. Though at 0.1 Pa saturation of the surface with CO obviously is not reached yet it is remarkable that at iron coverages much smaller than 1 ML the same amount of CO can be adsorbed. To be able to say more about this it is required to know more about the amount of CO adsorbed on the surface. An approximation of the absolute coverage can be given by using the absolute coverage of CO on Fe(110) as calculated by Gijzeman et al. [97]. For clean Fe(110) they found a saturation coverage of $\delta\Delta$=0.38°, which corresponds with $6.2 \cdot 10^{18}$ molecules per m^2 [25]. Assuming a linear sensitivity of Δ for θ_{CO} (which is done implicitly but with success for CO-adsorption on Fe, Ni, Ni(111)-Fe, Cu(111)-Fe and Cu(110)-Fe [6,29,56,97,101]) and transferability of the results for CO on Fe(110) to Cu(100)-Fe (which is correct for oxygen on Cu(100)-Fe [82]) 1 ML of adsorbed CO results in a change in Δ of 1°. A more direct determination of the absolute coverage was done by turning on the electron gun (2500 eV, 3 μA) during the desorption. This resulted in an oxygen and carbon contamination of about 40% of the value calculated using $\delta\Delta$, which is a reasonable agreement realising that low energy electron bombardment not necessarily leads to dissociation, but also induces desorption. Using this calibration it appears that the equilibrium coverage of CO at 0.01 Pa on 0.1 ML Fe is about 0.2 ML. Disregarding Fe enhanced adsorption of CO on Cu the average number of CO molecules bound to one Fe atom exceeds unity. In fact in the case of θ_{Fe}=0.01 and θ_{Fe}=0.04 at P_{CO}=0.01 Pa the ratio is about 2. Iron enhanced CO adsorption on Cu is not very likely under these circumstances. On catalysts this type of adsorption was suggested only for high pressures (1 kPa) [99]. An explanation for the high CO/Fe ratio may be the formation of iron carbonyl like species ($Fe(CO)_n$).

The assumption of a linear change in $\delta\Delta$ with θ_{CO} on these surfaces may not hold due to the different types of adsorbed CO. However, on Ni and Fe single crystal surfaces the change in Δ due to one CO molecule is the same. This indicates that the dipole of the CO molecule and the induced dipole in the surface are the same on both metals. There is no reason to expect this to be different on the Cu(100)-Fe surfaces as long as the CO/Fe ratio is smaller than unity (no dissociation occurs and a different ΔH_{ad} probably does not influence the dipole much, since also for Ni and Fe the difference in ΔH_{ad} is about 40 kJ/mol. As soon as the ratio CO/Fe exceeds unity one may expect the sensitivity to decrease since the dipoles probably weaken due to mutual interaction. In that case the number of CO molecules adsorbed is even larger than determined assuming linearity. Another cause for non linearity may be the a change in the dielectric constant due to reorganisation of the surface induced by adsorbed CO. This, however, is unlikely because it should also influence Ψ and, moreover reorganisation caused by heating did not show any effect on both Δ and Ψ.

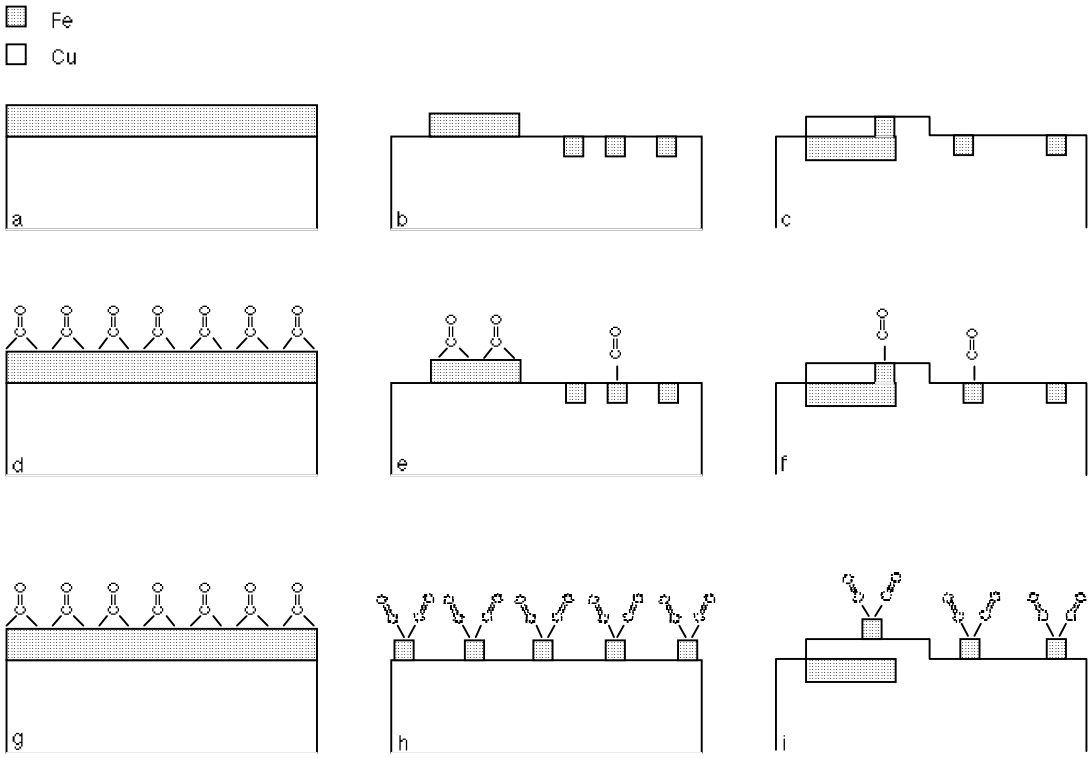

Figure 4 *A schematic model for the CO adsorptions on Cu(100)-Fe surfaces. a) represents a surface which is completely covered by Fe, b) shows a surface with both Fe clusters and dissolved iron atoms and c) gives the effect of a severe heat treatment at more than 500 K. d), e) and f) show what happens during a short exposure of CO and g), h) and i) show the results of prolonged exposure until equilibrium coverage.*

Supposing this carbonyl formation actually happens, one might expect to find some effects of it in the adsorption kinetics. Indeed, in the adsorption curves of Fig. 2 and Fig. 3 a fast and a slow stage can be observed. Since CO adsorption is usually a fast process [97] (with a initial sticking probability close to unity) there seems to be some evidence here for the existence of two different adsorption processes on this surface. The initial fast CO adsorption is probably similar to the molecular adsorption on other surfaces [6,29,97,98], whereas the slow stage may be caused by the carbonyl formation.

For a better understanding of what might happen on the surface during the experiments the discussion will be continued using a simple model based on the known growth behaviour of Fe on Cu(100). In the regime of θ_{Fe} as used ($0.01 < \theta_{Fe} < 1.7$) the iron is present after evaporation as clusters of at most 2 layers height and partly dissolved in the Cu surface layer (Fig. 4a for high θ_{Fe} and Fig. 4b for $\theta_{Fe} \bullet 0.1$) [9-13,20,102,105]. The structure of the iron is fcc. The effect of a heat treatment is that Cu atoms migrate over the iron clusters and depending on the time and temperature the Fe clusters are more or less buried. Though for these surfaces the equilibrium situation will be that the iron is completely dissolved in the copper crystal another 'extreme' will be found before. The maximum solubility of iron in the surface layers will be reached. The maximum solubility is probably below the bulk solubility of Fe in copper which is 4% [106]. The top layer of a Cu(100)-Fe surface after a short heating to 620 K might look like Fig. 4c. Since only the top layer is interesting for the CO adsorption the deeper buried iron is not really important in this figure.

It is worthwhile now to consider the circumstances under which both stages are found separately or together. Slow adsorption alone is found for all surfaces after a heat treatment to

more than 500 K and for freshly prepared surfaces with θ_{Fe}<0.05. Fast adsorption without a following slow stage is found only for θ_{Fe}=1.7. A combination of both processes is found on all other surfaces. A heat treatment always resulted in a decrease of extent of the fast adsorption.

Apparently fast adsorption only occurs on surfaces containing enough iron to present iron islands to the carbon monoxide (Fig. 4d-4e). After the fast adsorption the CO starts to adsorb on the single atoms dissolved in the surface layer. This can happen only for surfaces not completely covered with iron. These surfaces can be formed either by the deposition of small (< 0.1 ML) amounts of iron (Fig. 4b) or by a heat treatment of surfaces with a higher iron content (Fig. 4c). In either case the fast adsorption can be pictured as shown in Fig. 4d-4e for doubly co-ordinated CO and by the slow adsorption as shown in Fig. 4e-4f for singly co-ordinated CO. Of course it can not be excluded that already in the fast stage adsorption on these sites occurs. In this way on-top adsorption is required, which is also observed by Boellaard et al. on Cu/Fe catalysts [99]. The formation of iron carbonyl like species, $Fe(CO)_x$ ($2 \leq x \leq 5$), is now relatively easy. The iron can be lifted out of the surface maybe helped by a second CO molecule (Fig. 4h-4i), a process that costs less energy when the iron is surrounded by Cu atoms than by Fe atoms (CO induced iron segregation is even energetically favourable, -87 kJ/mol [105]). This process is slower than the first (normal) adsorption because the activation barrier should be higher.

It may be suggested that part of the slow adsorption stage is due to the formation of extra sites created by CO induced iron segregation from deeper layers. Segregation of Fe in the Cu/Fe system induced by the adsorption of CO is observed in Cu/Fe catalysts [99]. Adsorption experiments on heat treated surfaces never gave evidence for iron segregation. The Fe/Cu MVV ratio was checked before and after adsorption but no difference could be detected. Heating and cooling down under 0.1 Pa CO did not change these observations. However, in the case of the experiments on catalysts [99] both the CO pressure and the exposure are 4 orders of magnitude higher. Under those pressures even CO adsorption on Cu(100) is observed [102].

An other process which is may happen during the slow adsorption stage is the break up of the Fe clusters caused by the CO. This can, of course, only occur when enough space is available. This process is shown in Fig. 4h. CO induced cluster break-up is observed before [107]. In the UHV system used there was no experimental way either to prove or disprove this possibility.

For surfaces on which there is no space for the formation of carbonyl like species or cluster break-up (Fig. 4g) no slow adsorption is expected and found.

8.5 Conclusions.

1. Cu(100)-Fe surfaces show only molecular CO adsorption.
2. In contrast to Cu(111)-Fe and Cu(110)-Fe surfaces, CO does not dissociate on Cu(100)-Fe surfaces with iron coverages up to 1.7 ML, pressures up to 0.1 Pa and temperatures up to 620 K, which may be due to the square fcc structure of the iron on these surfaces.
3. The amount of molecularly adsorbed CO does not increase when a quantity of more than about 0.1 ML of iron is deposited.
4. Besides the initial fast adsorption of CO on the Fe islands, CO also adsorbs on Fe atoms dissolved in the surface layer causing a slow increase of the CO coverage. Since the amount of adsorbed CO exceeds θ_{Fe} for θ_{Fe}ε0.1 probably also carbonyl like species are formed in this stage.

5. After annealing the fast adsorption of CO on the Fe islands is obstructed by Cu atoms covering the Fe islands. The CO adsorption on annealed Cu(100)-Fe surfaces is therefore limited to single Fe atoms dissolved in the surface layer.

9

Low Energy Auger Electron Spectroscopy of clean and oxidised Cu(100) and Fe/Cu(100) surfaces.

Abstract

The background subtraction method for undifferentiated Auger spectra proposed by Peacock is shown to be reliable for the low energy Fe and Cu $M_{2,3}VV$ peaks. This is illustrated by the good results obtained for spectra of clean and oxidised Cu(100), Cu(100) containing 0 - 5 ML of Fe and oxidised surfaces. This variety of surfaces made it possible to test the method on spectra with overlapping peaks of different heights and on spectra in which the peak shape changed.

The spectra of the unoxidised Cu(100)/Fe surfaces could be described by weighted sum of the pure Cu and Fe $M_{2,3}VV$ peaks. The background intensity at energies higher than the Cu peak could be used as an internal calibration factor for the spectra. These results are used to calculate the inelastic mean free paths for the Cu and Fe $M_{2,3}VV$ electrons. These values were 0.36 ± 0.07 and 0.44 ± 0.09 nm respectively.

For the oxidised surfaces the Fe (oxide) peak could be extracted by a simple subtraction of a pure Cu $M_{2,3}VV$ peak. This Cu peak apparently did not change shape upon oxidation.

9.1 Introduction.

Auger Electron Spectroscopy is one of the most used techniques in surface science to determine the composition of the surface of many types of (conducting) samples. However, in some cases analysis of spectra is hampered by the overlap of peaks of different elements or by a change in peak shape. Both problems often occur in studies of low energy Auger peaks of transition metal (alloy) surfaces. The low energy Auger transitions contain valuable information about the composition of the top layers or the chemical compounds present at the surface e.g. Fe oxides [60], formation of vanadium and titanium nitrides [64,65], Fe/Cr alloys and Fe/Cu and Fe/Ni surface alloys and their oxides [32,52,108].

In the traditional analysis of AES data differentiated spectra are used. However, peak shape changes are a source of errors in quantification of these spectra and it is more difficult to analyse the change of shape. A second problem can occur in the derivative mode when the peaks are situated on a strongly changing background as is the case for features below 300 eV when using a Retarding Field Analyser (RFA). Labohm [44] solved this problem by developing a reasonably accurate correction method based on a linear approximation of the background. When using the peak area in the undifferentiated background subtracted spectrum, peak shape changes are of no influence any more but in practise the peaks as measured are on top of a background which has to be subtracted first. This procedure is not straightforward.

Most methods described in literature other than those that use a non-physical polynomial, spline or other fits as background, use a basic background of the form

$$B(E)=\frac{A_1}{E^{m_1}} \qquad (1)$$

which is based on models of the inelastic scattering of electrons and the generation of secondary electrons [47,75,109,110]. These models predict m_1 to be approximately unity. The parameters A_1 and m_1 of Eq (1) are fitted to the high energy side of the peak and subtracted. The next step in the procedure depends on the further use of the spectrum. If the spectrum is to be used for Auger fine-structure analysis both a second electron cascade (caused by the Auger electrons) has to be subtracted and a deconvolution with the instrument function has to be performed. The latter requires quite a lot of computation time and the determination of the instrument response function [111-113].

On the other hand if the spectrum is to be used for quantitative analyses, subtraction of a step of the form

$$S(E)=\frac{A_2}{E^{m_2}}\int_E^{E^T} N_A(E')dE' \qquad (2)$$

is relatively convenient and accurate [47]. $N_A(E)$ is the number of Auger electrons with energy E, E^T is the energy threshold at the high energy side of the peak and A_2 and m_2 are the parameters of the second cascade to be fitted at the low energy side of the peak.

The form of the background as described by both Eqn (1) and Eqn (2) requires the presence of linear regions in the log(N(E)) versus log(E) plots above and below the Auger features. These regions should be used to fit the values of m_1, m_2 and A_1.

Tougaard [76] proposed a more complicated method for background subtraction based on a more physical theory (taking into account the depth distribution and the scattering cross sections of the elements) that was proved to be valid for XPS and X-ray excited Auger

transitions. He also claims that the method is useful for electron excited Auger spectra after subtraction of the electron cascade due to other than the Auger electrons. However, the method becomes more complicated than for XPS because of the depth dependence of excitation probability of the exciting beam. Because of the relative simplicity of the use of Eqn (3) it was decided to use the method of Peacock.

According to Bender [110] a successful background subtraction method should satisfy the following criteria. The method should be:

1 accurate and reproducible;
2 universal: applicable to all kinds of elements in all kinds of compounds;
3 based on first principles and be independent of the fitting parameters;
4 not too much dependent on the choice of the input parameters;
5 fast from the computational point of few;
6 sensitive for small peaks;
7 able to distinguish peaks superimposed on the inelastic tail of peaks of other elements.

In this chapter it is shown that the method described by Peacock [47] in a slightly adapted form is successful in the background subtraction of low energy Auger features and satisfies the last two criteria, though some care is needed when small peaks are superimposed on the inelastic tails of other peaks. To test the reliability of the method the $M_{2,3}VV$ spectra of clean Cu(100), Cu(100) + Fe and the oxidised Cu and Cu/Fe surfaces were analysed. The spectra of these surfaces give a good opportunity to test the method because the Cu and Fe $M_{2,3}VV$ peaks (44 and 58 eV respectively) overlap slightly and the Fe $M_{2,3}VV$ peak exhibits a strong shape change upon oxidation. The procedure was used to calculate an Auger signal versus amount of Fe plot (AST - plot) from which a reasonable inelastic mean free path (imfp) for the Cu and Fe $M_{2,3}VV$ electrons can be calculated assuming monolayer growth for the first monolayer.

9.2 Results and discussion.

The Auger spectra were used for data analysis without any smoothing after sampling from the LIA. An energy range of 70 - 80 eV was used in all spectra to fit Eqn (1). A larger region expanding to higher energies gave the same results but required a longer sampling time. After subtraction of this basic background the inelastic tail under the peaks can be calculated by the iterative procedure described by Peacock [47]. Because of the small linear range in the log N(E) versus log E plot at very low energies (below 40 eV) the region to fit m_2 of Eqn (2) had to be chosen carefully. In most cases convergence within a few percent was reached after 5 iterations. Unless mentioned otherwise 5 iterations were used in the background calculations.

A typical spectrum in the Cu $M_{2,3}VV$ region obtained from a clean Cu(100) surface and the background calculated from the first 3 iterations are shown in Fig. 1. The fourth and fifth iteration are not visibly different from third on this scale and were thus omitted in this figure. The reproducibility of the peak shape and position was good and independent of small changes

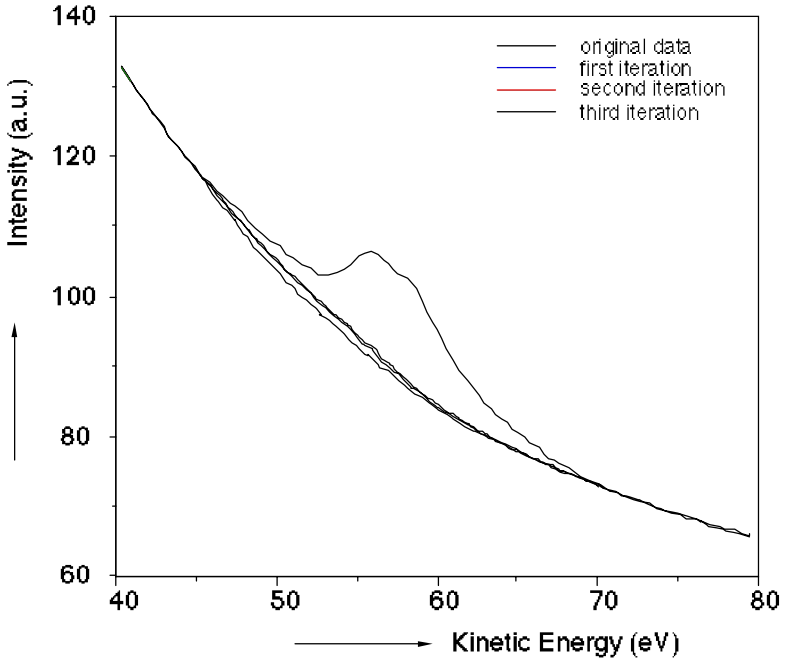

Figure 1 *Original Cu $M_{2,3}VV$ spectrum and three iterations of the background calculation.*

Table 1. Fit parameters of several Cu and Fe $M_{2,3}VV$ spectra of fresh and oxidised Cu(100) surfaces containing 0-5 ML Fe.

Surface	Region to fit m_2 (eV)	m_2	No. of it.	Cu $M_{2,3}VV$ area	Fe $M_{2,3}VV$ area
Cu(100)	40.0 - 45.0	2.0	5	254	-
Cu(100) + θ= 0.52 O_{ad}	40.0 - 45.0	2.0	5	232	
Cu(100) + 0.25 ML Fe	30.0 - 34.0	1.7	2	219	59.3
Cu(100) + 1.0 ML Fe	30.0 - 34.0	1.6	5	114	236
Cu(100) + 2.0 ML Fe	30.0 - 34.0	1.6	5	55.1	413
Cu(100) + 5.0 ML Fe	30.0 - 34.0	1.8	5	-	520
Cu(100) + 0.25 ML Fe oxidised	27.0 - 31.0	1.8	2	163	-
Cu(100) + 1.0 ML Fe oxidised	27.0 - 31.0	2.0	5	116	-

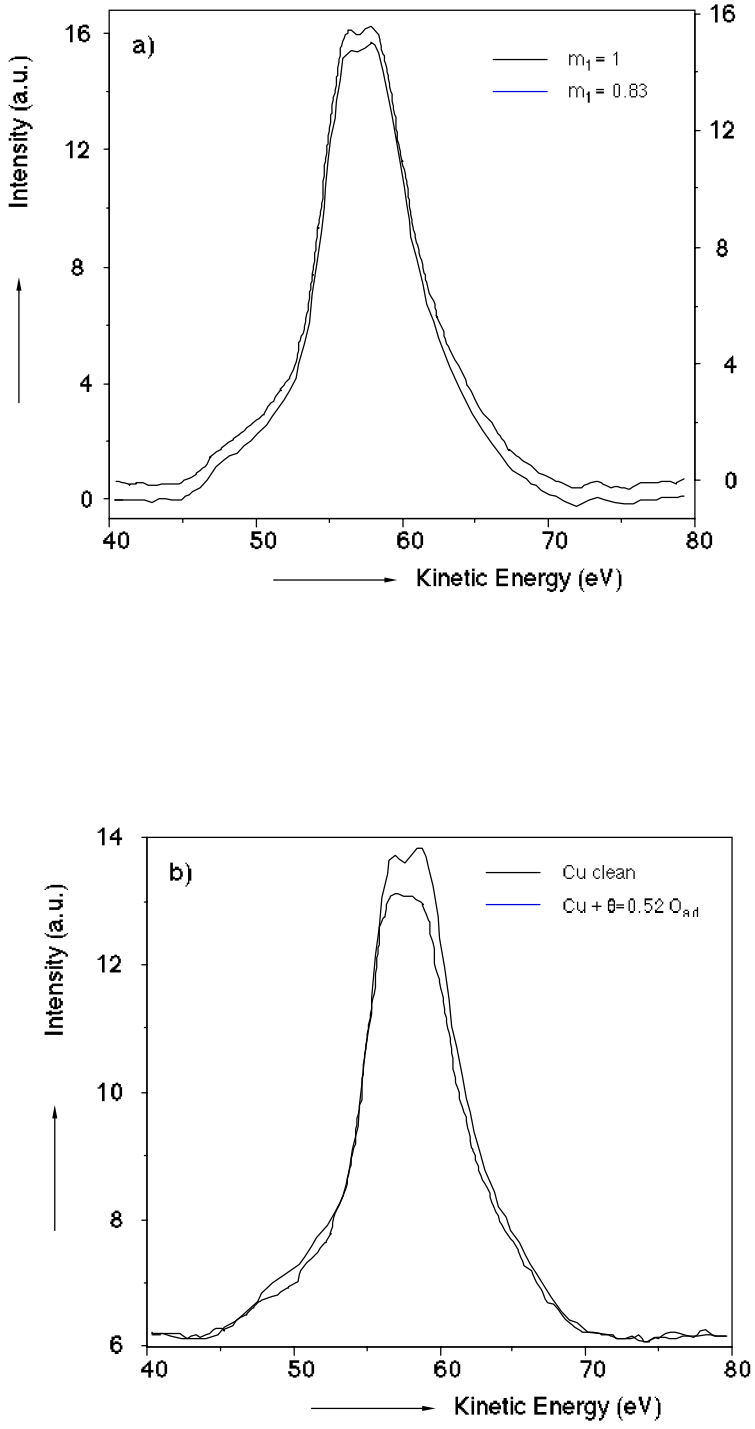

Figure 2 *(a) Influence of the two different basic backgrounds on the peak shape and area. The difference in peak area is 0.5%. (b) Cu $M_{2,3}VV$ spectra of a clean Cu(100) surface and an oxygen covered Cu(100) surface (θ_O = 0.52 ± 0.05).*

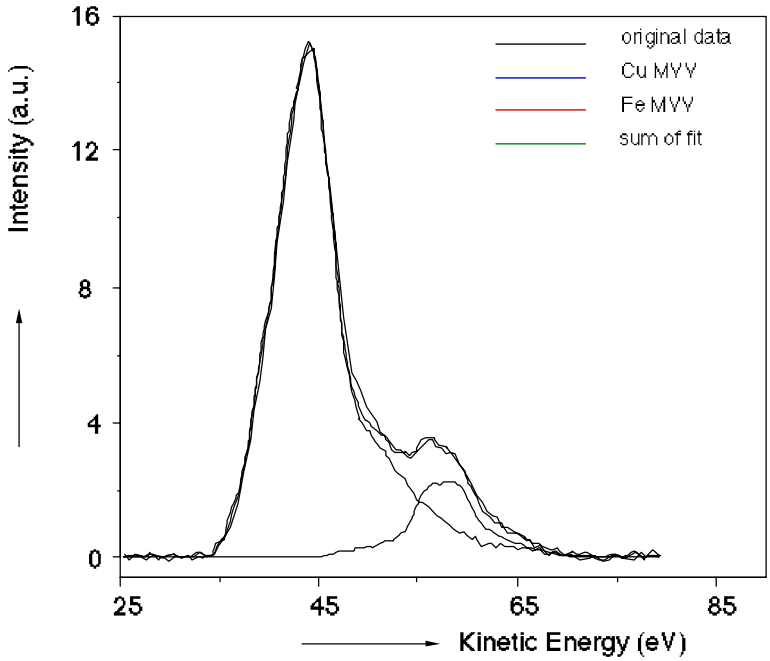

Figure 3 *Fit of a Cu $M_{2,3}VV$ and a Fe $M_{2,3}VV$ spectrum onto a spectrum of a Cu(100) with 2.0 ML Fe.*

in the instrumental configuration due to the sample movements which are required for cleaning, Fe evaporation and ellipsometry. Since it is sometimes convenient to use an offset in the output from the LIA, the high energy side of the spectra should be fitted to the expression

$$B(E) = C + \frac{A_1}{E^{m_1}} \qquad (3)$$

where C is the offset. This equation cannot be linearised with respect to its parameters. Because experience shows that m_1 is always close to unity I fitted one spectrum (taken without offset, C=0) to Eqns. 1 and 2 (A_1, m_1, A_2 and m_2 variable) and fitted the same spectrum with Eqns. 3 and 2 (C, A_1, A_2 and m_2 variable and m_1=1). Fig. 2a shows the result for the Cu $M_{2,3}VV$ peaks using the two procedures. The difference in the peak areas is smaller than 1%. This result is consistent with the observation of Sickafus [75] that deviations in the fit parameters of Eqn (1) are corrected by the parameters in the second step of the background subtraction (Eqn (2)).

An amount of adsorbed oxygen corresponding to θ=0.52 ± 0.05, which is the saturation value of adsorbed O at Cu(100) [51], apparently had no influence on background, peak shape and peak position. This can be seen in Fig. 2b which shows the $M_{2,3}VV$ peak of a clean and an oxidised Cu(100) surface and in Table 1 which lists the important fit parameters for the two spectra. Both spectra were normalised to the background intensity at 79 eV. This normalisation procedure will be discussed in more detail later. The difference in area between the two peaks is caused by screening of the Cu atoms by the adsorbed oxygen.

So far it has been shown that the method used for background subtraction does indeed give reliable results for Cu(100) and Cu(100)/O. The peak shape and position of Cu does not change after oxidation, a result that will be used later.

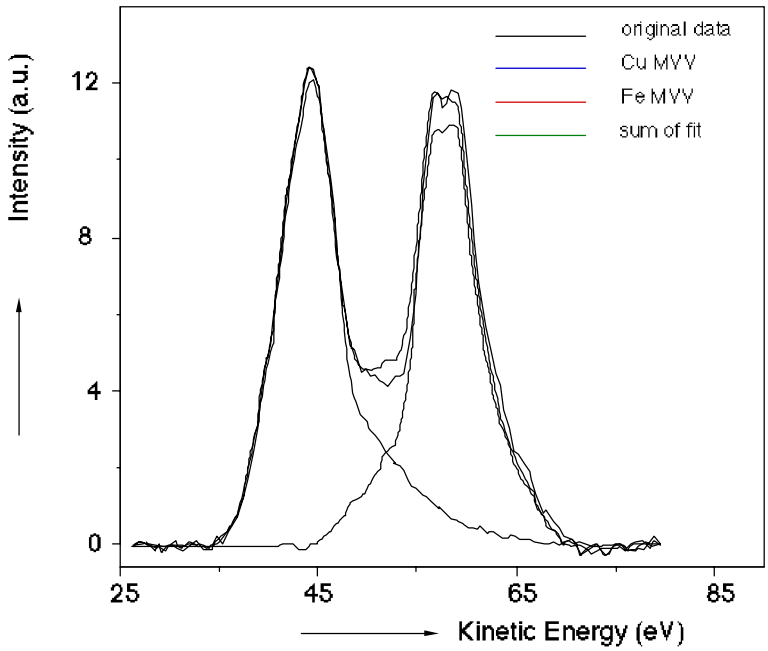

Figure 4 *Fit of a Cu $M_{2,3}VV$ and a Fe $M_{2,3}VV$ spectrum onto a spectrum of a Cu(100) with 1.0 ML Fe.*

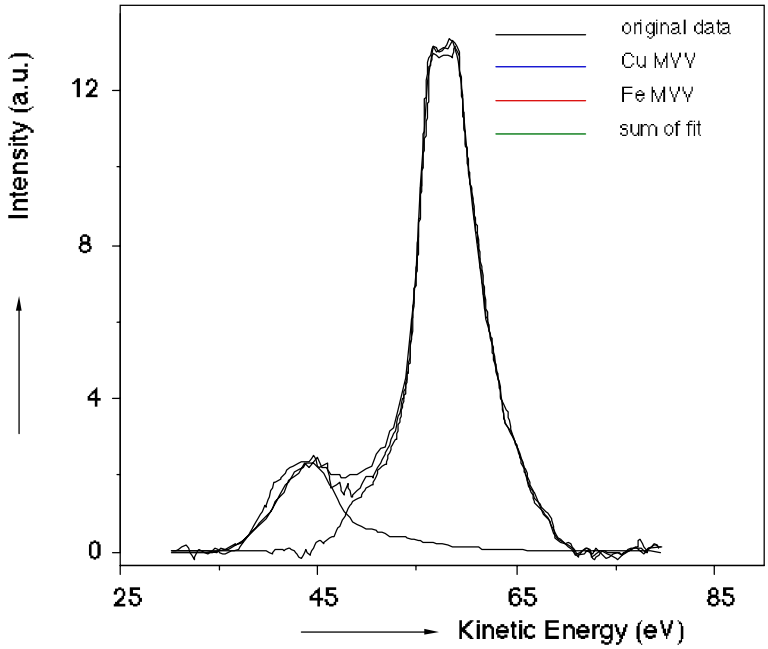

Figure 5 *Fit of a Cu $M_{2,3}VV$ and a Fe $M_{2,3}VV$ spectrum onto a spectrum of a Cu(100) with 0.25 ML Fe.*

A more complicated spectrum is obtained from the copper-iron system. Figs. 3 and 4 show the $M_{2,3}VV$ spectra of 2.0 and 1.0 monolayer of Fe on Cu(100) after background subtraction. A monolayer of Fe, as used here, contains the same number of atoms per unit area as the Cu(100) surface. This assumption is based on the epitaxial growth mode of Fe on Cu(100) [16]. Background subtraction from these spectra works satisfactory, as can be seen in Figs. 3 and 4. In Table 1 it can be seen that the fit procedure gave the same m_2 values for these surfaces and that 5 iterations were used. The separate Fe and Cu peaks calculated with the least squares fit of the pure Cu and Fe $M_{2,3}VV$ peaks and the sum of both are also shown in the Figs. 3 and 4.

The quality of the least squares fits of the two pure metal peaks onto the overlapping Fe and Cu peaks (Figs. 3 and 4) also indicates that the background subtraction method is quite reliable. It furthermore indicates that within the accuracy of the method no change in the peak shape occurs. This means that the $M_{2,3}VV$ spectrum of the bimetallic surface can be represented by the weighted sum of the two $M_{2,3}VV$ spectra of both constituents.

For surfaces containing small amounts of Fe (< 0.5 ML) some problems in the background determination occurred. These problems arise from a change in the background due to the presence of Fe causing the linear region at the low energy side of the $M_{2,3}VV$ peaks in the log(N) versus log(E) plot to shift to lower energies. Sometimes the linear region was very small or even absent. This often resulted in an extraordinary low value for m_2 compared to spectra of surfaces containing more Fe and either a strong apparent deformation of the Cu peak or no convergence in the iterative process. So analysis of the spectra with small amounts of Fe had to be done very carefully. Good results could be obtained by changing the region in which m_2 was fitted or by stopping the iteration after 2 or 3 steps. One should realise that convergence is not reached in this case. The peak shape of the Cu peak was used as criterion, assuming that the shape is independent of the amount of Fe on the surface. This assumption seems to be valid because at larger amounts of Fe no change was observed. The final result is given in Fig. 5.

A still more complicated case for background subtraction is presented by the spectra of oxidised Cu-Fe surfaces, where the Fe peak splits into two peaks. In Figs. 6a and 7a the spectra of the oxidised surfaces containing 0.25 and 1.0 ML Fe are shown. As with the spectra of the unoxidised surfaces background subtraction of spectra with high amounts of Fe worked without complications. With low amounts of Fe the same kinds of problems occurred as for the unoxidised surfaces. These problems could be 'solved' in the same way, i.e. subtraction of a copper peak (which does not change upon oxidation) should result in a reasonable spectrum for oxidised iron. Figs. 6b and 7b show the Fe (oxide) $M_{2,3}VV$ peak . The quality of the baseline in these spectra which were obtained after subtraction of a pure Cu $M_{2,3}VV$ peak normalised to the high energy flank of the peak, indicates that the procedure is working correctly. It also supports the earlier results that no change in the peak shape and position of the Cu $M_{2,3}VV$ peak due to the presence of iron and oxygen occurs within the accuracy of the instrument and the background subtraction method. Now the iron oxide peak can be separated from the Cu peak and it is possible to analyse the iron oxide peak in more detail as is done in chapter 4.

As a simpler application of these results the extraction of the inelastic mean free path (imfp) for the Cu and Fe Auger electrons from the data will be considered. Because the electron gun

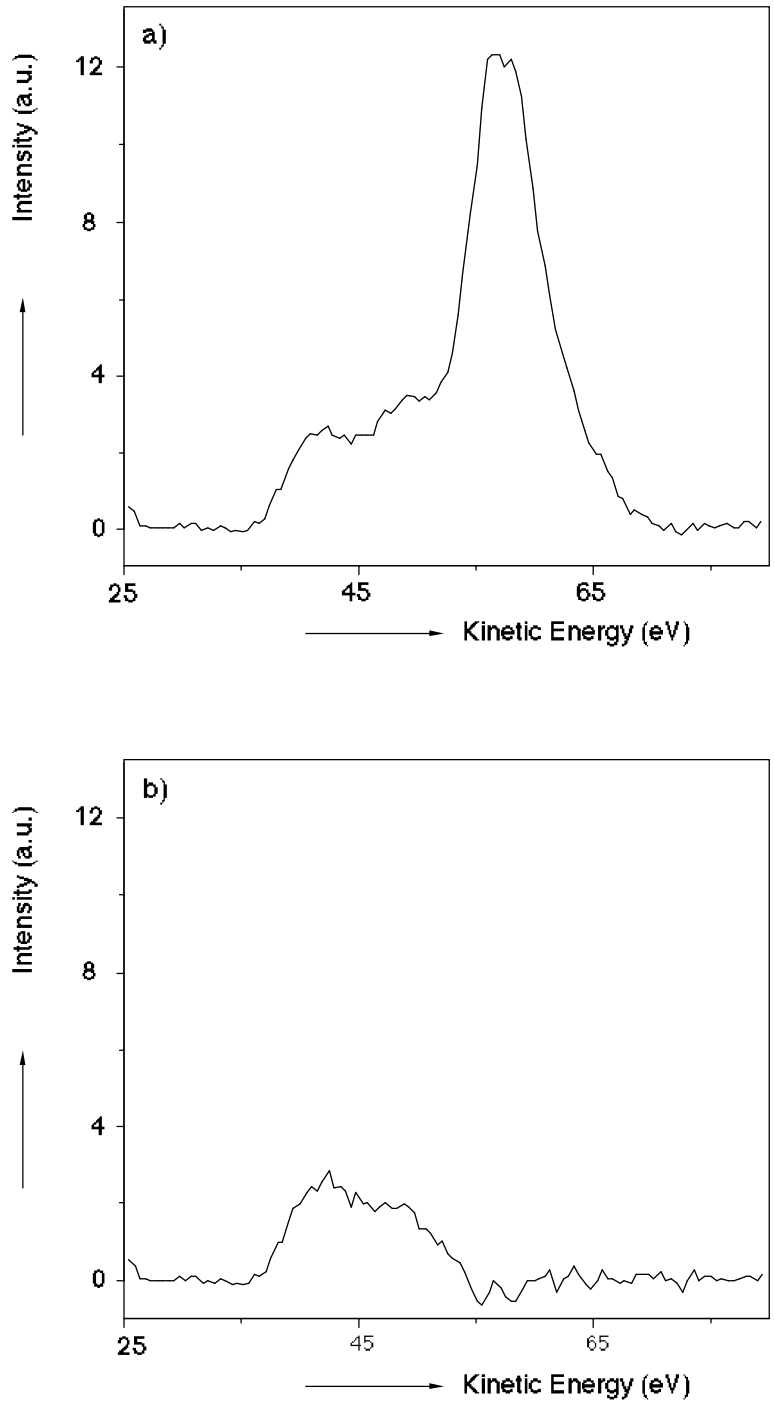

Figure 6 *Spectrum of an oxidised Cu(100) surface containing 0.25 ML Fe (a) and the spectrum after subtraction of the Cu $M_{2,3}VV$ peak (b).*

power supply was not emission stabilised a (preferably internal) calibration method had to be found. Langeron et al. [48] showed that the peak height/background ratio at the energy of the peak position only depends on the surface composition and the primary beam energy.

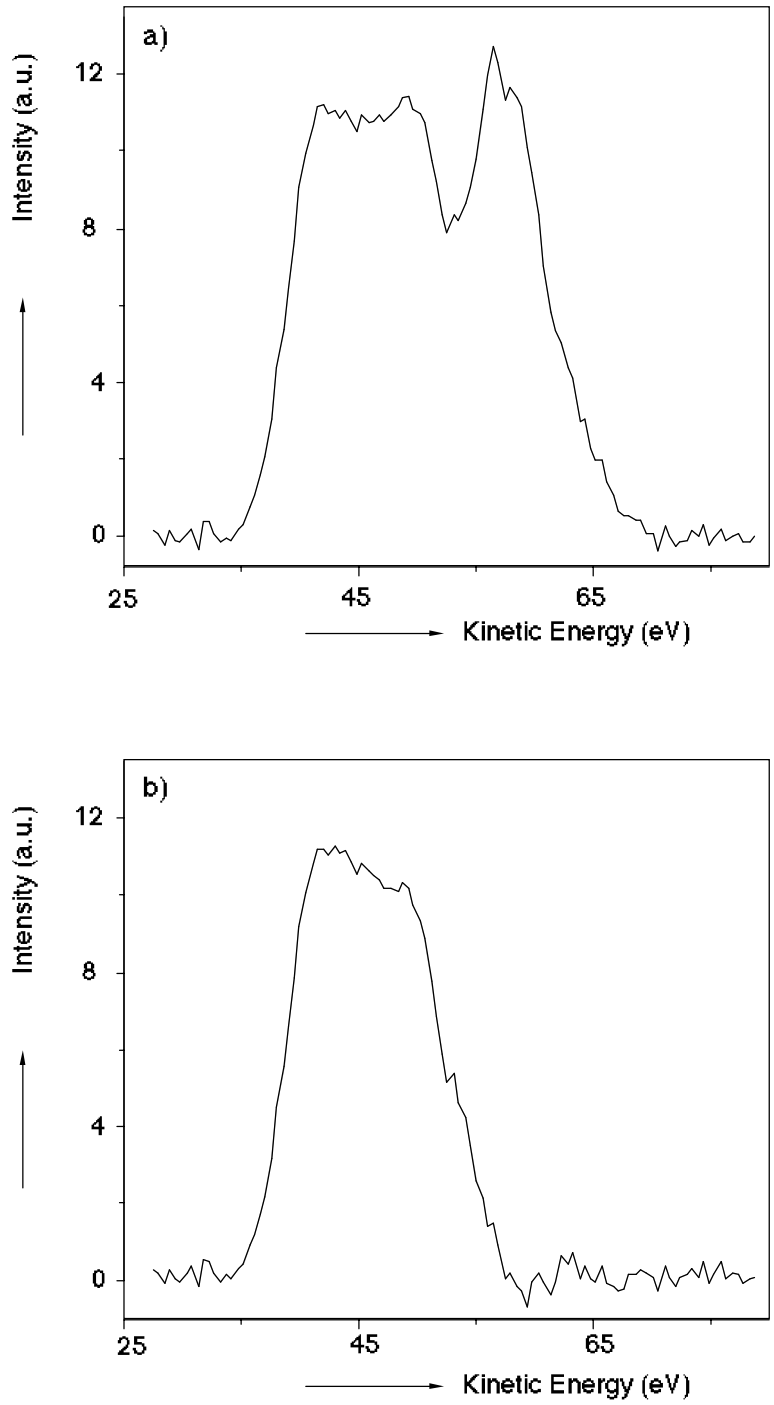

Figure 7 *Spectrum of an oxidised Cu(100) surface containing 1.0 ML Fe (a) and the spectrum after subtraction of the Cu $M_{2,3}VV$ peak (b).*

Therefore it was checked whether it is possible to use the background intensity at a higher energy than the Auger feature as a calibration factor. A point at higher energy was chosen because the shape of the background in that region appeared to be independent of changes in

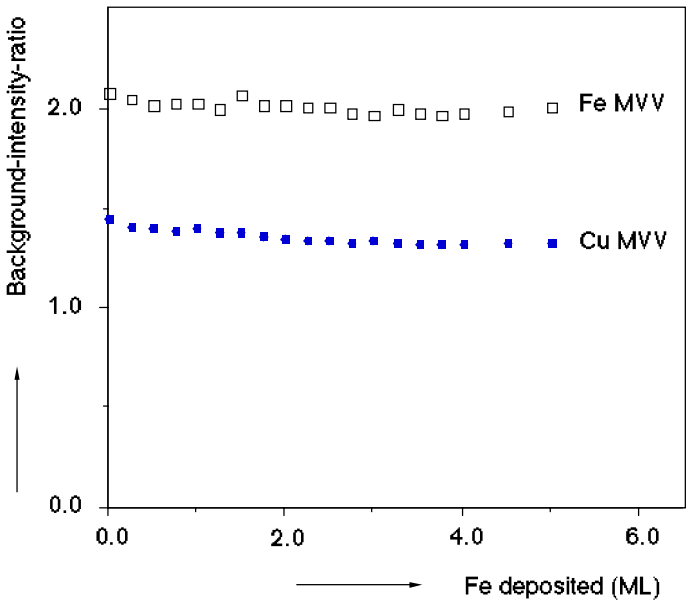

Figure 8 *The ratios of the background intensity under the Auger peaks and the intensity at 79 eV for the Fe and the Cu $M_{2,3}VV$ peaks during the evaporation.*

the amount of Fe or O at the surface. Instead of the Auger peak height used the peak area was used because the latter is less sensitive to peak shape changes. In Fig. 8 the ratios of the background intensity at the peak position (as calculated with the procedure described above) and the background at 79 eV are plotted for both the Fe and the Cu peaks against the amount of Fe deposited. The constant ratios during the complete experiment confirm the validity of both the background subtraction method and the use of the background intensity at 79 eV as internal calibration factor.

The area of the Cu and Fe peaks for surfaces containing 0 - 5 ML of Fe are plotted against the amount of Fe in Fig. 9. The calibration method described above is used to calculate the data in Fig. 9. Now it is possible to calculate the imfp of the Cu and Fe $M_{2,3}VV$ peaks from the initial slope of the curves in Fig. 9. This requires an assumption about the growth mode of Fe on Cu(100). Most authors find proof for a monolayer by monolayer growth [8,21,26]. Glatzel et al. [16] were the first to suggest a bi-layer by bi-layer growth mode. This was based on breakpoints in a high energy Fe $L_{2,3}M_{2,3}V$/ (Fe $L_{2,3}M_{2,3}V$ + Cu $L_{2,3}VV$) versus time of evaporation plot calibrated with Rutherford back scattering. Landskron et al. [17] observed breakpoints in the high energy Fe $L_{2,3}VV$ (703 eV) versus evaporation time plot at 3 and 6 ML. They ascribed these breakpoints to a reconstruction of the surface. Though the most significant results to determine the growth mode should be expected when the imfp's have almost the same length as the interlayer spacing of the layers (the larger the ratio between the inter-layer-spacing and the imfp the larger the change in the slope before and after the breakpoints) the results shown in Fig. 9 exhibit no clear breakpoints. While the Fe curve can be fitted reasonably well for both monolayer and bi-layer growth, the Cu curve can be fitted significantly better for monolayer growth. Part of the inconsistency of these results and the results mentioned in literature may be due to the strong temperature dependence of Cu segregation/interlayer mixing as reported by Steigerwald et al. [19]. They also observed some evidence for what may be bi-layer growth: half of the Cu atoms remained exposed at the

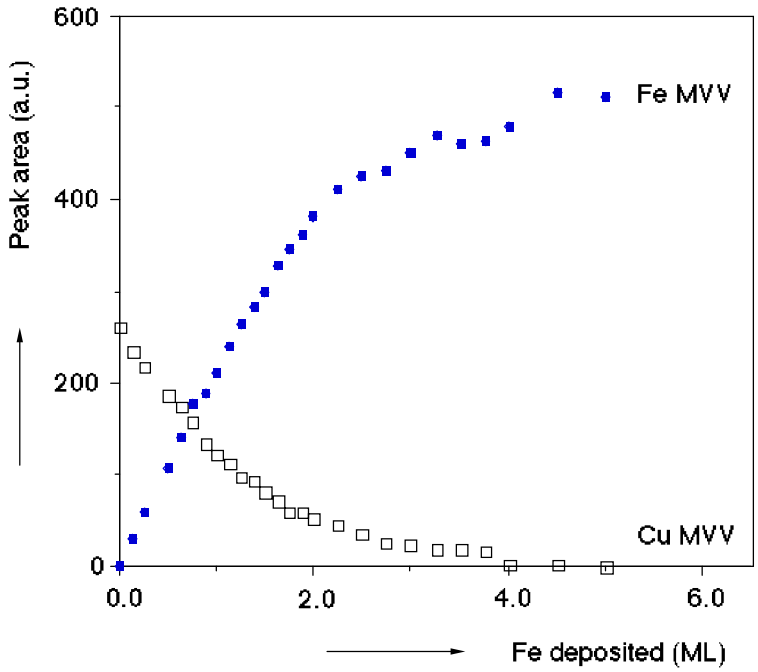

Figure 9 *Peak area of the Cu $M_{2,3}VV$ and the Fe $M_{2,3}VV$ peak as function of the amount of Fe evaporated.*

surface after evaporation of 1.0 ML of Fe at 295 K. But after evaporation at slightly higher temperatures even more Cu atoms remained exposed at the surface. The imfp's calculated from the monolayer fits are 0.36 ± 0.07 and 0.44 ± 0.09 nm for Cu $M_{2,3}VV$ and Fe $M_{2,3}VV$ electrons respectively. These imfp's are corrected for the effective angle of detection of an RFA ($\cos\theta = 0.74$) [114] and agree well with values given in literature [43].

9.3 Conclusions.

1 The background subtraction method supposed by Peacock gives good results in the analysis of the (low energy) Cu and Fe $M_{2,3}VV$ Auger spectra. Peak overlap and peak shape changes due to oxidation do not influence the quality of the results. Still some care is required in analysing spectra with small peaks superimposed on inelastic tails of peaks of other elements.

2 The combined Cu-Fe $M_{2,3}VV$ spectra can be described by a simple linear fit of the $M_{2,3}VV$ peaks of the pure metals in the complete composition range. For oxidised surfaces the Fe peaks can be separated by simply subtracting the copper peak from the observed spectra.

3 The background intensity at energies slightly higher than the Cu peak can be used as internal calibration factor. This is used to normalise the peak area's.

4 The inelastic mean free paths of the Cu and Fe $M_{2,3}VV$ electrons are found to be 0.36 ± 0.07 and 0.44 ± 0.09 nm respectively.

10

Conclusion

As was expected the reactivity of the Cu(100)-Fe surfaces exhibits many differences with clean copper and iron surfaces. Most of the differences described in this thesis concern the iron (oxide) on the surface. Since the surfaces nearly always consisted of an iron (oxide) layer on top of the Cu(100) surface the interaction between the copper surface and the iron (oxide) must be responsible for the different reactivity of the iron. The growth of fcc iron instead of bcc iron on Cu(100) already indicated a good interaction. Also the iron oxide formed on the Cu(100) surface (for θ_{Fe}<2 ML) appeared to have a good interaction with the copper as could be concluded from the LEED pattern that was observed for Cu(100)+0.8 ML Fe after saturation with oxygen (chapter 3). This LEED pattern exhibited a strong contraction. An other indication for this good interaction is the very low reactivity of the oxidised surfaces towards H_2 and CO (chapter 7) when the surfaces are completely covered with iron oxide.

For oxidation at room temperature no differences in initial oxidation rate were observed with ellipsometry for surfaces containing more than 0.19 ML of iron. This means that the oxidation probably proceeds via a precursor mechanism since the oxygen is initially bound to the iron on the surface (chapter 3-6). A precursor mechanism is also observed on pure copper single crystal surfaces [115].

Analysis of the Fe $M_{2,3}VV$ Auger spectra obtained during the oxidation of 1 ML of Fe on Cu(100) made it possible to exclude a successive oxidation of the iron from Fe^0 to Fe^{2+} to Fe^{3+} (chapter 4). Repetition of the same experiment using XPS revealed the presence of both Fe^{2+} and Fe^{3+} during the oxidation until all iron was oxidised to Fe^{3+}. On all surfaces saturated with

oxygen at 300 K (θ_{Fe} • 16 ML) a top layer of Fe_2O_3 was found with AES (chapter 3 and 4), XPS (chapter 5) and UPS (chapter 6). As for oxidation at 300 K of Fe(100) the amount of oxygen adsorbing on Cu(100)-Fe surfaces is limited. Quantitative analysis of the AES spectra of oxygen saturated Cu(100)-Fe surfaces containing up to 16 ML of iron showed that somewhat more than 2 ML of Fe can be oxidised to Fe_2O_3 (on surfaces containing less than 2 ML Fe all iron is oxidised to Fe_2O_3 and 0.5 ML of oxygen adsorbs on the Cu(100) interface). The ellipsometric data confirmed these findings assuming the same sensitivity of Δ for oxygen as on pure iron (chapter 3). However, equivalent experiments in a different UHV system equipped with XPS showed evidence for a much thicker iron oxide layer. This difference can possibly be explained by differences in surface structure after iron evaporation: the oxygen contamination on these surfaces was ~4 times higher than on the surfaces used for the AES and ellipsometry experiments.

The formation of closed layer of Fe_2O_3 on the Cu(100)-Fe surfaces also seems to be contradicted by results of Leibbrandt et al. [61]. They used High Energy Ion Scattering - Shadowing and Blocking (HEIS-SB) to determine the stoichiometry of the iron oxide formed on Fe(100). They concluded that FeO_x (wüstite) was present on their surfaces based on the number of displaced Fe atoms as function of the number of oxygen atoms adsorbed. The difference between their results and those presented in this thesis might be due to the strong interaction between the copper substrate and the oxide which also seems to cause a very low reactivity of the oxidised (at 300 K) Cu(100)-Fe surfaces towards CO and H_2 (chapter 7). This low reactivity is probably due to both a very small number of defect sites in the iron oxide and the small mobility of ions in this oxide. So Cu(100)-Fe surfaces may stabilise a 'different' iron oxide than Fe(100) does. On the other hand, when the interaction of the iron oxide on Fe(100) with the underlying iron lattice is strong enough to displace one 'extra' layer of iron atoms without oxidising them this exactly counts for the difference. Their argument against this is that for higher oxygen contents the number of displaced iron atoms still indicates FeO_x. However, those oxygen contents were obtained at 473 K and also on the Cu(100)-Fe surfaces strong indications for a different oxide structure were indirectly found in reduction experiments (chapter 7).

CO-adsorption on the Cu(100)-Fe surfaces appeared to be non dissociative and reversible. Apparently the close packed square symmetry of the fcc-Fe(100) surface is not able to dissociate CO though the interaction with the iron is strong enough to break iron clusters into single atoms and to form iron carbonyl like species on the surface. The hypothesis that CO breaks iron clusters and forms carbonyl like species is based on the number of CO molecules adsorbing per iron atom and the observation of a fast ('normal' molecular adsorption) and a slow (cluster breaking and carbonyl formation) adsorption stage.

The detailed analysis of the Fe $M_{2,3}VV$ Auger peak obtained during oxidation (chapter 4) was made possible by using an unconventional non-derivative data acquisition method and by using a background subtraction method that was originally developed for high energy AES spectra obtained with a cylindrical mirror analyser, for low energy AES spectra (chapter 9). Combination of the results of this analysis with XPS results (and a literature study into the origin of the Fe $M_{2,3}VV$ peak shape) indicated that it is difficult to determine the type of iron oxide from the $M_{2,3}VV$ peak shape.

Samenvatting

De interesse van veel wetenschappers voor systemen bestaande uit twee metalen komt voort uit het feit dat het samenvoegen van twee metalen vaak resulteert in het ontstaan van nieuwe eigenschappen. Het bestuderen van deze systemen en hun (nieuwe) eigenschappen verschaft meer inzicht in materie in het algemeen. Van veel directer belang voor de samenleving is dat deze nieuwe eigenschappen kunnen leiden tot nieuwe producten of verbeteringen aan bestaande producten.

Net als voor zuivere metalen geldt voor metaallegeringen dat bulk- en oppervlakte-eigenschappen verschillen. Dit uit zich zowel op het fysische als het chemische vlak. Met name de (chemische) reactiviteit van metaaloppervlakken is van belang voor vele toepassingen. Hierbij kan worden gedacht aan corrosie en aan heterogene katalyse. In beide gevallen kan gekozen worden voor een combinatie van bepaalde metalen om de gewenste eigenschappen te combineren.

Om de chemische reactiviteit van oppervlakken goed te kunnen bestuderen is het wenselijk om met goed gedefinieerde oppervlakken en omstandigheden te kunnen werken. Dat is de reden dat het in dit proefschrift beschreven onderzoek is uitgevoerd aan een éénkristaloppervlak onder ultra hoog vacuum condities. Een monokristallijn oppervlak is de basis voor een goed gedefinieerd oppervlak en het vacuum garandeert dat het oppervlak lang genoeg schoon blijft om de gewenste reacties gecontroleerd uit te kunnen voeren en achteraf de oppervlaktesamen-steling te kunnen bepalen. Omdat gewerkt wordt onder goed gedefinieerde omstandigheden ligt het voor de hand om de reactiviteit ten opzichte van betrekkelijk eenvoudige moleculen als O_2, CO en H_2 te bestuderen. Overigens zijn dit belangrijke reactanten in veel processen en de reacties blijken nog complex genoeg te zijn. De genoemde omstandigheden vormen een model-situatie die grote verschillen vertoont met de praktijk. Toch blijkt dit 'model' één van de betere mogelijkheden om een relatie te leggen tussen oppervlaktereactiviteit enerzijds en structuur op atomair niveau anderzijds[1].

De reden dat in dit proefschrift gekozen is voor het koper-ijzer-systeem is dat deze twee metalen een aantal punten verschillen. De belangrijkste verschillen zijn: de kristalstructuur bij kamertemperatuur (fcc voor Cu en bcc voor Fe), de oppervlaktespanning (van koper een stuk lager dan van ijzer) en de reactiviteit voor zuurstof en koolmonoxide (ijzeroxides zijn veel stabieler dan koperoxides, CO dissocieert op ijzer terwijl het op koper nauwelijks adsorbeert bij 300 K). Bovendien was al een en ander bekend over de reactiviteit van koper-ijzer-opper-vlakken. Van Pruissen [116] heeft de reactiviteit van Cu(111)-Fe en Cu(110)-Fe voor O_2, CO en H_2 uitgebreid bestudeerd. De bereiding van die oppervlakken gebeurde echter met behulp van $Fe(CO)_5$ ontleding. Dit resulteert in minder goed gedefinieerde oppervlakken dan met de opdampmethode zoals beschreven in dit proefschrift, omdat koolstof- en zuurstof-verontreinig-ingen bij hoge temperatuur verwijderd moesten worden. Voor een aantal waarnemingen zal dit verschil echter weing uitmaken.

De mogelijkheid om ijzer op te dampen in combinatie met de ruime hoeveelheid literatuur over de groei van ijzer op Cu(100) heeft de keus geleid tot het Cu(100)-Fe-systeem. Het bijzondere van het Cu(100)-Fe-oppervlak is dat het ijzer epitaxiaal (fcc) aangroeit terwijl bij kamertemperatuur nauwelijks menging optreedt. Overigens wordt het mengen in dit systeem gedreven door entropie en oppervlakte-energie aangezien de mengenthalpie van koper en ijzer positief is. Enige menging treedt wel op, zeker op monolaag-niveau en bij hogere

tempera-turen. Daarom zijn de meeste experimenten beschreven in dit proefschrift bij kamertemperatuur uitgevoerd.

In de hoofdstukken 3-6 wordt de interactie van de Cu(100)-oppervlakken, die (gedeeltelijk) met fcc-ijzer bedekt zijn, met zuurstof beschreven. In de verschillende hoofdstukken worden de resultaten van verschillende technieken beschreven en gecombineerd. Zo is in hoofdstuk 3 ellipsometrie, Auger-electronen-spectroscopie en lage-energie-electronen-diffractie toegepast om tot een model te komen voor de oxidatie van Cu(100)-Fe-oppervlakken met verschillende hoeveelheden ijzer. Hierbij worden voornamelijk uitspraken gedaan over het oppervlak na verzadiging met zuurstof. In hoofdstuk 4 wordt een poging gedaan de verandering van de piekvorm van de Fe-$M_{2,3}$VV-Auger-piek tijdens de oxidatie van 1 ML (monolaag) Fe te benutten om meer inzicht te krijgen in het verloop van de oxidatie. Literatuuronderzoek, de resultaten van de piekvorm-analyse en de XPS-resultaten (Fe 2p), die in hoofdstuk 5 gepresen-teerd worden, geven aan dat de Fe-$M_{2,3}$VV-piek niet echt geschikt is om (makkelijk) te kunnen waarnemen of er FeO, Fe_3O_4 danwel Fe_2O_3 aan het oppervlak aanwezig is. De analyse van de XPS-resultaten (hoofdstuk 5) geeft echter wel een goed inzicht in het verloop van de oxidatie. Verder bevestigen de XPS-resultaten het in hoofdstuk 3 beschreven model grotendeels en daar waar zij afwijken wordt een verklaring gesuggereerd. Tot slot wordt in hoofdtsuk 6 UPS gebruikt om nogmaals het oxide bij verzadiging te determineren en om te bestuderen of de veranderingen in de valentieband tijdens oxidatie in verband gebracht kunnen worden met initieel lagere gevoeligheid van de ellipsometer voor zuurstof.

De oxidatie van Cu(100)-Fe-oppervlakken blijkt te verlopen via een precursor-mechanisme. Dit kan worden afgeleid uit de initiële oxidatiesnelheid die niet afhankelijk blijkt te zijn van de hoeveelheid ijzer op het oppervlak. Zonder precursor-mechanisme mag namelijk verwacht worden dat voor $\theta_{Fe}<1$ een afname in de oxdatiesnelheid wordt waargenomen als θ_{Fe} afneemt omdat de initiële reactiekans voor adsorptie van O_2 op Cu(100) ongeveer twee ordes van grootte kleiner is dan op ijzer. Het ijzer op het oppervlak wordt eerst geoxideerd. Daarbij ontstaan in eerste instantie zowel Fe^{2+} als Fe^{3+}. Op oppervlakken met minder dan 2 ML ijzer wordt uiteindelijk alle ijzer geoxideerd tot Fe_2O_3, waarna een halve monolaag zuurstof op het koperoppervlak adsorbeert. Als meer dan 2 ML ijzer aanwezig is wordt 3.5 ML zuurstof opgenomen die gebonden wordt in de vorm van Fe_2O_3. Dit ijzeroxide ligt dan dus op een laagje metallisch (fcc-) ijzer. De mobiliteit van de ionen in het oxide dat gevormd is bij 300 K is kennelijk niet groot genoeg om verdere oxidatie te bewerkstelligen.

De reactiviteit van de geoxideerde oppervlakken voor CO en H_2, zoals beschreven in hoofdstuk 7, geeft vervolgens meer informatie over de structuur van het oxide. Voor oppervlakken waarvan de hoeveelheid ijzeroxide naar alle waarschijnlijkheid voldoende is om het koper geheel af te dekken is -indien de oppervlakken bij kamertemperatuur geoxideerd zijn- geen enkele reactiviteit ten opzichte van CO en H_2 waar te nemen voor drukken tot 0.2 Pa en bij een kristaltemperatuur van 630 K. Van oppervlakken met minder ijzer kan H_2 alle zuurstof verwijderen terwijl CO alleen reageert met de zuurstof die gebonden is aan koper. Voor alle oppervlakken geldt dat wanneer na de oxidatie bij 300 K ook nog zuurstof is geadsorbeerd bij 630 K, H_2 het oppervlak geheel kan reduceren terwijl CO alleen de zuurstof gebonden aan het koper verwijdert. Dit leidt tot een tweetal conclusies: Fe_2O_3 bevat te weinig defecten om reactief te zijn ten opzichte van H_2 en CO

onder genoemde omstandigheden en er is 'vrij' koper-oppervlak nodig om CO met zuurstof van het koper te laten reageren of om H_2 te dissociëren. De dan gevormde waterstofatomen kunnen het ijzeroxide wel reduceren.

Dat het fcc-ijzer op de Cu(100) oppervlakken unieke eigenschappen heeft blijkt ook uit de reactiviteit voor CO. De adsorptie van CO op Cu(100)-Fe (beschreven in hoofdstuk 8) blijkt moleculair en reversibel. Op alle ijzer-éénkristaloppervlakken dissocieert CO bij 350 K. Ook op de Cu-Fe-oppervlakken van Van Pruissen dissocieert het. Vreeburg et al. [56] neemt geen dissociatie waar op Ni(111)-Fe-oppervlakken mits de ensembles van ijzeratomen uit minder dan drie atomen bestaan. Ensembles die uit drie of meer atomen bestaan dissociëren wel CO. Ook op Ni(111) is het ijzer aanwezig in fcc-structuur. Kennelijk beschikt de vierkante symmetrie van het fcc-Fe(100) niet over adsorptie plaatsen met de juiste geometrie voor dissociatie. Er zijn wel sterke aanwijzingen dat de interactie tussen het ijzer en de CO sterk genoeg is om de ijzeratomen uit elkaar te trekken en zelfs carbonyl-achtige structuren te vormen. Dit is gebaseerd op de verhouding van het aantal ijzeratomen en het aantal geadsorbeerde CO-moleculen enerzijds en op twee duidelijk verschillende stadia in de 'adsorptie'-snelheid op verschillende oppervlakken anderzijds.

Een gedeelte van het werk beschreven in dit proefschrift was alleen mogelijk dankzij verbeteringen van de wijze waarop Auger-spectra worden verkregen en geanalyseerd. Automatisering en softwarematige data-analyse openden een weg om meer informatie uit de spectra te halen door niet-afgeleide spectra op te nemen en te analyseren. In hoofdstuk 2 wordt onder andere aandacht besteed aan de voordelen van deze onconventionele techniek en in hoofdstuk 9 wordt een methode beschreven waarmee spectra van hun achtergrond ontdaan kunnen worden. Het succes van de methode blijkt uit de analyse van de Fe-$M_{2,3}$VV-piek zoals die is beschreven in hoofdstuk 4.

Literature

[1] C.T. Campbell, Ann. Rev. Phys. Chem. **41** (1990) 775-837.

[2] H. Landolt and R. Börnstein, 'Zahlenwerte und Funktionen aus Naturwissenschaften und Technik.', Springer Verlag, Berlin 1988.

[3] J.H. Weaver, C. Krafka, D.W. Lynch and E.E. Kock, 'Physics data. Optical properties of metals', Fachinformationszentrum, Karlsruhe 1981.

[4] 'Thermochemical Properties of Inorganic Substances', O. Knacke, O. Kubaschewske and K. Hesselmann (Eds.) Springer Verlag, Berlin 1991.

[5] G.A. Somorjai in 'Chemistry in two dimensions: surfaces', Cornell University Press, Ithaca 1981

[6] T.J. Vink, O.L.J. Gijzeman and J.W. Geus, Surf. Sci. **150** (1985) 14.

[7] M. Arnott, E.M. McCash and W. Alisson, Surf. Sci. **269/270** (1992) 724.

[8] A. Clarke, P.J. Rous, M. Arnott, G. Jennings ans R.F. Willis, Surf. Sci. **192** (1987) L843

[9] A. Brodde and H. Neddermeyer, Surf. Sci. **287/288** (1993) 988.

[10] D.D. Chambliss, R.J. Wilson and S. Chiang, J. Vac. Sci. Technol. A **10** (1992) 1993.

[11] M.T. Kief and W.F. Egelhoff, Jr., Phys. Rev. B **47** (1993) 10 785.

[12] Th. Detzel. N. Memmel and Th. Fauster, Surf. Sci. **293** (1993) 227.

[13] M. Wuttig, B. Feldmann, J. Thomassen, F. May, H. Zillgen, H. Hannemann and H. Neddermeyer, Surf. Sci. **291** (1993) 14.

[14] Y. Darici, J. Marcano, H. Min and P.A Montano, Surf. Sci. **217** (1989) 521.

[15] P. Dastoor, M. Arnott, E.M. McCash and W. Allison, Surf. Sci. **272** (1991) 154.

[16] H. Glatzel, Th. Fauster, B.M.U. Scherzer and V. Dose, Surf. Sci. **254** (1989) 58.

[17] H. Landskron, G. Schmidt, K. Heinz, K. Müller, C. Sthulmann, U. Beckers, M. Wuttig and H. Ibach, Surf. Sci. **256**, (1991) 115.

[18] H. Magnan, D. Chandersis, B. Vilette, O. Heckmann and J. Lecante, Surf. Sci. **251/25**2 (1991) 597.

[19] D.A. Steigerwald, I. Jacob, and W.F. Egelhoff Jr., Surf. Sci. **202** (1988) 472.

[20] J. Thomassen, B. Feldmann and M. Wuttig, Surf. Sci. **264** (1992) 406.

[21] W. Daum, C. Stuhlman and H. Ibach, Phys. Rev. Letters **60** (1988) 2558.

[22] W.F. Egelhoff Jr. and M..T. Kief, Phys. Rev. B **45** (1992) 7795.

[23] J.F. Cochran, J.M. Rudd, M. From, B. Heinrich, W. Bennelt, W. Schwarzacher and W.F. Egelhoff Jr., Phys. Rev. B **45** (1992) 4676.

[24] D. Pescia, M. Stampanoni, G.L. Bona, A. Vaterlaus, R.F. Willis and F. Meier, Phys. Rev. Lett. **58** (1987) 2126.

[25] C. Rau, C. Schneider, G. Xing and K. Jamison, Phys. Rev. Lett. **57** (1986) 3221.

[26] M. Stampanoni, A. Vaterlaus, M. Aeschlimann, F. Meier and D. Pescia, J. Appl. Phys. **64** (1988) 5321.

[27] C.L. Chien, S.H. Lion, D. Kofalt, Wu Yu, T. Egami and T.R. McGuire, Phys. Rev. B. **33** (1986) 3247.

[28] F.J. Himpsel, Phys. Rev. Lett. **67** (1991) 2363.

[29] O.P. van Pruissen and O.L.J. Gijzeman, Appl. Surf. Sci. **27** (1986) 52.

[30] O.P. van Pruissen, E. Boellaard, O.L.J. Gijzeman and J.W. Geus, Appl. Surf. Sci. **27** (1986) 1.

[31] O.P. van Pruissen, M.M.M. Dings, E. Boellaard, O.L.J. Gijzeman and J.W. Geus, Appl. Surf. Sci. **27** (1986) 24.
[32] O.P. van Pruissen, G.C. van Leerdam, O.L.J. Gijzeman and J.W. Geus, Appl. Surf. Sci. **29** (1987) 86.
[33] O.P. van Pruissen, O.L.J. Gijzeman and J.W. Geus, Appl. Surf. Sci. **29** (1987) 317.
[34] O.P. van Pruissen, M.M.M. Dings and O.L.J. Gijzeman, Surf. Sci. **179** (1987) 377.
[35] K. Kishi and J. Nishioka, Surf. Sci. **229** (1989) 199.
[36] S. Di Nardo, M. Passacantando, P. Picozzi, S. Santucci, L. Lozzi, M. De Crescenzi and H. den Daas, Surf. Interface Anal. **18** (1992) 98.
[37] S. Di Nardo, M. Passacantando, P. Picozzi, S. Santucci, L. Lozzi, M. De Crescenzi and H. den Daas, Surf. Interface Anal. **19** (1992) 478.
[38] R.M.A. Azzam and N.M Bashara, 'Ellipsometry and polarised light', North-Holland, Amsterdam NL 1977.
[39] A. Zangwill, 'Physics at Surfaces.', Cambridge Univeristy Press, Cambridge UK 1988.
[40] Briggs and Seah, 'Practical surface analysis by Auger and X-ray Photo electron spectroscopy', John Wiley and Sons, Chichester UK 1990.
[41] D.P. Woodruff and T.A. Delchar, 'Modern techniques of surface science.', Cambridge University Press, Cambridge UK 1986.
[42] L.J. Clarke, 'Surface crystallography', John Wiley and Sons, Chichester UK 1985.
[43] M.P. Seah and W.A. Dench, Surf. Interface Anal.,**1** (1972) 2.
[44] F. Labohm, Surf. Interface Anal. **4** (1982) 767.
[45] H. den Daas, O.L.J. Gijzeman and J.W. Geus, Surf. Interface Anal. **18** (1992) 397 (chapter 9 of this thesis).
[46] H. den Daas, O.L.J. Gijzeman and J.W. Geus, Surf. Sci. **290** (1993) 26 (chapter 4 of this thesis).
[47] D.C. Peacock, Surf. Sci. **152/153** (1985) 895.
[48] J.P. Langeron, L. Minel, J.L. Vignes, S. Bouquet, F. Pellerin, G. Lorang, P. Ailloud and J. Le Héricy, Surf.Sci. **138** (1984) 610.
[49] J.P. Langeron, Surf. Interface Anal. **14** (1989) 381.
[50] S. Tanuma, C.J. Powell and D.R. Penn, Surf. Interface Anal. **17** (1991) 911.
[51] M. Wiegel, A.R. Balkenende, O.L.J. Gijzeman, G.W.R. Leibbrandt and F.H.P.M. Habraken, Surf. Sci. **254**, (1991) L428..
[52] R.J. Vreeburg, O.L.J. Gijzeman and J.W. Geus, Surf. Sci. **245** (1991) 111.
[53] Handbook of X-ray photoelectron spectroscopy, J. Chastain (ed.) Perkin-Elmer Corporation, Minnesota (1992).
[54] R.E. Hummel, 'Optische Eigenschaften von Metallen und Legierungen', Springer (Berlin) 1971.
[55] G.W.R Leibbrandt, S. Deckers, M. Wiegel and F.H.P.M. Habraken, Surf. Sci. **244** (1991) L101
[56] R.J. Vreeburg, J. van de Loosdrecht, O.L.J. Gijzeman and J.W. Geus, Catalysis Today **10** (1991) 329.
[57] F.H.P.M. Habraken, E.Ph. Kiefer and G.A. Bootsma, Surf. Sci. **83** (1979) 45.
[58] F.H.P.M. Habraken, C.M.A.M. Mesters and G.A. Bootsma, Surf. Sci. **97** (1980) 264.
[59] T.J. Vink, J.M. der Kinderen, O.L.J Gijzeman and J.W. Geus, Appl. Surf. Sci. **26** (1986) 357.
[60] M. Seo, J.B. Lumsden and R.W. Staehle, Surf. Sci. **50**, 541 (1975).

[61] G.W.R. Leibbrandt, G. Hoogers and F.P.H.M. Habraken, Phys. Rev. Lett. **68** (1992) 1947.
[62] P.K. de Bokx, F. Labohm, O.L.J. Gijzeman, G.A. Bootsma and J.W. Geus, Appl. Surf. Sci. **5** (1980) 321.
[63] G.W. Simmons and D.J. Dwyer, Surf. Sci. **48** (1975) 373.
[64] P.T. Dawson and K.K. Tzatzov, Surf. Sci. **171** (1986) 339.
[65] P.T. Dawson and K.K. Tzatzov, Surf. Sci. **234** (1990) 239.
[66] V.S. Smentkovski and J.T. Yates Jr., Surf. Sci. **232** (1990) 113.
[67] T. Miyano, Y. Sakisaka, T. Komeda and M. Onchi, Surf. Sci. **169** (1986) 157.
[68] Y. Sakisaka, T. Miyano, T. Komeda and M. Onchi, Phys. Rev. B **30** (1984) 6849.
[69] M. Arbab and B. Hudson, Surf. Sci. **206** (1988) 317.
[70] C. Jansson and P. Morgen, Surf. Sci. **232** (1990) 84.
[71] G. Lorang, M. Da Cunha Belo and J.P. Langeron, J. Vac. Sci. Technol. A **5** (1987) 1213.
[72] G. Ertl and K. Wandelt, Surf. Sci. **50** (1975) 479.
[73] K. Ueda and R. Shimizu, Surf. Sci. **43** (1974) 77.
[74] S. Hofmann and H.J. Steffen, Surf. Interface Anal. **14** (1989) 59.
[75] E.N. Sickafus, Surf. Sci. **100** (1980) 529.
[76] S. Tougaard, Surf. Sci. **216** (1989) 343.
[77] M.G. Ramsey and G.J. Russell, Phys. Rev B **30** (1984) 6960.
[78] C.R. Brundle, Surf. Sci. **66** (1977) 581.
[79] K. Wandelt, Surf. Sci. Rept. **2** (1982) 1.
[80] C.S. Kuivila, J.B. Butt and P.C. Stair, Appl. Surf. Sci. **32** (1988) 99.
[81] G.W.R Leibbrandt, thesis, Utrectht 1992, chapter 4 and 5.
[82] H. den Daas, O.L.J. Gijzeman and J.W. Geus, Surf. Sci. **285** (1993) 15. (chapter 3 of this thesis.)
[83] J.R. Lince, S.V. Didziulis, D.K. Shuh, T.D. Durbin and J.A. Yarmoff, Surf. Sci. **277** (1992) 43.
[84] R.L. Kurtz and V.E. Henrich, Surf. Sci. **129** (1983) 345.
[85] H. den Daas, O.L.J. Gijzeman and J.W. Geus, Appl. Surf. Sci. **68** (1993) 557. (chapter 7 of this thesis.)
[86] H. den Daas, E.H. Voogt, O.L.J. Gijzeman and J.W. Geus, accepted for publication in Surf. Sci. (chapter 8 of this thesis.)
[87] P. Heimann, J. Hermanson, H. Miosga and H. Neddermeyer, Phys. Rev. B **20** (1979) 3059.
[88] R. Matzdorf, G. Meister and A. Goldmann, Surf. Sci. **286** (1993) 56.
[89] K.W. Jacobsen and J.K. Nørskov, Phys. Rev. Lett. **65** (1990) 1788.
[90] I.K. Robinson, E. Vlieg and S. Ferrer, Phys. Rev. B **42** (1990) 6954.
[91] S.G. Bishop and P.C. Kemeny, Solid State Commun. **15** (1974) 1877.
[92] A. Fujimori, M. Saeki, N. Kimizuka, M. Taniguchi and S. Suga, Phys. Rev B **34** (1986) 7318.
[93] H. den Daas, M. Passacantando, L. Lozzi, S. Santucci and P. Picozzi, submitted to Surf. Sci.
[94] C.M.A.M. Mesters, T.J. Vink, O.L.J. Gijzeman and J.W. Geus, Surf. Sci. **135** (1983) 428.

[95] A.R. Balkenende, H. den Daas, M. Huisman, O.L.J. Gijzeman and J.W. Geus, **47** (1991) 341.
[96] A.R. Balkenende, O.L.J. Gijzeman and J.W. Geus, Cat. Sci. Technol., **1** (1991) 22.
[97] O.L.J. Gijzeman, T.J. Vink, O.P. van Pruissen and J.W. Geus, J. Vac. Sci. Technol. A **5** (1987) 718.
[98] R.J. Vreeburg, Thesis Utrecht 1992.
[99] E. Boellaard, Thesis Utrecht 1994.
[100] Ullmann's Encyklopädie der Technischen Chemie, Dritte Auflage (Urban und Schwarzenberg, München-Berlin, 1957), band 9 684-748.
[101] F. Labohm, C.W.R. Engelen, O.L.J. Gijzeman, J.W. Geus and G.A. Bootsma, J. Chem. Soc. Faraday Trans. 1, **78** (1982) 2435.
[102] C.M. Truong, J.A. Rodriguez and D.W. Goodman, Surf. Sci. **271** (1992) 385.
[103] O.L.J. Gijzeman, Appl. Surf. Sci. **62** (1992) 61.
[104] G. Brodén, G. Gafner and H.P. Bonzel, Surf. Sci. **84** (1979) 295.
[105] D. Tománek, S. Mukherjee, V. Kumar and K.H. Bennemann, Surf. Sci. **114** (1982) 11.
[106] J.L. Meijering, Acta Met. **14** (1966) 251.
[107] H.F.J. van 't Blik, J.B.A.D. van Zon, T. Huizinga, J.C. Vis, D.C. Koningsberger and R. Prins, J. Am. Chem. Soc. **107** (1985) 3139.
[108] S.C. Tjong, J. Eldridge and R.W. Hoffman, Appl. Surf. Sci. **14** (1982) 297.
[109] D.C. Peacock and J.P. Duraud, Surface Interface Anal. **8** (1986) 1.
[110] H.Bender, Surface Interface Anal. **15** (1990) 767
[111] E.N. Sickafus, Phys. Rev. B **16** (1977) 1436.
[112] E.N. Sickafus, Phys. Rev. B **16** (1977) 1448.
[113] E.N. Sickafus and C. Kukla, Phys. Rev. B **19** (1979) 4056.
[114] M.P. Seah, Surf. Sci. **32** (1972) 703.
[115] F.H.P.M. Habraken, thesis Utrecht 1980.
[116] O.P. van Pruissen, thesis Utrecht 1987.

Curriculum Vitae

De auteur van dit proefschrift werd geboren op 8 december 1965 te Meppel. Het voortgezet onderwijs werd gevolgd aan de Rijksscholengemeenschap te Meppel en in mei 1984 afgesloten met het VWO diploma. In het zelfde jaar werd begonnen met de studie scheikunde aan de Rijksuniversiteit te Utrecht. Na het propaedeutischexamen in augustus 1985 (c.l.) werd het doctoraalexamen afgelegd in augustus 1989 met als specialisatie fysische chemie (hoofdvak) en anorganische chemie (bijvak). Aansluitend werd begonnen aan het promotieonderzoek. In de functie van AIO, in dienst van de Faculteit Scheikunde aan de Rijksuniversiteit te Utrecht, werd aan dit proefschrift gewerkt van 1-9-1989 tot 1-12-1993. Gedurende de eerste helft van 1993 werd het onderzoek uitgevoerd in het Dipartimento di Fisica Università dell'Aquila in het kader van het Human Capital and Mobility Programme van de Europese Gemeenschap.